

Mining Science and Technology

Горные науки
и технологии

Vol. **10** № **3**
Tom
2025



<https://mst.misis.ru/>

<https://t.me/MinSciTech>



Activities of the *Mining Science and Technology (Russia) (Gornye nauki i tekhnologii)* international journal are aimed at developing international scientific and professional cooperation in the field of mining.

The journal target audience comprises researchers, specialists in the field of mining, representatives of academic and professional communities.

The journal publishes original papers describing research findings, experience in the implementation of projects in mining industry, review publications.

The journal seeks to develop interdisciplinary areas that contribute to progress in mining, for example, technological and environmental safety, project organization and management in mining industry, development of territories, legal aspects of natural resource use, and other areas studied by researchers and practitioners. The journal always welcomes new developments. Papers are accepted in English or Russian.

EDITOR-IN-CHIEF

Vadim L. Petrov, Prof., Dr.Sci.(Eng.), University of Science and Technology MISIS, Moscow, Russian Federation

DEPUTIES EDITOR-IN-CHIEF

Oleg I. Kazanin, Prof., Dr.Sci.(Eng.), Empress Catherine II Saint Petersburg Mining University, St. Petersburg, Russian Federation

Svetlana A. Epshtein, Dr.Sci.(Eng.), University of Science and Technology MISIS, Moscow, Russian Federation

EDITORIAL BOARD

Zach Agioutantis, Prof., Ph.D., University of Kentucky, Lexington, Kentucky, USA

Maksim A. Bogdasarou, Prof., Dr.Sci.(Geol. and Min.), Brest State A. S. Pushkin University, Brest, Belarus

Grigory Yu. Boyarko, Prof. Dr. Sci. (Econ.), Cand. Sci. (Geol. and Miner.), National Research Tomsk Polytechnic University, Tomsk, Russian Federation

Xuan Nam Bui, Prof., Dr.Sci., Hanoi University of Mining and Geology, Duc Thang – Bac Tu Liem, Hanoi, Vietnam

Carsten Drebenstedt, Prof., Ph.D., Freiberg University of Mining and Technology, Freiberg, Germany

Faramarz Doulati Ardejani, Prof., Ph.D., Colledge of Engineering, University of Tehran, Tehran, Iran

Mikhail S. Ershov, Prof., Dr.Sci.(Eng.), National University of Oil and Gas "Gubkin University", Moscow, Russian Federation

Alexandr N. Evdokimov, Dr.Sci. (Geol. and Min.), Empress Catherine II Saint Petersburg Mining University, St. Petersburg, Russian Federation

Alper A. Feyzullaev, Prof., Dr.Sci.(Geol. and Min.), Institute of Geology and Geophysics of the National Academy of Sciences of Azerbaijan, Baku, Azerbaijan

Ochir Gerel, Prof., Dr.Sci.(Geol. and Min.), Geoscience Center, the Mongolian University of Science and Technology, Ulaanbaatar, Mongolia

Zoran Gligorić, Prof., Dr.Sci. (Mining-Underground Mining), University of Belgrade, Belgrade, Republic of Serbia

Monika Hardygora, Prof., Ph.D., Wrocław University of Technology, Wrocław, Poland

Nikolae Ilias, Prof., Dr.Sci.(Eng.), University of Petrosani, Petrosani, Romania

Vladislav Kecojevic, Prof., Ph.D., Benjamin M. Statler College of Engineering and Mineral Resources, West Virginia University, Morgantown, West Virginia, USA

Aleksey A. Khoreshok, Prof., Dr.Sci.(Eng.), Gorbachev Kuzbass State Technical University, Kemerovo, Russian Federation

Vladimir I. Klishin, Prof., Dr.Sci.(Eng.), Institute of Coal, Siberian Branch, Russian Academy of Sciences, Kemerovo, Russian Federation

Vladimir N. Koshelev, Prof., Dr.Sci.(Chem.), National University of Oil and Gas "Gubkin University" (Gubkin University), Moscow, Russian Federation

Jyant Kumar, Prof., Ph.D-Geotech.Eng., Indian Institute of Science, Bengaluru, India

Vladimir A. Makarov, Prof., Dr.Sci.(Geol. and Min.), Siberian Federal University, Krasnoyarsk, Russian Federation

Sergey I. Malafeev, Prof., Dr.Sci.(Eng.), Vladimir State University named after Alexander and Nikolay Stoletovs, Vladimir, Russia

Oleg S. Misnikov, Prof., Dr.Sci.(Eng.), Tver State Technical University, Tver, Russian Federation

Valery V. Morozov, Prof., Dr.Sci.(Eng.), University of Science and Technology MISIS, Moscow, Russian Federation

Igor M. Petrov, Dr.Sci.(Eng.), Infomine Research Group LLC, Moscow, Russian Federation

Bakhadirzhan R. Raimzhanov, Prof., Dr.Sci.(Eng.), University of Science and Technology MISIS (branch), Almalyk, Uzbekistan

Bayan R. Rakishev, Prof., Dr.Sci.(Eng.), Kazakh National Research Technical University named after K.I. Satpayev, Alma-Ata, Kazakhstan

Oscar Jaime Restrepo Baena, Prof., Ph.D., National University of Colombia, Medellín, Colombia

Alexander N. Shashenko, Prof., Dr.Sci.(Eng.), National Mining University, Dnipro, Ukraine

Vadim P. Tarasov, Prof., Dr.Sci.(Eng.), University of Science and Technology MISIS, Moscow, Russian Federation

Denis P. Tibilov, Prof., Dr.Sci.(Econ.), Moscow State Institute of International Affairs (University) under the Ministry of Foreign Affairs of Russia, Moscow, Russian Federation

Niyaz G. Valiev, Prof., Dr.Sci.(Eng.), The Ural State Mining University, Ekaterinburg, Russian Federation

Natalia Zhuravleva, Prof., Dr.Sci.(Eng.), West Siberian Testing Center JSC (WSTCenter JSC), Novokuznetsk, Russian Federation

Vera V. Yurak, Assoc. Prof., Dr. Sci. (Econ.), Ural State Mining University, Yekaterinburg; Institute of Economics, Ural Branch of the Russian Academy of Sciences, Yekaterinburg, Russian Federation

EDITORIAL COUNCIL

Yuri G. Agafonov, Assoc. Prof., Cand.Sci.(Eng.), University of Science and Technology MISIS, Moscow, Russian Federation

Michael R. Filonov, Prof., Dr.Sci.(Eng.), University of Science and Technology MISIS, Moscow, Russian Federation

Leonid A. Plaschansky, Prof., Cand.Sci.(Eng.), University of Science and Technology MISIS, Moscow, Russian Federation

Yuri I. Razorenov, Prof., Dr.Sci.(Eng.), Empress Catherine II Saint Petersburg Mining University, Saint Petersburg, Russian Federation

EXECUTIVE SECRETARY

Daria P. Galushka, University of Science and Technology MISIS, Moscow, Russian Federation

QUARTERLY

FOUNDED in 2016

REGISTRATION

The journal science and applied research journal is registered by the Federal Service for Communication, IT and Mass Communication Control on August 10, 2015.
Registration Certificate E-No. ФС77-62652

INDEXATION

Scopus, CAS, EBSCO, DOAJ, РИНЦ, ВИНТИ РАН, Dimensions, BASE, J-Gate, Jisc Library Hub Discover.

FOUNDER AND PUBLISHER



MISIS UNIVERSITY
MISIS University of Science and Technology

CONTACT

4 Leninsky Prospect, Moscow 119049, Russian Federation
Phone: +7 (495) 955-00-77
e-mail: send@misis.ru



This work is licensed under a
[Creative Commons Attribution 4.0 License](https://creativecommons.org/licenses/by/4.0/).



Деятельность научно-практического журнала «Горные науки и технологии» (Mining Science and Technology (Russia)) направлена на развитие международного научного и профессионального сотрудничества в области горного дела.

Целевая аудитория журнала – исследователи, специалисты в области горного дела, представители академического и профессионального сообществ.

В журнале публикуются оригинальные статьи, описывающие результаты исследований, опыт реализации проектов в горнопромышленном комплексе, обзорные публикации.

Журнал стремится развивать такие междисциплинарные направления, как технологическая и экологическая безопасность, организация и управление проектами в горной промышленности, развитие территорий, правовые аспекты использования природных ресурсов и другие, которые способствуют прогрессу в горном деле и реализуются исследователями и практиками.

ГЛАВНЫЙ РЕДАКТОР

Петров Вадим Леонидович, проф., д.т.н., Университет науки и технологий МИСИС, г. Москва, Российская Федерация

ЗАМЕСТИТЕЛИ ГЛАВНОГО РЕДАКТОРА

Казанин Олег Иванович, проф., д.т.н., Санкт-Петербургский горный университет императрицы Екатерины II, г. Санкт-Петербург, Российская Федерация

Эпштейн Светлана Абрамовна, д.т.н., Университет науки и технологий МИСИС, г. Москва, Российская Федерация

РЕДАКЦИОННАЯ КОЛЛЕГИЯ

Агиутантис Зак, проф., д-р наук, Университет Кентукки, г. Лексингтон, Кентукки, США

Богдасаров Максим Альбертович, проф., д.г.-м.н., Брестский государственный университет им. А.С. Пушкина, г. Брест, Беларусь

Боярко Григорий Юрьевич – проф., д.э.н., к.г.-м.н., Национальный исследовательский Томский политехнический университет, г. Томск, Российская Федерация

Буи Суан Нам, проф., д-р наук, Ханойский университет горного дела и технологии, г. Ханой, Вьетнам

Валиев Нияз Гадым оглы, проф., д.т.н., Уральский государственный горный университет, г. Екатеринбург, Российская Федерация

Герел Очир, проф., д.г.-м.н., Центр геолого-геофизических исследований, Монгольский университет науки и технологий, г. Улан-Батор, Монголия

Глигорич Зоран, проф., д-р наук, Белградский университет, г. Белград, Република Сербия

Дребенштедт Карстен, проф., д-р наук, Технический университет Фрайбергская горная академия, г. Фрайберг, Германия

Дулати Ардежани Фарамарз, проф., д-р наук, Инженерный колледж, Тегеранский университет, г. Тегеран, Иран

Евдокимов Александр Николаевич, проф., д.г.-м.н., Санкт-Петербургский горный университет императрицы Екатерины II, г. Санкт-Петербург, Российская Федерация

Ершов Михаил Сергеевич, проф., д.т.н., Российский государственный университет нефти и газа (национальный исследовательский университет) им. И.М. Губкина, г. Москва, Российская Федерация

Журавлева Наталья Викторовна, проф., д.т.н., АО «Западно-Сибирский испытательный центр» (АО «ЗСИЦентр»), г. Новокузнецк, Российская Федерация

Илиаш Николае, проф., д.т.н., Университет Петрошани, г. Петрошани, Румыния

Кеоджевич Владислав, проф., д-р наук, Институт инженерного дела и минеральных ресурсов им. Бенджамина М. Статлера Университета Западной Вирджинии, г. Моргантаун, Западная Вирджиния, США

Клишин Владимир Иванович, проф., д.т.н., Институт угля Сибирского отделения Российской академии наук, г. Кемерово, Российская Федерация

Кошелев Владимир Николаевич, проф., д.х.н., Российский государственный университет нефти и газа им. И.М. Губкина, г. Москва, Российская Федерация

Кумар Джьянт, проф., д-р наук (геотехнический инжиниринг), Индийский институт науки (Indian Institute of Science), г. Бангалор, Индия

Макаров Владимир Александрович, проф., д.г.-м.н., Сибирский федеральный университет, г. Красноярск, Российская Федерация

Малафеев Сергей Иванович, проф., д.т.н., Владимирский государственный университет имени А.Г. и Н.Г. Столетовых, г. Владимир, Российская Федерация

Мисников Олег Степанович, проф., д.т.н., Тверской государственный технический университет, г. Тверь, Российская Федерация

Морозов Валерий Валентинович, проф., д.т.н., Университет науки и технологий МИСИС, г. Москва, Российская Федерация

Петров Игорь Михайлович, д.т.н., ООО «Исследовательская группа «Информайн»», г. Москва, Российская Федерация

Раимжанов Бахадиржан Раимжанович, проф., д.т.н., филиал Университета науки и технологий МИСИС, г. Алматы, Узбекистан

Ракишев Баян Ракишевич, проф., д.т.н., Казахский национальный исследовательский технический университет им. К.И. Сатпаева, г. Алма-Ата, Казахстан

Рестрепо Баэна Оскар Хайме, проф., д-р наук, Национальный университет Колумбии, г. Медельин, Колумбия

Тарасов Вадим Петрович, проф., д.т.н., НИТУ «МИСиС», г. Москва, Российская Федерация

Тиболов Денис Петрович, проф., д.э.н., Московский государственный институт международных отношений (Университет) Министерства иностранных дел России, г. Москва, Российская Федерация

Фейзуллаев Акпер Акпер оглы, проф., д.г.-м.н., Институт геологии и геофизики (ИГГ) Национальной Академии Наук Азербайджана, г. Баку, Азербайджан

Хорешок Алексей Алексеевич, проф., д.т.н., Кузбасский государственный технический университет им. М.С. Горбачева, г. Кемерово, Российская Федерация

Шашенко Александр Николаевич, проф., д.т.н., Национальный горный университет, г. Днепр, Украина

Хардигора Моника, проф., д-р наук, Вроцлавский технологический университет, г. Вроцлав, Польша

Юрак Вера Васильевна, доц., д.э.н., Уральский государственный горный университет, г. Екатеринбург; старший научный сотрудник, Институт экономики Уральского отделения Российской академии наук (ИЭ УрО РАН), г. Екатеринбург, Российская Федерация

РЕДАКЦИОННЫЙ СОВЕТ

Агафонов Юрий Григорьевич, доц., к.т.н., Университет науки и технологий МИСИС, г. Москва, Российская Федерация

Плащанский Леонид Александрович, проф., к.т.н., Университет науки и технологий МИСИС, г. Москва, Российская Федерация

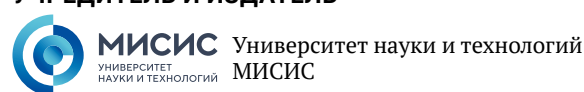
Разоренов Юрий Иванович, проф., д.т.н., Санкт-Петербургский горный университет императрицы Екатерины II, г. Санкт-Петербург, Российская Федерация

Филонов Михаил Рудольфович, проф., д.т.н., Университет науки и технологий МИСИС, г. Москва, Российская Федерация

ОТВЕТСТВЕННЫЙ СЕКРЕТАРЬ

Галушка Дарья Петровна, Университет науки и технологий МИСИС, г. Москва, Российская Федерация

УЧРЕДИТЕЛЬ И ИЗДАТЕЛЬ



АДРЕС УЧРЕДИТЕЛЯ И ИЗДАТЕЛЯ

119049, г. Москва, Ленинский проспект, д. 4

КОНТАКТЫ РЕДАКЦИИ

Адрес: 119049, г. Москва, Ленинский проспект, д. 4

Телефон: +7 (495) 955-00-77

e-mail: send@misis.ru



Контент доступен под лицензией
Creative Commons Attribution 4.0 License.

ПЕРИОДИЧНОСТЬ 4 раза в год

ОСНОВАН в 2016 году

РЕГИСТРАЦИЯ

Зарегистрирован Федеральной службой по надзору в сфере связи, информационных технологий и массовых коммуникаций 10 августа 2015 года.

Свидетельство о регистрации Эл № ФЦ77-62652.

ИНДЕКСИРОВАНИЕ

Scopus, CAS, EBSCO, DOAJ, РИНЦ, ВИНТИ РАН, Dimensions, BASE, J-Gate, Jisc Library Hub Discover.



Журнал открытого доступа.



CONTENTS

MINERAL RESOURCES EXPLOITATION

- Variation of ore grades in the boundary zone of subeconomic ore..... 205
B.R. Rakishev, A.I. Edil'baev, A.A. Orynbay, T.S. Ibyrkhanov

GEOLOGY OF MINERAL DEPOSITS

- Statistical analysis of determining porosity factor of oil and gas reservoir rocks using gas volumetry and X-Ray tomography methods..... 221
V.I. Galkin, O.A. Melkishev, Ya. V. Savitsky
- From visual diagnostics to deep learning: automatic mineral identification in polished section images 232
D.M. Korshunov, A. V. Khvostikov, G. V. Nikolaev, D. V. Sorokin, O.I. Indychko, M.A. Boguslavsky, A.S. Krylov
- Analysis of a digital terrain model for solving geological problems by the example of Aktogai ore field 245
N. Seib, Yu. Belov, N. Zimanovskaya, G. Orazbekova, A. Tretyakova, A. Muratova, I. Kasenov
- Geological and isotopic constraints on the copper ore formation in Ta Phoi area, Lao Cai province, Northwestern Vietnam..... 262
K. T. Hung, N.X. Dac

BENEFICIATION AND PROCESSING OF NATURAL AND TECHNOGENIC RAW MATERIALS

- Application of polystyrene sulfonates for the depression of magnesium-containing silicates in copper-nickel ore flotation..... 280
A.A. Lavrinenko, G. Yu. Golberg, I.N. Kuznetsova, O. G. Lusinyan, V.A. Tverskoy

MINING MACHINERY, TRANSPORT, AND MECHANICAL ENGINEERING

- Reliability analysis of mine ventilation fans based on Markov process theory..... 289
P.V. Vyatkin, N. G. Valiev, D.I. Simisinov, E.B. Volkov

DIGITAL TECHNOLOGIES AND ARTIFICIAL INTELLIGENCE

- Digital twins and digital technologies: specific features and prospects in the coal industry 298
S.M. Nikitenko, E. V. Goosen, A.A. Rozhkov, M.K. Korolev

EXPERIENCE OF MINING PROJECT IMPLEMENTATION

- Valuation of non-producing mining companies 306
A. N. Lopatnikov, A. Y. Rummyantsev



СОДЕРЖАНИЕ

РАЗРАБОТКА МЕСТОРОЖДЕНИЙ ПОЛЕЗНЫХ ИСКОПАЕМЫХ

- Изменение содержания полезных компонентов в приконтактной зоне
некондиционных руд 205
Б. Р. Ракишев, А. И. Едильбаев, А. А. Орынбай, Т. С. Ибырханов

ГЕОЛОГИЯ МЕСТОРОЖДЕНИЙ ПОЛЕЗНЫХ ИСКОПАЕМЫХ

- Статистический анализ определения коэффициентов пористости пород-коллекторов
нефти и газа методами газовой метрии и рентгеновской томографии 221
В. И. Галкин, О. А. Мелкишев, Я. В. Савицкий

- От визуальной диагностики к глубокому обучению: автоматическое определение
минералов на фотографиях аншлифов 232
*Д. М. Коршунов, А. В. Хвостиков, Г. В. Николаев, Д. В. Сорокин, О. И. Индычко,
М. А. Богуславский, А. С. Крылов*

- Анализ цифровой модели рельефа для решения геологических задач
на примере Актогайского рудного поля 245
Н. Сайб, Ю. Белов, Н. Зимановская, Г. Оразбекова, А. Третьякова, А. Муратова, И. Касенов

- Геологические и изотопные оценки условий образования медных руд в районе Та Фой,
провинция Лао Кай, северо-западный Вьетнам 262
Х. Т. Хунг, Н. С. Дак

ОБОГАЩЕНИЕ, ПЕРЕРАБОТКА МИНЕРАЛЬНОГО И ТЕХНОГЕННОГО СЫРЬЯ

- Применение полистиролсульфонатов для депрессии магнийсодержащих силикатов
при флотации медно-никелевых руд 280
А. А. Лавриненко, Г. Ю. Гольберг, И. Н. Кузнецова, О. Г. Лусинян, В. А. Тверской

ГОРНЫЕ МАШИНЫ, ТРАНСПОРТ И МАШИНОСТРОЕНИЕ

- Исследование надежности шахтных вентиляторов
на основе теории марковских процессов 289
П. В. Вяткин, Н. Г. Валиев, Д. И. Симисинов, Е. Б. Волков

ЦИФРОВЫЕ ТЕХНОЛОГИИ И ИСКУССТВЕННЫЙ ИНТЕЛЛЕКТ

- Цифровые двойники и цифровые технологии:
особенности и перспективы в угольной отрасли 298
С. М. Никитенко, Е. В. Гоосен, А. А. Рожков, М. К. Королев

ОПЫТ РЕАЛИЗАЦИИ ПРОЕКТОВ В ГОРНОПРОМЫШЛЕННОМ СЕКТОРЕ ЭКОНОМИКИ

- Оценка горных компаний с проектами на стадии оцененных ресурсов и запасов
до этапа строительства предприятия и добычи 306
А. Н. Лопатников, А. Ю. Румянцев












MINERAL RESOURCES EXPLOITATION

Research paper

<https://doi.org/10.17073/2500-0632-2025-04-395>

UDC 622.342

**Variation of ore grades in the boundary zone of subeconomic ore****B. R. Rakishev¹  , A. I. Edil'baev²  , A. A. Orynbay^{1,3}   , T. S. Ibyrkhanov¹ **¹ Satbayev University (Kazakh National Research Technical University named after K. I. Satpayev),
Almaty, Republic of Kazakhstan² Mining Bureau LLP, Almaty, Republic of Kazakhstan³ Almaty University of Power Engineering and Telecommunications named after Gumarbek Daukeyev,
Almaty, Republic of Kazakhstan a.orynbay@aes.kz**Abstract**

Deposits of non-ferrous, precious, and rare metals are predominantly complex-structured. Such bench blocks consist of economic and subeconomic ore. The boundary between the two types is defined by a cut-off ore grade. The numerical value of the ore grade in the subeconomic portion of a block determines the thickness of material that can potentially be admixed with shipped economic ore. Controlled admixing enables complete recovery of minerals from stopes while maintaining concentrate quality. For this purpose, exploration borehole data from five copper and gold deposits in Kazakhstan with complex structures were analyzed. Based on borehole data, trend equations were derived to describe ore grade variation in the subeconomic part of a block. A software tool was developed to automate the calculation of trend lines and their equations. Using this program, new dependencies were obtained for determining the ore grade in the shipped ore (α'). For the first time in mining science, a method has been substantiated for the complete recovery of economic ore from complex-structured bench blocks, based on admixing a controlled portion of subeconomic ore. This approach increases total ore extraction and improves valuable component recovery to concentrate. The potential increase in recovered components from shipped ore may reach 10–15% of total production.

Keywords

complex-structured bench blocks, ore grade, economic ore, subeconomic ore, admixed subeconomic ore layers, trend line, complete ore recovery, Kazakhstan

Financing










This article was prepared as part of the project funded by the Ministry of Science and Higher Education of the Republic of Kazakhstan, 2023/AP19676591: Development of innovative technologies for the complete extraction of disparate conditioned ores from complex blocks of ledges.

For citation

Rakishev B. R., Edil'baev A. I., Orynbay A. A., Ibyrkhanov T. S. Variation of ore grades in the boundary zone of subeconomic ore. *Mining Science and Technology (Russia)*. 2025;10(4):205–220. <https://doi.org/10.17073/2500-0632-2025-04-395>

РАЗРАБОТКА МЕСТОРОЖДЕНИЙ ПОЛЕЗНЫХ ИСКОПАЕМЫХ

Научная статья

**Изменение содержания полезных компонентов
в приконтактной зоне некондиционных руд****Б. Р. Ракишев¹  , А. И. Едильбаев²  , А. А. Орынбай^{1,3}   , Т. С. Ибырханов¹ **¹ Казахский национальный исследовательский технический университет имени К. И. Сатпаева,
г. Алматы, Республика Казахстан² ТОО «Горное бюро», г. Алматы, Республика Казахстан³ Алматинский университет энергетики и связи имени Гумарбека Даукеева,
г. Алматы, Республика Казахстан a.orynbay@aes.kz**Аннотация**

Месторождения руд цветных, благородных и редких металлов в основном являются сложноструктурными. Эти блоки состоят из балансовых (кондиционных) и небалансовых (некондиционных) руд в формате уступов. Границы между двумя типами руд устанавливаются некоторым предельным значением полезного компонента (ПК) в руде. Численное значение содержания ПК в некондиционной



части блока предопределяет слой возможного примешивания некоторой доли забалансовых руд к отгружаемым кондиционным рудам. Примешиванием можно достигнуть полного извлечения полезных ископаемых из забоев и получения концентрата требуемого качества. В этих целях были проанализированы данные по разведочным скважинам пяти меднорудных и золоторудных месторождений Казахстана со сложно-структурным строением. По данным разведочных скважин определены уравнения трендов изменения содержания руды в некондиционной части блока. Разработана программа для автоматизации расчета линий трендов и их уравнений. С ее использованием получены новые зависимости для определения содержания ПК в отгружаемой руде α' . В горной науке впервые обоснован новый метод полного извлечения кондиционных руд из сложноструктурных блоков уступов, основанный на примешивании определенного объема некондиционных руд. Такой подход способствует увеличению общего объема извлекаемой руды и повышению выхода полезных компонентов в концентрат. Прирост извлеченных компонентов из отгружаемой руды может достигать 10–15 % от общего объема производства.

Ключевые слова

сложноструктурные блоки уступов, содержание полезных компонентов, кондиционные руды, некондиционные руды, примешиваемые слои некондиционных руд, линия тренда, полное извлечение руд, Казахстан

Финансирование

Статья подготовлена в рамках проекта, финансируемого министерством науки и высшего образования Республики Казахстан 2023/AP19676591 «Разработка инновационных технологий полного извлечения разрозненных кондиционных руд из сложноструктурных блоков уступов».

Для цитирования

Rakishev B. R., Edil'baev A. I., Orynbay A. A., Ibyrkhanov T. S. Variation of ore grades in the boundary zone of subeconomic ore. *Mining Science and Technology (Russia)*. 2025;10(4):205–220. <https://doi.org/10.17073/2500-0632-2025-04-395>

Introduction

The overwhelming majority of deposits of non-ferrous, precious, and rare metals in Kazakhstan, as well as in other parts of the world, are characterized by complex structural organization [1–3]. Such deposits display a range of distinctive features: diversity of ore body morphology, significant variability in geometric parameters, intricate spatial distribution within the host rock mass, heterogeneity in the distribution of valuable components, and pronounced contrasts in the physical and mechanical properties of host rocks [4–6]. Together, these geological factors define the complexity of deposit sections with heterogeneous structure [7, 8]. Importantly, such deposits account for 60–90% of non-ferrous metal production in the CIS, while technologically unavoidable operational ore losses may reach 20–35% of total output [6, 9, 10].

Analysis shows that the main factors contributing to increased ore losses and dilution in open-pit mining of complex-structured deposits are:

- insufficient knowledge of the geological and morphological features of structurally heterogeneous bench blocks;

- mismatch between the applied mining technologies for excavation and haulage operations and the actual geological conditions of ore occurrence, both in situ and after drilling, blasting, and extraction.

Addressing these challenges requires the development of fundamentally new methods for assessing

ore grades in boundary zones between economic and subeconomic ore. The adoption of such approaches would markedly improve the accuracy of quantitative and qualitative assessment of mined material and provide more effective control over ore losses and dilution. This line of research is highly relevant for the modern mining industry, yet a review of earlier studies shows that it has not been sufficiently addressed in the literature.

A comprehensive solution calls for a systems approach that integrates:

- advanced digital technologies and information systems;
- conventional methods for evaluating ore quality;
- reliable data on deposit geology and morphology.

Only such an integrative approach can ensure the required accuracy in assessing the quality of mined ore at every stage of deposit development.

As shown in [6, 9], the combined influence of mining-technical factors, geological structure, and mineral composition of a deposit determines not only the choice of mining method, but also ore preparation and beneficiation technologies. Ore losses and dilution, the primary negative factors reducing ore quality, largely depend on the adjustment of operational sampling methods, preliminary delineation of ore bodies, and strict compliance with boundaries during stoping operations [10]. Moreover, identi-



fying types of complex-structured bench blocks, determining the ore saturation coefficient, and quantifying the structural complexity index serve as objective criteria for evaluating recovery [11]. Analytical relationships for calculating the grade of valuable components in shipped ore (α') have also been proposed to substantiate complete extraction of ore from complex-structured bench blocks [12]. At the same time, particular attention should be given to evaluating and regulating the extraction of boundary zones, analyzing the influence of complex ore body geometries, and characterizing the morphology of these zones [13].

As previously substantiated, the most effective solution combines traditional research methods with advanced digital technologies. In recent years, computer modeling of deposit geology and the spatial distribution of ore bodies has become increasingly common in specialized studies. This is carried out using modern geological and mining information systems (GMIS), specialized software platforms for three-dimensional modeling and deposit analysis.

Of particular interest are studies in which the application of GMIS has led to the development and successful testing of innovative methods for assessing ore grades and quality parameters. For example, [5] describes the use of block modeling techniques that allow accurate determination of the spatial distribution of valuable components within ore bodies. This approach offers fundamentally new opportunities for analyzing deposit morphology and predicting ore grades. The block modeling methodology enables reliable zoning of technological ore types and grade categories within the open-pit space. Another method involves geometrical modeling of quality parameters in titanomagnetite deposits to construct wireframe models of ore bodies within closed outlines of mine workings, thereby distinguishing technological ore types [14]. Furthermore, it has been demonstrated that the delineation of geological domains with complex morphologies, together with quantitative evaluation of associated uncertainty, can be achieved through geostatistical modeling [15]. Boundary delineation methods based on these models may be used to refine and extend ore grade prediction techniques in boundary zones. Earlier research also proposed a neural-network-based method for delineating lithological differences for 3D modeling of ore bodies and host rocks, improving both the quality and speed of geological data processing at all stages of deposit development [16]. However, despite the clear advantages of modern computer models, limitations remain [17]. In particular, block models often lack precision in delineating ore

bodies and may fail to accurately distinguish between economic and subeconomic ore.

The use of GMIS extends beyond deposit and ore body modeling; it is also an integral tool for ore flow quality management and monitoring. Studies [18, 19] highlight the importance of obtaining reliable data and forecasting ore grades across different parts of mined bench blocks for effective ore flow management based on a combination of segregation and blending principles. This approach has enabled a stable feed composition and optimal ore parameters for the beneficiation of low-grade apatite–nepheline ores [18] and copper–porphyry ores [19]. It has also been shown that determining ore grades at the boundaries and beyond the delineated limits of ore bodies is a critical task influencing both the quantity and quality of shipped ore. Enhancing the efficiency of mining and processing operations requires automated integration of extraction and beneficiation cycles, supported by information systems capable of handling tasks ranging from ore grade forecasting to real-time monitoring of ore flow quality and tonnage throughout the production process [20].

The reviewed studies highlight the importance of determining ore grades in boundary zones of subeconomic ore, in shipped ore, and in addressing ore losses and dilution during extraction. At the same time, determining ore grades in boundary zones requires targeted research aimed at maximizing recovery of economic ore through the selective incorporation of subeconomic material.

Objective: To establish variations in ore grades within the boundary zones of subeconomic ore based on borehole samples from several deposits of non-ferrous, precious, and rare metals in Kazakhstan.

Tasks:

1. To identify patterns of variation in valuable component grades with increasing distance from the boundary of economic ore at the Koktas-Sharykty, Kaskyrkazgan, Yuzhny-Mointy, and Naiman-Zhal deposits.

2. To determine the thickness of the admixed subeconomic ore layer in the boundary zone that ensures the required ore grades in shipped ore.

3. To establish new regularities in ore grades in shipped ore that guarantee production of concentrate of the required quality.

By controlling the thickness of the admixed subeconomic ore layer within limits that maintain the required ore quality for delivery to the concentrator, it is possible to reduce losses and increase the overall recovery of valuable minerals. To provide a scientific and technical basis for this concept, several real deposits in Kazakhstan are examined.



The ore bodies display a wide range of morphological characteristics. Lenticular and tabular forms are most common, although irregularly shaped bodies also occur (Fig. 1). A distinctive feature is the presence of numerous swellings and pinch-outs, reflecting the complex conditions under which the ore bodies formed. The spatial position of the mineralized zones is variable – they may be located either within the porphyrite massif or in the surrounding terrigenous rocks, composed mainly of conglomerates and, to a lesser extent, sandstones.

The exposed ore bodies are relatively small, with dimensions ranging from 10×2 to 160×120 m. Their spatial distribution is marked by the clustering of closely spaced bodies into four well-defined ore zones. All of these zones share a consistent northwest orientation (300–320°), which corresponds to the strike of both the andesite porphyrite body and the enclosing Givetian–Frasnian sedimentary rocks [22].

Detailed characteristics of the ore zones

First (southernmost) ore zone: Consists of two ore bodies measuring 10×2 m and 130×5–30 m. The first body lies directly within the bed of the Sharykty River. The second has a complex morphology, branching at its southeastern end where it gradually pinches out, while on the northwestern flank it dips beneath modern unconsolidated sediments.

Second ore zone: Located 60–70 m northeast of the first. It comprises five relatively small ore bodies that form a distinct chain about 120 m long. The largest body in this zone measures 50×10 m.

Third ore zone: Situated 40–50 m northeast of the second. Here, all ore bodies occur exclusively within the andesite–porphyrite massif. The zone is characterized by a discontinuous arrangement of bodies forming a chain with a total length of 440 m. The largest body reaches 120×20 m.

Fourth ore zone: Found 90–100 m northeast of the third. It includes two ore bodies measuring 160×15 m and 60×10 m. This is the northeasternmost of all the identified mineralized zones.

1.3. The Kaskyrkazgan copper–molybdenum deposit belongs to the Kaskyrkazgan group, which also includes the Kepcham and Kenkuduk porphyry copper deposits. Deposits of the Kaskyrkazgan group are located in the central part of the Tokrau intrusive–tectonic zone, characterized by a complex structure, with mineralization concentrated in the apical portion of a granite–porphyry stock enriched in xenoliths of host rocks.

In terms of composition, the ores at these deposits are complex copper–molybdenum types, divided into oxidized and primary sulfide zones.

The oxidized ores are poorly developed, extending to depths of up to 20 m and only rarely to 45 m. The main minerals are bornite, chalcocite, limonite, hematite, malachite, azurite, chrysocolla, cuprite, goethite, and hydrogoethite. Greater importance, however, is attached to the transition zone of mixed ores.

Copper–molybdenum mineralization is of disseminated–veinlet type within a granodiorite massif, typically associated with contacts containing xenoliths of sedimentary rocks and quartz porphyrites. Copper mineralization occurs mainly in disseminated form, whereas molybdenum mineralization is largely veinlet-type. The correlation between copper and molybdenum is weak: molybdenite veinlets often cut across zones of disseminated copper mineralization and in some cases extend well beyond them.

Overall, the deposit is marked by highly complex mineralization patterns. Ore intervals are usually interbedded with barren layers, with irregular thicknesses ranging from tens of meters to mere decimeters (Fig. 2). The disseminated mineralization is generally not massive but appears pockety, producing a “checkerboard” pattern in cross-sections – even between adjacent boreholes on the same exploration line. Dissemination of ore minerals observed in one borehole may be absent in the next, even at a distance of only 20–50 m, or may shift vertically either upward or downward [23].

1.4. The Naiman-Zhal ore field formed during the Cambrian–Ordovician in an island-arc system developed on oceanic crust. The host rocks are represented by a basalt–terrigeneous–siliceous formation corresponding to the initial stage of volcanic activity in the region. This formation is genetically associated with volcanogenic massive sulfide (VMS) polymetallic deposits containing gold and silver, most prominently expressed in the Maikain ore field, which serves as a reference example of this deposit type.

The geological structure of the Naiman-Zhal deposit, covering an area of 2.0 × 0.8 km, is dominated by volcanic and volcanogenic–sedimentary (volcaniclastic) rocks of the Lower and Middle Ordovician. Terrigenous and chemical sediments play a subordinate role, while subvolcanic and intrusive complexes are distinctly minor in the stratigraphic section.

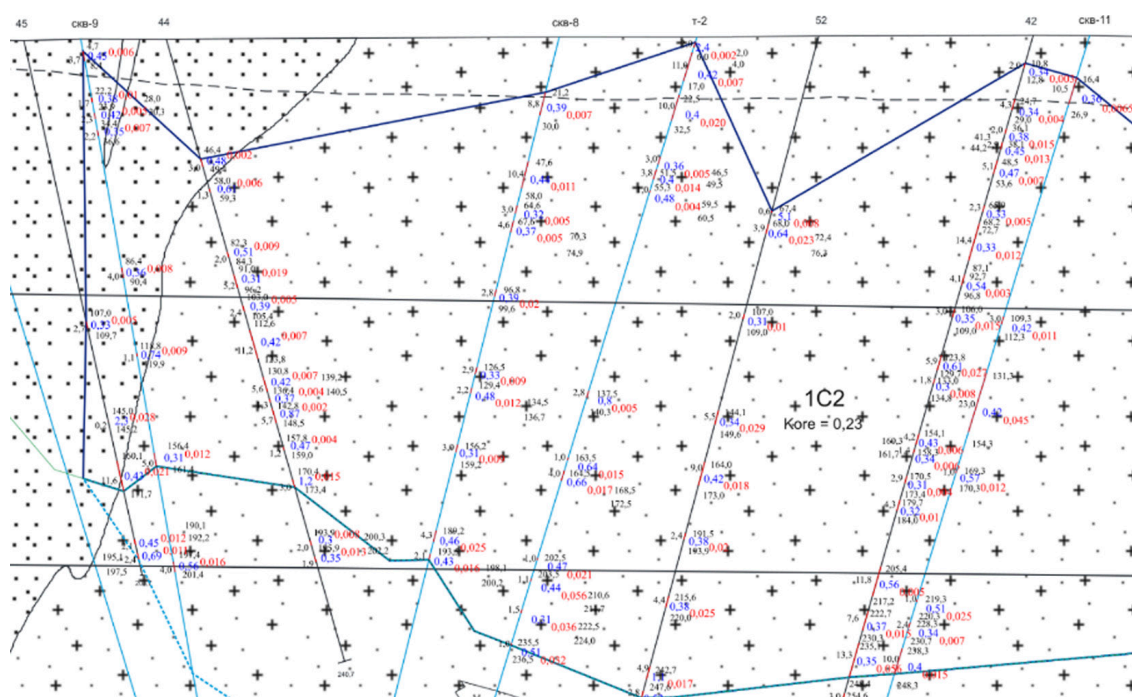
Within the Naiman-Zhal deposit, mineralized zones are distinguished, within which the ore bodies themselves are localized. These zones can be identified in surface workings and boreholes by their characteristic material composition and specific structural–textural features. However, delineating economically significant ore bodies with established

cut-off grades for gold (e.g., 0.5 g/t) requires detailed sampling (Fig. 3). The central parts of the ore bodies, enriched in gold and silver, are clearly recognizable by visual features, both in oxidized and semi-oxidized ores as well as in primary gold-bearing ores [24].

All of the examined deposits are characterized by complex structural organization. Bench blocks represent intricate combinations of ore bodies and host rocks (subeconomic ore) that differ in:

- configuration;
- size range;
- physical–technical properties;
- geological characteristics.

A distinctive feature of these deposits is the absence of visually discernible boundaries between economic and subeconomic ore, which makes their boundaries probabilistic in nature. A significant drawback is the lack of real-time information on the distribution of valuable components within different parts of a mined block. However, this problem can be addressed through integrated analysis of exploration borehole data. Applying regression analysis methods makes it possible to establish patterns in the variation of ore grades in the boundary zones of subeconomic ore, thereby significantly improving the effectiveness of exploration work.



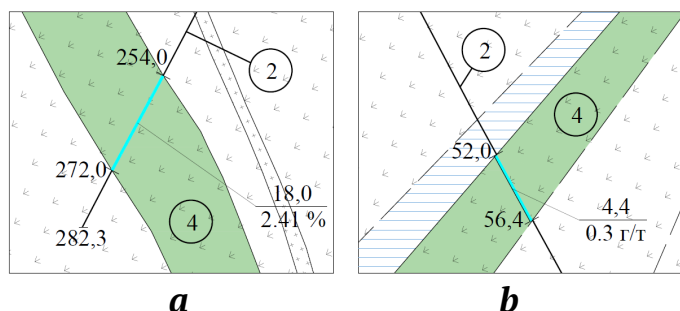


Fig. 4. Schematic representation of exploration boreholes and ore zones at the deposits: *a* – Koktas-Sharykty; *b* – Yuzhny-Mointy; 2 – exploration borehole; 4 – ore body

Table 1

Exploration borehole data from the Koktas-Sharykty (a), Kaskyrkazgan (b), and Yuzhny-Mointy (c) deposits

Deposit	Profile, station	Cu, % Au, g/t	Sample depth in borehole, m		Sample length, m
a	SP-5-155	0.0309	253	254	1
	SP-5-156	0.5738	254	255	1
	SP-5-157	3.2414	255	256	1
	SP-5-158	1.0086	256	257	1
	SP-5-159	3.1540	257	258	1
	SP-5-160	2.3665	258	259	1
	SP-5-161	3.0334	259	260	1
	SP-5-162	2.4180	260	261	1
	SP-5-163	1.5263	261	262	1
	SP-5-164	0.5374	262	263	1
	SP-5-165	0.8430	263	264	1
	SP-5-166	2.5454	264	265	1
	SP-5-167	2.8711	265	266	1
	SP-5-168	1.6061	266	267	1
	SP-5-169	1.0772	267	268	1
	SP-5-170	1.2598	268	269	1
	SP-5-171	1.4031	269	270.4	1.4
	SP-5-172	0.3113	270.4	272	1.6
	SP-5-173	0.0662	272	273	1
b	KAS 2013 72	0.155	71.4	72.4	1
	KAS 2013 73	0.309	72.4	73.4	1
	KAS 2013 74	0.766	73.4	74.4	1
	KAS 2013 75	0.248	74.4	75.4	1
	KAS 2013 76	0.027	75.4	76.4	1
c	UMP35b/55	0.09	51	52	1
	UMP35b/56	0.35	52	52.6	0.6
	UMP35b/57	0.48	52.6	53.2	0.6
	UMP35b/58	0.28	53.2	54	0.8
	UMP35b/59	0.1	54	54.8	0.8
	UMP35b/60	0.49	54.8	55.4	0.6
	UMP35b/61	0.24	55.4	56.4	1
	UMP35b/62	0.05	56.4	57.4	1

For a more detailed investigation of valuable component distribution, the following approaches are recommended:

- statistical analysis of sampling data;
- development of regression models for metal distribution;
- assessment of spatial grade variability;
- identification of patterns in ore quality variation within boundary zones.

These studies can substantially enhance the reliability of predictive estimates and support optimization of the mining process.

2. Analytical determination of ore grades in the boundary zones of subeconomic ore

This analysis is based on data from geological boreholes (Fig. 4). Exploration borehole results from the Koktas-Sharykty, Kaskyrkazgan, and Yuzhny-Mointy deposits are summarized in Table 1. These data make it possible to identify patterns of grade variation within the subeconomic portion of a bench block and to more accurately establish trend lines for valuable component distribution beyond the boundaries of economic ore.

The procedure for constructing a trend line and determining its equation involves several steps. First, select two consecutive points within the ore body with known ore grades and one point in the adjacent subeconomic ore zone with an established grade (see Fig. 4). Distances between these points are measured from core samples obtained in exploration or production boreholes. The coordinate system is then aligned so that its origin coincides with the first point of the trend line inside the ore body (Fig. 5, *a, b*). The selected points are connected by a smooth curve. The first segment of the curve (up to the economic ore boundary) reflects ore grade variation within the economic ore, while the second segment describes ore grade variation in the subeconomic portion of the block. The resulting trend line is expressed by the exponential equation:

$$y' = A \cdot e^{kx'}, \quad (1)$$

where y' is the ore grade at a given interval, A and k are coefficients to be determined, and x' is the distance from the first borehole point to the interval under consideration, m.

To determine the coefficients A and k , equation (1) is linearized by applying natural logarithms:

$$\ln y' = \ln A + kx', \quad Y' = C + kx', \quad (2)$$

where $\ln y' = Y'$, $\ln A = C$ represent the intercept terms of the linear equation.

The values of C and k are obtained using linear regression, which minimizes the sum of squared deviations between observed and estimated values:

$$E = \sum_{i=1}^n (Y'_i - (kx'_i + C))^2, \quad (3)$$

where E is the sum of squared deviations, n is the number of data points, and x'_i is the abscissa of the i -th point.

The coefficients k and C are then calculated as:

$$k = \frac{n \sum_{i=1}^n (x'_i Y'_i) - \sum_{i=1}^n x'_i \sum_{i=1}^n Y'_i}{n \sum_{i=1}^n (x'_i)^2 - \left(\sum_{i=1}^n x'_i \right)^2}, \quad (4)$$

$$C = \frac{\sum_{i=1}^n Y'_i - k \sum_{i=1}^n x'_i}{n}.$$

Once k and C are determined, coefficient A can be derived, completing the exponential dependence.

To determine the ore grade (y) in the subeconomic portion of the block, it is necessary to use the segment of the overall trend line corresponding to this zone. To isolate this segment, the origin of a new coordinate

system must be aligned with the boundary of the ore body (Fig. 5, c, d), then:

$$y = A \cdot e^{k(x+\lambda)} = A \cdot e^{k\lambda} \cdot e^{kx}, \quad y = A' \cdot e^{kx}, \quad (5)$$

where λ is the distance from the origin of the initial coordinate system to the ore body boundary, and $A' = e^{k\lambda}$ is the trend line coefficient in the subeconomic zone (Fig. 6).

Equation (5) can thus be used to compute ore grades (y) within the subeconomic ore zone. For automated calculations, a program was developed to plot the dependence of ore grade on distance within the boundary zone and determine the coefficients of the exponential equation. The program was written in C# using the Visual Studio 2022 environment (see Fig. 6). To use the program, a *.csv file containing borehole or production drill data for the area of interest (see Table 1) must be uploaded. By pressing the “Plot Data” button, the regression analysis is executed as described above. As shown in Fig. 6, two tables are produced with the trend curve coefficients for the left and right boundaries, presented both in the primary coordinate system (left) and in the transformed coordinate system (right). The graphs below display the grade variation curves for the left and right ore body boundaries in both coordinate systems.

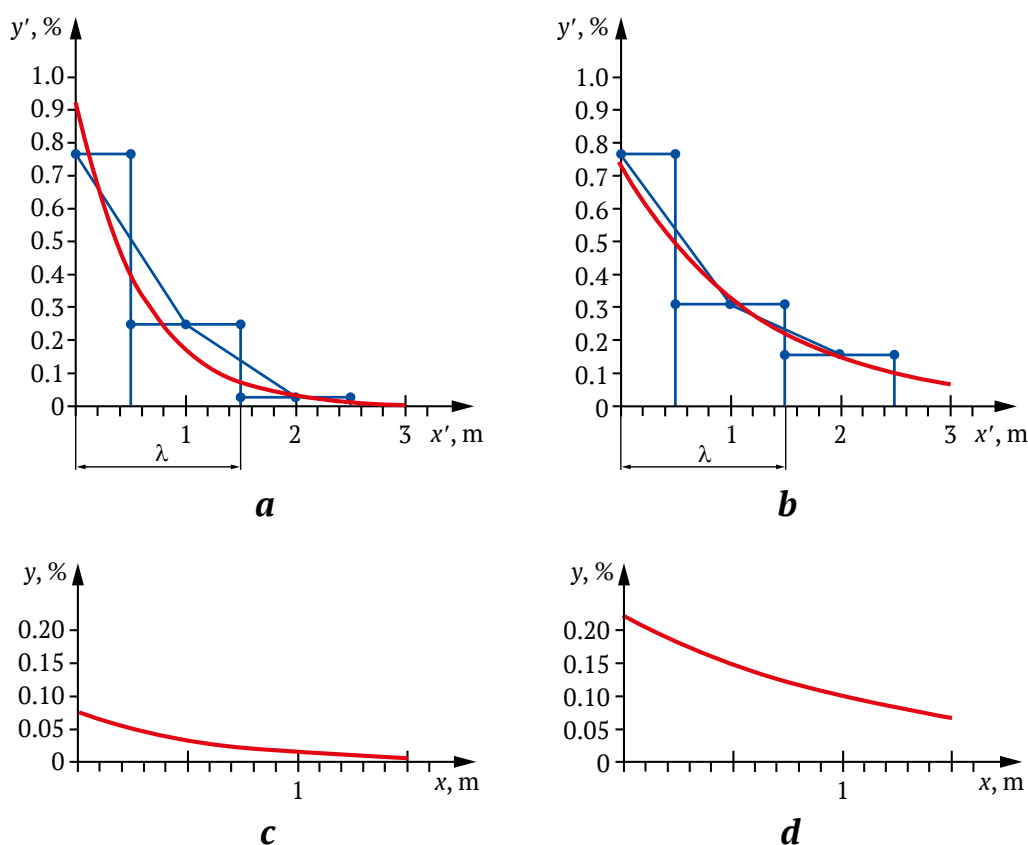


Fig. 5. General trend lines of ore grades in the boundary zones of economic and subeconomic ore based on exploration borehole KAS 2013 72–76 at the Kaskyrkazgan deposit: *a* – right boundary of the ore body; *b* – left boundary of the ore body; trend lines in the subeconomic zone: *c* – right flank; *d* – left flank

3. Technological justification for complete ore recovery from complex-structured blocks with inclusion of a subeconomic ore layer

Achieving complete ore recovery from complex-structured blocks with minimal losses and dilution requires consideration of several key beneficiation indicators:

- concentrate grade (β);
- tailings grade (δ);
- average ore grade in the feed (α);
- concentrate yield (γ_c);
- tailings yield (γ_t);
- recovery to concentrate (ε_c);
- recovery to tailings (ε_t).

These indicators are usually determined experimentally in laboratory and pilot-scale tests [25–27]. For theoretical calculations, however, mathematical relationships derived in our previous studies [25] can be applied:

$$\gamma_c = \frac{M_c}{M_o} = \frac{\alpha - \delta}{\beta - \delta}, \quad \gamma_t = \frac{M_t}{M_o} = \frac{\beta - \alpha}{\beta - \delta}, \quad (6)$$

$$\varepsilon_c = \frac{M_c \beta}{M_o \alpha} = \frac{\alpha - \delta}{\beta - \delta} \cdot \frac{\beta}{\alpha}, \quad \varepsilon_t = \frac{M_t \delta}{M_o \alpha} = \frac{\beta - \alpha}{\beta - \delta} \cdot \frac{\delta}{\alpha}.$$

Since the masses of the feed ore (M_o), concentrate (M_c), and tailings (M_t) can be measured with high

accuracy, the recoveries and beneficiation product yields can likewise be calculated precisely using the formulas given in (6).

The relationship between valuable component recovery and product yields is expressed by the following equations:

$$\varepsilon_c = \gamma_c \frac{\beta}{\alpha}, \quad \varepsilon_t = \gamma_t \frac{\delta}{\alpha}. \quad (7)$$

Principles of delineating economic ore

When tackling this problem, particular attention should be paid to the methodology for delineating the boundaries of economic ore. This procedure is based on determining the minimum cut-off grade of the valuable component in ore (α) that is both technologically and economically justified. Ore volumes with ore grades below this threshold ($< \alpha$) are classified as subeconomic and regarded as part of the host rock.

Research has shown that ore grades decrease gradually with distance from the ore body boundary. In the boundary zone of subeconomic ore directly adjacent to the economic ore, the grade corresponds to the cut-off value [12]. With increasing distance from this boundary, the average ore grade of the total mined ore mass (α') declines.

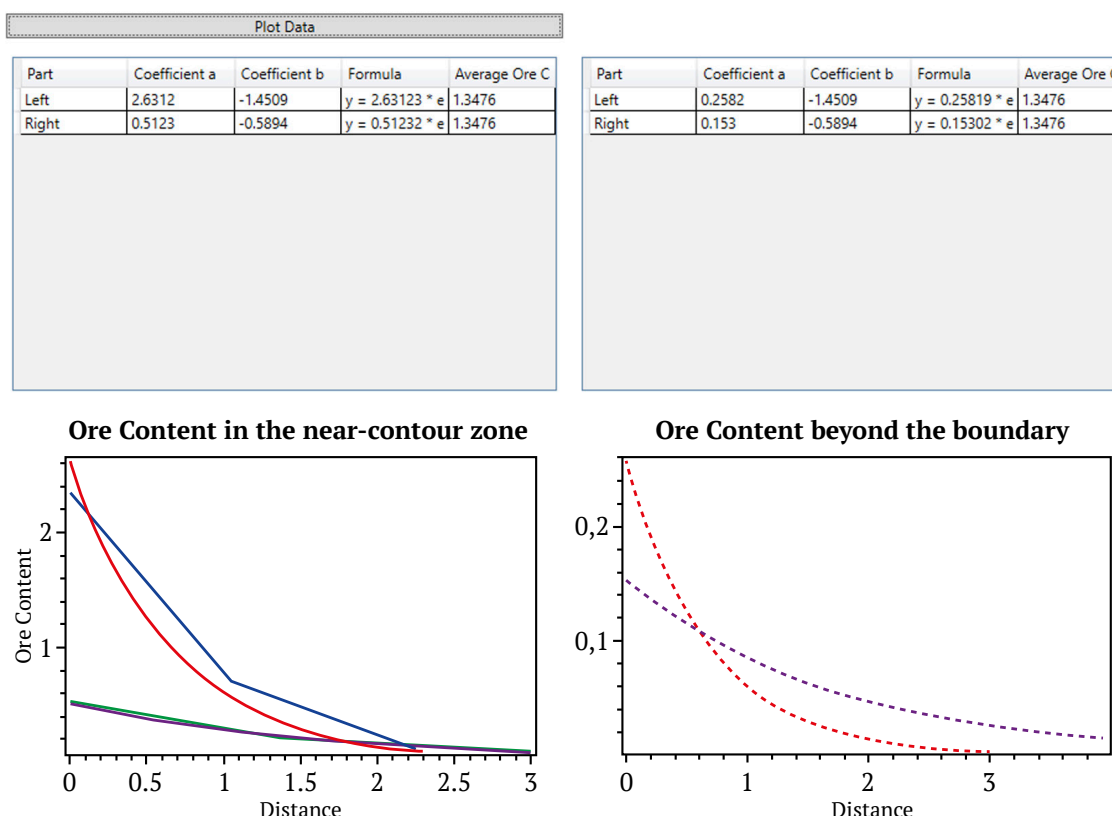


Fig. 6. Program interface for calculating ore grade equations in the boundary zone of subeconomic ore (Coefficient $a = A'$)

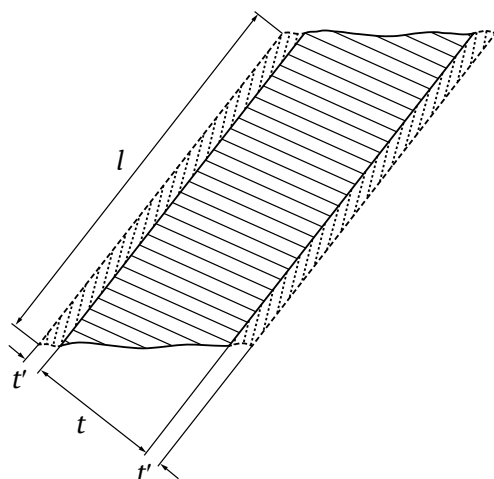




Fig. 7. Schematic for determining ore grade in the shipped ore:
 – economic ore;  – subeconomic ore

To quantify this process in two-dimensional representation (Fig. 7), the following equation is applied:

$$\alpha' = \frac{S_{eo} \cdot \alpha + S_{so} \cdot \alpha''}{S_{eo} + S_{so}}, \quad (8)$$

where S_{eo} is the area of economic ore, m^2 ; S_{so} is the area of the admixed subeconomic ore layer, m^2 , and α'' is the ore grade in the admixed subeconomic ore.

These mathematical relationships make it possible to:

- delineate economic ore bodies more precisely;
- calculate optimal mining parameters;
- design algorithms that minimize ore losses;
- reduce ore dilution;
- substantiate the economic feasibility of extracting boundary zones.

This methodology is especially relevant for complex-structured deposits with indistinct ore body

boundaries, where conventional delineation approaches often prove inadequate.

To calculate the grade $\alpha'' = y$ in the admixed layer of subeconomic ore, equation (5) is applied, giving:

$$\alpha'' = \frac{1}{t'} \int_0^{t'} y(x) dx = \frac{1}{t'} \int_0^{t'} A' e^{kx} dx = \frac{A'}{kt'} (e^{kt'} - 1), \quad (9)$$

where t' is the thickness of the admixed subeconomic ore layer. The calculated values of α'' are presented in Tables 2 and 3.

To determine the ore grade in the shipped ore, the following algorithm is applied:

1. Define the complex-structured bench block under investigation.

2. Compile ore grade data for the boundary zones of economic and subeconomic ore based on samples from exploration or production boreholes.

3. Input the boundary zone grade data into the developed software, which calculates the coefficients A' , k for the exponential dependence (5) describing grade variation in subeconomic ore.

4. Using the calculated coefficients, determine the ore grade in the admixed subeconomic ore layer according to dependence (9).

5. Substitute the calculated α'' value into equation (8) to obtain the ore grade of the total shipped ore.

For practical verification of the proposed algorithm, three scenarios of integrated ore extraction were examined in detail. Each scenario involved combined mining of economic ore with adjoining layers of subeconomic mineralization within complex-structured blocks. The ore bodies considered varied substantially in thickness, from 4 to 30 m, which allowed assessment of the algorithm's performance under diverse geological conditions.

Table 2

Data for the Kaskyrkazgan copper deposit (a) and the Koktas-Sharykty area (b)

Deposit	Ore body No.	Average ore grade in the ore body, α , %	Ore body thickness, m	A'	k	Ore grade, α'' , in the boundary layer of subeconomic ore, m		
						0–0.3	0–0.7	0–1.0
a	1	0.30	13.7	0.10	–1.15	0.085	0.069	0.059
	2	0.33	9.8	0.19	–0.74	0.170	0.148	0.134
	3	0.35	6.5	0.23	–0.32	0.219	0.206	0.197
	4	0.39	6.8	0.20	–0.65	0.182	0.161	0.147
	5	0.43	6	0.19	–1.00	0.164	0.137	0.120
b	1	0.30	16.5	0.13	–0.50	0.121	0.110	0.102
	2	0.38	13.5	0.11	–0.46	0.103	0.094	0.088
	3	0.53	6	0.18	–1.94	0.136	0.098	0.079
	4	0.74	13	0.21	–0.78	0.187	0.162	0.146
	5	0.97	8.37	0.15	–1.34	0.124	0.097	0.083



Study parameters for copper ores:

Scenario 1: admixed subeconomic ore layer thickness (t') = 0.3 m; the ore grade in the admixed layer (α'') varied within the range 0.008–0.02.

Scenario 2: $t' = 0.7$ m; $\alpha'' = 0.034$ –0.101.

Scenario 3: $t' = 1.0$ m; $\alpha'' = 0.059$ –0.197.

Study parameters for gold-bearing ores:

Scenario 1: $t' = 0.3$ m; $\alpha'' = 0.008$ –0.028.

Scenario 2: $t' = 0.7$ m; $\alpha'' = 0.033$ –0.13.

Scenario 3: $t' = 1.0$ m; $\alpha'' = 0.054$ –0.236.

Ore quality and beneficiation product characteristics:

Feed ore grades: copper ores $\alpha_{Cu} = 0.3$ –1.0%; gold-bearing ores $\alpha_{Au} = 0.00005$ –0.0002% (0.5–2.0 g/t).

Concentrate grades: copper concentrate $\beta_{Cu} = 20.0\%$; gold-bearing concentrate $\beta_{Au} = 0.04\%$ (40.0 g/t).

Tailings grades: copper ores $\delta_{Cu} = 0.06\%$; gold-bearing ores $\delta_{Au} = 0.00001\%$ (0.1 g/t).

Experimental results

The calculated ore grades in the shipped ore and their recoveries to concentrates for copper and gold-bearing ores are summarized in Tables 4 and 5, respectively. Relative deviations of these indicators are analyzed in Tables 6 and 7, providing an assessment of the algorithm's stability under different initial conditions.

Table 3

Data for the Yuzhny-Mointy gold-bearing area (a) and the Naimanjal deposit (b)

Deposit	Ore body No.	Average ore grade in the ore body, α , %	Ore body thickness, m	A'	k	Ore grade, α'' , in the boundary layer of subeconomic ore, m		
						0–0.3	0–0.7	0–1.0
a	1	0.30	6.4	0.15	–1.25	0.125	0.100	0.086
	2	0.35	16.2	0.12	–1.87	0.092	0.067	0.054
	3	0.43	5.1	0.13	–1.39	0.106	0.083	0.070
	4	0.48	6.5	0.12	–1.06	0.103	0.085	0.074
	5	0.65	10.9	0.36	–0.91	0.315	0.266	0.236
b	1	0.31	9.9	0.10	–0.45	0.094	0.086	0.081
	2	0.47	4	0.18	–2.19	0.132	0.092	0.073
	3	0.67	12	0.20	–0.84	0.177	0.151	0.135
	4	0.76	30	0.20	–0.80	0.178	0.153	0.138
	5	1.00	6	0.30	–1.25	0.250	0.200	0.171

Table 4

Ore grades in shipped ore and their recovery to concentrate at different thicknesses of admixed subeconomic ore layers in the Kaskyrkazgan deposit (a) and the Koktas-Sharykty area (b)

Deposit	Scenarios							
	Initial		I		II		III	
	α	ϵ_c	α'	ϵ_c	α'	ϵ_c	α'	ϵ_c
a	0.30	80.24	0.291	79.62	0.279	78.72	0.270	78.03
	0.33	82.06	0.321	81.54	0.307	80.72	0.297	80.04
	0.35	83.11	0.339	82.54	0.324	81.72	0.314	81.12
	0.39	84.87	0.373	84.16	0.351	83.14	0.334	82.29
	0.43	86.31	0.406	85.47	0.375	84.27	0.355	83.34
b	0.30	80.24	0.294	79.80	0.285	79.18	0.278	78.67
	0.33	84.46	0.368	83.96	0.353	83.26	0.343	82.74
	0.35	88.95	0.493	88.10	0.447	86.83	0.415	85.79
	0.39	92.17	0.716	91.89	0.684	91.50	0.661	91.20
	0.43	94.10	0.913	93.71	0.844	93.17	0.798	92.76



The findings demonstrate the effectiveness of the proposed approach to mining complex-structured ore blocks, ensuring:

- higher recovery of valuable minerals;
- controlled incorporation of subeconomic ore into production;
- opportunities for optimizing process parameters;

- reduction of valuable component losses;
- reduced dilution of the mined ore mass.

The validation results confirm the versatility of the developed algorithm across different ore types and a wide range of geological conditions.

As shown by the data in Tables 4 and 5, there is a clear dependence of the ore grade in the shipped ore mass on two key factors. First, there is a direct

Table 5

Ore grades in shipped ore and their recovery to concentrate at different thicknesses of admixed subeconomic ore layers in the Yuzhny-Mointy area (a) and the Naimanjal deposit (b)

Deposit	Scenarios							
	Initial		I		II		III	
	α	ϵ_c	α'	ϵ_c	α'	ϵ_c	α'	ϵ_c
a	0.3	80.24	0.285	79.15	0.263	77.45	0.248	76.02
	0.35	83.11	0.341	82.63	0.327	81.92	0.317	81.33
	0.43	86.31	0.396	85.11	0.356	83.39	0.329	82.03
	0.48	87.76	0.448	86.88	0.410	85.63	0.385	84.67
	0.65	91.04	0.633	90.80	0.610	90.44	0.593	90.14
b	0.31	80.89	0.298	80.08	0.278	78.66	0.266	77.65
	0.47	87.50	0.426	86.17	0.359	83.54	0.324	81.74
	0.67	91.32	0.646	90.99	0.610	90.43	0.586	90.03
	0.76	92.38	0.749	92.26	0.731	92.07	0.719	91.93
	1	94.28	0.931	93.84	0.824	93.00	0.765	9.43

Table 6

Relative deviations of the studied indicators from the required values at different thicknesses of admixed subeconomic ore layers in the Kaskyrkazgan deposit (a) and the Koktas-Sharykty area (b)

Deposit	I		II		III	
	$\Delta\alpha'$	$\Delta\epsilon_c$	$\Delta\alpha'$	$\Delta\epsilon_c$	$\Delta\alpha'$	$\Delta\epsilon_c$
a	3.02	0.78	7.05	1.90	9.94	2.76
	2.77	0.63	6.88	1.64	10.00	2.47
	3.21	0.69	7.44	1.66	10.35	2.39
	4.38	0.83	10.07	2.04	14.32	3.04
	5.64	0.97	12.68	2.35	17.50	3.44
b	2.14	0.55	5.01	1.32	7.24	1.95
	3.06	0.59	7.05	1.42	9.81	2.04
	6.91	0.95	15.70	2.38	21.75	3.55
	3.31	0.30	7.58	0.72	10.67	1.05
	5.89	0.41	13.04	0.99	17.74	1.42

Table 7

Relative deviations of the studied indicators from the required values at different thicknesses of admixed subeconomic ore layers in the Yuzhny-Mointy area (a) and the Naimanjal deposit (b)

Deposit	I		II		III	
	$\Delta\alpha'$	$\Delta\epsilon_c$	$\Delta\alpha'$	$\Delta\epsilon_c$	$\Delta\alpha'$	$\Delta\epsilon_c$
a	5.14	1.36	12.21	3.48	17.38	5.26
	2.68	0.57	6.44	1.42	9.34	2.13
	7.89	1.39	17.23	3.38	23.38	4.95
	6.59	1.01	14.53	2.43	19.76	3.52
	2.56	0.27	6.15	0.67	8.84	0.99
b	4.00	1.00	10.28	2.75	14.29	4.00
	9.39	1.52	23.59	4.52	31.00	6.57
	3.52	0.36	8.99	0.97	12.57	1.41
	1.49	0.13	3.79	0.34	5.37	0.49
	6.91	0.47	17.59	1.36	23.50	1.96



correlation between the ore grade in economic ore and its concentration in the shipped material. Second, an inverse relationship is observed with respect to the distance from the ore body boundary: as the distance from the boundary of economic mineralization increases, the ore grade consistently decreases. This relationship is equally characteristic of both copper and gold-bearing ores, and it is evident in all the extraction scenarios considered. It is noteworthy that a similar trend, though somewhat less pronounced, is also observed in the recovery of copper and gold to concentrate. In this case, however, the amplitude of variations is much smaller, indicating the relatively stable nature of the beneficiation process.

For a more detailed assessment of how these changes affect the final technological outcome – namely, the recovery of the valuable component to concentrate – a comparative analysis of deviations across all three scenarios is required. Such an approach makes it possible to:

- determine the sensitivity of the technological process to variations in the initial ore grade;
- assess the influence of distance from the ore body boundary on beneficiation efficiency;
- define mining parameters for each ore type;
- evaluate the stability of processing equipment performance under changing conditions;
- develop corrective measures to minimize the negative effects of the identified factors.

According to the data presented in Tables 6 and 7, clear patterns can be observed in the variation of ore grades in shipped ore.

For copper ores, the maximum relative deviation does not exceed 6% in Scenario I, increases to 16% in Scenario II, and reaches 22% in Scenario III.

For gold-bearing ores, the maximum deviation is 10% in Scenario I, rises to 24% in Scenario II, and reaches 31% in Scenario III.

Analysis of valuable component recovery to concentrate reveals a clear trend.

For copper ores, deviations range from 0.3 to 0.97% in Scenario I, from 0.72 to 2.38% in Scenario II, and from 1.05 to 3.55% in Scenario III.

For gold-bearing ores, deviations range from 0.13 to 1.52% in Scenario I, from 0.34 to 4.52% in Scenario II, and from 0.49 to 6.57% in Scenario III.

All observed deviations in recovery remain within technologically acceptable limits, confirming the effectiveness of the proposed method.

The application of new technological solutions for recovering economic ore from complex-structured blocks with partial inclusion of subeconomic ore makes it possible to:

- ensure the required quality of shipped ore mass;
- significantly increase the volume of extracted raw material;
- enhance the overall efficiency of deposit exploitation.

The implementation of this new technology for mining complex-structured blocks results in the following:

- a portion of subeconomic ore previously considered as diluting waste is reclassified as recoverable reserves;
- the volume of extracted ore mass increases substantially;
- the percentage recovery of valuable components to the final concentrate improves.

4. Economic impact

Under actual production conditions at a copper open-pit mine with an annual ore output of 6–7 Mt, an average copper grade of 0.45%, and complex-structured blocks accounting for 50–60% of the total, the additional recovery of valuable components may reach 10–15% of overall production.

Thus, the proposed technology delivers a significant technological and economic impact while maintaining the required quality of the mined ore mass.

Conclusion

1. Based on analysis of exploration borehole data from five copper and gold-bearing ore deposits in Kazakhstan (Kaskyrkazgan, Koktas-Sharykty, Yuzhny-Mointy, Naiman-Zhal, and others), regularities in the variation of ore grades in the boundary zones of subeconomic ore have been established. It was determined that these grades follow an exponential relationship of the form $y = A' \cdot e^{kx}$ with parameters varying as follows: for copper ores, $A' = 0.10\text{--}0.23$, $k = -0.32\text{--}1.94$, for gold-bearing ores, $A' = 0.10\text{--}0.36$, $k = -0.45\text{--}2.19$.

2. An automated software tool was developed in C# within the Visual Studio 2022 environment to calculate exponential trend equations, determine coefficients A' and k , and forecast ore grades in the admixed subeconomic ore layer.

3. Using this software, calculations were performed to determine grades in the shipped ore (α') when admixing subeconomic ore layers of varying thickness ($t' = 0.3, 0.7, \text{ and } 1.0 \text{ m}$). It was shown that for copper ores, α' varied from 0.406 to 0.270%, with recovery to concentrate ε_c decreasing from 94.10 to 78.03%; for gold-bearing ores, α' varied from 0.931 to 0.248 r/r, with recovery to concentrate ε_c decreasing from 94.28 to 76.02%.



4. In the first case of admixing a 0.3 m subeconomic ore layer, relative deviations in ore grade of shipped ore were 2.14–6.91% for copper ores and 1.49–9.39% for gold-bearing ores. The corresponding deviations in recovery to concentrate were 0.3–0.97% for copper and 0.13–1.52% for gold, all within acceptable technological limits.

5. The proposed approach for complete recovery of economic ore through controlled admixing of boundary subeconomic material ensures the required quality of shipped ore while increasing extractable reserves. This has been confirmed by calculations for admixed layers of varying thickness.

6. For the first time in mining science, the theoretical feasibility of reclassifying part of the diluting

subeconomic ore into recoverable reserves has been substantiated. This leads to an increase in shipped ore tonnage and recovery of valuable components to concentrate without compromising concentrate quality.

The results obtained are of considerable practical significance. In the case of an open-pit mine with an annual ore production of 6–7 Mt, an average copper grade of 0.45%, and complex-structured blocks accounting for 50–60% of total production, additional copper recovery may reach 10–15% of overall output. In monetary terms, this corresponds to an additional annual profit of approximately USD 15.3 million, assuming a market copper price of USD 8,500 per ton.

References

1. Shabarov A.N., Kuranov A.D. Basic development trends in mining sector in complicating geotechnical conditions. *Gornyi Zhurnal*. 2023;(5):5–10. <https://doi.org/10.17580/gzh.2023.05.01>
2. Trubetskoy K.N., Peshkov A.A., Matsko N.A. Determination of application scope for steeply dipping deposit mining methods using pre-formed worked-out space. *Gornyi Zhurnal*. 1994;(1):51–59. (In Russ.)
3. Trushko V.L., Protosenya A.G. Prospects of geomechanics development in the context of new technological paradigm. *Journal of Mining Institute*. 2019;236:162–166. <https://doi.org/10.31897/pmi.2019.2.162>
4. Yakovlev V.L., Kornilov S.V., Sokolov I.V. *Innovative basis for the strategy of integrated mineral resource development*. Ed. by corresponding member of RAS V. L. Yakovlev. Yekaterinburg: Ural Branch of RAS; 2018. 360 p. (In Russ.)
5. Kantemirov V., Iakovlev A., Titov R. Applying geoinformation technologies of block modelling to improve the methods of assessing quality indicators of minerals. *Gornyi Zhurnal*. 2021;(1):63–73. (In Russ.)
6. Cheban A., Sekisov G. Complex structural ore blocks and their systematization. *Transbaikal State University Journal*. 2020;26(6):43–53. (In Russ.) <https://doi.org/10.21209/2227-9245-2020-26-6-43-53>
7. Boyarko G. Yu., Bolsunovskaya L.M. Mineral resource base of Russia's cobalt: current state and development prospects. *Mining Science and Technology (Russia)*. 2025;10(2):118–147. <https://doi.org/10.17073/2500-0632-2025-02-368>
8. Kirsanov A.K. Chinese mining industry: state of the art review. *Mining Science and Technology (Russia)*. 2023;8(2):115–127. <https://doi.org/10.17073/2500-0632-2022-11-35>
9. Lobyntsev A.K., Fomin S.I. Assessment of the influence of mining factors degree on the standard of prepared reserves when designing open-pit mining of complexstructure ore deposits. *Ratsionalnoe Osvoenie Nedr*. 2021;(5):40–43. (In Russ.)
10. Kushnarev P.I. Hidden losses and ore dilution. *Zoloto i Tekhnologii*. 2017;(3):82–87. (In Russ.)
11. Rakishev B.R. Mining and geological models of virtual complex ore blocks of the bench. *Naukovyi Visnyk Natsionalnoho Hirnychoho Universytetu*. 2023;(4):11–17. <https://doi.org/10.33271/nvngu/2023-4/011>
12. Rakishev B.R. Complete extraction of conditioned ores from complex-structured blocks due to partial admixture of substandard ores. *Journal of Mining Institute*. 2024;270:919–930.
13. Nurzhumin E.K., Toleubekova Ja.Z., Kamarov R.K., et al. Mining in marginal areas of complicated-structure ore bodies and the ore body structure complexity evaluation. *Interexpo GEO-Siberia*. 2014;2(4):23–30. (In Russ.)



14. Yakovlev I.M. Planning of mining operations in the quality management mode based on geoinformation modeling. *Mining Informational and Analytical Bulletin*. 2021;(5–1):258–268. (In Russ.) https://doi.org/10.25018/0236_1493_2021_51_0_258
15. Veliz V., Maleki M., Madani N. et al. Plurigaussian modeling of non-stationary geological domains to assess geological uncertainty in a porphyry copper deposit. *Ore Geology Reviews*. 2023;162:105707. <https://doi.org/10.1016/j.oregeorev.2023.105707>
16. Melnichenko I.A., Kirichenko Yu.V. Spatial zoning of mineral deposits. *Mining Informational and Analytical Bulletin*. 2021;(4):46–56. (In Russ.) https://doi.org/10.25018/0236_1493_2021_4_0_46
17. Kantemirov V.D., Yakovlev A.M., Titov R.S., Timokhin A.V. Improvement of mineral processing methods in mining structurally-complex deposits. *Mining Industry Journal*. 2022;(1S):63–70. (In Russ.) <https://doi.org/10.30686/1609-9192-2022-1s-63-70>
18. Pavlishina D.N., Tereshchenko S.V. Analysis of systems of quality management of low-grade apatite-nepheline ores during their processing. *Vestnik of MSTU*. 2014;17(2):254–258. (In Russ.)
19. Maleki M., Mery N., Soltani-Mohammadi S., et al. Geological Control for in-situ and recoverable resources assessment: a case study on Sarcheshmeh Porphyry Copper Deposit, Iran. *Ore Geology Reviews*. 2022;150:105133. <https://doi.org/10.1016/j.oregeorev.2022.105133>
20. Kaplunov D.R., Ryl'nikov A.G. Generalization of modern approaches to quality management technology at operating mines. *Izvestiya Tulkogo Gosudarstvennogo Universiteta. Nauki o Zemle*. 2020;(4):40–53. (In Russ.)
21. Glukhov A.M., et al. *Report on gold exploration works at the Yuzhno-Moyuntinskaya area in Karaganda Region (2015–2016)*. Sheets L-43-40-A, B. Karaganda: Tsentrkaznedra; 2016. 350 p. (In Russ.)
22. Katsyuba E.A., et al. *Report on exploration and evaluation works for copper, gold, and associated components at the Koktas-Sharyktinskaya area within the Spasskaya Copper Ore Zone (2014–2015)*. Karaganda: Tsentrkaznedra; 2015. 154 p. (In Russ.)
23. Nitsenko P.A., et al. *Report on exploration and evaluation works at the Kaskyrkazgan Site in Karaganda Region with calculation of copper and molybdenum reserves under C2 category as of 01.10.2014*. Karaganda: Tsentrkaznedra; 2014. 144 p. (In Russ.)
24. Danilov V.I., et al. *Multi-variant reserve estimation and technical-economic substantiation of cut-off grades for ores of the Naimanjal Deposit*. Almaty: Tsentrkaznedra; 2007. 135 p. (In Russ.)
25. Rakishev B.R. Technological resources for improving the quality and completeness of use of the mineral raw materials. *News of the National Academy of Sciences of the Republic of Kazakhstan, Series of Geology and Technical Sciences*. 2017;2(422):116–124.
26. Pelikh V.V., Salov V.M., Burdonov A.E., Lukyanov N.D. Model of baddeleyite recovery from dump products of an apatite-baddeleyite processing plant using a CVD6 concentrator. *Journal of Mining Institute*. 2021;248:281–289. <https://doi.org/10.31897/PMI.2021.2.12>
27. Mutalova M.A., Khakimova D.Yu. Investigation of the recovery of useful components from slags by the flotation method. *International Journal of Advanced Technology and Natural Sciences*. 2020;1(2):26–30. (In Russ.)

Information about the authors

Bayan R. Rakishev – Academician of the National Academy of Sciences of the Republic of Kazakhstan, Dr. Sci. (Eng.), Professor at the Department of Mining Engineering, Satbayev University (Kazakh National Research Technical University named after K.I. Satpayev), Almaty, Republic of Kazakhstan; ORCID [0000-0001-5445-070X](https://orcid.org/0000-0001-5445-070X), Scopus ID [6603178936](https://orcid.org/6603178936); e-mail b.rakishev@mail.ru

Abdraman I. Edil'baev – Dr. Sci. (Eng.), General Director, Mining Bureau LLP, Almaty, Republic of Kazakhstan; ORCID [0000-0001-8498-7049](https://orcid.org/0000-0001-8498-7049), Scopus ID [23396734100](https://orcid.org/23396734100); e-mail byedilbayev@gmail.com

Asfandyar A. Orynbay – PhD (Mining Eng.), Associate Professor of the Department of Electronic Engineering, Almaty University of Power Engineering and Telecommunications named after Gumarbek Daukeyev, Almaty, Republic of Kazakhstan; Senior Research of the Department of Mining Engineering, Satbayev University (Kazakh National Research Technical University named



after K.I. Satpayev), Almaty, Republic of Kazakhstan; ORCID [0000-0002-3720-7625](https://orcid.org/0000-0002-3720-7625), Scopus ID [57204864631](https://scopus.org/57204864631); e-mail a.orynbay@au.es.kz

Temirlan S. Ibyrkhanov – PhD-Candidate of the Department of Mining Engineering, Satbayev University (Kazakh National Research Technical University named after K.I. Satpayev), Almaty, Republic of Kazakhstan; ORCID [0009-0001-6344-8270](https://orcid.org/0009-0001-6344-8270); e-mail ibir.tem@mail.ru

Received 21.04.2025

Revised 24.06.2025

Accepted 27.06.2025



GEOLOGY OF MINERAL DEPOSITS

Research paper

<https://doi.org/10.17073/2500-0632-2024-08-299>

UDC 550.837:553.98

**Statistical analysis of determining porosity factor of oil and gas reservoir rocks using gas volumetry and X-Ray tomography methods**V. I. Galkin  , O. A. Melkishev  , Ya. V. Savitsky   

Perm National Research Polytechnic University, Perm, Russian Federation

 yansavitsky@yandex.ru**Abstract**

To address the current challenges in oil industry related to modeling a pore space structure in a 3D core model and evaluating permeability and porosity ("Digital Core"), it is necessary to obtain representative characteristics of the void space. A similar characteristic is required to solve geotechnical problems related to modeling and evaluating the strength properties of heterogeneous rocks. In addition, it is also important for research on capillary processes in porous media. The paper is devoted to the comparative analysis of the values of porosity of oil and gas reservoir rocks obtained by gas volumetry and X-ray computer tomography methods. The aim of this work is to develop statistical models for assessing the discrepancy between the porosity factor K_p , determined using computer tomography (CT) data and more reliable laboratory petrophysical data for two lithological rock types: terrigenous and carbonate. The research objectives include: assessing the impact of lithology on the K_p evaluation using various methods (petrophysics and CT); examining and evaluating the impact of the reservoir rocks porosity factor range on the convergence of the results from these two methods for different lithological rock types; building statistical models to adjust the K_p values based on CT results for different lithological rock types. The solution to these problems is based on a detailed statistical analysis of the studies of terrigenous and carbonates rocks in oil fields in the Perm region. Porosity measurement was carried out on a AP-608 automated porosimeter-permeameter and a Nikon XT H 225 X-ray tomography system. The techniques for measuring the volume of pores in samples using the gas volumetry method, image binarization, and porosity calculation using the X-ray tomography method are described. The results of the analysis showed that the studied methods give different values of porosity factors depending on the lithology. For carbonate rocks, a greater correspondence of the porosity factor estimates obtained by different methods is characteristic that is due to the structural features of the pore space. Significant differences were found for terrigenous rocks, which are explained by the limited resolution of X-ray tomography. The analysis resulted in statistical models for evaluating and correcting K_p data obtained by X-ray tomography for terrigenous and carbonate rocks in various K_p value ranges. The results of the study can be used for petrophysical substantiation of the permeability and porosity of reservoir rocks in oil and gas fields.

Keywords

porosity, core, terrigenous reservoirs, carbonate reservoirs, petrophysics, X-ray tomography, gas volumetry, statistical analysis

For citation


Galkin V. I., Melkishev O. A., Savitsky Ya. V. Statistical Analysis of determining porosity factor of oil and gas reservoir rocks using gas volumetry and X-Ray tomography methods. *Mining Science and Technology (Russia)*. 2025;10(3):221–231. <https://doi.org/10.17073/2500-0632-2024-08-299>

ГЕОЛОГИЯ МЕСТОРОЖДЕНИЙ ПОЛЕЗНЫХ ИСКОПАЕМЫХ

Научная статья

Статистический анализ определения коэффициентов пористости пород-коллекторов нефти и газа методами газоволюметрии и рентгеновской томографииВ. И. Галкин  , О. А. Мелкишев  , Я. В. Савицкий   

Пермский национальный исследовательский политехнический университет, г. Пермь, Российская Федерация

 yansavitsky@yandex.ru**Аннотация**

Для решения актуальных задач в нефтяной отрасли, связанных с моделированием структуры порового пространства в 3D-модели керна и оценкой фильтрационно-емкостных свойств («Цифровой керн»), необходимо получение представительной характеристики пустотного пространства.



Аналогичная характеристика требуется для решения задач геомеханики, связанных с моделированием и оценкой прочностных свойств неоднородных горных пород. Кроме того, она важна для исследований капиллярных процессов в пористых средах. Статья посвящена сравнительному анализу значений пористости пород-коллекторов нефти и газа, полученных методами газовойolumетрии и рентгеновской компьютерной томографии. Целью работы является разработка статистических моделей для оценки расхождения определения коэффициента пористости K_p по данным компьютерной томографии (КТ) с более достоверными данными лабораторной петрофизики для двух литологических типов пород – терригенных и карбонатных. Задачи исследования включают: оценку влияния литологического состава пород на оценку K_p разными методами (петрофизика и КТ); рассмотрение и оценку влияния диапазона варьирования пористости пород коллекторов на сходимость результатов этих двух методов для разных литологических типов пород; построение статистических моделей для корректировки значений K_p по результатам КТ для разных литологических типов пород. Решение данных задач основывается на проведении детального статистического анализа исследований терригенных и карбонатных пород нефтяных месторождений Пермского края. Измерение пористости проводилось на автоматизированном порозиметре-пермеамetre AP-608 и системе рентгеновской томографии Nikon XT H 225. Описаны методики измерения объемов пор образцов газовойolumетрическим методом, бинаризации изображений и расчета пористости по методу рентгеновской томографии. Результаты анализа показали, что изучаемые методы дают различающиеся значения коэффициентов пористости в зависимости от литологического состава пород. Для карбонатных пород характерно большее соответствие оценки коэффициента пористости, полученных различными методами, что обусловлено структурными особенностями порового пространства. В терригенных породах установлены значительные различия, объясняемые ограниченной разрешающей способностью рентгеновской томографии. По итогам анализа получены статистические модели для оценки и корректировки данных K_p , полученных методом рентгеновской томографии для терригенных и карбонатных пород в различных диапазонах значений K_p . Результаты исследования могут быть использованы при петрофизическом обосновании фильтрационно-емкостных свойств пород-коллекторов месторождений нефти и газа.

Ключевые слова

пористость, керн, терригенные коллекторы, карбонатные коллекторы, петрофизика, рентгеновская томография, газовойolumетрия, статистический анализ

Для цитирования

Galkin V.I., Melkishev O.A., Savitsky Ya.V. Statistical Analysis of determining porosity factor of oil and gas reservoir rocks using gas volumetry and X-Ray tomography methods. *Mining Science and Technology (Russia)*. 2025;10(3):221–231. <https://doi.org/10.17073/2500-0632-2024-08-299>

Introduction

One of the most important characteristics that allow for the estimation of reserves and are taken into account in the prospecting, exploration, and development of oil and gas fields is porosity factor K_p . Despite the existence of the problem of scaling physical characteristics between a reservoir and individual samples [1, 2], the most accessible and reliable methods of studying are direct laboratory petrophysical testing of core samples, among which the estimation of a porosity factor is one of the most accurate and reliable.

Over the past two decades, a significant number of publications with the results of tomographic studies of a core have appeared. The works of foreign and domestic researchers provide data for samples of various sizes and lithology. Thus, the works [3, 4] are devoted to reviewing the capabilities of the method in a number of types of geological research, including the study of carbonate reservoir rocks. The papers [5, 6] are devoted to the study of marine sediment cores. Although statistical analysis of the porosity of terrigenous and carbonate sediments is

carried out in [6], unfortunately, it only applies to full-size samples, which were the subject of the study. The papers [7, 8] are also review papers, providing only general descriptions of the principles of tomography and examples of the method's use without statistical analysis. The paper [9] presents experience on core porosity research, but due to low resolution, the authors limit themselves to calculating cavernous porosity. The authors of [10] compared the results of porosity measurements obtained by tomography and gas volumetry with breakage by lithology, but only 14 samples were studied. In addition, for tomography, the samples were cut into cylinders with sides of 5–20 mm that significantly affected the results. Thus, a full statistical comparison of determining the porosity of samples of standard sizes by X-ray tomography and other methods, taking into account the peculiarities of the lithology of the studied reservoirs, has not been carried out, although some researchers recognize the need for such a comparison [11].

To address the current challenges in oil industry related to modeling the pore space structure in a 3D



core model and evaluating permeability and porosity ("Digital Core"), it is necessary to obtain a representative characteristic of a void space. A similar characteristic is required to solve geotechnical problems related to modeling and evaluating the strength properties of heterogeneous rocks. In addition, it is important for research on capillary processes in porous media.

Laboratory petrophysical studies of core samples allow to evaluate only a single integral characteristic of a core sample, comprising the effective porosity and total porosity of a sample. However, for computer 3D modeling of various processes in a rock core, such integral values are insufficient that necessitates the use of non-destructive volumetry methods for researching core samples, such as X-ray computer tomography (CT), which allows for the study of the internal heterogeneity of core samples in volume. The application of CT, despite its modernity and technological nature, has a number of problems associated with the method's resolution for evaluating the heterogeneity of rock in the region of physical small-scale heterogeneities (small pores), that is, microporosity.

In order to bring the porosity estimates determined by different methods to a unified value, the study included a statistical analysis of the values of porosity factors obtained from standard laboratory petrophysical studies of core samples and from the results of a core CT.

The aim of this work is to develop statistical models for assessing the discrepancy between the porosity factor K_p determined using computer tomography (CT) data and more reliable laboratory petrophysical data for terrigenous and carbonate rocks. The assessment of this discrepancy will enable the estimation of the proportion of microporosity in computer 3D core models based on the CT results. The separate consideration of terrigenous and carbonate rocks is due to the significant differences in mineralogical composition, structural-textural features of the sediments, and pore space structures of these two main lithological types of sedimentary rocks.

The research objectives include:

- an assessment of the impact of lithology on the K_p assessment using various methods (petrophysics and CT);
- an assessment of the influence of the K_p variation range on the convergence of the results of these two methods (petrophysics and CT) for different lithologies;
- building models for adjusting K_p values based on CT results for different lithologies.

The solution to these problems is based on a detailed statistical analysis.

Theory

There are two standard methods for determining porosity factor that are widely used in petrophysics, which differ in a phase used: determination of porosity by liquid saturation and determination of porosity by gas (gas volumetry). These methods do not measure the entire pore volume, but only those pores that are connected to a sample surface and to each other, which, according to classification [12], constitute effective porosity. The use of liquid or gas allows them to be filled and the entire volume of these open and connected pores to be measured with sufficient accuracy. Of course, there is also a method for measuring total and closed porosity (K_p estimation through mineralogical density), but it is less commonly used because it requires the destruction of samples [13].

At the same time, in recent years, a relatively new method of studying pore space has become increasingly widespread in petrophysical research, computer X-ray tomography. This method allows the visualization of the pore space inside a sample, which makes it possible to qualitatively assess the porosity and establish a relationship between its distribution and the lithological characteristics of the sample being studied. However, the main disadvantage of using the X-ray computer tomography method in a standard petrophysical research complex is its low resolution. This method can only visualize pores that are up to a few micrometers in size that leads to a significant underestimation of the volume of the pore space, resulting in a porosity factor calculated using the X-ray tomography method being lower than that measured by standard liquid saturation and gas volumetry methods.

It can be assumed that the degree of closeness of the porosity factor values calculated using the gas volumetry-liquid saturation methods and the X-ray tomography method will depend significantly on the dominant sizes and quantitative ratios of individual pore types in a studied core sample: open (effective porosity) and closed, connected and isolated, large and small. In the opinion of the authors of this paper, this will mainly be determined by the samples lithology. Among the types of reservoir rocks studied, the pore space structure will differ most significantly between carbonate and terrigenous rocks.

Carbonate reservoirs are known to have an extremely heterogeneous pore space structure, consisting of intergranular and intragranular pores, cavities, and fractures. Often in some types of carbonate reservoirs, for example, in grainstone structural type of limestones [14], most of the reservoir space can be represented by large cavities and fractures, which makes it easily visualizable using X-ray tomography.



At the same time, the nature of the structure of the carbonate pore space does not exclude the presence of a certain proportion of closed pores in a sample, which may not be detected by gas volumetry and liquid saturation methods, which are only capable of measuring effective (open) porosity. Therefore, it can be expected that the porosity factors of carbonate rocks determined by standard methods and by X-ray tomography may be close in value to each other, but at the same time be composed of different volumes.

The pore space of terrigenous reservoir rocks is characterized by greater homogeneity and connectivity due to its predominantly intergranular nature. Rocks of this composition form granular-type reservoirs, closely described by the Slichter model, in which permeability is determined by porosity and particle diameter [15]. At the same time, the dimensions of individual elements of the void space in this type of rock are smaller than the resolution limit of the X-ray tomography method. It should be noted that, despite the existence of high-resolution micro- and nanotomography methods, these methods can only be used for separately manufactured samples of millimeter dimensions, as shown in [16] that excludes comparison with the determination of the porosity factor using standard methods carried out on cylindrical samples with a standard diameter of 30 or 25 mm.

Thus, this study compares the porosity factors obtained by different methods on the same standard-size samples of carbonate and terrigenous rocks.

Research Materials and Techniques

The studied samples of core from the oil fields of the Perm region were cut from full-size cores into cylinders with a standard diameter and a height of 30 mm. The samples belonged to two lithologies: terrigenous and carbonate rocks.

The terrigenous samples were mainly represented by sandstone, silt-rich sandstone composed of quartz and feldspar-quartz; gray, dark gray, brown, and brown; fine-grained, medium-fine-grained, and coarse-grained; of varying degrees of sorting; orthomorphous or cemented with clayey, calcite, or ferruginous cement; strong or of medium strength, with mineral inclusions of mica, ore minerals, and pyrite.

The carbonate samples were represented by limestone, dolomite, and dolomitized limestone light gray, gray, dark gray; organogenic, detrital, organogenic-detrital, lumpy-detrital, lumpy-algal, and algal; sometimes slightly clayey and clayey; porous, porous-cavernous, and cavernous; strong with frequent stylolitic joints and cracks sometimes filled with calcite crystals.

The research involved measuring porosity using the gas volumetry method (K_p , %) and X-ray computer tomography (K_p^t , %).

The gas volumetry method was chosen by the authors for several reasons: firstly, this method is quite fast (on average, it takes no more than an hour to measure one sample) and relatively simple, and, as a result, it is most often used in petrophysical laboratories; secondly, the use of a chemically inert gas instead of a liquid allows to reliably exclude changes in the samples caused, for example, by accidental violation of the procedure of washing and drying a sample after the saturation test or chemical interaction between the liquid and the mineral matrix of a sample.

Porosity measurements were performed on an AP-608 automated porosimeter-permeameter (Coretest Systems, USA). The principle of operation of this unit is based on the method of non-stationary filtration [17].

The essence of the method lies in measuring a pore volume using the principle of helium expansion according to Boyle's law, which states that the pressure P of any ideal gas multiplied by its volume V gives a constant value at a constant temperature. In the context of core analysis, Boyle's law allows to determine an unknown volume by the expansion of a gas with known pressure and temperature values into an empty space and using the resulting pressure to calculate the unknown volume. Therefore, knowing P_1 , P_2 and V_2 , it is possible to calculate V_1 :

$$V_1 = \frac{P_2 \cdot V_2}{P_1}. \quad (1)$$

In an AR-608 porosimeter-permeameter, helium is pumped in from both ends of a sample. The permeability range of samples available for measurement on this unit is from 0.001 mD (rocks with such permeability are not considered to be reservoirs) to 5000 mD. Accordingly, the porosity measuring range is from 0.1 to 40%, which also covers the ranges typical of terrigenous and carbonate reservoirs.

The method of sample preparation and measurement complies with GOST¹ and involved pre-drying of samples that were carefully extracted in an alcohol-benzene mixture using a drying cabinet. The drying time and temperature were at least 8 h and 105°C for the carbonate rocks and at least 12 h and 80°C for the terrigenous rocks. After drying, the samples were cooled in a desiccator, their geometric characteristics were measured using an electronic

¹ GOST 26450.0-85–GOST 26450.2-85. Rocks. Methods for determining reservoir properties. M.: Standards Publishing House; 1985. 16 p. (In Russ.)

caliper, and then the porosity factor was determined using the AR-608 unit. All measurements were taken at least five times, and the arithmetic mean was calculated based on the results of all five measurements, which was the final value for each sample.

The second method analyzed in the paper is X-ray computer tomography of a core. The method was developed by A. Cormack and G. Hounsfield [18] and is based on Radon transformations [19]. The essence of the method lies in creating a series of X-ray images obtained when X-rays pass through a sample rotating along a single axis. The resulting X-ray images are transformed through the inverse transform of the integral of a function of a straight line perpendicular to a vector that is directed along the direction of the radiation at a certain distance measured along it.

In our study, an X-ray inspection system with a computer tomography function, Nikon XT H 225 (Nikon Metrology, Great Britain) was used for X-ray tomography. This system consists of a stationary X-ray source forming a focal spot measuring 3 μm , a three-position rotating table, and a 2048 \times 1408 pixel detector with a physical pixel size of 142 μm . The system allows studying samples of a standard diameter of 30 mm with a resolution of up to 20 μm .

Samples were surveyed at a radiation source voltages ranging from 150 to 180 kV, current strengths ranging from 100 to 150 mA, using a 0.5 mm thick copper filter, exposure time of 0.5 s, and at least 3000 images. All samples were positioned so that the resolution of the resulting reconstruction was at

least 25 μm . Inhomogeneities smaller than 1 voxel (25 μm) are referred to as microporosity, which, unlike larger macroporosity, cannot be distinguished with high accuracy and directly geometrically identified in a sample. In practice, a number of assumptions are made to identify such porosity in samples. For example, that the micropores are located on the surface of large pores, or micropores can be located in the contact areas of mineral grains, or they are distributed fairly evenly throughout the volume of a mineral matrix. However, for all these assumptions, it is necessary to estimate the proportion of this microporosity.

The reconstruction of a 3D image was performed using proprietary CT Pro 3D software (Nikon Metrology, UK), which uses an improved version of one of the most widely used FDK algorithms [20] for the reconstruction procedure. The reconstructed images were processed in the Avizo Fire program (Visualization Science Group, France).

The technique for processing the images of the samples in order to obtain the volume of the pore space was used as follows. In the initial reconstruction, a 32-bit black and white three-dimensional image, where the brightest areas correspond to areas of maximum density (mineral matrix), and the darkest areas correspond to the void space, a binarization procedure was performed. The essence of the binarization procedure is that the entire range of gray shades is divided into two volumes with values of 0 and 1, corresponding to the volumes of pores and matrix (Fig. 1).

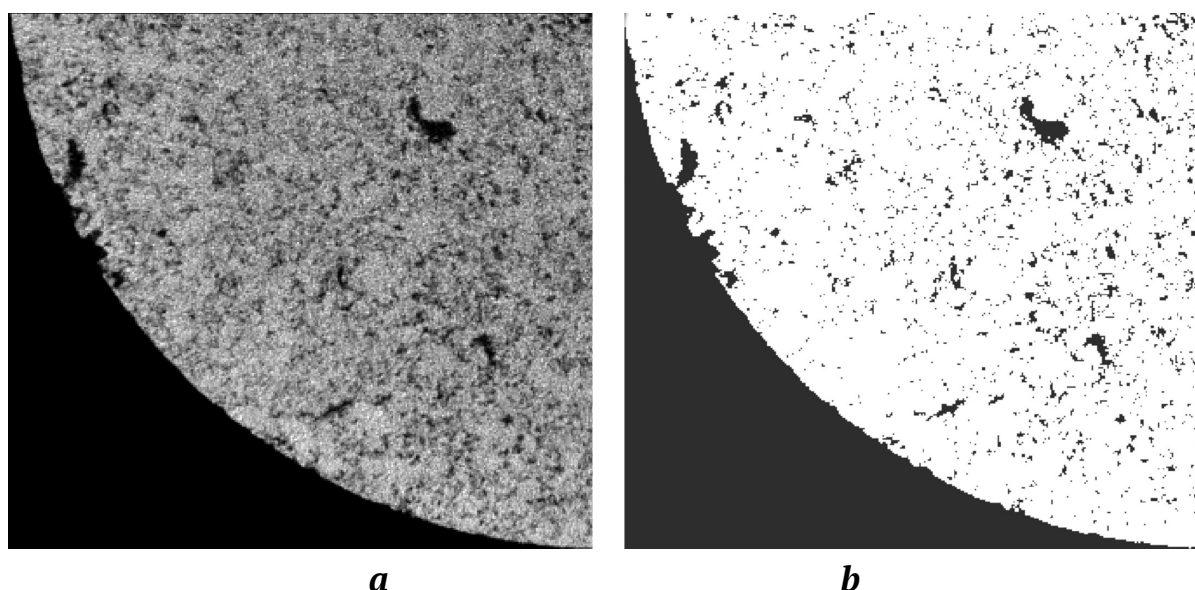


Fig. 1. Distinguishing on a fragment of a black and white image of a rock:

a – reconstructed image of a sample cross-section in shades of gray, proportional to the absorption of the material (black – does not absorb, white – absorbs); *b* – distinguishing void space in a black-and-white image of rock (black – air in pores and around the sample; white – mineral matrix)

These volumes, in turn, can already be measured using software tools.

The porosity factor of the sample was calculated based on tomography data using the standard porosity calculation formula:

$$K_p^t = \frac{V_{por}}{V_{vol}} \cdot 100, \quad (2)$$

where V_{por} is the volume of the binarized model of a sample pore space, mm^3 ; V_{vol} is the volume of the binarized model of the entire sample space, mm^3 .

Findings and Analysis of the Data Obtained

This chapter deals with the statistical analysis of the porosity factor values obtained by the methods described above. Fig. 2 shows a comparison of the porosity factor values obtained by the gas volumetry method (K_p , %) and those obtained by the X-ray tomography method (K_p^t , %) for terrigenous and carbonate rocks.

For terrigenous rocks, the average porosity values for K_p^t and K_p are 8.71 and 10.76%, respectively, with standard deviations of 6.17 and 5.82%.

For carbonate rocks, the average porosity values for K_p^t and K_p are 21.43 and 22.00%, respectively, with standard deviations of 5.51 and 5.43%.

The analysis of the given correlation fields shows that the relationships of the values of K_p and K_p^t for the studied rocks depend of the values range. For terrigenous rocks the values of K_p and K_p^t lower than those for carbonate ones. Comparisons of the average values of K_p and K_p^t for the studied rocks were performed using Student's t-test and are presented in Table 1.

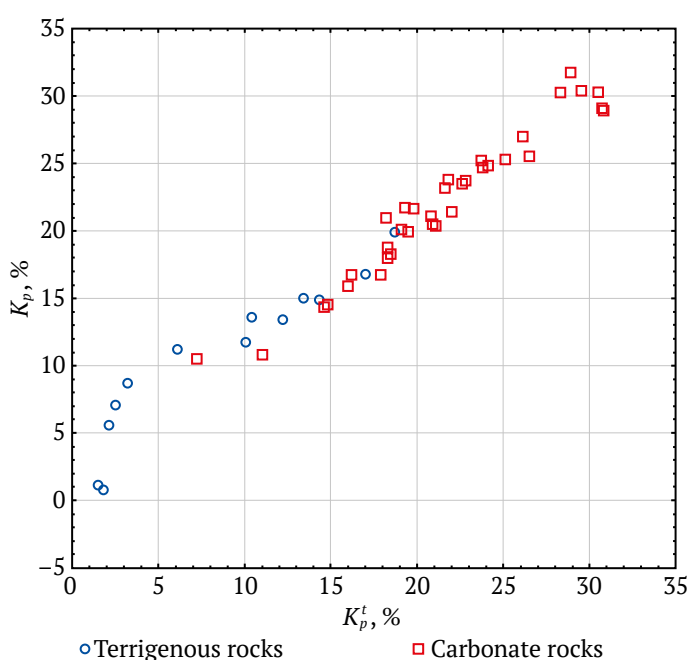


Fig. 2. Fields of correlation between K_p and K_p^t for different rocks

Table 1

Comparison of average values of K_p and K_p^t for different rock types

Rock	Mean \pm standard deviation		Criteria $\frac{t}{p}$
	K_p , %	K_p^t , %	
Terrigenous	10.76 ± 5.82	8.71 ± 6.17	$\frac{0.866}{0.395}$
Carbonate	22.00 ± 5.43	21.43 ± 5.51	$\frac{0.431}{0.668}$

It can be seen from here that the average values of the porosity factors, determined by different methods, do not statistically differ (the level of significance achieved $p > 0.05$). At the same time, visual analysis of the fields of correlation between K_p and K_p^t for both terrigenous and carbonate rocks shows that within the correlation fields, different relationships are observed depending on the values of K_p and K_p^t . Overall, the results of the evaluation of the average K_p and K_p^t are not statistically contradictory to each other, but require a more detailed examination by the porosity ranges. At the same time, the average values obtained by CT method are always lower, despite the different lithology that indicates the complexity and some underestimation of K_p for microporosity due to the physical limitations of the CT method.

To determine various relationships between K_p and K_p^t , we subdivided them by lithology and K_p range and arrange the values of K_p of the samples in ascending order, where their number increased by one ($n = 3, n = 4, n = 5, \dots, n = 33$ for carbonate rocks and $n = 13$ for terrigenous rocks). The total number of models considered was determined by the sample collection amount. For each considered range of values of K_p , we performed a $K_p = f(K_p^t)$ regression analysis by n values with assessing the paired correlation coefficient r and statistical characteristics of the regression equation coefficients.

The regression equation is as follows:

$$K_p = b + k \cdot K_p^t, \quad (3)$$

where K_p is porosity factor obtained by the gas volumetry method, %; K_p^t is porosity factor obtained by X-ray tomography, %; b is intercept (free term) in the regression equation; k is slope in the regression equation.

For carbonate rocks, the regression equation parameters are given in Table 2.

33 regression equations were built for carbonate rocks, and the correlation coefficient values r ranged from 0.892 to 0.975.



The statistical characteristics of the developed models were used to build dependencies of the values of the intercepts of the regression equations and the slopes for K_p^t on the values of the correlation coefficients r (Figs. 3–5).

The analysis shows that the relationships between the studied parameters are of two types: at $K_p < 24\%$; when increasing the range of K_p , there is a regular de-

crease in an intercept value; with even greater increase of K_p , the value of an intercept changes insignificantly.

The analysis shows that the relationships between the studied parameters are also of two types: at $K_p < 24\%$, when increasing K_p , there is a regular increase in the slopes at K_p^t ; with even greater increase of K_p , the values of the slopes changes insignificantly, being in a range of 0.97–0.98.

Table 2

Regression equations for K_p dependence on K_p^t (arborate rocks)

Range of K_p values, %	Intercept b	t at intercept	Slope k at K_p^t	t at K_p^t	Correlation coefficient r	Achievable level of significance of $r-p$
10.51–14.35	6.260	2.281	0.515	1.974	0.892	$p = 0.299$
10.51–14.53	5.842	2.889	0.636	3.428	0.924	$p = 0.076$
10.51–15.91	5.842	2.998	0.630	4.754*	0.939	$p = 0.018$
10.51–16.74	4.609	2.666	0.692	5.474*	0.939	$p = 0.005$
10.51–16.74	4.745	3.306*	0.679	6.797*	0.949	$p = 0.001$
10.51–17.98	4.388	3.352*	0.709	8.096*	0.957	$p = 0.0002$
10.51–18.29	4.112	3.369*	0.735	9.242*	0.961	$p = 0.00004$
10.51–18.77	3.773	3.030*	0.765	9.629*	0.959	$p < 10^{-5}$
10.51–19.97	3.329	2.675*	0.801	10.329*	0.960	$p < 10^{-5}$
10.51–20.10	2.952	2.284*	0.832	10.515*	0.957	$p < 10^{-5}$
10.51–20.42	2.986	2.550*	0.83	11.864*	0.963	$p < 10^{-5}$
10.51–20.53	2.925	2.693*	0.834	13.112*	0.967	$p < 10^{-5}$
10.51–20.96	2.764	1.973	0.855	10.469*	0.945	$p < 10^{-5}$
10.51–21.10.	2.629	1.978	0.865	11.325*	0.946	$p < 10^{-5}$
10.51–21.40	2.705	1.879	0.860	12.262*	0.953	$p < 10^{-5}$
10.51–21.64	2.705	1.899	0.860	11.979*	0.948	$p < 10^{-5}$
10.51–21.72	2.313	1.644	0.895	11.388*	0.940	$p < 10^{-5}$
10.51–23.19	1.981	1.419	0.918	11.912*	0.942	$p < 10^{-5}$
10.51–23.51	1.787	1.341	0.931	12.815*	0.946	$p < 10^{-5}$
10.51–23.76	1.614	1.264	0.942	13.705*	0.950	$p < 10^{-5}$
10.51–23.78	1.456	1.01	0.957	12.402*	0.938	$p < 10^{-5}$
10.51–24.71	1.238	1.015	0.968	15.046*	0.954	$p < 10^{-5}$
10.51–24.86	1.169	1.008	0.972	16.076*	0.958	$p < 10^{-5}$
10.51–25.18	0.989	0.874	0.984	16.894*	0.960	$p < 10^{-5}$
10.51–25.30	1.076	1.074	0.978	17.877*	0.963	$p < 10^{-5}$
10.51–25.54	1.437	1.384	0.957	18.349*	0.963	$p < 10^{-5}$
10.51–27.02	1.303	1.321	0.964	19.559*	0.966	$p < 10^{-5}$
10.51–28.94	1.321	1.387	0.970	20.292*	0.967	$p < 10^{-5}$
10.51–29.14	1.385	1.396	0.961	21.476*	0.969	$p < 10^{-5}$
10.51–30.25	1.585	1.643	0.962	22.080*	0.970	$p < 10^{-5}$
10.51–30.27	1.436	1.532	0.961	23.640*	0.973	$p < 10^{-5}$
10.51–30.40	1.575	1.541	0.979	24.909*	0.975	$p < 10^{-5}$
10.51–31.76	1.419	1.647	0.970	24.639*	0.973	$p < 10^{-5}$

* – statistically significant values ($p \leq 0.05$).

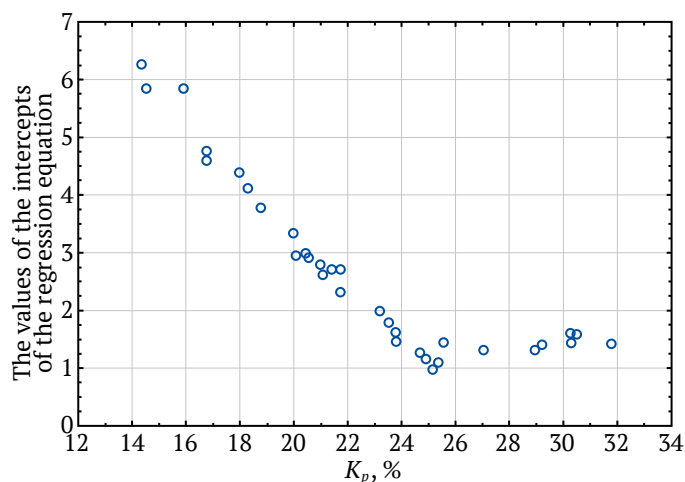


Fig. 3. The values of intercepts of the regression equations depending on K_p (carbonate rocks)

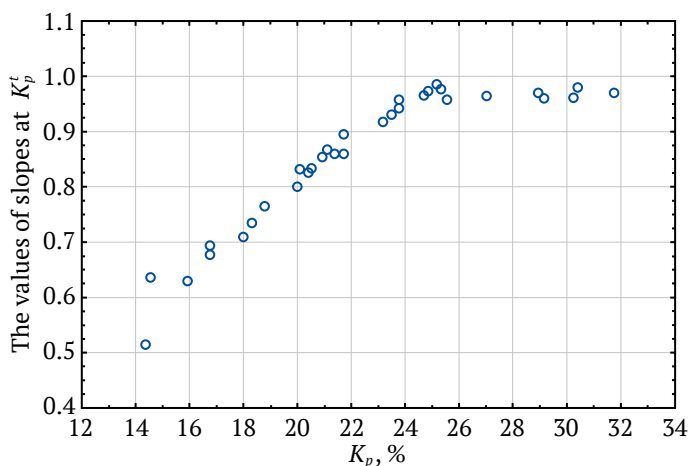


Fig. 4. Slope at K_p^t in regression equations depending on K_p (carbonate rocks)

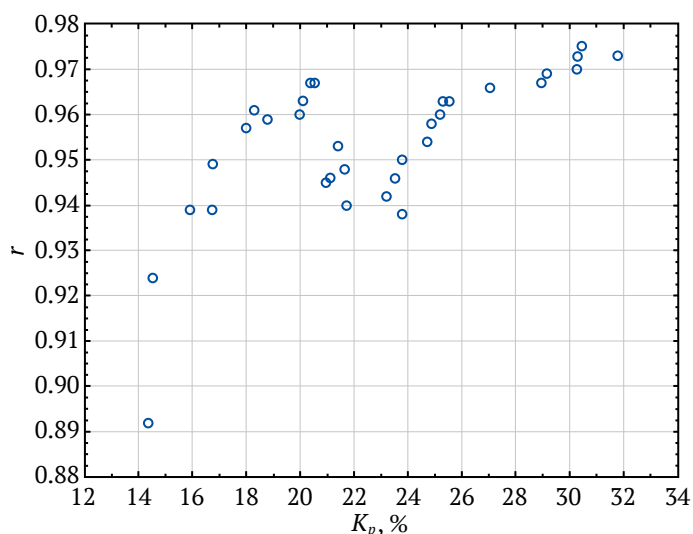


Fig. 5. Correlation coefficient r as a function of K_p (carbonate rocks)

It can be seen from here that the relationships between the studied parameters are also of two types: at $K_p < 22\%$, when increasing K_p , there is an initial increase in r . At $K_p < 23\%$, r decreases. With an even greater increase in the range of K_p , the values of the coefficients increase along a complex trajectory.

The above K_p and K_p^t dependency analysis for carbonate rocks showed that it seems possible to determine two boundaries that differentiate the values of K_p^t into three groups: the first one, when $K_p^t < 16.0\%$; the second, at $16.0\% \leq K_p^t < 22.6\%$; and the third one, when $K_p^t \geq 22.6\%$.

The first group is at $K_p^t < 16.0\%$, in which the dependency of K_p on K_p^t is statistically insignificant. At K_p^t from 16.0 to 22.6%, statistically significant correlations between the studied parameters were observed. To determine the values of K_p from K_p^t it is necessary to make an adjustment using the regression equation given in Table 4. At $K_p^t \geq 22.6\%$, it is also necessary to make an adjustment using the regression equation given in Table 3.

Thus, the studies conducted showed that the values of K_p^t obtained by X-ray tomography for carbonate rocks, despite the statistical equality of the mean values, are characterized by different statistical relationships. At $K_p^t < 16.0\%$, there is no significant correlation with K_p . This indicates that different values of porosity factors are obtained using these methods. At $K_p^t \geq 16.0\%$, the values of K_p^t and K_p are statistically interconnected. It should be noted that at certain intervals of the values, the intercepts values are statistically significant. This indicates that there is an adjustment of the values K_p by the intercepts of the regression equations. Therefore, to correctly use the values of K_p^t and K_p in carbonate rocks, it is necessary to use the obtained regression equations for the identified ranges of K_p .

A similar analysis was performed for terrigenous rocks (Table 4).

11 regression equations were built for terrigenous rocks, and r values ranged from 0.806 to 0.937. The analysis of the intercepts of the regression equations showed that when $K_p^t < 11.75\%$, the intercepts changed from negative to positive values. The values of slope at K_p^t are also characterized by a regular change from higher values (more than 1) to lower values (less than 1). Correlation coefficients r trends are shown in Fig. 6.

The analysis shows that the relationships between the studied parameters are also of two types: when $K_p < 12\%$, increasing K_p causes a chaotic change in the values of r ; when the K_p range increases, there is a regular increase in r values from 0.849 to 0.937.



Table 3

Regression equations for K_p dependence on K_p^t (carbonate rocks)

Range of K_p values, %	Intercept b	t at intercept	Slope k at K_p^t	t at K_p^t	Correlation coefficient r	Achievable level of significance of $r-p$
$K_p^t < 16.0\%$	6.260	2.116	0.514849	1.974	0.892	$p = 0.299$
$16.0\% \leq K_p^t < 22.6\%$	-0.940	-0.359	1.080430	8.054	0.884	$p < 10^{-5}$
$K_p^t \geq 22.6\%$	7.709	3.408	0.766514	8.932	0.942	$p < 10^{-5}$

Table 4

Regression equations for K_p dependence on K_p^t (terrigenous rocks)

Range of K_p values, %	Intercept b	t at intercept	Slope k at K_p^t	t at K_p^t	Correlation coefficient r	Achievable level of significance of $r-p$
0.8–5.6	-10.703	-1.267	7.312	1.579	0.844	$p = 0.360$
0.8–7.1	-9.935	-2.535	6.864	3.528	0.928	$p = 0.072$
0.8–8.7	-6.456	-2.427	5.000	4.324*	0.928	$p = 0.002$
0.8–11.2	-0.248	-0.118	2.091	3.238*	0.850	$p = 0.032$
0.8–11.75	2.166	1.195	1.14	3.053*	0.806	$p = 0.028$
0.8–13.43	2.638	1.698	0.997	3.942*	0.849	$p = 0.008$
0.8–13.60	2.579	1.805	1.004	4.812*	0.876	$p = 0.0001$
0.8–14.88	2.864	2.187*	0.927	5.607*	0.892	$p = 0.0005$
0.8–15.00	2.887	2.373*	0.92	6.477*	0.907	$p = 0.0001$
0.8–16.8	3.098	2.736*	0.875	7.384*	0.919	$p = 0.00002$
0.8–19.9	3.048	2.923*	0.884	8.943*	0.937	$p < 10^{-5}$

* – statistically significant values ($p \leq 0.05$).

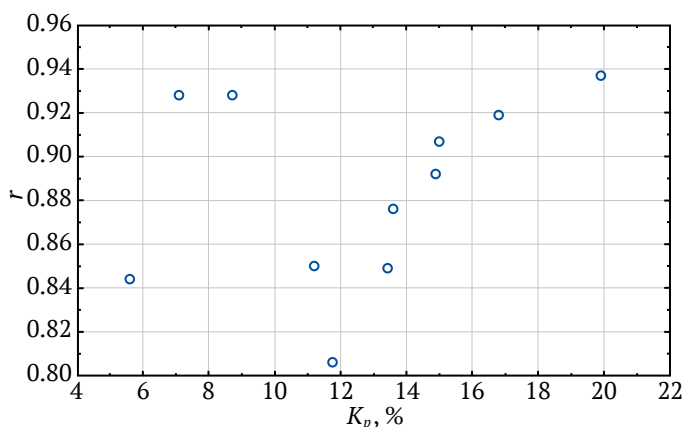


Fig. 6. Correlation coefficients r depending on K_p (terrigenous rocks)

An analysis of the constructed regression equations showed that when $K_p^t \leq 7.1\%$, the dependence K_p on K_p^t is statistically insignificant. At $K_p^t > 7.1\%$ a statistically significant regression equation was obtained:

$$K_p = 6.349 + 0.63905 K_p^t, \quad (4)$$

at $r = 0.964, p = 0.00002$.

This indicates that the relationships between K_p and K_p^t are characterized by the presence of a statistical relation.

Practical Application and Areas of Further Research

Thus, the conducted research showed that these methods do not replace, but complement each other, as they have different limitations in application. At the same time, the statistical analysis carried out showed that the use of both methods gives naturally different, but statistically related results, which demonstrates the possibility of their joint application. It is also important that, when researching samples of different lithological types of collectors, the methods have different limitations:

1. In the study of carbonate samples, both methods showed statistically significant correlation coefficients between K_p and K_p^t at the values of K_p obtained by the gas volumetry method of above 16% that may be due to larger void sizes.

2. When testing terrigenous samples, porosity was most accurately determined at porosity factor values K_p more than 7.1% that may be due to poor filling of intergranular voids with cement or good sorting of the material.

The application of the recommended equations for the lithologies in different ranges of K_p enables an integral estimation of microporosity as the difference between the estimation of K_p according to the equation and the values of K_p^t obtained based on CT data.



This is especially true for samples of irregular or complex shapes, which are not always possible to fully examine in a petrophysical laboratory. This integrated assessment of microporosity allows for a constraint on the total volume of distributable micropores, which will improve the quality of three-dimensional computer models of core and pore space of reservoir rocks.

The results of the study can be used for petrophysical substantiation of the permeability and porosity of reservoir rocks in oil and gas fields.

The use of the proposed approach enables improving the quality of 3D models of rock core, which will ultimately lead to an increase in the accuracy of various modeling methods related to rock properties, and will allow for more rational and economically efficient development of oil and gas fields (or other natural resources).

Further research areas appear to the authors in the continuation of the tests with an increase in the number and variety of samples that will enable a refinement of the obtained dependencies, as well as in the consideration of additional standard characteristics of core (values of a residual oil saturation factor, capillary curves, etc.).

Conclusion

The research carried out convincingly showed that when using the data on porosity factors obtained by different methods for both carbonate and

terrigenous rocks, the results obtained should be comparable.

The results of the assessment of the averages of K_p and K_p^t for terrigenous and carbonate rocks are not statistically contradictory to each other. At the same time, the average values obtained by the CT method are always lower, despite the different lithology that indicates the complexity and some underestimation of K_p for microporosity due to the physical limitations and other features of the CT method.

The studies carried out showed that the values of K_p^t obtained by X-ray tomography for carbonate rocks, when $K_p^t < 16.0\%$, have no statistical relationship with K_p . For the values outside this range, the equations for estimating and adjusting the K_p values were proposed.

An analysis of the constructed regression equations for terrigenous rocks showed that when $K_p^t \leq 7.1\%$, the dependence of K_p on K_p^t was statistically insignificant. For the values outside this range, the equations for estimating and adjusting the K_p values were proposed.

The application of the recommended equations for the lithologies by the range of K_p allows for an integral estimation of microporosity as the difference between the estimate of K_p according to the equation and the values of K_p^t obtained based on CT data. The proposed approaches make it possible to improve the quality of 3D models of the pore space structure of rocks.

References

1. Petersilie V.I., Poroskun V.I., Yatsenko G.G. (eds.) *Methodological guidelines for calculating geological reserves of oil and gas using the volumetric method*. Moscow: Nedra; 2003. 258 p. (In Russ.)
2. Khassanov D.I., Lonshakov M.A. Investigation of the scale effect and the concept of a representative volume element of rocks in relation to porosity. *Georesources*. 2020;22(4):55–69. <https://doi.org/10.18599/grs.2020.4.55-69>
3. Ketcham R.A., Carlson W.D. Acquisition, optimization and interpretation of X-ray computed tomographic imagery: applications to the geosciences. *Computers & Geosciences*. 2001;27(4):381–400. [https://doi.org/10.1016/S0098-3004\(00\)00116-3](https://doi.org/10.1016/S0098-3004(00)00116-3)
4. Vinegar H.J. X-ray CT and NMR imaging of rocks. *Journal of Petroleum Technology*. 1986;38(03):257–259. <https://doi.org/10.2118/15277-PA>
5. Renter J.A.M. Applications of computerized tomography in sedimentology. *Marine Geotechnology*. 1989;8(3):201–211. <https://doi.org/10.1080/10641198909379868>
6. Wolanski K., Zarudzki W., Kiersnowski H., et al. X-ray computed tomography (CT) applied for rock core analysis. *Bulletin of the Russian Academy of Natural Sciences*. 2017;17(5):43–50.
7. Khoziainov M.S., Weinberg E.I. Computational microtomography – a new information technology for non-destructive study of internal microstructure of geological rock samples. *Geoinformatika*. 1992;(1):42–50. (In Russ.)
8. Vorobyev K.A., Vorobev A.E., Tcharo H. Oil industry digitization: technology “digital” core. *The Eurasian Scientific Journal*. 2018;10(3). URL: <https://esj.today/PDF/78NZVN318.pdf> (In Russ.)
9. Kostin D.K., Kuznetsov E.G., Vilesov A.P. Experience of TNNC LLC in core study using CT SCANNER. *Scientific and Technical Bulletin of Rosneft*. 2014;(3):18–21. (In Russ.)



10. Eremenko N.M., Murav'eva Yu.A. Application of the X-ray microtomography for porosity determination in borehole core. *Petroleum Geology. Theory and Practice*. 2012;7(3):5. (In Russ.)
11. Shtyrlyayeva A.A., Zhuravlev A.V., Gerasimova A.I. Prospects and problems of computer microtomography using for core samples studies. *Petroleum Geology. Theory and Practice*. 2016;11(1):12. (In Russ.) https://doi.org/10.17353/2070-5379/8_2016
12. Dobrynin V.M., Vendelstein B. Yu., Kozhevnikov D.A. *Petrophysics (Physics of Rocks)*. Moscow: Gubkin Russian State University of Oil and Gas; 2004. 367 p. (In Russ.)
13. *Methodological recommendations for the study of oil and gas reservoir rocks by physical and petrographic methods*. Compiled by Goryan V.I., Berezin B.M., Belov Yu.A. et al. Proceedings of VNIGNI. Moscow: Nedra; 1978. Pp. 87–111. (In Russ.)
14. Dunham R.J. Classification of carbonate rocks according to depositional texture. In: Ham V.E. (Ed.). *Classification of carbonate rocks: Symposium. American Association of Petroleum Geologists Memoir*. 1962;1:108–121.
15. Romm E.S. *Structural models of pore space in rocks*. Leningrad: Nedra; 1985. P. 8. (In Russ.)
16. Betelin V.B., Smirnov N.N., Stamov L.I., Skryleva E.I. Developing the structure of core pores based on processing of tomography data. *Proceedings in Cybernetics*. 2018;(2):86–91. (In Russ.)
17. Jones S.C. A Rapid accurate unsteady-state klinkenberg permeameter. *Society of Petroleum Engineers Journal*. 1972; 12(5):383–397. <https://doi.org/10.2118/3535-pa>
18. Hounsfield G.N. Computerized transverse axial scanning (tomography). Part 1: Description of system. *British Journal of Radiology*. 1973;46:1016–1022.
19. Radon J. Über die Bestimmung von Funktionen durch ihre Integralwerte langs gewisser Mannigfaltigkeiten. *Berichte Sachsische Akademie der Wissenschaften, Leipzig. Journal of Mathematical Physics*. 1917;69:262–267
20. Feldkamp L.A., Davis L.C., Kress J.W. Practical cone-beam algorithm. *Journal of the Optical Society of America A*. 1984;1(6):612–619.

Information about the authors

Vladislav I. Galkin – Dr. Sci. (Geol. and Mineral.), Professor, Head of the Department of Petroleum and Gas Geology, Perm National Research Polytechnic University, Perm, Russian Federation; ORCID [0000-0003-4867-2298](https://orcid.org/0000-0003-4867-2298), Scopus ID [55418067700](https://scopus.org/55418067700); e-mail vgalkin@pstu.ru

Oleg A. Melkishev – Cand. Sci. (Eng.), Associate Professor of the Department of Petroleum and Gas Geology, Perm National Research Polytechnic University, Perm, Russian Federation; ORCID [0000-0001-7056-3173](https://orcid.org/0000-0001-7056-3173), Scopus ID [55531674700](https://scopus.org/55531674700); e-mail melkishev@pstu.ru

Yan V. Savitsky – Cand. Sci. (Eng.), Engineer of the Department of Petroleum and Gas Geology, Perm National Research Polytechnic University, Perm, Russian Federation; ORCID [0000-0003-2405-4508](https://orcid.org/0000-0003-2405-4508), Scopus ID [57211543253](https://scopus.org/57211543253), ResearcherID [AHI-0193-2022](https://orcid.org/AHI-0193-2022); e-mail yansavitsky@yandex.ru

Received 27.08.2024

Revised 24.02.2025

Accepted 14.05.2025




GEOLOGY OF MINERAL DEPOSITS

Research paper

<https://doi.org/10.17073/2500-0632-2025-05-416>

UDC 550.8

**From visual diagnostics to deep learning:
automatic mineral identification in polished section images****D.M. Korshunov¹ , A.V. Khvostikov²  , G.V. Nikolaev² , D.V. Sorokin² ,
O.I. Indychko² , M.A. Boguslavsky² , A.S. Krylov²  **¹ *Geological Institute of the Russian Academy of Sciences (GIN RAS), Moscow, Russian Federation*² *Lomonosov Moscow State University, Moscow, Russian Federation* dmit0korsh@gmail.com**Abstract**

Studying mineralogical composition of ores is a fundamental step in the exploration of new deposits, as it allows determining the forms in which useful components are found, the processes of ore formation, and the potential recoverability of valuable elements. The mineral associations, textures, and structures of ores not only provide key information about the geology of a deposit, but also determine the choice of beneficiation methods. Despite the development of modern analytical tools and existing solutions for automatic mineral diagnosis, such as those based on the SEM-EDS method, optical microscopy remains the most accessible means of quantitative mineralogical analysis. However, it remains labor-intensive and requires highly skilled specialists. In addition, its visual nature limits the accuracy and reproducibility of results, creating a need for more effective approaches. One promising area is the automation of ore mineral identification based on images of polished sections. The aim of the work was to develop and validate a universal segmentation model based on deep learning. In the course of the research, related problems were also solved, including the creation of an open LumenStone dataset, the development of color adaptation methods, joint analysis of PPL and XPL images, panorama construction, and the development of a fast annotation method. The work applied convolutional neural network architectures, color correction and joint image processing algorithms, as well as an original sampling method that compensates class imbalance. The proposed segmentation model demonstrated high accuracy (IoU up to 0.88, PA up to 0.96) for nine minerals. The obtained results confirmed the effectiveness of integrating deep learning and modern image processing algorithms in mineralogical analysis systems and laid the foundation for further development of digital methods in automated petrography.

Keywords

mineralogy, mineragraphy, digital petrography, automatic image analysis methods, segmentation, deep learning, color adaptation, panoramic images

Financing


This research was supported by the Russian Science Foundation (project no. 24-21-00061).

For citation

Korshunov D.M., Khvostikov A.V., Nikolaev G.V., Sorokin D.V., Indychko O.I., Boguslavsky M.A., Krylov A.S. From visual diagnostics to deep learning: automatic identification of minerals in polished section photographs. *Mining Science and Technology (Russia)*. 2025;10(3):232–244. <https://doi.org/10.17073/2500-0632-2025-05-416>

ГЕОЛОГИЯ МЕСТОРОЖДЕНИЙ ПОЛЕЗНЫХ ИСКОПАЕМЫХ

Научная статья

**От визуальной диагностики к глубокому обучению:
автоматическое определение минералов на фотографиях аншлифов****Д. М. Коршунов¹ , А. В. Хвостиков²  , Г. В. Николаев² , Д. В. Сорокин² ,
О. И. Индычко² , М. А. Богуславский² , А. С. Крылов²  **¹ *Геологический институт РАН, г. Москва, Российская Федерация*² *Московский государственный университет им. М. В. Ломоносова, г. Москва, Российская Федерация* dmit0korsh@gmail.com**Аннотация**

Изучение минерального состава руд является основополагающим этапом при разведке новых месторождений, поскольку именно оно позволяет определить формы нахождения полезных компонентов, процессы рудообразования и потенциальную извлекаемость ценных элементов. Минеральная ассоциация, текстуры и структуры руд не только дают ключевые сведения о геологии месторождения, но



и определяют выбор методов обогащения. Несмотря на развитие современной аналитической базы и существующие решения автоматической диагностики минералов, например, на основе СЭМ-EDS метода, оптическая микроскопия является самым доступным средством количественного минералогического анализа. Однако она остаётся трудоёмкой и требует высокой квалификации специалиста. А её визуальный характер ограничивает точность и воспроизводимость результатов, что создает необходимость в разработке более эффективных подходов. Одним из перспективных направлений является автоматизация идентификации рудных минералов по фотоизображениям шлифов. Целью работы являлась разработка и валидация универсальной сегментационной модели на основе глубокого обучения. В процессе исследования также были решены сопутствующие задачи, включая формирование открытого набора данных LumenStone, разработку методов цветовой адаптации, совместного анализа PPL- и XPL-изображений, построения панорам и разработки метода быстрой разметки. В работе были применены свёрточные нейросетевые архитектуры, алгоритмы коррекции цвета и совместной обработки изображений, а также оригинальный метод семплирования, компенсирующий дисбаланс классов. Предложенная модель сегментации продемонстрировала высокую точность (IoU до 0,88, RA до 0,96) по девяти минералам. Полученные результаты подтвердили эффективность интеграции глубокого обучения и современных алгоритмов обработки изображений для задач минералогического анализа и заложили основу для дальнейшего развития цифровых методов в автоматизированной петрографии.

Ключевые слова

минералогия, минераграфия, цифровая петрография, автоматические методы анализа изображений, сегментация, глубокое обучение, цветовая адаптация, панорамные изображения

Финансирование

Исследование выполнено за счет гранта Российского научного фонда (проект № 24-21-00061).

Для цитирования

Korshunov D.M., Khvostikov A.V., Nikolaev G.V., Sorokin D.V., Indychko O.I., Boguslavsky M.A., Krylov A.S. From visual diagnostics to deep learning: automatic identification of minerals in polished section photographs. *Mining Science and Technology (Russia)*. 2025;10(3):232–244. <https://doi.org/10.17073/2500-0632-2025-05-416>

Introduction

Studying mineralogical composition of ores is a fundamental step in the exploration of new deposits, as it allows determining the forms in which useful components are found, the processes of ore formation, and the potential recoverability of valuable elements. The mineral associations, textures, and structures of ores not only provide key information about the geology of a deposit, but also determine the choice of beneficiation methods.

Despite the development of modern analytical tools and existing solutions for automatic mineral diagnosis, such as those based on the SEM-EDS method [1, 2], optical microscopy remains the most accessible means of quantitative mineralogical analysis. However, it remains labor-intensive and requires highly skilled specialists. In addition, its visual nature limits the accuracy and reproducibility of results, creating a need for more effective approaches.

A promising area is the automation of ore mineral identification based on photographs of polished sections. This approach not only reduces span time, but also minimizes subjective errors associated with visual diagnostics and enables the implementation of accurate statistical analysis methods. The aim of this work is to describe our experience in developing a segmentation model for automatic detection of minerals in photographs of polished sections and

solving a number of related problems that arose during the research. The paper systematically outlines the main problems encountered by the authors and the solutions they propose.

Current state of the problem

The first attempts to create tools for the automatic diagnostics of ore minerals under a microscope were made in the second half of the 20th century [3, 4]. At that time, spectrophotometers were used to measure the color of minerals, in particular, a mineral type was interpreted based on the absorption spectra of light in the visible range. Due to its low accuracy, this method was not widely used. More advanced methods of automatic mineral identification were developed in the second half of the 1990s and were based on the analysis of photographs of polished sections under a microscope [5, 6].

Attempts were made to automatically analyze mineral associations using cluster analysis in order to find patterns between different objects in photographs [7]. Special mention should be made of the attempt by the authors [8] to compile a digital atlas of all minerals and to identify the minerals themselves using a dendrogram based on a digital questionnaire.

To date, existing classical solutions (without the use of deep learning) for automatic mineral identification can be divided into two main groups:



1. Based on reflected light intensity in conjunction with color characteristics expressed in the RGB or LAB color space [9];

2. Based on statistical principles of color palette separation to identify minerals in a specific sample [10–12].

Both approaches have significant limitations. Methods that use color and reflectivity are unable to distinguish between minerals with similar optical properties. Statistical methods, in turn, require recalibration for each new geological object, making their application "situational" and limited. This is well illustrated in [12], which shows the features of applying this principle to separate copper ore into three minerals and three lithological types at a specific deposit.

It is worth noting that there are also highly specialized solutions available in the form of extensions for popular image analysis software packages such as Fiji/ImageJ. For example, [13] describes a method for automatic determining hematite grade, size, and intergrowth types in ore using this software. The problem with such solutions is that they solve a narrow, specific problem and lack the necessary level of versatility.

The most effective way to overcome the shortcomings of the classical methods and achieve fundamentally better results in the automatic analysis of such images is to use trainable deep models (e.g., convolutional neural networks) that are capable of extracting complex hierarchical features from images, taking into account not only local textures and shapes, but also global relationships between image fragments. Instead of manually selecting color and statistical characteristics, such models – whether traditional convolutional neural networks (CNN) [13–15], modern transformers with a self-attention mechanism [16], or hybrid architectures (e.g., Mamba [17]) – learn to identify the distinctive morphological and structural-textural features of each mineral.

For instance, convolutional neural networks were used to detect surface defects and examine polishing quality of metal products [18, 19] and to analyze carbon distribution in cast iron based on microphotographs of rough workpiece surfaces [20]. In [21], a method is presented for separating hematite and quartz in iron ore polished sections, with the determining their size classes to optimize the feed for a processing plant. It is also worth noting a number of works devoted to the assessment and classification of the dimensionality of individual mineral individuals [22, 23], as well as the analysis and typification of the morphology of intergrowths in a system with known mineral associations [24, 25]. The segmen-

tation model proposed in these works achieved 98% accuracy in predicting iron ore quality and hematite recoverability, highlighting the potential of deep models in solving industrial problems.

In [14], the effectiveness of deep convolutional networks for three-dimensional mineral identification and free grain analysis was demonstrated, and in [26], the authors showed that combined analysis of optical micrographs using CNN improves the accuracy of mineral content estimation in charge. In [15], the authors improved the methods of feature downsampling, classifying rocks more accurately based on polished section images.

It is worth noting that applying modern deep learning approaches facilitates transition from image fragment classification [27] to full semantic segmentation, which allows for accurate pixel-level segmentation of images by mineral, see [17, 26] and [14, 28]. At the same time, works [14, 29] demonstrated the fundamental feasibility of creating high-quality ore mineral segmentation models with high identification accuracy (> 0.8 by to the IoU metric).

The main advantage of using deep trainable neural networks when working with images of ore samples is their ability to take into account the context of an image and adapt to the variability of mineral associations. Most importantly, it allows reliable differentiation even between minerals with very similar characteristics (pyrite–marcasite, covellite–chalcocite, etc.) without the need for permanent recalibration of the algorithm for new samples, unlike other computer vision methods. However, there are still relatively few studies devoted directly to the diagnostics of mineral species using such approaches. Deep learning models can also be used in conjunction with domain adaptation methods, which allow the segmentation model to be retrained on “new” images – taken with different equipment or under different lighting conditions, and thus maintain high performance even with significant variations in input data. Extensive reviews on domain adaptation [14] and examples of successful application in semantic segmentation of geological and satellite images [30, 31] confirm that this approach provides versatility and stability in a wide variety of conditions. The fundamental feature of most deep learning methods is the need for complete image annotation for training. This is often a very labor-intensive process, but the use of specialized weak supervision methods, which appear to the user as annotation the image with rough strokes (ScribbleSup [32], ScribbleSeg [33]) or clicks [34], allows in many cases to significantly speed up the collection and preparation of training data.



To build a reliable system based on deep learning, the following fundamental problems must be solved, which are discussed in detail in this paper:

1. Development of neural network methods for mineral segmentation.
2. Development of adaptive methods for image calibration and preprocessing.
3. Development of methods for joint processing of heterogeneous images.
4. Development of a method for creating panoramic images.
5. Development of auxiliary methods for processing and analyzing images of polished sections.

Research Materials and Techniques

This study used a collection of polished sections provided by the Department of Geology, Geochemistry, and Mineral Resources of the Faculty of Geology at Lomonosov Moscow State University. A Carl Zeiss AxioScope 40 polarizing microscope with a Canon PowerShot G10 camera was used to obtain images of the polished sections. All photos were taken with a magnification of $\times 50$ and have a resolution of 3396×2547 pixels.

The main drawback of existing solutions that use deep neural network models in the considered problems of analyzing photos of polished sections [23, 35], according to the authors, are the proprietary image sets used and the proprietary code base, which makes it impossible to compare the methods being developed. Therefore, all annotated (indexed) image sets created as part of the work are presented as a single open dataset LumenStone¹, and the software implementation of all developed methods is published as a petroscope² library with open source code for the Python 3 programming language.

The LumenStone image dataset contains several subsets focused on solving various image analysis problems for polished sections. The main subsets are S1, S2, and S3, which are aimed at the problem of mineral segmentation (automatic identification) and are formed taking into account mineral associations and mineral properties:

- LumenStone S1 (84 images): complex ores (galena, sphalerite, chalcopyrite, bornite, fahlore);
- LumenStone S2 (39 images): sulfide copper-nickel ores (pyrrhotite, pentlandite, chalcopyrite);
- LumenStone S3 (35 images): minerals with strong anisotropic properties (arsenopyrite, covellite).

Pixel masks of the corresponding minerals were created for all images of the datasets using Super-

visely and Adobe Photoshop software. The masks are necessary for training and testing deep learning models.

It should be noted that due to natural reasons (frequency of occurrence in nature), the collected set of images has a significant minerals imbalance (the percentage ratio is given in Table 1). This fact is an additional complication for the development of methods for automatic mineral segmentation and must be taken into account.

The authors also collected additional subsets of images necessary for solving related problems:

1. LumenStone V1: a special dataset of images of the same 10 specimens (sections) with different shooting conditions, designed for developing and testing color adaptation methods. The images were obtained using the same equipment with blue and yellow light filters, as well as using a LOMO Microsystems PLM-215 microscope with a Canon EOS 40D camera.

2. LumenStone P1: 875 images obtained for 35 polished sections. For each polished section, 25 photographs were taken with 20–30% overlap, intended for creating panoramic microscopic images.

To solve the problem of simultaneous analysis of anisotropic mineral photographs in PPL and XPL, “rotated” photographs of a single field of view were taken with the microscope stage rotation increment of 5 and 15° and additionally included in LumenStone S3.

Problems and their solutions (discussion)

The descriptions of the problems in the field of image processing and analysis that are to be considered the complex problem of automatic mineral identification in microscopic images of polished sections and the approaches proposed by the authors to solve these problems are given below.

1. Neural network methods for mineral segmentation. In this work, we consider convolutional neural networks to solve segmentation problems. Transformer-based alternatives, although promising, remain excessively resource-intensive for standard laboratory conditions [36]. Despite the good generalization ability of convolutional neural networks, they are quite sensitive to class imbalance in training dataset [37, 38], which is characteristic of the collected data (Table 1). Furthermore, neural network methods cannot be directly applied to high-resolution images due to hardware limitations. To mitigate these shortcomings, we proposed a specialized method for sampling the training dataset during the training process, which extracts small fragments from images (patches) and acts as a data balancer.

¹ LumenStone Dataset. URL: <https://imaging.cs.msu.ru/en/research/geology/lumenstone>

² GitHub. URL: <https://github.com/xubiker/petroscope>



Table 1

Distribution of minerals on labeled photographs of polished sections in the LumenStone S1, S2, and S3 sets for solving segmentation problems (the distribution when divided into training and test datasets is Provided in square brackets)

Mineral	Percentage in set S1 [training, test], %	Percentage in set S2 [training, test], %	Percentage in the S3 set [training, test], %	Total percentage (S1 + S2 + S3), %
Nonmetallic minerals	16.4 [12.6. 3.8]	9.8 [8.0. 1.8]	11.4 [8.8. 2.6]	37.6
Chalcopyrite	2.0 [1.1. 0.9]	3.1 [2.7. 0.4]	0.9 [0.6. 0.3]	6
Galena	3.9 [3.2. 0.8]	–	1.1 [0.9. 0.3]	5
Magnetite	–	0.4 [0.4. 0.1]	0.1 [0.1. < 0.1]	0.5
Bornite	2.0 [1.7. 0.3]	–	0.5 [0.4. 0.1]	2.5
Pyrrhotite	–	8.9 [6.2. 2.7]	–	8.9
Pyrite	12.9 [9.5. 3.4]	–	1.9 [1.5. 0.4]	14.8
Pentlandite	–	2.4 [1.6. 0.8]	–	2.4
Sphalerite	13.8 [10.9. 2.9]	–	0.5 [0.3. 0.2]	14.3
Arsenopyrite	–	–	3.9 [3.0. 1.0]	3.9
Tennantite	2.1 [1.6. 0.5]	–	–	2.1
Covellite	–	–	1.8 [1.4. 0.3]	1.8
Other (not used)	–	0.1	0.1	0.2

The objective of the developed sampling method is to equalize the distribution of mineral classes fed into a neural network during training. For each pair “training image – mineral type”, a matrix containing the extracted area of a selected mineral at each point in the case of selecting a patch centered at that point is calculated. The resulting set of matrices is used as probability maps when selecting patches for training. For instance, at each sampling iteration, for the mineral that is currently the least represented, 1) an image from the training sample collection is selected (proportional to the content of this mineral), 2) the center of the patch is selected in accordance with the previously calculated probability maps, 3) the patch is extracted, and 4) the information about the representation of minerals in the used data is updated. With moderate patch sizes (256–384 px), this method allows for a significant equalization of the distribution of minerals in the LumenStone S1, S2, and S3 sets that has a positive effect on the training speed of segmentation models and on the final segmentation quality metrics.

When developing neural network models for mineral segmentation, we reviewed and investigated a number of convolutional architectures, ranging from the traditional UNet [40] and its modification ResUNet [29] to more modern PSPNet [41] and UPerNet [42]. The advantage of the latter lies in the ability to analyze images at different scales, correctly identify both small and very large objects simultaneously, and take

into account local and global context that significantly improves the quality of segmentation based on the available data.

To evaluate the quality of segmentation in this work, IoU (Intersection over Union) metric was used [43]. This is one of the simplest and most common methods of geometric evaluation of segmentation when reference labeling is available. The metric takes values from the range [0, 1], where 1 corresponds to a complete match between the predicted and reference labelings (ideal case), and 0 corresponds to no intersections between the predicted and reference segmentation annotation. An IoU value greater than 0.7 is usually considered satisfactory, although this depends, of course, on the subject area.

In our case, training the PSPNet neural network with the ResNet18 encoder on the LumenStone S1 and S2 datasets, together with the class-balanced sampling method described above, allowed segmenting nine minerals and a generalized class of non-metallic minerals with very high quality (the average IoU value on the test set was 0.88). The training uses a cross-entropy loss function, random augmentations (rotation, slight changes in scale, brightness, and color), an Adam optimizer with an initial learning rate of 0.001 and a decrease upon reaching a plateau. The training took approximately 3 hours using a Nvidia A6000 GPU. An example of applying the trained mineral segmentation model to an image from a test set is shown in Fig. 1.

2. Adaptive methods for image calibration and preprocessing. One of the main problems encountered by the authors when working with primary data is high sensitivity of segmentation models to the color palette of images. Differences in color characteristics between training images and real images lead to a significant deterioration in the quality of mineral identification. The color and brightness characteristics of images are determined by many factors: microscope parameters, camera settings, lighting, etc.

A solution to this problem is to use automatic color correction based on the color difference between the received image and a known reference (e.g., [44]).

We proposed the method for correcting color distortions in [45]. The main idea is to construct a tran-

sition matrix (Color Correction Matrix, CCM) [46] between the color spaces of a distorted and reference images (images from the training set are taken as reference).

The process includes extracting the averaged colors of minerals and the background using partial labeling, linearizing colors through gamma correction ($\gamma = 2.2$), and calculating the affine transformation. The minimization problem is solved in LAB space, using the sum of the squares of color differences calculated using the CIEDE2000 formula [47] as a loss function. The work uses a 4×3 matrix with initial approximation initialization based on the “white balance” method [46]. The final step is to transform the distorted image through matrix multiplication by the previously calculated color correction matrix.

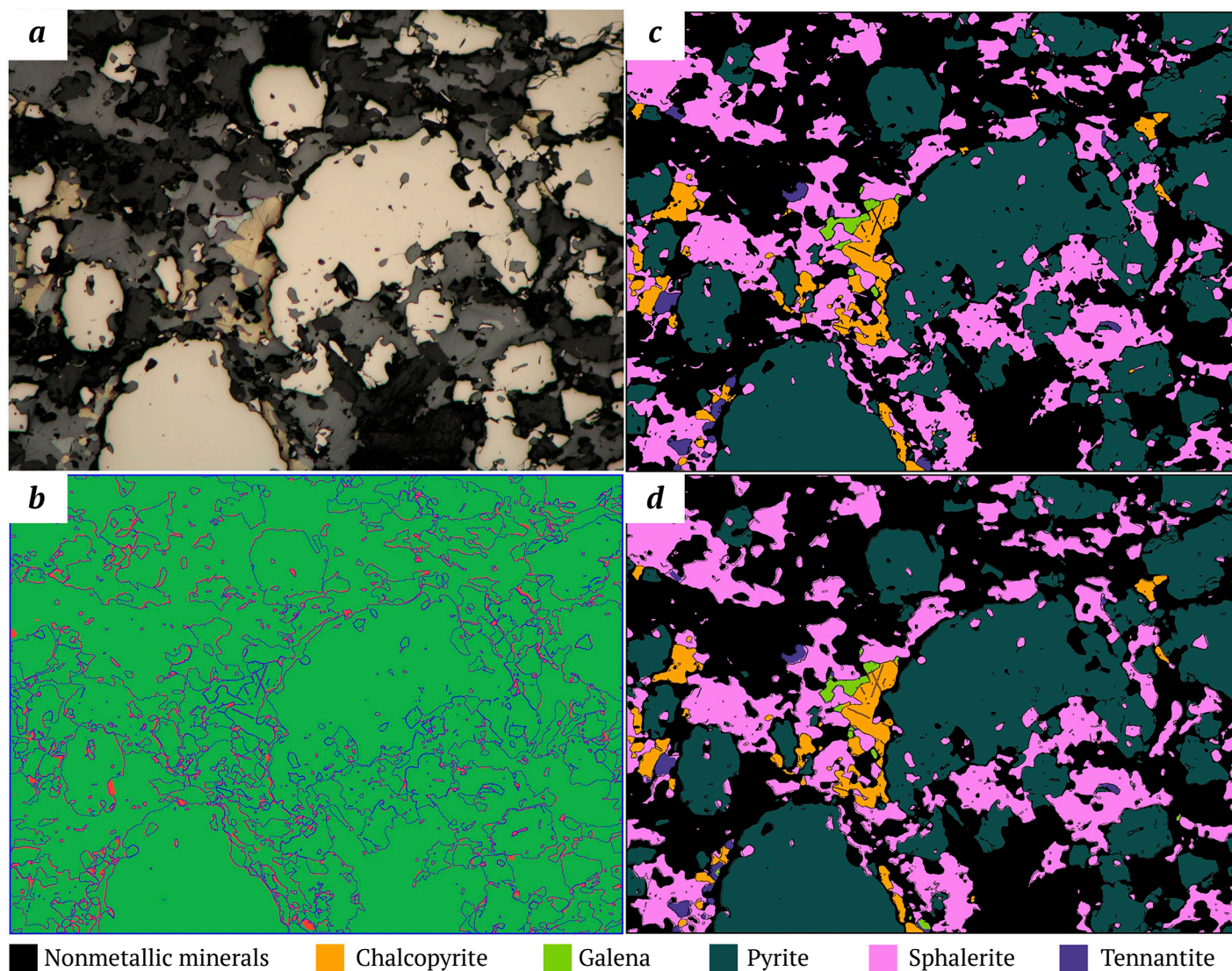


Fig. 1. Example of a polished section image segmentation with the trained PSPNet model:
a – image; *b* – error map (correctly recognized areas are highlighted in green, segmentation errors are highlighted in red);
c – mineral mask (expert annotation); *d* – model prediction

The proposed method allows preserving color differences that are critical for mineral identification (Fig. 2), while minimizing the influence of lighting changes and equipment settings. The algorithm supports two operating modes: an individual correction for each image and a “calibration” mode for a series of images, where the correction matrix is calculated once and applied to the entire group. The method does not require any prior training, and processing a single image takes less than 10 seconds on an Intel Xeon Gold 6226R CPU.

3. Methods for joint processing of heterogeneous images. Many minerals are identified not only by their color and reflectivity, but also by the presence or absence of anisotropic properties. Anisotropy manifests itself in the ability of minerals to “fade” in doubly polarized light (crossed nicols) when the optical axes of a mineral coincide with the direction of the microscope polarizers. This property is a key to distinguishing minerals with similar reflectance and color parameters. For example, pyrite (isotropic) and marcasite (anisotropic) have similar optical characteristics but differ in the manifestation

of anisotropy. Similarly, pyrite and arsenopyrite, although they have slightly different reflectivity and color, can also be reliably separated based on the manifestation of anisotropy by arsenopyrite.

We developed a neural network segmentation method that uses XPL and PPL images as additional input data for the segmentation neural network to improve the accuracy of mineral segmentation [48]. The key step in this method is to align images taken at different angles of rotation with the reference PPL image. For this purpose, SIFT algorithms [49] were used to detect stable key points in images, and RANSAC algorithm [50] was used to calculate the affine transformation between images based on the found matches. Thus, all images were referred to a single coordinate system (Fig. 3). Then XPL images referred to a single coordinate system were used as additional input channels for a neural network based on the architecture proposed earlier by the authors [29]. The used hyperparameters are described in [29], and the model training time is approximately 6 hours with the use of a Nvidia A6000 GPU.

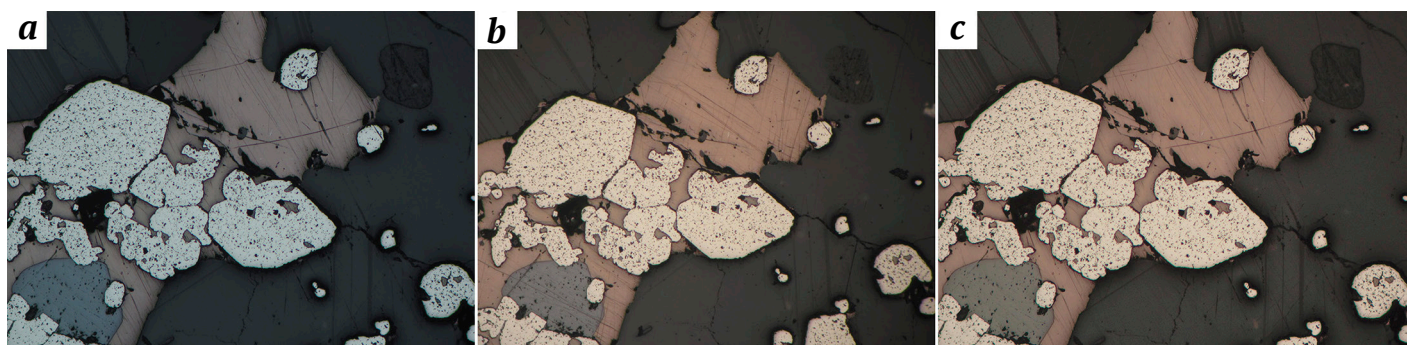


Fig. 2. An example of how the proposed color calibration method works:

a – original image taken with alternative equipment; *b* – reference image; *c* – initial image after applying the method

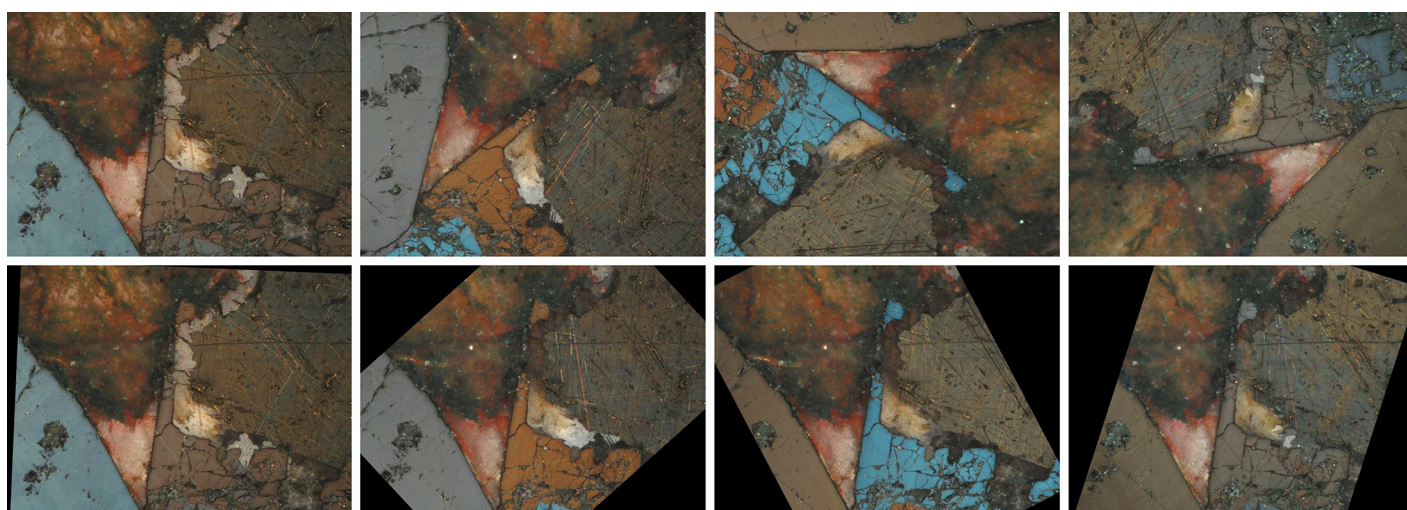


Fig. 3. Alignment of XPL images of arsenopyrite: top row – images of arsenopyrite in different orientations; bottom row – images of arsenopyrite in different orientations after alignment. Four different orientations out of 24 are presented for each image with anisotropic minerals

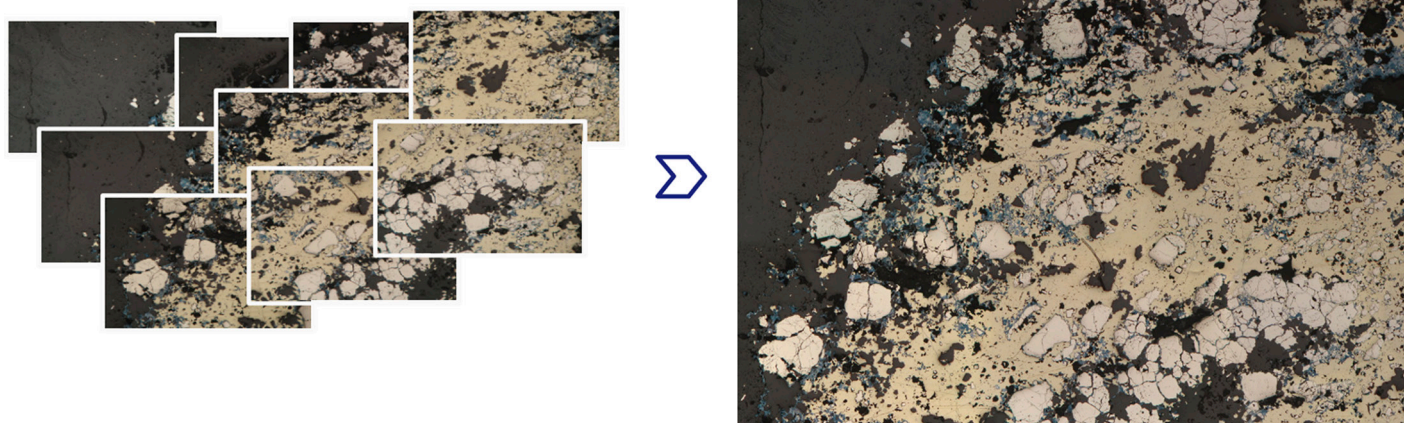


Fig. 4. Illustration of the developed method for constructing panoramas:

on the left, several images of the same polished section, taken with overlap; on the right, the constructed panorama

4. Methods for creating panoramic images.

The average polished section area is several square centimeters, with typical x50 magnification. Under such conditions, only a small part of a polished section, measuring a few square millimeters, is visible in each photograph. The use of photographs covering a large area of a sample would allow more accurate information to be obtained about the distribution of minerals in a sample and their relative positions, which would have a positive effect on the quality of the analysis.

Scanning electron microscopes (SEM) can be used to obtain large images in geology, but such equipment is very expensive, structural and textural features may be lost due to the nature of the method, and the identification of mineral phases requires additional effort. Therefore, like other researchers [51], we have opted for software stitching series of overlapping images into a single panorama.

Currently, there are many examples of software for automatic stitching disparate photos into a single panoramic image. These include Adobe Photoshop, Fiji/ImageJ, and many others. However, using third-party software has a number of disadvantages. Powerful tools such as Adobe Photoshop can overly transform a panorama (unnaturally change colors, remove important details, mistaking them for artifacts of stitching). Integrating a third-party implementation into own system is tricky and it also makes it impossible to make the changes needed to the algorithm to fit the specifics of the problem you're trying to solve.

We developed our own algorithm for stitching photographs into a panoramic image of the surface of a polished section [52] (Fig. 4). The algorithm con-

sists of two main stages: image alignment and further post-processing to improve visual perception. At the first stage, with the use of calibration images, geometric distortions of images are corrected using the Brown–Conrady model [53], and photometric distortions are corrected using flat field compensation [54]. Then, using the LoFTR neural network [55], common key points are found in images that have overlapping areas. These are used to calculate perspective transformations (homographies) for pairs of adjacent images using RANSAC [50], after which all images are transformed into the coordinates of a single image (reference image). Finally, global panorama optimization is performed to minimize the alignment errors. The result of this stage is a preliminary panorama, a collage. The second stage involves improving the initial panorama. The differences in exposure between images are compensated. The seams between images are masked by constructing the least noticeable seam using the graph-cut method [56], taking into account the differences in color and gradients of neighboring pixels. The final step is to blend the images near the joints of the panorama tiles to remove any remaining stitching artifacts. The LumenStone P1 dataset, compiled for the panorama construction, was used to test the algorithm. The method does not require prior training, and the processing speed for a single panorama consisting of 25 images at an Intel Xeon Gold 6226R CPU is approximately 5 minutes.

5. Additional methods for processing and analyzing images of polished sections. The application of deep learning methods for mineral segmentation in images requires accurate annotation of a large number of images, which is a labor-intensive process. To sim-

plify the annotation process and create a segmentation model capable of recognizing the main ore minerals, the authors are developing a method of accelerated interactive annotation using superpixel clustering based on the SLIC [57] and Felzenswalb [58] methods. A geologist roughly annotates minerals with strokes, labeling entire areas of an image with the label of a particular mineral based on the scribble data and the superpixel map. The user adjusts the method's predictions until the final annotation is obtained. A distinctive feature of this approach is multi-scale clustering, which allows to quickly label both large homogeneous areas and small fragments, automatically breaking large clusters into smaller ones as needed.

One can also reduce the labor costs of data annotating by extending the training set with partially annotated data. The main idea behind this approach is to highlight areas of uncertainty (lack of confidence) in the trained segmentation model on images. The authors suggest highlighting areas of uncertainty in images [59] using a hyperbolic radius [60] that reduces the scope of annotation to 5–10% of the original image (Fig. 5).

The final stage after recognizing and segmenting all minerals in the images is the statistical analysis of an image. It is responsible for conducting quantitative analysis to assess the areal ratio of mineral phases and their particle size analysis with separating fractions by size class for each mineral. This stage is currently under development.

Findings

The result of the authors' research into the automatic analysis of microscopic images of geological polished sections to determine mineral composition was the creation of an open image dataset called LumenStone and a number of algorithms and methods that solve the main problems encountered:

1. Neural network methods for mineral segmentation. A convolutional neural network model for mineral segmentation and a special method for

sampling training data have been developed, allowing the existing class imbalance to be neutralized. The accuracy of mineral segmentation according to the IoU metric was as follows: non-metallic minerals – 0.912, bornite – 0.938, chalcopyrite – 0.899, galena – 0.905, magnetite – 0.650, pentlandite – 0.790, pyrrhotite – 0.928, pyrite – 0.964, sphalerite – 0.922, tennantite – 0.882. The overall pixel accuracy (PA) of the segmentation was 0.96. The differences in mineral identification results can be explained by the difference in the size of the training sets used for LumenStone S1 and LumenStone S2.

2. Adaptive methods for image calibration and preprocessing. An algorithm has been developed for adapting images of polished sections obtained under different shooting conditions using partial user annotation. Pixel segmentation accuracy for distorted images increased from 0.29 (before) to 0.87 after adaptation using annotation covering approximately 30–35% of the image.

3. Methods for joint processing of heterogeneous images. The developed algorithm for segmenting anisotropic minerals using additional rotated XPL images improved the quality of anisotropic mineral segmentation by 3–12%. It has been shown that the best results can be achieved by using 6 additional rotated images.

4. Methods for creating panoramic images. A method for constructing panoramic microscopic images of polished sections has been developed. The root mean square error of alignment of panorama tiles from 25 images was 0.5–0.6 px. The resulting panoramas have a resolution of 12000×8000 pixels and can be used for automatic mineral segmentation. The implemented method does not have the disadvantages of less specialized solutions such as Adobe Photoshop, Fiji, and Panorama Studio.

5. Additional methods for processing and analyzing images of polished sections. A prototype method for interactive annotation of polished section images has been developed, which significantly speeds

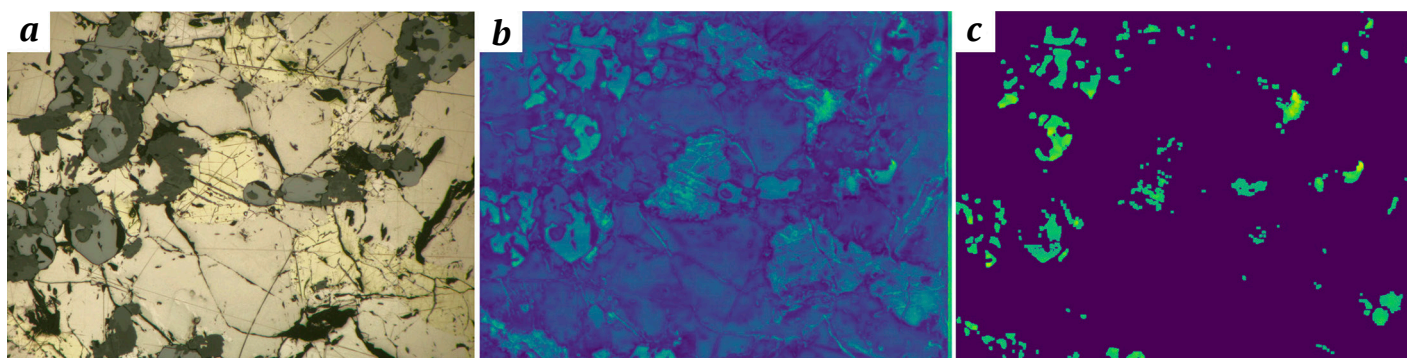


Fig. 5. The result of uncertainty area assessment method:
a – original image; b – prediction of segmentation model uncertainty areas; c – areas for manual labeling



up the process of preparing data for training segmentation models. A method for automatically searching for areas of uncertainty has also been developed, allowing image annotation to be prioritized and significantly reducing the scope of annotations required.

Conclusion

This paper presents the authors' experience in developing a set of methods for the automatic analysis of images of polished sections for the identification of ore minerals. The developed segmentation method based on a convolutional neural network is capable of identifying nine ore minerals (with correct distinguishing between ore minerals and non-metallic phases) with an IoU accuracy = 0.88 and PA = 0.96. The potential of using additional information from XPL images to increase the accuracy of anisotropic mineral identification was demonstrated.

The developed methods of interactive annotation and image adaptation significantly accelerate and improve the training and use of segmentation models on new data. It is worth noting the method developed by the authors for obtaining panoramic images of polished sections, which allows detailed images of the entire surface of polished sections to be obtained in high resolution without expensive equipment. Unlike existing software solutions, this method does not distort the final panorama that has a positive effect on the segmentation results. Wor-

king with large-format images opens up new possibilities for the automatic analysis of images of polished sections.

The results obtained justify the need for further development of the area under consideration and form the basis for the creation of an intelligent quantitative assessment system capable not only of identifying minerals and calculating their areal fractions and performing particle-size analysis by size class, but also determining the types of minerals intergrowths. The implementation of this methodology will open up new possibilities in digital petrography, enabling fast, economical, and reproducible mineralogical analysis on optical microscopes in reflected light. Ultimately, this will enable the formation of unified criteria for analyzing the structural and textural characteristics of mineral associations for genesis comparison of different deposits.

Currently, the authors are integrating most of the methods and algorithms described in this paper into their PathScribe software platform [61]. This platform is a cloud-based client-server solution with cross-platform clients for working with ultra-high-resolution images and is designed for universal use in both scientific and educational applications. The authors hope that the ability to work with panoramic images of polished sections using convenient tools for annotation and fully automatic analysis will be useful for geologists of various specializations.

References

1. De Castro B., Benzaazoua M., Chopard A., et al. Automated mineralogical characterization using optical microscopy: Review and recommendations. *Minerals Engineering*. 2022;189:107896. <https://doi.org/10.1016/j.mineng.2022.107896>
2. Duncan P., Gavyn K.R. Unlocking the applications of automated mineral analysis. *Geology Today*. 2011;27(6):226–235. <https://doi.org/10.1111/j.1365-2451.2011.00818.x>
3. Yushko S.A. *Methods of laboratory ore research*. Moscow: Nedra; 1984. 389 p. (In Russ.)
4. Craig J.R., Vaughan D.J. *Ore microscopy and ore petrography*. Manchester: A Wiley-interscience Publication; 1994. 446 p.
5. Bonifazi G. Digital multispectral techniques and automated image analysis procedures for industrial ore modelling. *Minerals Engineering*. 1995;8(7):779–794. [https://doi.org/10.1016/0892-6875\(95\)00039-S](https://doi.org/10.1016/0892-6875(95)00039-S)
6. Marschallinger R. Automatic mineral classification in the macroscopic scale. *Computers & Geosciences*. 1997;23(1):119–126. [https://doi.org/10.1016/S0098-3004\(96\)00074-X](https://doi.org/10.1016/S0098-3004(96)00074-X)
7. Berry R., Walters S.G., McMahon C. Automated mineral identification by optical microscopy. In: *Ninth International Congress for Applied Mineralogy*. Brisbane, Australia, 8–10 September 2008. Brisbane: QLD; 2008. Pp. 91–94.
8. Shoji T., Keneda H. An interactive system to assist mineral identification in ore microscopy. *Mathematical Geology*. 1994;26:961–972. <https://doi.org/10.1007/BF02083424>
9. López-Benito A., Catalina J.C., Alarcón D., et al. Automated ore microscopy based on multispectral measurements of specular reflectance. I—A comparative study of some supervised classification techniques. *Minerals Engineering*. 2020;146:106136. <https://doi.org/10.1016/j.mineng.2019.106136>
10. Berrezueta E., Ordóñez-Casado B., Bonilla W., Banda R., Castroviejo R., Carrión P., Puglla S. Ore petrography using optical image analysis: application to Zaruma-Portovelo deposit (Ecuador). *Geosciences*. 2016;6(2):30. <https://doi.org/10.3390/geosciences6020030>



11. Köse C., Alp I., İkibaş C. Statistical methods for segmentation and quantification of minerals in ore microscopy. *Minerals Engineering*. 2012;30:19–32. <https://doi.org/10.1016/j.mineng.2012.01.008>
12. Krawczykowska A., Trybalski K., Krawczykowski D. The application of modern techniques and measurement devices for identification of copper ore types and their properties. *Archives of Mining Sciences*. 2013;58(2):433–448. <https://doi.org/10.2478/amsc-2013-0029>
13. Iglesias J.C.A., Augusto K.S., Gomes O.D.F.M., et al. Automatic characterization of iron ore by digital microscopy and image analysis. *Journal of Materials Research and Technology*. 2018;7(3):376–380. <https://doi.org/10.1016/j.jmrt.2018.06.014>
14. Tang K., Chen J., Zhou H., Liu J. Deep convolutional neural network for 3D mineral identification and liberation analysis. *Minerals Engineering*. 2022;183:107592. <https://doi.org/10.1016/j.mineng.2022.107592>
15. Zhou Z., Yuan H., Cai X. Rock Thin section image identification based on convolutional neural networks of adaptive and second-order pooling methods. *Mathematics*. 2023;11(5):1245. <https://doi.org/10.3390/math11051245>
16. Kirillov A., Mintun E., Ravi N., et al. Segment anything. In: *Proceedings of the IEEE/CVF International Conference on Computer Vision*. 2023;4015–4026. <https://doi.org/10.48550/arXiv.2304.02643>
17. Hatamizadeh A., Kautz J. Mambavision: A hybrid mamba-transformer vision backbone. arXiv preprint arXiv: 2407.08083. 2024. <https://doi.org/10.48550/arXiv.2407.08083>
18. Liu M.W., Lin Y.H., Lo Y.C., et al. Defect Detection of grinded and polished workpieces using faster R-CNN. In: *Proceedings of the IEEE Conference on Computer Vision and Pattern Recognition*. 2021. Pp. 1290–1296. <https://doi.org/10.1109/AIM46487.2021.9517664>
19. Zhongliang L.V., Zhenyu Lu., Kewen Xia., et al. LAACNet: Lightweight adaptive activation convolution network-based defect detection on polished metal surfaces. *Engineering Applications of Artificial Intelligence*. 2024;133(E):108482. <https://doi.org/10.1016/j.engappai.2024.108482>
20. Sivkova T., Gusev A., Syropyatov A. Technology for cast iron microstructure analysis in SIAMS software using neural networks. In: *Proceedings of the 31st International Conference on Computer Graphics and Vision*. September 27–30, 2021, Nizhny Novgorod, Russia. 2021;2:772–780.
21. Amaral B., Soares A.K., Iglesias J.C.Á., Caldas T.D.P., Santos R.B.M., Paciornik S. Instance segmentation of quartz in iron ore optical microscopy images by deep learning. *Minerals Engineering*. 2024;211:108681. <https://doi.org/10.1016/j.mineng.2024.108681>
22. Maitre J., Bouchard K., Bédard L.P. Mineral grains recognition using computer vision and machine learning. *Computers & Geosciences*. 2019;130:84–93. <https://doi.org/10.1016/j.cageo.2019.05.009>
23. Song Y., Huang Z., Shen C., et al. Deep learning-based automated image segmentation for concrete petrographic analysis. *Cement and Concrete Research*. 2020;135:106118. <https://doi.org/10.1016/j.cemconres.2020.106118>
24. Donskoi E., Hapugoda S., Manuel J.R., et al. Automated optical image analysis of iron ore sinter. *Minerals*. 2021;11(6):562. <https://doi.org/10.3390/min11060562>
25. Donskoi E., Poliakov A. Advances in optical image analysis textural segmentation in ironmaking. *Applied Sciences*. 2020;10(18):6242. <https://doi.org/10.3390/app10186242>
26. Santoro L., Lezzerini M., Aquino A., et al. A novel method for evaluation of ore minerals based on optical microscopy and image analysis: preliminary results. *Minerals*. 2022;12(11):1348. <https://doi.org/10.3390/min12111348>
27. Su C., Wang Y., Zhu J., Zhang X.C. Rock classification in petrographic thin section images based on concatenated convolutional neural networks. *Earth Science Informatics*. 2020;13:1477–1484. <https://doi.org/10.1007/s12145-020-00505-1>
28. Tang H., Wang H., Wang L., et al. An improved mineral image recognition method based on deep learning. *JOM*. 2023;75:2590–2602. <https://doi.org/10.1007/s11837-023-05792-9>
29. Khvostikov A.V., Korshunov D.M., Krylov A.S., Boguslavskii M.A. Automatic identification of minerals in images of polished sections. *The International Archives of the Photogrammetry, Remote Sensing and Spatial Information Sciences*. 2021;XLIV-2/W1-2021:113–118. <https://doi.org/10.5194/isprs-archives-XLIV-2-W1-2021-113-2021>
30. Chen H., Zhang H., Yang G.A., Zhang L. Mutual information domain adaptation network for remotely sensed semantic segmentation. In: *IEEE Transactions on Geoscience and Remote Sensing*. 2022;60:1–16. <https://doi.org/10.1109/TGRS.2022.3203910>
31. Nasim M.K., Tannistha M., Shrivastava A., Singh T. Seismic facies analysis: a deep domain adaptation approach. In: *IEEE Transactions on Geoscience and Remote Sensing*. 2020;60:1–16. <https://doi.org/10.1109/TGRS.2022.3151883>



32. Lin D., Dai J., Jia J., et al. Scribblesup: Scribble-supervised convolutional networks for semantic segmentation. In: *Proceedings of the IEEE Conference on Computer Vision and Pattern Recognition*. Las Vegas, NV, USA; 2016. Pp. 3159–3167. <https://doi.org/10.1109/CVPR.2016.344>
33. Chen X., Cheung Y.S.J., Lim S.N., Zhao H. *ScribbleSeg: Scribble-based interactive image segmentation*. arXiv preprint arXiv: 2303.11320. 2023. <https://doi.org/10.48550/arXiv.2303.11320>
34. Cheng B., Parkhi O., Kirillov A. Pointly-supervised instance segmentation. In: *IEEE/CVF Conference on Computer Vision and Pattern Recognition (CVPR)*. New Orleans, LA, USA; 2022. Pp. 2617–2626. <https://doi.org/10.1109/CVPR52688.2022.00264>
35. Tang H., He L., Huang B., et al. Segmentation and labeling of polished section images based on deep learning. *Mining, Metallurgy & Exploration*. 2025;42:1053–1063. <https://doi.org/10.1007/s42461-025-01205-4>
36. Tabani H., Balasubramaniam A., Marzbanet S., et al. Improving the efficiency of transformers for resource-constrained devices. In: *24th Euromicro Conference on Digital System Design (DSD)*. Palermo, Italy; 2021. Pp. 449–456. <https://doi.org/10.1109/DSD53832.2021.00074>
37. Bressan P.O., Junior J.M. Martins J.A.C., et al. Semantic segmentation with labeling uncertainty and class imbalance. *International Journal of Applied Earth Observation and Geoinformation*. 2022;108:102690. <https://doi.org/10.1016/j.jag.2022.102690>
38. Li Z., Kamnitsas K., Glocker B. Analyzing overfitting underclass imbalance in neural networks for image segmentation. In: *IEEE Transactions on Medical Imaging*. 2021;40(3):1065–1077. <https://doi.org/10.1109/TMI.2020.3046692>
39. Kochkarev A., Khvosticov A., Korshunov D., Boguslavskii M. Data balancing method for training segmentation neural networks. In: *Proceedings of the 30th International Conference on Computer Graphics and Machine Vision (GraphiCon 2020)*. Saint Petersburg, Russia, 22–25 September. Saint Petersburg: Ceur Workshop Proceedings; 2020.
40. Ronneberger O., Fischer P., Brox T. U-Net: Convolutional networks for biomedical image segmentation. In: Navab N. *Medical Image Computing and Computer-Assisted Intervention – MICCAI 2015*. Cham: Springer; 2015. Pp. 234–41. https://doi.org/10.1007/978-3-319-24574-4_28
41. Zhao H., Shi J., Qi X., et al. Pyramid scene parsing network. In: *Proceedings of the IEEE Conference on Computer Vision and Pattern Recognition*. Honolulu, HI, USA; 2017. Pp. 2881–2890. <https://doi.org/10.1109/CVPR.2017.660>
42. Xiao T., Liu Y., Zhou B., et al. Unified perceptual parsing for scene understanding. In: Ferrari V., Hebert M., Sminchisescu C., Weiss Y. (eds.) *Computer Vision – ECCV 2018. ECCV 2018. Lecture Notes in Computer Science. Vol 11209*. Springer, Cham; 2018. Pp. 418–434. https://doi.org/10.1007/978-3-030-01228-1_26
43. Rezatofighi H., Tsoi N., Gwak J., et al. Generalized intersection over union: A metric and a loss for bounding box regression. In: *Proceedings of the IEEE*. 2019. Pp. 658–666. <https://doi.org/10.48550/arXiv.1902.09630>
44. Reinhard E., Adhikhmin M., Gooch B., Shirley P. Color transfer between images. *IEEE Computer Graphics and Applications*. 2001;21(5):34–41. <https://doi.org/10.1109/38.946629>
45. Indychko O.I., Khvostikov A.V., Korshunov D.M., Boguslavskii M.A. Color adaptation in images of polished sections of geological specimens. *Computational Mathematics and Modeling*. 2022;33:487–500. <https://doi.org/10.1007/s10598-023-09588-z>
46. Wolf S. *Color correction matrix for digital still and video imaging systems*. Washington, D.C.: National Telecommunications and Information Administration; 2003. 28 p.
47. Sharma G., Wu W., Dalal E.N. The CIEDE2000 color-difference formula: Implementation notes, supplementary test data, and mathematical observations. *Color Research & Application*. 2005;30(1):21–30. <https://doi.org/10.1002/col.20070>
48. Razzhivina D.I., Korshunov D.M., Boguslavskiy M.A., et al. Registration and segmentation of PPL and XPL images of geological polished sections containing anisotropic minerals. *Computational Mathematics and Modeling*. 2024;34:16–26. <https://doi.org/10.1007/s10598-024-09592-x>
49. Lowe D.G. Distinctive image features from scale invariant keypoints. *International Journal of Computer Vision*. 2004;60:91–110. <https://doi.org/10.1023/B:VISI.0000029664.99615.94>
50. Fischler M.A., Bolles R.C. Random sample consensus: a paradigm for model fitting with applications to image analysis and automated cartography. *Communications of the ACM*. 1981;24(6):381–395.
51. Ro S.-H., Kim S.-H. An image stitching algorithm for the mineralogical analysis. *Minerals Engineering*. 2021;169:106968. <https://doi.org/10.1016/j.mineng.2021.106968>



52. Nikolaev G., Korshunov D., Khvostikov A. Automatic stitching of panoramas for geological images of polished sections. *ISPRS Annals of the Photogrammetry, Remote Sensing and Spatial Information Sciences*. 2024;X-2/W1-2024:39–46. <https://doi.org/10.5194/isprs-annals-X-2-W1-2024-39-2024>
53. Brown D. C. Decentering distortion of lenses. *Photogrammetric Engineering*. 1966;32(3):444–462.
54. Seibert J. A., Boone J. M., Lindfors K. K. Flat-field correction technique for digital detectors. In: *Proceedings of SPIE, Medical Imaging 1998: Physics of Medical Imaging*. 1998:3336;348–354. <https://doi.org/10.1117/12.317034>
55. Sun J., Shen Z., Wang Y., et al. LoFTR: Detector-free local feature matching with transformers. In: *Proceedings of the IEEE/CVF Conference on Computer Vision and Pattern Recognition (CVPR)*. 2021. Pp. 8922–8931. <https://doi.org/10.48550/arXiv.2104.00680>
56. Boykov Y., Kolmogorov V. An experimental comparison of min-cut/max-flow algorithms for energy minimization in vision. In: *IEEE Transactions on Pattern Analysis and Machine Intelligence*. 2004;26(9):1124–1137. <https://doi.org/10.1109/TPAMI.2004.60>
57. Achanta R., Shaji A., Smith K., et al. SLIC superpixels compared to state-of-the-art superpixel methods. In: *IEEE Transactions on Pattern Analysis and Machine Intelligence*. 2012;34(11):2274–2282. <https://doi.org/10.1109/TPAMI.2012.120>
58. Felzenszwalb P. F., Huttenlocher D. P. Efficient graph-based image segmentation. *International Journal of Computer Vision*. 2004;59:167–181. <https://doi.org/10.1023/B:VISI.0000022288.19776.77>
59. Indychko O., Korshunov D., Khvostikov A. Using uncertainty to expand training sets for mineral segmentation in geological images. *The International Archives of the Photogrammetry, Remote Sensing and Spatial Information Sciences*. 2025. In press.
60. Franco L., Mandica P., Kallidromitis K., et al. Hyperbolic Active Learning for Semantic Segmentation under Domain Shift. In: *Proceedings of the 41st International Conference on Machine Learning*. 2024. <https://doi.org/10.48550/arXiv.2306.11180>
61. Khvostikov A., Ippolitov V., Krylov A., et al. PathScribe: new software to work with whole slide histological images for education and research. In: *Proceedings of the 2023 8th International Conference on Biomedical Imaging, Signal Processing*. Singapore: ACM; 2023. Pp. 63–70. <https://doi.org/10.1145/3634875.3634884>

Information about the authors

Dmitrii M. Korshunov – Cand. Sci. (Geol. and Miner.), Researcher, Geological Institute of the Russian Academy of Sciences (GIN RAS), Moscow, Russian Federation; ORCID [0000-0002-8500-7193](https://orcid.org/0000-0002-8500-7193); e-mail dmit0korsh@gmail.com

Alexander V. Khvostikov – Cand. Sci. (Phys. and Math.), Senior Researcher of the Laboratory of Mathematical Methods for Image Processing, Faculty of Computational Mathematics and Cybernetics (CMC), Lomonosov Moscow State University, Moscow, Russian Federation; ORCID [0000-0002-4217-7141](https://orcid.org/0000-0002-4217-7141), Scopus ID [57188856261](https://orcid.org/57188856261); e-mail khvostikov@cs.msu.ru

Gleb V. Nikolaev – M. Sc. Student, Faculty of Computational Mathematics and Cybernetics (CMC), Lomonosov Moscow State University, Moscow, Russian Federation; ORCID [0009-0003-0814-3997](https://orcid.org/0009-0003-0814-3997); e-mail nickolaev.gleb03@gmail.com

Dmitry V. Sorokin – Cand. Sci. (Phys. and Math.), Senior Researcher of the Laboratory of Mathematical Methods for Image Processing, Faculty of Computational Mathematics and Cybernetics, Lomonosov Moscow State University, Moscow, Russian Federation; ORCID [0000-0003-3299-2545](https://orcid.org/0000-0003-3299-2545); e-mail dsorokin@cs.msu.ru

Olesya I. Indychko – PhD-Student, Faculty of Computational Mathematics and Cybernetics (CMC), Lomonosov Moscow State University, Moscow, Russian Federation; ORCID [0009-0007-0936-4088](https://orcid.org/0009-0007-0936-4088); e-mail olesyaindychko@gmail.com

Mikhail A. Boguslavskii – Cand. Sci. (Geol. and Miner.), Associate Professor of the Department of Geology, Geochemistry and Mineral Economics, Faculty of Geology, Lomonosov Moscow State University, Moscow, Russian Federation; ORCID [0000-0003-0133-7185](https://orcid.org/0000-0003-0133-7185), ResearcherID [V-4671-2017](https://orcid.org/V-4671-2017); e-mail mboguslavskiy@yandex.ru

Andrey S. Krylov – Dr. Sci. (Phys. and Math.), Professor, Head of the Laboratory of Mathematical Methods for Image Processing, Faculty of Computational Mathematics and Cybernetics, Lomonosov Moscow State University, Moscow, Russian Federation; ORCID [0000-0001-9910-4501](https://orcid.org/0000-0001-9910-4501), Scopus ID [7202280261](https://orcid.org/7202280261), ResearcherID [B-9651-2014](https://orcid.org/B-9651-2014); e-mail kryl@cs.msu.ru

Received 30.05.2025

Revised 05.07.2025

Accepted 07.07.2025



GEOLOGY OF MINERAL DEPOSITS

Review paper

<https://doi.org/10.17073/2500-0632-2025-06-422>

UDC 550.8:551.4



Analysis of a digital terrain model for solving geological problems by the example of Aktogai ore field

N. Seib^{1,2}  , Yu. Belov³ , N. Zimanovskaya²  , G. Orazbekova⁴ ,
A. Tretyakova⁵  , A. Muratova²  , I. Kasenov³ 


¹ KeplerGroup LLP, Almaty, Republic of Kazakhstan

² D. Serikbayev East Kazakhstan Technical University, Ust-Kamenogorsk, Republic of Kazakhstan

³ KazGeoExploration LLP, Astana, Republic of Kazakhstan

⁴ Shakarim University, Semey, Republic of Kazakhstan

⁵ Biruk-Altyn LLP, Almaty, Republic of Kazakhstan

 nata_zim@mail.ru

Abstract

The formation of terrain reflects a combination of geological processes, including tectonics, magmatism, and erosion. A digital terrain model (DTM) is an important tool for solving geological problems, including the prediction of ore deposits, especially in areas of low exploration maturity. The paper discusses the surface imprinting of geological processes that form a terrain, and also considers a method of digital terrain model analysis. The presented method allows identifying specific landforms similar to those formed above known deposits that makes it possible to add one more prospecting criterion when prospecting for porphyry deposits and deposits formed under similar conditions. The Aktogai ore field was selected as the object for studying the terrain above the known deposits. The Aktogai ore field is located in the northeastern part of Near-Balkhash territory. It includes two major porphyry copper deposits, Aktogai and Aidarly, a small copper deposit Kyzylkia, as well as a number of copper and polymetallic occurrences of porphyry and vein types associated with the Koldar granite massif of the “variegated batholith” formation. All objects identified within the Aktogai ore field were formed under specific structural conditions of ore formation and were affected by erosion processes to varying degrees. This, in turn, is expressed by the presence of local landforms of these objects on the day surface, which are characterized by different “terrain energy” factors. Analysis of the DTM surface allows not only to identify local landforms above an ore body and their morphological features, but also to indirectly assess the erosional truncation of the ore body. Based on morphological characteristics, it is also possible to classify host rocks lithological units. An assessment of the applicability of the method depending on the characteristics of an ore body and an indirect assessment of the tectonic conditions of deposit formation are provided. It has been established that large ore deposits (Aktogai, Aidarly, Zapadny Stockwork) manifest themselves in the terrain as local cauldron subsidences. These zones are characterized by a high degree of textural heterogeneity and coincide with areas of intense metasomatism. Areas morphologically and spectrally similar to the areas of known ore bodies have been identified, indicating their potential for further exploration. DTM and textural analysis methods allow identifying geological and structural features associated with porphyry systems and serve as an additional tool for predicting new ore bodies/deposits. The integration of morphometric (physiographic) and spectral analysis increases the reliability of the interpretation of geological processes.

Keywords

digital terrain model (DTM), Aktogai ore field, porphyry copper deposit, Koldar massif, textural analysis, satellite data, ring structures, radial structures

Financing

This work was performed with state financing backing from the Ministry of Science and Higher Education of the Republic of Kazakhstan (grant No. AR 23484205).

Acknowledgements

We would like to express our gratitude to the entire geological team of KAZ Minerals Aktogai LLP and, in particular, to Chief Geologist Sofia Adamopoulos for their interest and support in conducting a series of researches, which resulted in this paper. We would also like to express our gratitude to the director and founders of Geokhimeksploraishn LLP, Yuri Anatolyevich Barabash and Ruslan Rafkatovich Ivlev, and to the Chief Geologist of KAZ Minerals LLP, Alexander Grigoryevich Rassokhin, for their professional advices and support in conducting the research work.

For citation








Seib N., Belov Yu., Zimanovskaya N., Orazbekova G., Tretyakova A., Muratova A., Kasenov I. Analysis of a digital terrain model for solving geological problems by the example of Aktogai ore field. *Mining Science and Technology (Russia)*. 2025;10(3):245–261. <https://doi.org/10.17073/2500-0632-2025-06-422>



ГЕОЛОГИЯ МЕСТОРОЖДЕНИЙ ПОЛЕЗНЫХ ИСКОПАЕМЫХ

Обзорная статья

Анализ цифровой модели рельефа для решения геологических задач на примере Актогайского рудного поля

Н. Сайб^{1,2}  , Ю. Белов³ , Н. Зимановская²  , Г. Оразбекова⁴ ,
А. Третьякова⁵ , А. Муратова²  , И. Касенов³ ¹ ТОО «KeplerGroup», г. Алматы, Республика Казахстан² Восточно-Казахстанский технический университет им. Д. Серикбаева, г. Усть-Каменогорск, Республика Казахстан³ ТОО «KazGeoExploration», г. Астана, Республика Казахстан⁴ Университет Шакарима, г. Семей, Республика Казахстан⁵ ТОО «Бирюк-Алтын», г. Алматы, Республика Казахстан nata_zim@mail.ru

Аннотация

Формирование рельефа отражает совокупность геологических процессов, включая тектонику, магматизм и эрозию. Цифровая модель рельефа (ЦМР) является важным инструментом при решении геологических задач, включая прогнозирование рудных объектов, особенно в условиях недостаточной геологической изученности территории. В статье рассмотрено отражение на поверхности геологических процессов, формирующих рельеф, также рассмотрен метод анализа цифровой модели рельефа (ЦМР). Представленный метод позволяет выделять особые формы рельефа, подобные тем, что были сформированы над известными месторождениями, что дает возможность добавить еще один поисковый признак при поисках порфириновых месторождений и месторождений, образованных в схожих условиях формирования. Объектом для изучения рельефа над сформированными месторождениями было выбрано Актогайское рудное поле. Актогайское рудное поле расположено в Северо-Восточном Прибалхашье. Оно включает в себя два крупнейших медно-порфириновых месторождения – Актогай и Айдарлы, мелкое медное месторождение Кызылкия, а также ряд медных и полиметаллических проявлений порфириновой и жильной формации, приуроченных к Колдарскому массиву гранитоидов формации «пестрых батолитов». Все объекты, выявленные в пределах Актогайского рудного поля, были сформированы в определенных структурных условиях рудообразования и в разной степени затронуты эрозийными процессами. Это, в свою очередь, выражено наличием локальных форм рельефа этих объектов на дневной поверхности, которые характеризуются различными коэффициентами «энергии рельефа». Анализ поверхности ЦМР позволяет не только выделить надрудные локальные формы рельефа и их морфологические особенности, но и косвенно оценить эрозионный срез рудного объекта. По морфологическим признакам также можно разделить литологические разности вмещающих пород. Дана оценка применимости метода в зависимости от характеристик объекта, и косвенная оценка тектонической обстановки формирования месторождений. Установлено, что крупные рудные объекты (Актогай, Айдарлы, Западный штокверк) выражаются в рельефе как локальные понижения кальдерообразной формы. Эти зоны характеризуются высокой степенью текстурной неоднородности и совпадают с областями интенсивного метасоматоза. Выделены участки, морфологически и спектрально сходные с известными рудными телами, что указывает на их перспективность для дальнейших поисков. ЦМР и методы текстурного анализа позволяют выявлять геолого-структурные признаки, ассоциированные с порфириновыми системами, и служат дополнительным инструментом при прогнозировании новых рудных объектов. Интеграция морфометрического и спектрального анализа повышает достоверность интерпретации геологических процессов.

Ключевые слова

цифровая модель рельефа (ЦМР), Актогайское рудное поле, медно-порфириновое месторождение, Колдарский массив, текстурный анализ, спутниковые данные, кольцевые, радиальные структуры

Финансирование

Данная работа была выполнена при финансовой поддержке Министерства науки и высшего образования Республики Казахстан (грант №AR 23484205).

Благодарности

Выражаем благодарность всему геологическому коллективу ТОО «KAZ Minerals Aktogay» и непосредственно главному геологу Софии Адамопулос за проявленный интерес и поддержку в проведении целого ряда научно-исследовательских работ, результатом которых и явилась настоящая статья. Также выражаем благодарность директору и учредителям компании ТОО «Геохимэксплорэйшн» Юрию Анатольевичу Барабашу, Руслану Рафкатовичу Ивлеву и главному геологу ТОО «KAZ Minerals» Александру Григорьевичу Рассохиному за профессиональные консультации и поддержку в проведении исследовательских работ.

Для цитирования

Seib N., Belov Yu., Zimanovskaya N., Orazbekova G., Tretyakova A., Muratova A., Kassenov I. Analysis of a digital terrain model for solving geological problems by the example of Aktogai ore field. *Mining Science and Technology (Russia)*. 2025;10(3):245–261. <https://doi.org/10.17073/2500-0632-2025-06-422>



Introduction

The analysis of physiographic structures is necessary for solving many geological problems. A present-day terrain is usually an indication, manifestation of several superimposed geological processes. The identification of individual landforms and analysis of their relative positions make it possible to establish the frequency of occurring geological processes/phenomena in a region. Accordingly, specific geological tasks involve identifying individual landforms: this includes identifying the outlines and structural positions of the objects under study, their relative location and scale of manifestation, as well as certain physiographic features, such as assessing erosion processes, which in turn indicate tectonic changes in the region. In some cases, it is necessary to distinguish regional terrain, while in others, local landforms need to be distinguished. A wealth of experience has been accumulated in recognizing and interpreting landforms to reconstruct various geological processes [1–3].

With the development of matrix electronic models of elevation surfaces and computer technologies, new opportunities for analysis have emerged [4–6]. Elevation matrices can be constructed using radar data, through reconstructing the terrain using stereoscopic pair images, or by obtaining elevation data using GPS and laser technologies. These methods are often combined and supplemented with information from various sources [7, 8]. The ability to use both absolute and relative elevation values allows not only for a qualitative assessment of objects, but also for a quantitative assessment of certain processes [9, 10].

The aim of this study is to develop a methodology for interpreting the geomorphological features of the formation and erosion of porphyry copper deposits based on a digital terrain model (DTM) and textural analysis, with the subsequent application of the findings to identify mineralization prospects using the Aktogai ore field as a reference example.

The study proposes using terrain parameters as an additional prospecting criterion for assessing the tectonic setting, the depth of the erosional truncation, and the spatial position of ore bodies relative to daylight surface. The novelty of the study lies in the integration of DTM analysis, textural characteristics, and satellite image classification data for a comprehensive forecast of metasomatic alteration zones and potential valuable mineralization.

In performing this study, we set the following tasks:

- Conducting a geological and structural analysis of the Aktogai ore field and justify its selection as a reference site for assessing the terrain above porphyry deposits;

- Building and interpreting a digital terrain model (DTM) based on GeoEye-1 satellite data and other sources, identifying local depressions and residual surface;

- Performing textural analysis of the terrain (including entropy, skewness, terrain energy, etc.) in order to identify structural and lithological nonuniformities;

- Comparing the results of the terrain analysis with known areas of metasomatic alteration and ore stockworks, identifying relationships between terrain physiography and erosion depth;

- Classifying spectral data to identify lithological units and secondary mineral halos, comparing with the results of the terrain analysis;

- Evaluating the informative value of each method and proposing an integrated approach to predicting prospects with signs of valuable mineralization.

The example below demonstrates the feasibility of using terrain analysis to solve geological problems. The study was carried out by the example of the Aktogai ore field, located in the Ayagoz district of the East Kazakhstan region. The basis is finding a background (regional) surface that simultaneously provides information about the regional terrain or relative to which it is possible to calculate the residual (remaining) surface for distinguishing local surface landforms and analyzing the textural features of the terrain.

1. Geological position and fundamentals

The Aktogai group of porphyry copper-molybdenum deposits, Aktogai, Aidarly, and Kyzylkya, are located northeast of Balkhash Lake in Eastern Kazakhstan, 450 km northeast of Almaty. Together, they have total resources of more than 3 billion tons of ore containing more than 10 million tons of copper and about 60 tons of gold.

There is a considerable interest in studying the patterns of porphyry mineralization in the Central Asian region. A body of research conducted in recent years reveals a clear pattern linking mineralization to specific regional structural and tectonic conditions. Based on the studies reconstructing the geological conditions in the region [11, 12], patterns in the distribution of known large porphyry copper systems in the Asian region were identified [13, 14].

Porphyry-epithermal mineral systems are mainly considered to form in magmatic arcs (both continental and oceanic) associated with active continental margins [15, 16]. The Aktogai ore field located on the active margin of the Balkhash-Ili volcanic-plutonic belt of the Kazakh-Mongolian magmatic arc and associated with the post-collision intrusive complex of the early Late Paleozoic (Fig. 1) [12] is no exception.

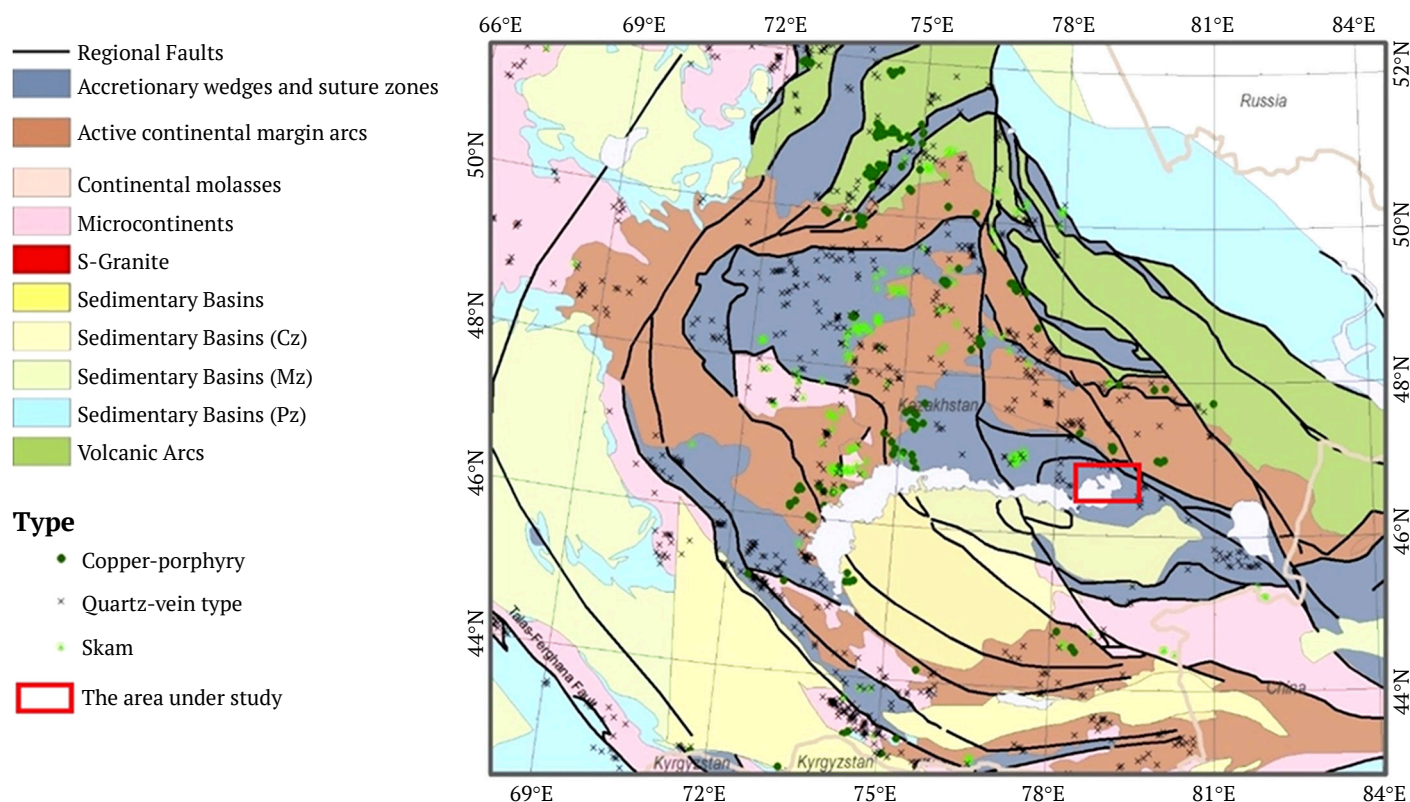


Fig. 1. Location of the study area on the geological map of the Balkhash-Dzungarian metallogenic province (modified from Windley et al., 2007)

It is assumed that in all cases, the deposits were formed at shallow crustal levels: <1.5 km for epithermal systems and <6 km for porphyry systems. Due to their shallow depth, the deposits are subject to relatively rapid erosion and have low conservation potential that explains why such geologically old (Paleozoic or older) deposits are rare. Mineralization formed in porphyry-epithermal mineral systems is usually spatially and temporally associated with intermediate and felsic subaerial volcanic rocks and corresponding subvolcanic intrusions.

The ore-forming intrusions of the Aktogai deposit were formed in an arc setting 331.4–327.5 million years ago as a result of partial melting of the thickened, eclogitized, and sulfide-rich juvenile lower crust [17]. The ore-bearing Koldar pluton formed in an arc setting 366–336 million years ago [18] during the collision of the Siberian Platform with the Kazakh continent and the Baltic-Ural block [19] and during the closure of the Dzungarian-Balkhash Sea [20]. The Koldar massif is considered to be co-magmatic with the Keregetas volcanic complex, which formed in the late Carboniferous period.

The Koldar pluton, covering an area of 75 km², is a complex intrusion (Fig. 2) [21]. Three phases can be distinguished within the Koldar massif: 1 – gabbro-diorite, gabbro-diabase, melanocratic diorite,

quartz diorite, granodiorite; 2 – batholith granite; 3 – porphyritic microgranite, granite-porphyry (probably marginal facies of the intrusion). The massif is predominantly represented by diorites and quartz diorites [22].

The three main deposits of the Aktogai ore field are associated with stock-like granodiorite and plagiogranite porphyries intruding the extensive Late Carboniferous Koldar laccolith-like massif [23], and with a large xenolith of Carboniferous rocks within the pluton. When intruding, the ore-forming intrusions caused significant hydrothermal alteration.

The cross-sections show layers of Middle-Upper Carboniferous volcanogenic-sedimentary rocks of the Keregetas series and Upper Carboniferous-Lower Permian Koldar series. The former series consists of andesite with a small amount of rhyolite, sandstone, and siltstone, while the latter includes sedimentary rocks, volcanogenic-sedimentary rocks, and a small amount of felsic tuff [18, 24].

1.1. Aktogai Deposit

The Aktogai deposit is located in the eastern part of the Central Aktogai Massif. This pluton, a porphyritic granodiorite body, intruded through the diorite, quartz diorite, and granodiorite of the Koldar pluton. The porphyritic granodiorite is cut by an elongated stock con-

sisting of ore-bearing granodiorite and plagiogranite (tonalite) porphyries, accompanied by a series of chimney bodies of explosive breccias with quartz-biotite and sericite-tourmaline matrices, formed together with the porphyry intrusion. The magmatic complex's vein rocks represented by diorite and diabase porphyrites, quartz and dacite porphyries are not widespread. A special group is represented by small bodies and dykes of fine-grained matrix granodiorite-porphyry and glassy matrix granodiorite-porphyry, as well as large dyke-like granite bodies in the Aidarly area [25, 26].

The ore-bearing stockwork is located in the exo-contact of a porphyry stockwork, forming a cone-shaped body that tapers downward and transits at depth into a series of linear west-northwestward mineralized zones. On the surface, the ore body has an elliptical ring shape, partially exposed to the west, with a maximum diameter of about 2,500 m and a radial width of 80 to 530 m [26]. The most recent vein for-

mations, possibly already Permian, are represented by post-mineralization diabase and andesite porphyrites.

All rocks in the vicinity of the ore body area, except for late mafic dikes, were altered. The barren core of the cone consists of a siliceous zone composed of quartz bodies surrounded by a dense network of barren quartz veinlets and a thin zone of sericite-quartz alteration. At the margins, the silicified core changes into a dense zone of early potassium alteration, including potassium feldspar and biotite, which surrounds the main ring-shaped ore body. This potassium zone includes several linear intervals, which are weakly mineralized but heavily altered with feldspar and surrounded by a wide biotite halo. Phyllic alteration, characterized by the presence of quartz-(carbonate)-chlorite-sericite association, manifest itself in the form of irregular thin linear zones, confined to the contacts of granodiorite porphyry apophyses and fracturing zones along the flanks of the ore body.

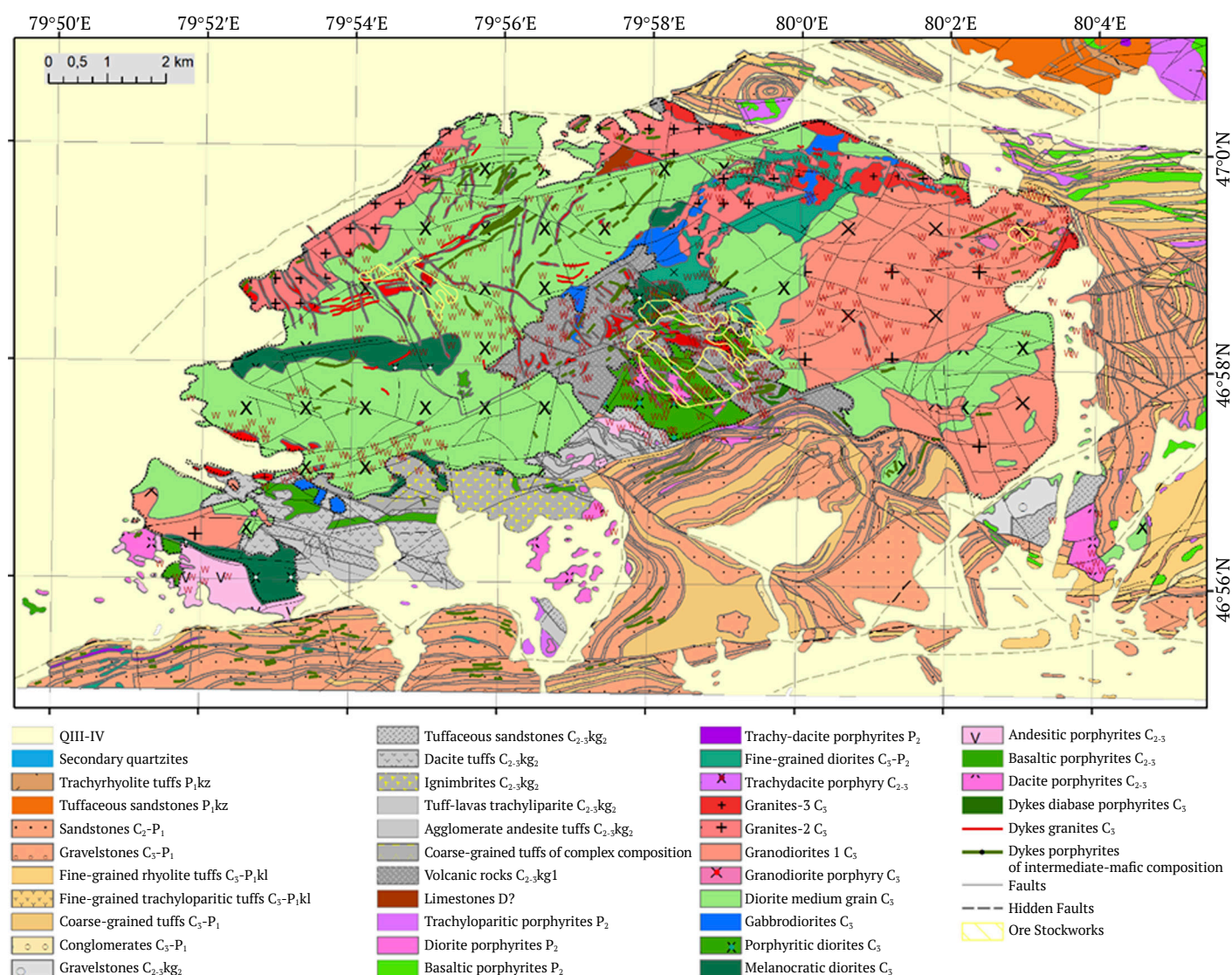


Fig. 2. Geological map of the Koldar massif (according to Sergiyko Yu.A. et al., 1980)



The periphery of the porphyry copper system is surrounded by a large propylite halo containing epidote-amphibole and albite-chlorite-prehnite. The mineralized system exhibits external zoning from bornite-chalcopryrite in the center to chalcopryrite-pyrite and pyrite halo in the outer parts. Copper and molybdenum overlap each other, while lead-zinc mineralization is limited to carbonatization zones on the sides of the ore body [27].

1.2. Aidarly deposit

The Aidarly deposit is located approximately 4 km northwest of the Aktogai deposit and lies within the same elongated 8×2 km sulfide alteration zone. It is concentrated on a small northwestern extension of ore-bringing granodiorite porphyry, which intruded into the diorite, quartz diorite, and granite phases of the Koldar pluton. The edge of the granodiorite porphyry has steep contacts characterized by numerous apophyses and is accompanied by a series of northeastward and northwestward fragmented dikes of the same composition. All these intrusions are cut through by late quartz diorites and dolerites. Small chimney breccia bodies in the vicinity of granodiorite porphyry consist of cemented fragments of mineralized rocks [27].

The mineralization is limited by the outer boundaries of the stock and the surrounding Koldar pluton and is closely associated with the stock. On the surface, the ore body is exposed in the form of an elongated northwestward ring, surrounding slightly mineralized granodiorite porphyry. Unlike Aktogai, the ore body resembles a downward-expanding cone with a barren core occupied by weakly mineralized granodiorite porphyry and a zone of silicification. The alteration and mineral zoning are similar to those described at Aktogai. The exposed granodiorite porphyry has undergone minor silicification and sericitization. At a depth of 600 m, the porphyry has a non-mineralized intensively silicified core with disseminated anhydrite at its outer edges. At the periphery of the porphyry system, silicification transits outward into a potassium alteration zone containing quartz-potassium feldspar-biotite. Higher up in the system, at medium and near-surface depths, a zone of phyllitization characterized by quartz-sericite-chlorite-carbonate association with rare tourmalinization is found. In turn, the potassium zone is surrounded by a wide halo of propylite alteration.

The Cu-Mo ore stockwork is confined to the early potassic zone, where sericitization is evident. Although most aspects of the mineralization and alteration at Aidarly are similar to those described above for Aktogai, the Aidarly deposit differs in that it has

a more extensive and better developed zone of polymetallic (Pb-Zn) veins and veinlets on the outer margins. Comparisons show that the Aidarly deposit is less eroded than the Aktogai.

1.3. Kyzylkiya deposit

The small Kyzylkiya deposit is located 4 km east of the Aktogai deposit, on the opposite side of the Aidarly deposit (see Fig. 2). At the deposit, Cu-Mo mineralization is associated with a small stock of granodiorite porphyry intruding into the granodiorites of the Koldar pluton. Ore bodies are present as en-echelon zones of chalcocite-bornite-chalcopryrite ores, accompanied by uneven kalifeldsparization-silicification and sericitization [27]. The Kyzylkiya ore stockwork is characterized by lower sulfur content than at Aktogai and Aidarly, and, accordingly, weak pyritization and significantly lower amounts of supergene chalcocite and bornite. In terms of the morphology of ore bodies, the composition and nature of metasomatic alteration, the quality of ore mineralization, and their zoning, the Kyzylkiya deposit is comparable to the root parts of the Aktogai deposit¹ that indicates deep erosion in the eastern part of the ore field.

The specific nature of metasomatic alteration at the Kyzylkiya deposit is observed. High-temperature amphibole-epidote facies propylites are developed in the form of narrow bands in the northwest and southeast of the stockwork. Medium-temperature albite-prehnite-chlorite propylites in the form of a semicircle frame the stockwork north-easterly and south-easterly². The biotitization process at the deposit is very widespread. Quartz-kalifeldspath meta-somatites with relics of the original rocks have been recorded in the south, southwest, and northwest (outside the ore stockwork). Slight kalifeldsparization is observed in the center of the ore stockwork and in the form of thin zones to the north and east beyond its boundaries. Quartz-sericite metasomatites are found only at the southern border of the ore stockwork, extending slightly beyond its limits. Argillization within the Kyzylkiya stockwork is manifested only in the southwest in the form of two narrow zones. Tourmalinization is widely manifested at the deposit, especially in its southwestern tip. Carbonatization covers almost the entire stockwork; zeolitization covers its northern part and is observed in separate patches in the south³. It should be noted that metasomatism leading to significant rock destruction (argillization, sericitization) is not very pronounced here.

¹ Ivlev R.R. Volumetric geochemical zoning of porphyry copper systems and its practical significance. [PhD Dissertation]. 1987.

² Ibid.

³ Ibid.



The Aktogai and Aidarly deposits are confined to the Aktogai deep fault zone, while the Kyzylkiya deposit is confined to the parallel Ikbass fault zone. The sulfide mineralization total area is 26 km². It has a slightly arched shape with the convex side facing south. The zone extends from west to east for about 14 km, with a width ranging from 1–1.5 to 3–3.5 km. The apparent polarizability of rocks in the anomalous zone varies from 4 to 26%.

Less significant IP anomalies are located 1–1.5 km north of the Aktogai deposit, at the same distance south of the deposit, and in the extreme southwest. Some of them correspond to small manifestations of porphyry copper formation.

1.4. Geological and lithological features affecting the terrain of porphyry deposits

The surface terrain reflects the tectonic and erosional processes occurring in a region. Assessment of the nonuniformity of the terrain, its texture, and the relative differences in erosion truncation, along with other methods, make it possible to characterize the features of the region [28, 29].

All porphyry copper deposits in Kazakhstan were formed more than 200–400 million years ago. Most of the oldest deposits were denuded as a result of repeated tectonic processes that occurred in the territory of present-day Kazakhstan. The terrain of preserved deposits turned out to be in near-surface conditions is determined not only by their original shape, but also by the lithological characteristics and wall-rock alteration of the deposits and host rocks.

1.5. Ore control structures

The formation of calderas is often associated with ore deposits, including porphyry copper, epithermal, polymetallic veins, and volcanogenic massive sulfide deposits [4]. Calderas often form above magmatic chambers because the magma inside a chamber is a large source of heat and magmatic volatiles that drive hydrothermal systems [30, 31] above magmatic chambers. As a result of heating, the rocks above a magmatic chamber undergo expansion and deformation, the nature of which depends on the heat source, the isotropy of the host medium, and the tectonic stresses that existed during the intrusion of magma into the Earth's crust. Subsequent structures are superimposed within the formed calderas, and despite the fact that over millions of years the originally formed calderas have been partially denuded and buried, their influence on the formation of the denudation terrain remains. In a relatively isotropic environment, radial and annular structures can be expected to form as magma cools.

Systems of fractures, veins, and breccias are an inevitable consequence of porphyritic magmatism. As noted by Tosdal R.M. and Richards J.P. (Tosdal R.M.,

Richards J.P., 2001), porphyritic intrusions can be cork-shaped and in some cases associated with both steeply dipping radial fractures and gentle concentric fractures reflecting stress conditions dominated by magma, where the two main horizontal stresses are almost equal that, in turn, affects the formation of the terrain above eroded porphyry systems.

Numerous examples of concentric and radial fracture systems are known in Climax-type rhyolite and porphyry deposits (molybdenum) [4, 32], but such fracture geometry is not characteristic of porphyry copper deposits. In conditions of differing horizontal stresses, subparallel dyke-like porphyry intrusions are more common [33–35]. Such conditions are more likely to reflect the stress regime in a remote area. Tabular veins and fractures ranging in size from centimeters to decimeters are characteristic of high-temperature potassium alteration zones [33, 34], but may extend to the near-surface fully developed argillitization zone. Veins D (with sericite halos) tend to be wider, more continuous, more widely spaced, and more variable in strike and dip than the earlier higher-temperature tabular veins. In some cases, they are radial [35, 36]. In some areas, such veins occupy groups of conjugated faults with minor (from meters to tens of meters) shear and normal displacements, which are concentrated on the porphyry hydrothermal system but can extend several kilometers laterally. The Main Stage veins in Butte ("Copper City", Montana, USA) extend 10 km from east to west and follow two types of faults that indicate minor compression from east to west and expansion from north to south [4].

The main structures are formed in the tension zones. Fracture systems drain ore fluids from magmatic source rocks at depth to higher levels of the Earth's crust (both epithermal and porphyry), where mineral deposition occurs, while epithermal fluids evolve during upward migration. Permeable fractures form the geometry of ore stocks. Synmineral structures displace ore systems. Post-mineral structural shears also affect the geometry of the ore system and require analysis during the exploration of displaced ores.

The resulting ore deposits may be located at different levels of the Earth's crust between a magmatic chamber and the surface. The most suitable conditions for the ascent of heated volatile substances to shallower levels of the Earth's crust occur along preferred permeable zones, such as existing regional structures (faults) or, more commonly, caldera structures. On the one hand, tension stresses above magmatic sources, destruction, and fragmentation of rocks create caudron subsidence landforms; on the other hand, fluids flow along existing structures resulting in the superimposition of structures and the enlargement of

existing fractures and faults [1]. Often, most of the mineralization in calderas is grouped along ring faults. In nested calderas, ore deposits commonly occur along the outer ring system. There are examples of mineralization confined to the inner ring system, coinciding with an outward-dipping thrust fault [5].

When intense metasomatism and fracturing develop above deposits, more intense weathering of rocks should be expected and, as a result, the formation of cauldron subsidence terrain. When denudation reaches a quartz core or feeding fine-crystalline dikes, the terrain is inverted, and positive landforms are created in places where more durable rocks outcrop. When stocks intrude under compression conditions, deformation of the above-intrusion alteration zones occurs, leading to the formation of elliptical and more complex denudation shapes above porphyry copper deposits.

It is quite natural to find cauldron subsidence structures in the Aktogai ore field, the shape of which can be compared to the erosional truncation of the deposits and extrapolated to objects of poor exploration maturity.

1.6. Terrain Energy

It can be assumed that multiphase intrusive complexes have varying strengths and destructibility. In turn, cuts of varying amplitudes are created in the terrain, which allows the “terrain texture” to be used to distinguish lithological units and emphasize implicit landforms [37, 38]. In addition, by removing the regional component of a terrain, it is possible to compare local landforms located at different altitudes.

In his work, Mark [39] describes three elevation characteristics of a terrain:

– H – terrain energy (Relief energie) – the value between the minimum and maximum terrain elevations in any arbitrarily limited space;

– H_a – available terrain – the vertical distance between the assumed leveling surface and the surface connecting adjacent drainage channels;

– H_d – drainage terrain – the vertical distance between adjacent watersheds and rivers.

In practice, it is often difficult to distinguish between these three concepts with sufficient accuracy. The degree of generalization of the sampling of river networks and watersheds blurs the precise definition of the term “drainage terrain”. If a watershed coincides with the leveling surface, then in this case the “drainage terrain” is equal to the “available terrain”. If we consider the “terrain energy” in the area between adjacent river and watershed, then the “terrain energy” will be equal to the “drainage terrain”. Next, we will discuss “terrain energy” as a collective term describing the nonuniformity of terrain – its texture – and representing the vertical distance between a watershed and an adjacent river. In our study, “terrain energy” will be expressed through the textural analysis of terrain presented below.

2. Techniques

2.1. Digital Terrain Model (DTM)

The digital terrain model (DTM) was obtained by processing a stereopair of GeoEye-1 satellite data and is provided by TerraLink (<http://www.terralink.kz>).

The terrain model was visualized by combining an elevation matrix colored in a color palette with a semi-transparent shadow surface matrix superimposed on it, obtained by recalculating the elevation surface (Fig. 3).

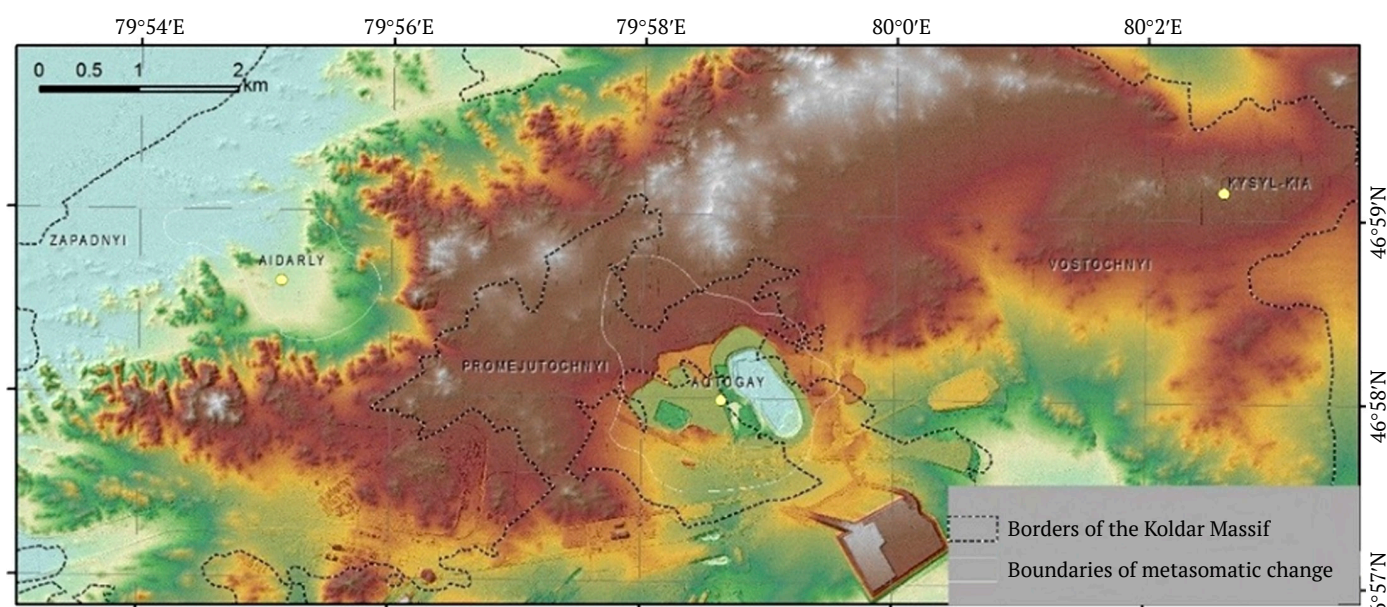


Fig. 3. Visualization of the DTM. The surface of the DTM is displayed with a color gradient with a semi-transparent overlay of a shaded terrain surface

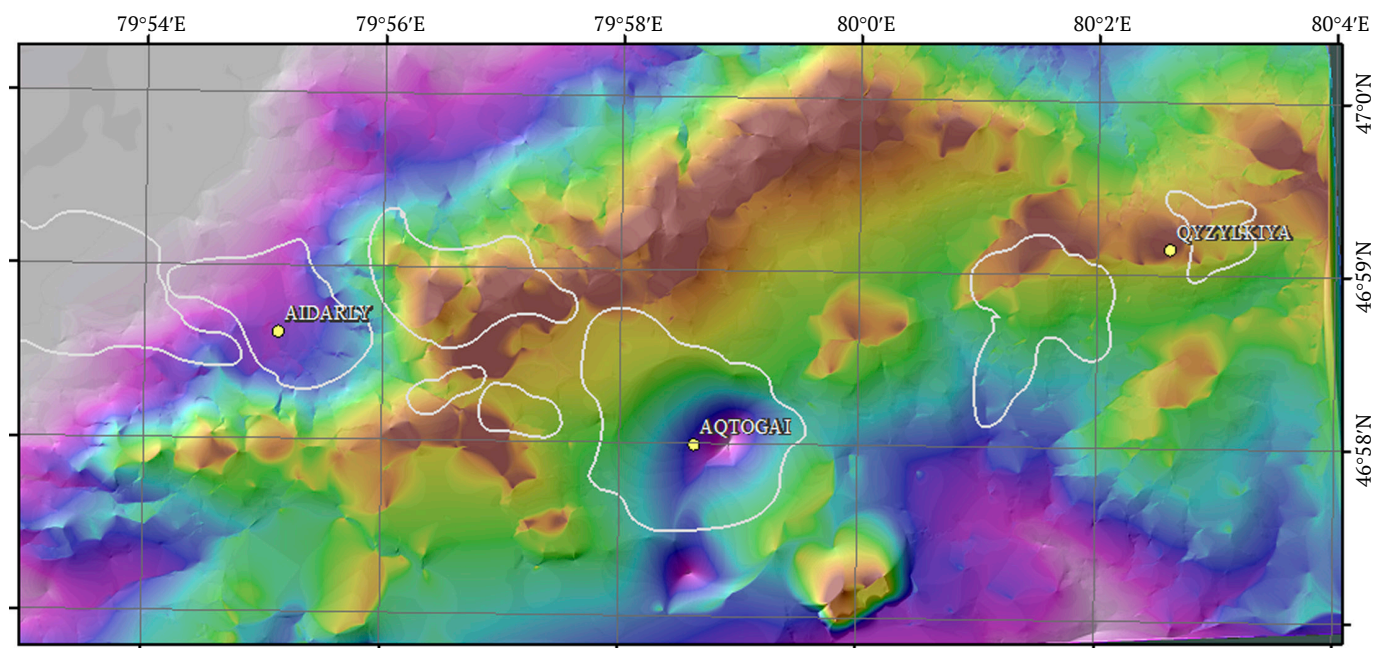


Fig. 4. Residual terrain surface – the difference between the surface constructed on the basis of local topographic maxima and the surface based on local minima. The metasomatic alteration areas are outlined

2.2. Construction of the Residual Terrain Surface

The goal is to calculate the difference between the smoothed upper surface, connecting peaks and ridges, and the lower surface, connecting river valleys. However, at first glance, the seemingly simple task of finding a smoothed surface presents certain difficulties. This immediately rules out the possibility of using standard mathematical functions such as “Median”, “Low Pass” filters, Fourier analysis, or polynomials. All of them provide a regional background, but do not allow for control of the edge elevation marks. What remains is the application of a smoothing surface constructed along the inflection points. That is, it is necessary to find extreme points, or the second derivative of the surface, and divide the obtained extreme values according to their position in the terrain. This function is implemented in the ENVI software package.

The algorithm used in the ENVI Topographic Features module to calculate channels and ridges was described by Wood⁴. Another option for selecting boundary elevation marks is possible as a result of calculating surfaces from a river network created in ArcMap (ArcScript⁵) with a specified catchment threshold. Moreover, to distinguish ridges, it is possible to use a river network constructed on the basis of inverted terrain [40].

When selecting peaks, ridges, pits, and valleys, it is important to select the correct smoothing threshold, i.e., the restriction on the selection of ridges and river valleys based on their scale characteristics. Elevation interpolation was performed using the ArcMap software package.

When processing the DTM data, we constructed smoothing surfaces based on local maxima and local minima of the terrain (Fig. 4).

As a result, a quantitative assessment of the elevation difference for the Aktogai ore field was obtained, which can be shown in color. The difference between the surfaces allows to distinguish local landforms and areas that differ in terms of terrain texture characteristics.

Areas of local depression in the terrain are distinguished. Areas of local depression in the terrain were obtained by subtracting the DTM values from the surface constructed based on local terrain maxima (Fig. 5).

2.3. Textural Analysis of Terrain

Texture is a set of repeating or regular variations in brightness in local areas of an image. It reflects the spatial relationships between pixels and can describe characteristics such as: uniformity; codimension; smoothness; skewness.

Textural analysis, which is widely used to analyze geological structures, can be performed using several methods.

A textural analysis was performed for the DTM, comparing the statistical dependence of pixel values in a given filter window. The surfaces of incline, cur-

⁴ Wood J.D. The geomorphological characterisation of digital elevation models. [PhD thesis]. University of Leicester, UK; 1996. 466 p.

⁵ Galang J. ArcGIS Script #13836 ArcScripts; 2005. URL: <http://arcscripsts.esri.com/details.asp?dbid=13836>

vature, local minima and local maxima, as well as entropy, uniformity, mean value, and skewness of a histogram were calculated. These methods evaluate texture based on statistical characteristics of an image: Gray-Level Co-Occurrence Matrix (GLCM). A matrix is created showing how often a pair of pixels with specific brightness values occur at a given distance and angle to each other.

The texture parameters are calculated from this matrix:

- Energy – a measure of texture uniformity;

- Contrast – evaluates the differences between neighboring pixels;

- Correlation – the degree of linear dependence between adjacent pixels;

- Entropy – characterizes the chaotic nature of the texture;

- Skewness – characterizes a clearly expressed direction.

For the matrices obtained, classification intervals were empirically selected and visualized for contrast in a color palette.

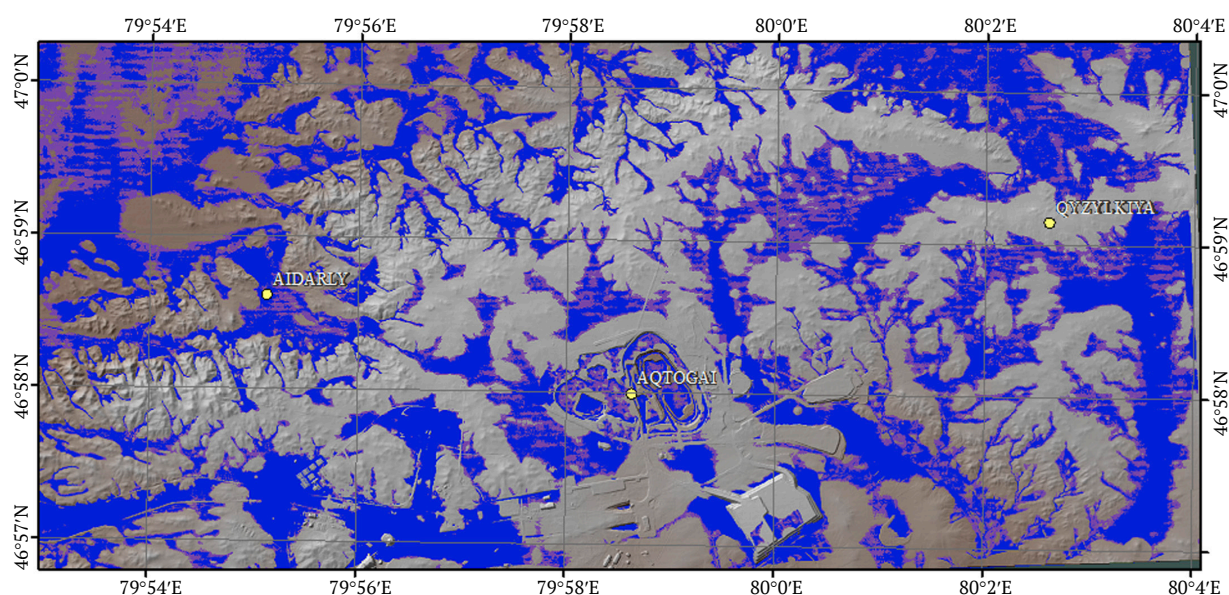


Fig. 5. Display of areas of local depression in the terrain (highlighted in blue)

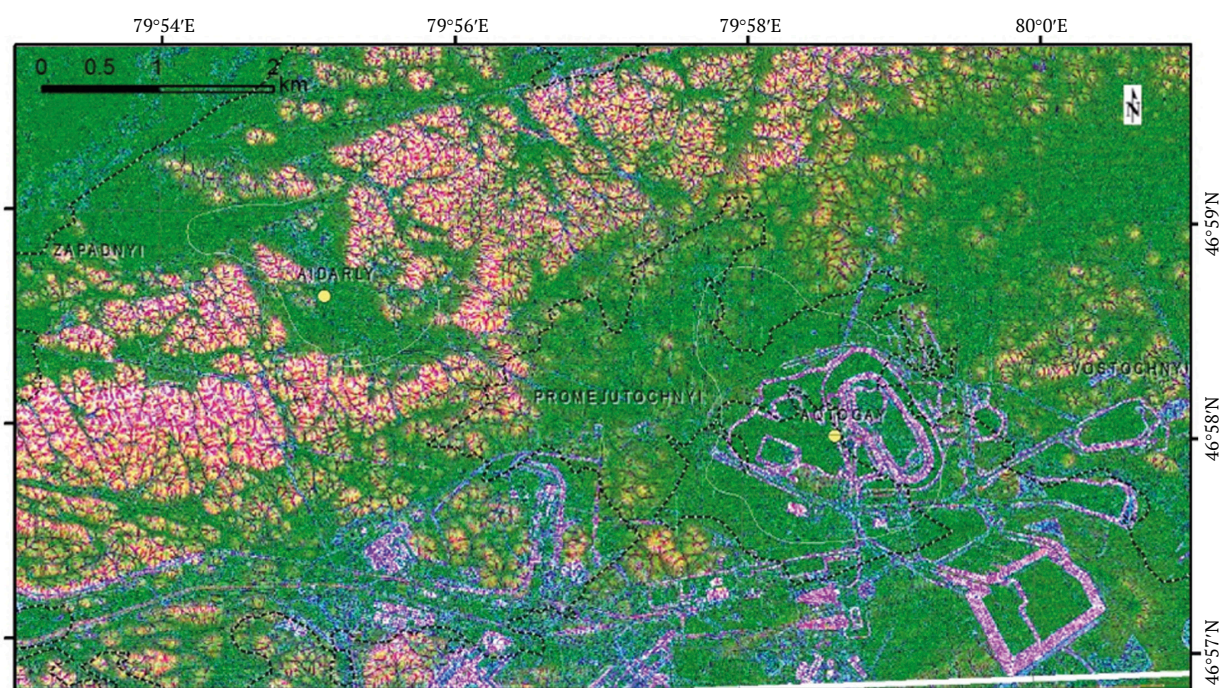


Fig. 6. RGB channel combination: *R* – incline, *G* – shaded terrain, and *B* – root mean square value. Intrusive complexes and anthropogenic changes are clearly distinguished

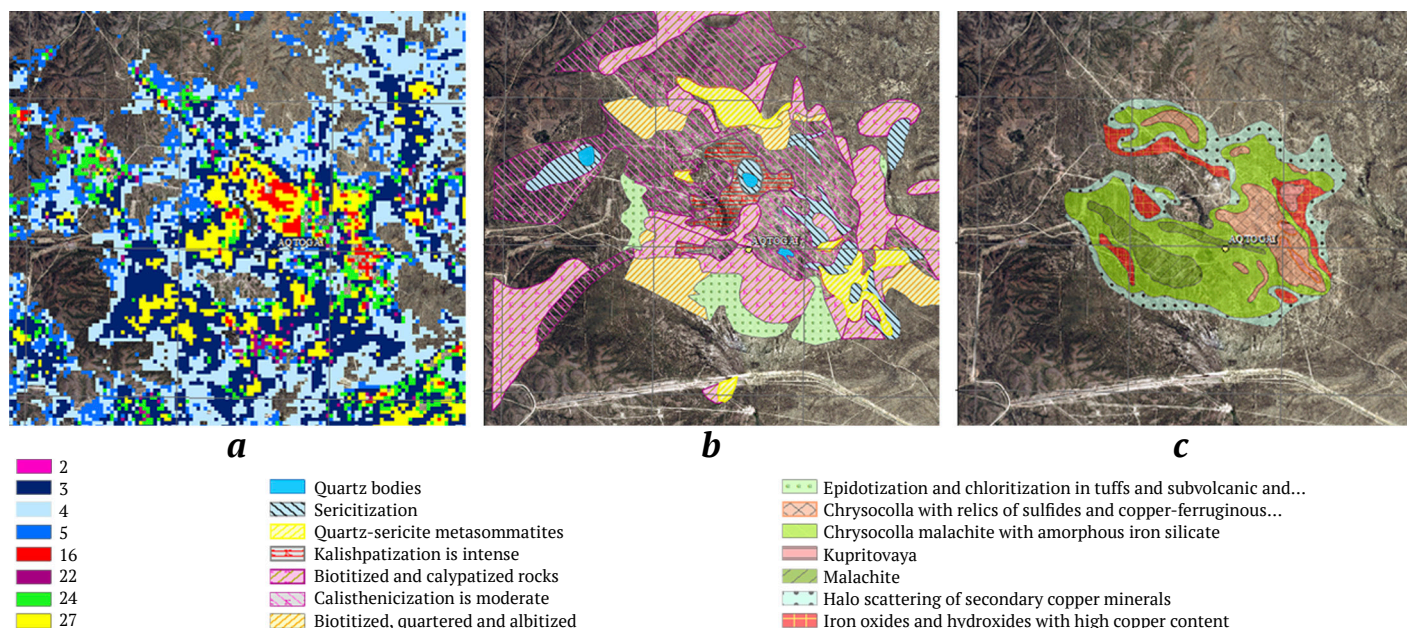


Fig. 7. Uncontrolled classification (a), map of metasomatic alteration at the Aktogai deposit (modification from: Zhukov et al., 1979) (b), map of supergene mineral associations (modification from: Sergiyko et al., 1980) (c)

Using textural analysis provides the following advantages: increased accuracy in object classification; detection of hidden patterns that cannot be identified by analyzing spectral characteristics alone. Topographic modeling software in ENVI was used to analyze the surface terrain.

Combinations of RGB channels allow creating contrasting differences in terrain caused by lithological features and geological processes involved in its formation. Fig. 6 uses the most informative combination of RGB channels, where R = incline, G = shaded terrain, and B = root mean square value. The image clearly shows the lithological differences between rock types and anthropogenic changes caused by mineral extraction.

Using textural analysis, we achieve the following advantages: improving the accuracy of object classification and discovering hidden patterns that cannot be identified solely by analyzing spectral characteristics.

2.4. Classification of Spectral Data

The project used various methods to identify an ore zone, which will be described in a new paper. In this work, we compare the results obtained from processing the surface terrain with the results obtained after classifying spectral data, so we present the methodology of this method here.

At the first stage, classes were selected based on objects identified as a result of processing. Thirty-seven classes were identified and used for classification using several statistical analysis methods. As a result, some lithological units and zones of secondary mineralization above ore stockworks were identified.

For uncontrolled classification in a small area comprising the Aktogai and Aidarly deposits, and Promezhutochny stockworks, 30 classes were empirically selected using the *K-means* algorithm.

For uncontrolled classification, the number of classes was selected so that areas of known deposits were revealed. After applying the method, eight classes were selected that fall within the outline of the Aktogai deposit. The identified classes were compared with the map of metasomatic zoning compiled by Zhukov et al., 1979 (Fig. 7, b) [41], and with the map of supergene mineralization from the report of Sergiyko et al., 1980 (Fig. 7, c) [42].

With the expansion of the area to the Kyzylkiya deposit, the number of uncontrolled classes has increased to 35. The classes were converted into a mask that can be applied to matrices obtained as a result of other processing stages.

3. Findings and Discussion

In terms of their characteristics, the Aktogai, Aidarly, and Kyzylkiya deposits and the Zapadny, Promezhutochny, and Vostochny ore stockworks share common features that are typical of porphyry copper-molybdenum deposit system as a whole, and have their own distinctive features each.

The most informative findings were selected from all the processed material, and their comparative analysis with the initial information was performed.

Analysis of the terrain shows that the large Aidarly and Aktogai deposits and the Zapadny stockwork form local depressions in the terrain, large calderas comparable to the morphology of partially eroded maars. This

shape is due to the formation of a system of near-stockwork fractures and the fact that hydrothermally altered and fragmented rocks in the center of the structure are more susceptible to erosion than the surrounding rocks. The intrusion of numerous dikes along fractures at the deposit led to the complication of the cauldron subsidence landforms. The elongated shapes of the Zapadny stockwork depression and the distortion of the isometric shapes of the Aidarly and Aktogai deposits indicate that the deposits were formed under compression.

This is confirmed by the direction of the dikes, which develop in two main directions under conditions of transpression. The deeper erosional truncation of the Aktogai deposit leads to the flattening of the cauldron subsidence landforms, probably due to the equalization of the erodibility of host rocks and ore-bearing rocks. The image showing the depression in the terrain clearly shows that the cauldron subsidence landforms occupy the deposit open pit and extends westward toward the Promezhutochny stockwork.

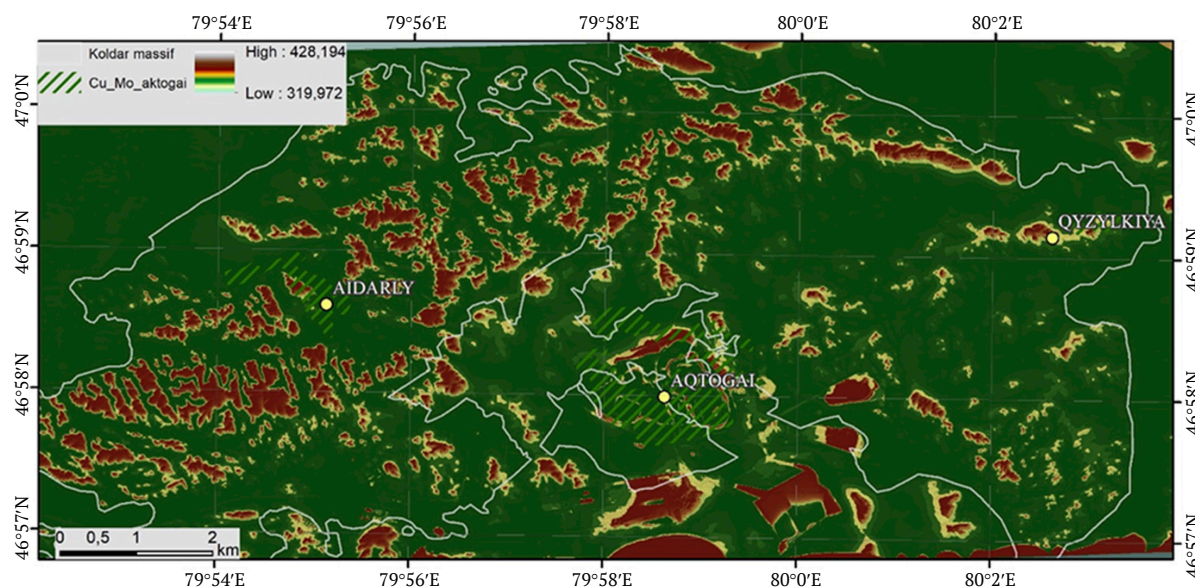


Fig. 8. Local depressions in the terrain
(the difference between the digital surface model and the surface connecting local minima)

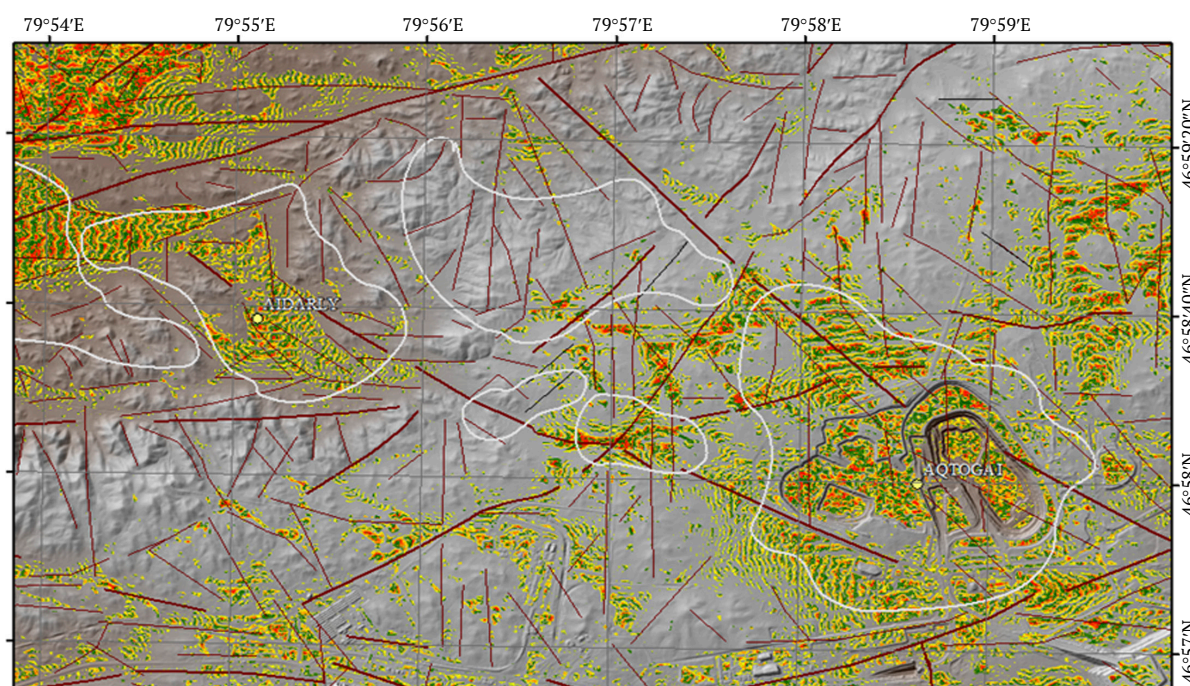


Fig. 9. DTM and superimposed mask of positive values of skewness of histogram of digital terrain surface values. The outlines indicate known areas of mineralization showing quartz-sericite-chlorite metasomatic alteration. The arrow indicates a cluster that spatially coincides with an area promising for further exploration, identified by other methods

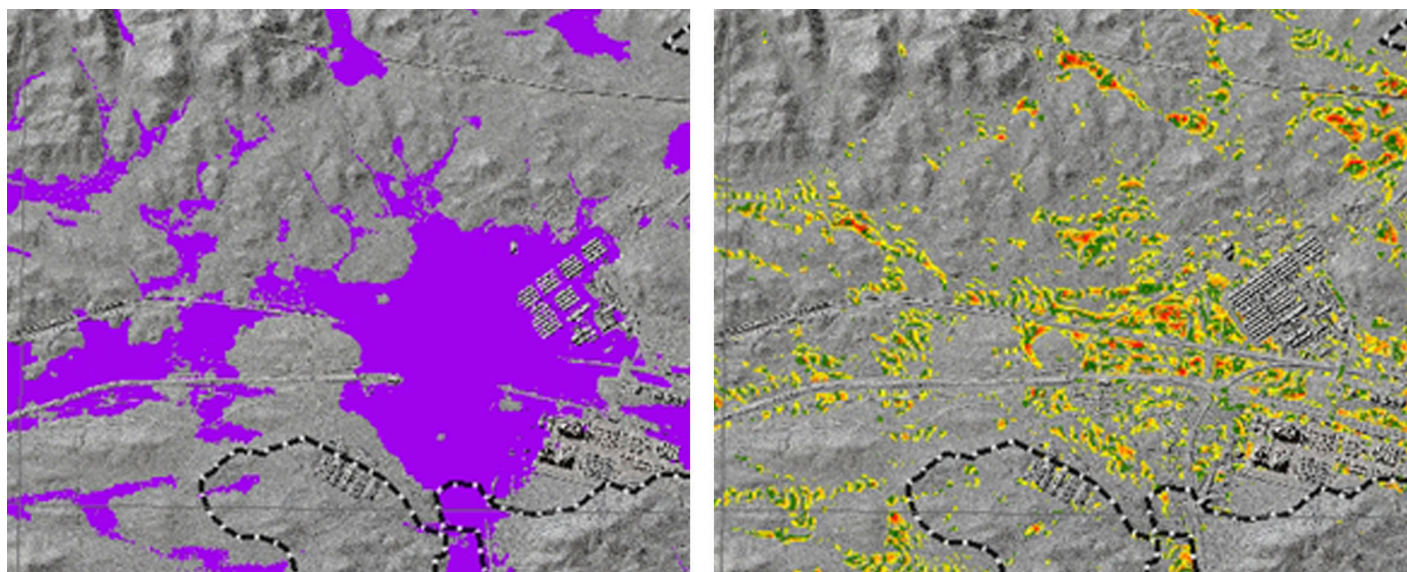


Fig. 10. Left: Area outlined by a local topographic depression; right: Positive values of skewness of the histogram of the digital terrain surface

The Kyzylkiya deposit and the Vostochny stockwork have a positive terrain morphology that is probably due to the fact that the upper part of the deposit has been eroded and the rock outcrop on the surface is more resistant to erosion processes.

The Promezhutochny stockwork is expressed in the terrain as a small local depression and a rise, which has probably been preserved as a result of partially manifested silicification, the manifestation of which makes the above-ore horizons more resistant to erosion.

Local depressions in the terrain (Fig. 8) emphasize the structure of ore stockworks and reflect, to some extent, the structure of the Koldar massif. For instance, in terms of its pattern, the diorite massif differs from the granodiorite massif. Depressions formed by the river system differ from those caused by superimposed stockworks and accompanying hydrothermal alteration, which include a greater number of radial and ring structures. In addition to the well-known ore stockworks, there are a number of other depressions similar to those already known.

The most interesting result of the textural analysis is the change in the skewness of the DTM surface histogram. The result was an image with contrasting distribution of values and a characteristic pattern of distinguished areas, most of which coincided with the zones of metasomatic alteration correlating with depressions in the terrain (Figs. 9, 10).

Conclusions

In the course of processing and analysis, images were obtained that allowed the identification of tectonic disturbances (faults) and certain lithological

varieties of rocks in the Koldar massif that are not reflected in existing geological maps of the ore field. The analysis of images shows that the areas of positive skewness values coincide with the general outline of metasomatic alteration developed at known deposits. The areas that stand out most are those where sericitization is more developed with a formation of supergene mineralogical association, including chrysocolla with relics of sulfides and copper-ferrous silicates. This area probably corresponds to the most fully developed metasomatism.

The areas of positive skewness confirmed the outlines of the Promezhduyuschiye and Zapadny ore stockworks and the outlines of the Aidarly deposit.

South of the Aidarly deposit, there is an anomalous cluster of the elevation histogram positive skewness values. The distinguished cluster is located at the intersection of faults and in a local depression in the terrain, similar to the location of the Aktogai and Aidarly deposits.

To identify similar areas, data on local depressions in the terrain were compared with the distribution of pixels of spectral data classes obtained by uncontrolled classification and characteristic of the Aktogai deposit outline. The characteristic areas of local depressions with manifestations of metasomatism may be promising for further exploration for ore deposits, but it should be noted that local depressions may also be caused by other geological processes, so they should be considered in conjunction with other signs of ore associations (Fig. 11).

When analyzing the terrain, the individual phases of the intrusive complexes of the Koldar massif are clearly distinguished (see Figs. 4, 5).

The Aidarly deposit and the Promezhutochny stockwork are associated with an intrusion that probably became exposed at a later time. It is most clearly expressed in the terrain and has a higher terrain activity index.

The Aktogai and Kyzylkiya deposits are spatially associated with an intrusion that has a characteristic appearance, a more smoothed terrain.

Based on the results of processing and analyzing satellite data, the characteristics of ore deposits were summarized according to their degree of distinguishing (Table 1).

The outlines of the terrain nonuniformities at the Aktogai deposit based on the results of the processing broadly coincide with the established outlines of hydrothermally altered rocks. The areas of quartz-sericite metasomatism especially closely coincide with the known outlines.

The outlines of the terrain nonuniformities at the Aidarly deposit also coincide with the identified areas of metasomatic alteration of quartz-sericite and propylite facies. Based on the digital terrain model (DTM) processing data, the central (axial) part of the deposit was distinguished as quasi-isometric in plan view, while elongated local depressions in the caldera are indicative of the deposit formation under conditions of horizontal tectonic compression.

The spatial identification of the Kyzylkiya deposit is poorly expressed in the terrain compared to the Aktogai and Aidarly deposits and cannot be reliably distinguished when processing the DTM surface. The deposit is characterized by small-size spectral anomalies distinguished by certain methods of processing.

Promezhutochny ore stockwork cannot be clearly distinguished based on the analysis of terrain characteristics.

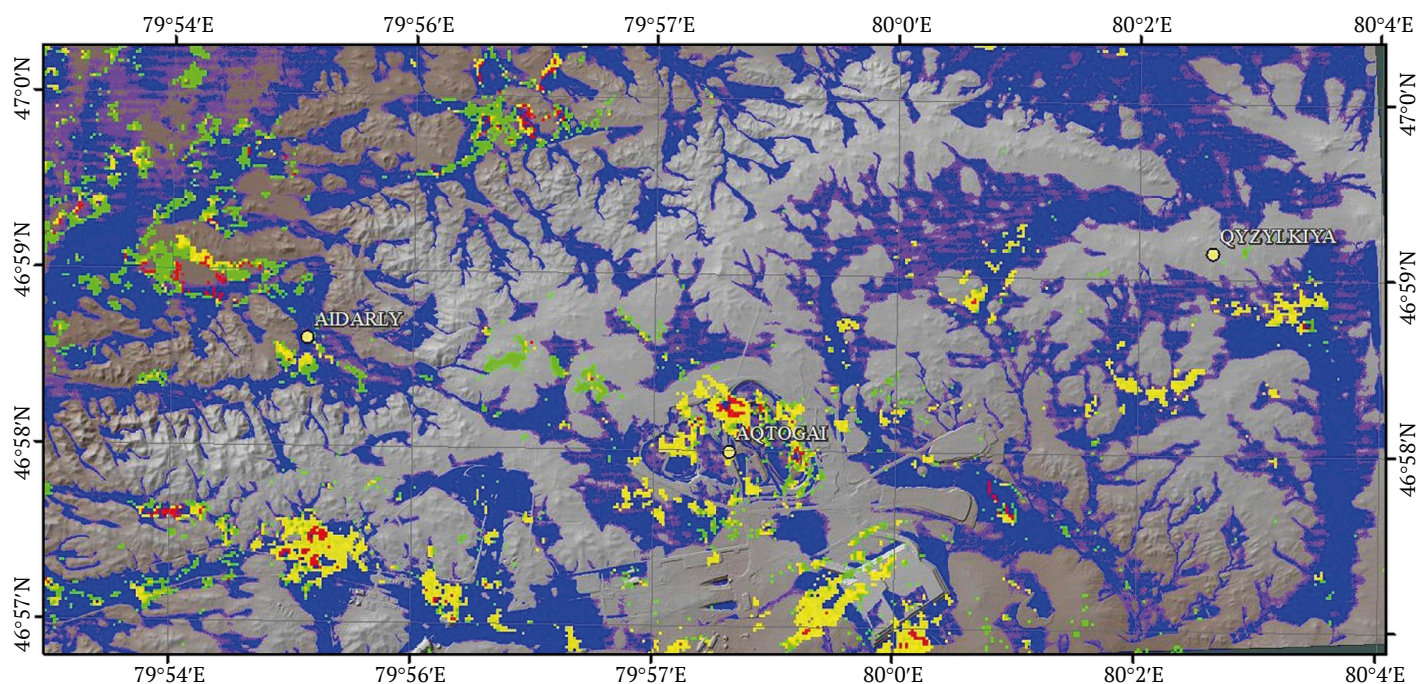


Fig. 11. Superimposition of classification results on distinguished areas of local terrain depression (DTM data substrate)

Table 1

Comparative characteristics of ore deposits by degree of distinguishing

No.	Ore stockwork	Degree of visualization as a result of satellite data processing	
		Skewness for DGM	Cauldron subsidence
1	Aktogai Deposit	Pronounced and coincides with the outlines of intensely manifested metasomatism	A slight saucer-shaped depression in the terrain with radial branches
2	Aidarly deposit	Pronounced and coincides with the outlines of intensely manifested metasomatism	Distinct, with radial branches
3	Kyzylkiya deposit	Weakly pronounced	Not observed
4	Promezhutochny ore stockwork	Pronounced	Distinct, with radial branches
5	Zapadny ore stockwork	Stands out well	Clearly
6	Vostochny ore stockwork	Weakly pronounced	Not observed



The Zapadny stockwork is distinguished at every stage of satellite data processing and occupies a distinctly lowered position in the terrain. Its elongated shape is probably due to its formation under compression in a north-northwest direction.

The Vostochny ore stockwork cannot be clearly distinguished.

The description shows that not all stockworks can have a characteristic terrain shape and, same to the interpretation of geophysical data, assessing the terrain shape can contribute to prospecting/exploration, but is not a sufficient indicator for the reliable identification of ore stockworks.

In the course of processing, the following additional areas can be identified, which are commensurable to known ore deposits in terms of their spectral characteristics and landforms:

1. A zone near the northern margin of the area at the intersection of the Main Koldar Fault and the North-Koldar Fault, limited by the Koldar Fault in the south. The distinguished zone is complicated by higher-order faults radiating outwards from the center of the manifestation. To some extent, the zone also manifests itself when using other processing methods. Field observations have revealed a monzonite

stock, numerous veins and streaks of quartz-epidote and feldspar mineralization. Chloritization zones, as well as a strip with manifestation of malachitization are found here.

2. The zone south of the Aidarly deposit in a local topographic low at the intersection of the Maly Koldar Fault and higher-order faults is distinguished by textural analysis of the DTM data. Zones of intense chlorite-carbonate metasomatism and zones of intense fracturing are observed here.

The zones of wall-rock alteration were identified using a combination of methods. Superimposition of the results enhances the contrast of the wall-rock alteration halos, and the areas identified should subsequently be compared with the results of geophysical surveys and a comprehensive geochemical survey.

We recommend analyzing the terrain morphology as an additional measure. When combined, all these methods allow for the most successful solution of forecasting problems: identifying areas that are similar in their spectral characteristics to known ore deposits and indirectly assessing their position relative to the surface. The areas may be promising for further exploration and should be verified by field observations.

References

1. Eggers M.J. Engineering geological modelling for pit slope design in the porphyry copper-gold deposits of Southeast Asia. In: Dight P.M. (ed.) *APSSIM 2016: Proceedings of the First Asia Pacific Slope Stability in Mining Conference*. Australian Centre for Geomechanics, Perth; 2016. Pp. 49–82. https://doi.org/10.36487/ACG_rep/1604_0.4_Eggers
2. Seib N., Kley J., Torizin J., et al. Identification of volcanic forms in a digital terrain model of the West Eifel. *Zeitschrift der Deutschen Gesellschaft für Geowissenschaften*. 2008;159:657–670. <https://doi.org/10.1127/1860-1804/2008/0159-0657>
3. Grohmann C.H., Riccomini C., Alves F.M. SRTM-based morphotectonic analysis of the Poços de Caldas Alkaline Massif, southeastern Brazil. *Computers & Geosciences*. 2007;33(1):10–19. <https://doi.org/10.1016/j.cageo.2006.05.002>
4. John D.A., Ayuso R.A., Barton M.D., et al. *Porphyry copper deposit model*. USGS Scientific Investigations Report, 2010–5070–B, 169 p.
5. Acocella V. Understanding caldera structure and development: An overview of analogue models compared to natural calderas. *Earth-Science Reviews*. 2007;85(3–4):125–160. <https://doi.org/10.1016/j.earscirev.2007.08.004>
6. Németh K., Cronin S.J. Syn- and post-eruptive erosion in tropical climate tephra ring (West Ambrym, Vanuatu). *Geomorphology*. 2007;86(1–2):115–130. <https://doi.org/10.1016/j.geomorph.2006.08.016>
7. Németh K. Long-term erosion-rate calculation in the Waipiata Volcanic Field (New Zealand). *Géomorphologie: Relief, Processus, Environnement*. 2001;7(2):137–152
8. Németh K. Calculation of long-term erosion in Central Otago, New Zealand, based on erosional remnants of maar/tuff rings. *Zeitschrift für Geomorphologie*. 2003;47(1):29–49. <https://doi.org/10.1127/zfg/47/2003/29>
9. Seib N., Kley J., Büchel G. Identification of maars and volcanic landforms in the West Eifel Volcanic Field using DTM data. *International Journal of Earth Sciences*. 2013;102:875–891. <https://doi.org/10.1007/S00531-012-0829-5>
10. Seib N., Kley J. Problems of residual surface modelling for geological applications. In: *Proceedings of the Kolmogorov Readings*. Moscow, Russia; 2010. Pp. 146–151.



11. Şengör A.M.C., Natal'in B.A., Burtman V.S. Evolution of the Altaid tectonic collage and Palaeozoic crustal growth in Eurasia. *Nature*. 1993;364:299–307. <https://doi.org/10.1038/364299a0>
12. Windley B.F., Alexeiev D., Xiao W., et al. Tectonic models for accretion of the Central Asian Orogenic Belt. *Journal of the Geological Society*. 2007;164(1):31–47. <https://doi.org/10.1144/0016-76492006-022>
13. Seltnmann R., Kröner A., Kovach V., et al. Reassessment of continental growth during the accretionary history of the Central Asian Orogenic Belt. *Gondwana Research*. 2014;25(1):103–125. <https://doi.org/10.1016/j.gr.2012.12.023>
14. Shen P., Pan H., Hattori K., et al. Large Paleozoic and Mesozoic porphyry deposits in the Central Asian Orogenic Belt: Geodynamic settings, magmatic sources, and genetic models. *Gondwana Research*. 2018;58:161–194. <https://doi.org/10.1016/j.gr.2018.01.010>
15. Seedorff E., Dilles J.H., Proffett J.M., et al. Porphyry deposits: Characteristics and origin of hypogene features. *Economic Geology, One Hundredth Anniversary Volume*. 2005;251–298. <https://doi.org/10.5382/AV100.10>
16. Simmons S.F., White N.C., John D.A. Epithermal precious and base metal deposits. *Economic Geology, One Hundredth Anniversary Volume*. 2005;485–522.
17. Yermolov P.V., Portnov V.S., Makat D.K. Age and geodynamics of Central Kazakhstan carbon ore copper provinces. *Naukovyi Visnyk Natsionalnoho Hirnychoho Universytetu*. 2017;(6):5–15.
18. Li C., Shen P., Pan H., et al. Geology and ore-forming fluid evolution of the Aktogai giant porphyry Cu deposit, Kazakhstan. *Journal of Asian Earth Sciences*. 2018;165:192–209. <https://doi.org/10.1016/j.jseaes.2018.07.009>
19. Buslov M.M., Fujiwara Y., Iwata K., Semakov N.N. Late Palaeozoic–early Mesozoic geodynamics of Central Asia. *Gondwana Research*. 2004;7(3):791–808. [https://doi.org/10.1016/S1342-937X\(05\)71064-9](https://doi.org/10.1016/S1342-937X(05)71064-9)
20. Filippova I.B., Bush V.A., Didenko A.N. Middle Paleozoic subduction belts: the leading factor in the formation of the Central Asian fold-and-thrust belt. *Russian Journal of Earth Sciences*. 2001;3(6):405–426. <https://doi.org/10.2205/2001ES000073>
21. Cao M.J., Li G.M., Qin K.Z., et al. Assessing the magmatic affinity and petrogenesis of granitoids at the giant Aktogai porphyry Cu deposit, Central Kazakhstan. *American Journal of Science*. 2016;316:614–668. <https://doi.org/10.2475/07.2016.02>
22. Poletaev A.I., Krasnovikov A.T., Nurtuganov B.N., Timofeeva S.N. Geological structure and age of the Koldar intrusive. *Izvestiya Akademii Nauk Kazakhskoi SSR, Seriya Geologicheskaya*. 1987;(6): 3–13.
24. Mao J.W., Pirajno F., Lehmann B., et al. Distribution of porphyry deposits in the Eurasian continent and their tectonic settings. *Journal of Asian Earth Sciences*. 2014;79(B):576–584. <https://doi.org/10.1016/j.jseaes.2013.09.002>
24. Shen P., Pan H.D., Xiao W.J., et al. Two geodynamic–metallogenic events in the Balkhash (Kazakhstan) and the West Junggar (China): Carboniferous porphyry Cu and Permian greisen W–Mo mineralization. *International Geology Review*. 2013;55(13):1660–1687. <https://doi.org/10.1080/00206814.2013.792500>
25. Li C., Shen P., Pan H. Mineralogy of the Aktogai giant porphyry Cu deposit in Kazakhstan: Insights into the fluid composition and oxygen fugacity evolution. *Ore Geology Reviews*. 2018;95:899–916. <https://doi.org/10.1016/j.oregeorev.2018.03.027>
26. Seltnmann R., Shatov V., Yakubchuk A. *Mineral deposits database and thematic maps of Central Asia*. London: CERCAMS, Natural History Museum; 2004. 117 p.
27. Zvezdov V.S., Migachev I.F., Girfanov M.M. Porphyry copper deposits of the CIS and models of their formation. *Ore Geology Reviews*. 1993;7(6):511–549. [https://doi.org/10.1016/0169-1368\(93\)90013-O](https://doi.org/10.1016/0169-1368(93)90013-O)
28. Burbank D.W. Rates of erosion and their implications for exhumation. *Mineralogical Magazine*. 2002;66(1):25–52. <https://doi.org/10.1180/0026461026610014>
29. Sobel E.R., Oskin M., Burbank D., Mikolaichuk A. Exhumation of basement uplifts: Kyrgyz Range, using fission track thermochronology. *Tectonics*. 2006;25(2). <https://doi.org/10.1029/2005TC001809>
30. Corbett G.J., Leach T.M. *Southwest Pacific gold–copper systems: Structure, alteration, and mineralisation*. Society of Economic Geologists; 1998. <https://doi.org/10.5382/SP.06>
31. Skirrow R.G., Huston D.L., Mernagh T.P., et al. *Critical commodities for a high-tech world: Australia's supply potential*. Geoscience Australia, Canberra; 2013.
32. Carten R.B., White W.H., Stein H.J. High-grade granite-related molybdenum systems: classification and origin. *Mineral Deposit Modeling*. 1993; 40:521–554.



33. Heidrick T.L., Title S.R. Fracture and dike patterns in Laramide plutons and their structural and tectonic implications. In: Titley S.R. (Ed.) *Advances in Geology of Porphyry Copper Deposits. Southwestern North America*. Tucson: University of Arizona Press; 1982. Pp. 73–92.
34. Sillitoe R.H. Porphyry copper systems. *Economic Geology*. 2010;105:3–41. <https://doi.org/10.2113/gsecongeo.105.1.3>
35. Tosdal R.M., Richards J.P. Magmatic and structural controls on porphyry copper \pm Mo \pm Au deposits. *Reviews in Economic Geology*. 2001; 14:157–181.
36. Gustafson L.B., Hunt J.P. The porphyry copper deposit at El Salvador, Chile. *Geological Bulletin of China*. 1975;21:768–776.
37. Bostjančić I., Gulam V., Pollak D., Frangen T. Comparative analysis of slope and relief energy for small-scale landslide susceptibility mapping: insights from Croatia. *Remote Sensing*; 2025; 17:2142. <https://doi.org/10.3390/rs17132142>
38. Zograban L.N., Gevorgian F.S. “Relief energy”, its mapping and significance in the erosion process. *Izvestiya of the Academy of Sciences of the Armenian SSR, Earth Sciences*. 1969;(4):80–86. (In Russ.)
39. Mark D.M. Geomorphometric parameters: A review and evaluation. *Geografiska Annaler: Series A*. 1975;57(3–4):165–177.
40. Chernova I.Yu., Khasanov D.I., Zharkov I.Ya., et al. Detection and study of the zones of the latest crustal movements using GIS tools. *Arc Review*. 2005;(1):6–7. (In Russ.)
41. Zhukov N.M., Filimonova L.E., Vizigina V.G. *Metasomatizes and hypogene mineralization of the Aktogay porphyry copper deposit*. Almaty; 1979. 230 p.
42. Sergiyko Yu.A., et al. *Report on the detailed exploration of the Aktogay copper-porphyry deposit with reserve estimation as of 01.01.1980*. Alma-Ata; 1980. (In Russ.)

Information about the authors

Nadine Seib – PhD (Earth Sci.), Senior Geologist, KeplerGroup LLP, Almaty, Republic of Kazakhstan; Senior Research Fellow, School of Earth Sciences, D. Serikbayev East Kazakhstan Technical University, Ust-Kamenogorsk, Republic of Kazakhstan; ORCID [0000-0001-7092-1671](https://orcid.org/0000-0001-7092-1671), Scopus ID [8417022400](https://scopus.org/authorid/8417022400); e-mail snv63@yandex.com

Yury Belov – Senior Geologist, KazGeoExploration LLP, Astana, Republic of Kazakhstan; ORCID [0009-0003-9596-4952](https://orcid.org/0009-0003-9596-4952); e-mail belov010885@mail.ru

Natalya Zimanovskaya – PhD (Geology and Mineral Exploration), Associate Professor, Senior Researcher, Center of Competence and Technology Transfer in Geology and Mining, D. Serikbayev East Kazakhstan Technical University, Ust-Kamenogorsk, Republic of Kazakhstan; ORCID [0000-0002-9881-690X](https://orcid.org/0000-0002-9881-690X); e-mail nata_zim@mail.ru

Gulizat Orazbekova – PhD (Geology and Mineral Exploration), Lecturer, Department of Automation and Information Technologies, Shakarim University, Semey, Republic of Kazakhstan; ORCID [0000-0002-4503-6838](https://orcid.org/0000-0002-4503-6838); e-mail orazbekova@bk.ru

Aizhan Tretyakova – Senior Geologist, Biruk-Altyn LLP, Almaty, Republic of Kazakhstan; ORCID [0000-0002-0803-1587](https://orcid.org/0000-0002-0803-1587); e-mail A.Tretyakova@ordabasy.kz

Assem Muratova – PhD student (Geology and Mineral Exploration), D. Serikbayev East Kazakhstan Technical University, Ust-Kamenogorsk, Republic of Kazakhstan; ORCID [0009-0003-7241-5571](https://orcid.org/0009-0003-7241-5571), Scopus ID [58574678800](https://scopus.org/authorid/58574678800); e-mail muratova.assem@gmail.com

Issatay Kassenov – Chief GIS Specialist, KazGeoExploration LLP, Astana, Republic of Kazakhstan; ORCID [0009-0002-7787-3427](https://orcid.org/0009-0002-7787-3427); e-mail is.kassenov@gmail.com

Received 20.06.2025

Revised 21.07.2025

Accepted 22.07.2025



GEOLOGY OF MINERAL DEPOSITS

Research paper

<https://doi.org/10.17073/2500-0632-2025-03-386>

UDC 553.43/.44:553.065(597)

**Geological and isotopic constraints on the copper ore formation in Ta Phoi area, Lao Cai province, Northwestern Vietnam**K. T. Hung¹   , N. X. Dac²¹ Hanoi University of Mining and Geology, Hanoi, Vietnam² Vietnam Institute of Geosciences and Mineral Resources, Hanoi, Vietnam khuongthehung@humg.edu.vn**Abstract**

The Ta Phoi copper deposit, located in the northeastern Phan Si Pan zone, Northwestern Vietnam, is a significant site of Neoproterozoic Cu mineralization. Its distinct geological characteristics justify its investigations, especially in comparison to nearby IOCG Sin Quyen deposit. This study is aimed at clarifying the genesis, ore-forming conditions, and fluid evolution of the Ta Phoi deposit through an integrated approach combining geological, petrographic, geochemical, and isotopic data analysis. The research specifically employs U-Pb dating of sphene, sulfur isotope analysis, and fluid inclusion microthermometry to identify the age, origin, and physicochemical environment of the mineralization. Sphene U-Pb dating yielded concordant ages of 810.7 ± 4.6 Ma and 819.5 ± 2.0 Ma, indicating a Neoproterozoic mineralization event temporally linked to regional granodiorite and diorite intrusions. Sulfur isotope values ($\delta^{34}\text{S} = +2.2$ to $+3.1\text{‰}$) suggest a magmatic origin for ore-forming fluids. Fluid inclusion data detected fluid temperatures ranging from 163.1°C to 410°C , fluid salinities of 2.1–16.25 wt% NaCl equiv., and formation pressures of 44–100 MPa at depths of 3.4–6.5 km. These results confirmed that the Ta Phoi deposit formed from medium- to high-temperature, magmatogene hydrothermal fluids in a subduction-related continental arc setting; it may represent a porphyry-related skarn or endoskarn system that developed in response to magmatic fluid migration along lithological contacts and faults. These findings provide new insights into the metallogenic framework of the Ta Phoi deposit and highlight its potential for further Cu exploration in Northwestern Vietnam.

Keywords


Copper ore, U-Pb dating, sphene, metallogeny, Ta Phoi deposit, North-Western Vietnam

For citation

Hung K. T., Dac N. X. Geological and isotopic constraints on the copper ore formation in Ta Phoi area, Lao Cai province, Northwestern Vietnam. *Mining Science and Technology (Russia)*. 2025;10(3):262–279. <https://doi.org/10.17073/2500-0632-2025-03-386>

ГЕОЛОГИЯ МЕСТОРОЖДЕНИЙ ПОЛЕЗНЫХ ИСКОПАЕМЫХ

Научная статья

Геологические и изотопные оценки условий образования медных руд в районе Та Фой, провинция Лао Кай, северо-западный ВьетнамХ. Т. Хунг¹   , Н. С. Дак²¹ Ханойский университет горного дела и геологии, г. Ханой, Вьетнам² Вьетнамский институт наук о Земле и минеральных ресурсах, г. Ханой, Вьетнам khuongthehung@humg.edu.vn**Аннотация**

Месторождение меди Та Фой (Ta Phoi), расположенное в северо-восточной части зоны Фан Си Пан на северо-западе Вьетнама, является важным объектом проявления неопротерозойской медной минерализации. Его отличительные геологические характеристики оправдывают его изучение, особенно в сопоставлении с близлежащим месторождением типа Fe-оксидных Au-Cu гидротермальных месторождений (IOCG) Синь Куен (Sin Quyen). Цель данного исследования – выявить генезис, условия рудообразования и эволюцию флюидов месторождения Та Фой с помощью комплексного подхода, сочетающего анализ геологических, петрографических, геохимических и изотопных данных. В частности, в исследовании используются U-Pb датирование сфена, изотопный анализ серы и микротермометрия флюидных включений для определения возраста, происхождения и физико-химических условий формирования минерализации. Определение возраста сфена U-Pb методом дало согласующиеся возрасты $810,7 \pm 4,6$ млн лет и $819,5 \pm 2,0$ млн лет, что указывает на неопротерозойский возраст минерализации, совпадающий с возрастом региональных гранодиоритовых и диоритовых интрузий. Изотопный анализ серы ($\delta^{34}\text{S} = +2,2$ до $+3,1\text{‰}$) указывает на магматическое происхождение рудообразующих флюидов. Данные по флюидным включениям показали,



что температура флюидов колебалась от 163,1 °C до 410 °C, солёность флюидов составляла 2,1–16,25 вес. % в эквиваленте NaCl, а пластовое давление – 44–100 МПа на глубине 3,4–6,5 км. Эти результаты подтвердили, что месторождение Та Фой образовалось в результате воздействия магматогенных гидротермальных флюидов средней и высокой температуры в субдукционных условиях континентальной дуги; оно может представлять собой порфировую скарновую или эндоскарную систему, которая сформировалась в результате миграции магматических флюидов вдоль литологических контактов и разломов. Эти результаты дают новое представление о металлогенической обстановке формирования месторождения Та Фой и подчеркивают потенциал дальнейшей разведки на медь в северо-западной части Вьетнама.

Ключевые слова

медная руда, U-Pb определение возраста, сфен, металлогения, месторождение Та Фой, северо-западный Вьетнам

Для цитирования

Hung K. T., Dac N. X. Geological and isotopic constraints on the copper ore formation in Ta Phoi area, Lao Cai province, Northwestern Vietnam. *Mining Science and Technology (Russia)*. 2025;10(3):262–279. <https://doi.org/10.17073/2500-0632-2025-03-386>

Introduction

The mineralization process typically occurs over a wide spatial range and is closely associated with deformation, metamorphism, faulting, and magmatic intrusion events during specific tectonic stages. These processes contribute to the formation of significant mineral deposits, containing copper (Cu), gold (Au), lead (Pb), zinc (Zn), and rare earth elements (REE), along with other associated minerals [1–3].

Lao Cai province located in the Phan Si Pan zone in northwestern Vietnam has significant mineral resource potential, particularly as for Cu-Au mineralization, which has been assessed as highly prospective [4]. Consequently, in 2015, the Vietnam government approved the establishment of the Lao Cai copper metallurgical industrial zone, with a processing capacity exceeding 10,000 tons of cathode copper/year. Geological mapping and mineral exploration conducted along the northeastern margin of the Phan Si Pan zone have identified several large copper ore deposits, including the Sin Quyen, Ta Phoi, and Vi Kem deposits, as well as valuable copper mineralization occurrences such as Nam Chac, Trinh Tuong, Lung Thang, and Lung Po [5–9]. However, these studies remain fragmented, lack in-depth analysis, and have yet to incorporate modern mineralization research techniques. In recent years, some studies on mineralization have focused on copper deposits in Lao Cai area, first of all, the Sin Quyen deposit [10–12]. These investigations have introduced new perspectives on the nature and formation age of copper mineralization in the northeastern Phan Si Pan zone, particularly at the Sin Quyen deposit, revealing the presence of gold and rare earth elements (REE) alongside copper as major economic commodities [13]. This raises the question of whether deposits with economic significance, similar to Sin Quyen, exist along the Lung Po–Ta Phoi metallogenic belt. The Ta Phoi copper deposit within this belt has been estimated to contain substantial copper re-

serves [14, 15], but its potential for associated gold and REE mineralization remains uncertain. Furthermore, the genetic mechanisms of ore formation at Ta Phoi and Sin Quyen require clarification – do they share similar mineralization processes and metallogenic periods? Addressing these questions necessitates comprehensive research into the material composition, formation conditions, spatial distribution, and genesis of the mineralization. Such studies would provide a scientific basis for more precise mineral exploration strategies and resource estimation in the region.

The **aim** of this study is to clarify the geological and isotopic features of copper ore formation in the Ta Phoi area through an integrated analysis of field observations, petrography, and geochemical data.

To achieve this aim, the study was focussed on the following key **tasks**:

- characterizing geological setting and lithological units that host copper mineralization;
- analyzing petrographic features and mineral assemblages to interpret alteration patterns and paragenetic sequences;
- integrating U-Pb sphene geochronology to constrain the mineralization formation timing;
- applying sulfur isotope analysis to identify the source of ore-forming materials;
- conducting fluid inclusion studies to determine the temperature, salinity, pressure, and depth conditions of ore formation.

The outcomes of this research will enhance the understanding of metallogenic processes in the region and provide valuable insights for future mineral exploration in northwestern Vietnam.

1. Geological setting

Northwestern Vietnam belongs to the South China and Indochina blocks (Figs. 1, *a*, *b*). These blocks are integral components in the palaeogeographic reconstruction of the Rodinia supercontinent [16–19]. Several copper deposits, including the Iron Oxide

Copper-Gold (IOCG) deposits of Sin Quyen, and copper Suoi Thau, Ta Phoi, are located in Northwestern Vietnam (Fig. 1, c).

The Ta Phoi copper deposit is located in the northwestern Vietnam, which is bordered by the Song Chay fault to the north and the Song Ma belt to the south [4]. This region comprises three major tectonic units: the Phan Si Pan zone, the Song Da rift, and the Tu Le basin (Fig. 2, a). The Song Da rift is an elongated, northwest-southeast trending structure characterized by Devonian to Middle Triassic sedimentary-volcanic sequences. A prominent feature of this rift is the well-developed Permian-Triassic alkaline basalts (~260 Ma), which predominantly occur along the Da River [24]. These basalts, along with silicic volcanic rocks, rest atop Early Permian limestone and are subsequently overlain unconformably by Triassic limestone and schist containing coal deposits [25, 26]. Some studies suggest that the Song Da volcanic suite is linked to the Emeishan plume [27–29]. The Tu Le Basin is predominantly composed of rhyolite, trachy-

rhyolite, and trachydacite. Zircon U-Pb dating indicates that the rhyolites in this basin formed during the Late Permian (262–252 Ma), contemporaneously with the mafic rocks of the Song Da Rift [30, 31].

The Phan Si Pan zone serves as a tectonic link between two major crustal blocks: the North Vietnam–South China block and the Indochina block (Fig. 2, b). It is positioned between the Red River shear zone and the Tu Le basin and is composed primarily of Mesoarchean to Early Paleoproterozoic basement rocks, including biotite quartzite, quartz-biotite-garnet schist, and amphibolite [23, 33]. Paleo-Mesoproterozoic units in the zone consist of biotite schist, two-mica schist, and amphibolite [23, 33]. Precambrian magmatism in the Phan Si Pan zone is characterized by several granitoid and mafic intrusive events, including: Mesoarchean granitoids (2.9–2.8 Ga) [33–35], Paleoproterozoic granitoids (1.8–2.2 Ga) [33, 35–37], Paleoproterozoic mafic dykes (1.8–2.3 Ga) [33], and Neoproterozoic granitoids (760–751 Ma) [20, 21, 23, 38].

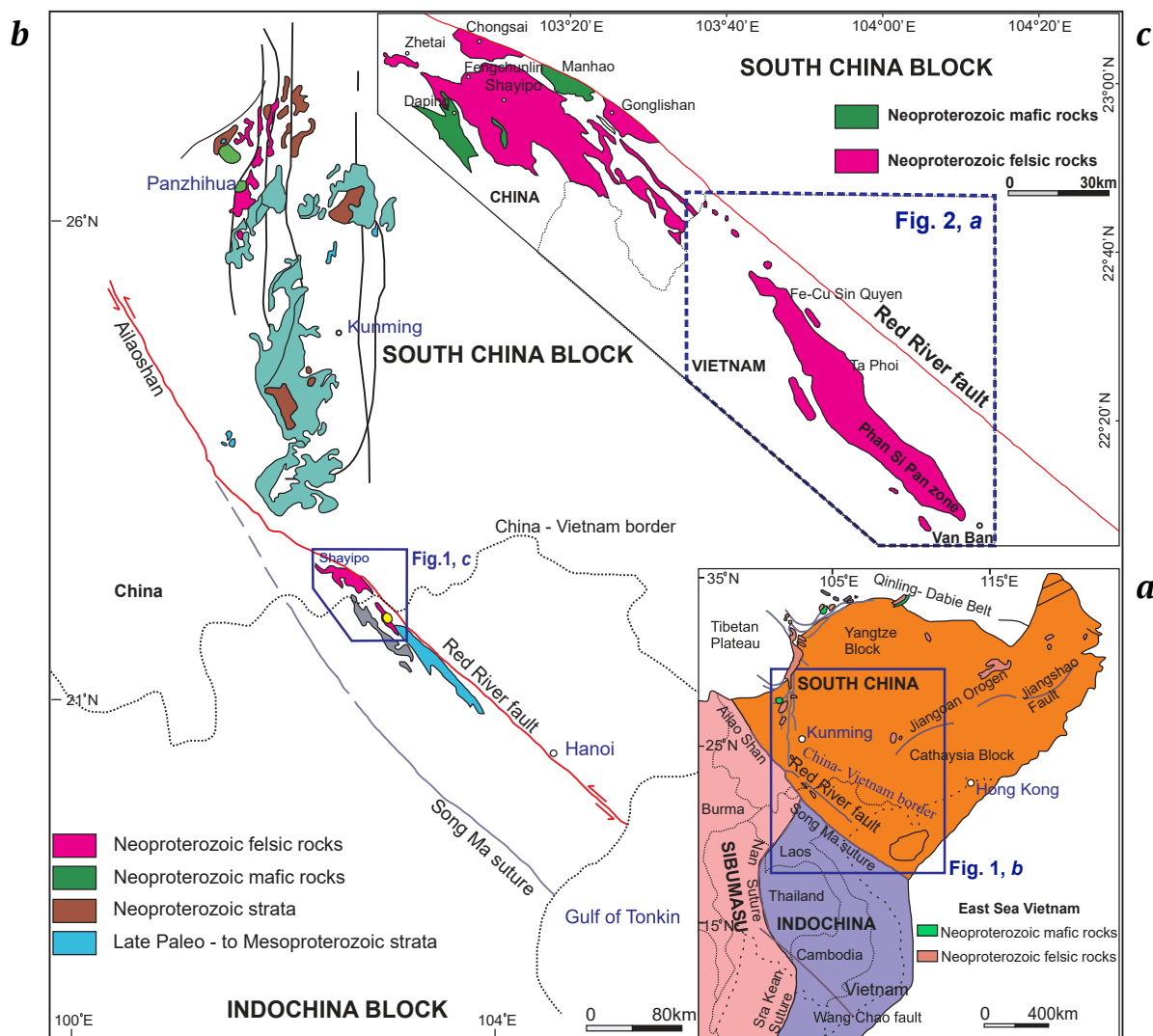


Fig. 1. Simplified tectonics map of NW Vietnam and adjoining areas ([20–23] and references therein)

The Mesoproterozoic–Paleoproterozoic crystalline basement is unconformably overlain by Paleozoic–Mesozoic meta-sedimentary and sedimentary sequences, which include quartz-sericite-chlorite schist, quartzite, limestone, and dolomite (see Figs. 2, *a, b*). In addition to the Precambrian granitoids, voluminous A-type granites intruded during the Late Permian–Early Triassic, closely associated with the Emeishan mantle plume [29–31, 39]. Cenozoic plutons have also been identified in the region [40, 41].

The Neoproterozoic granitoid intrusions in the Phan Si Pan zone include the Po Sen, Phin Ngan, and Lung Thang plutons, along with several smaller bodies and lenses (Fig. 2, *b*) [42]. These intrusions are comparable to the widespread Neoproterozoic granitoids (~860–740 Ma) in the western and southwestern Yangtze Block (see Fig. 1) [42–47].

2. Geology of the Ta Phoi deposit

2.1. Stratigraphy and Lithology

The Ta Phoi copper deposit is located in Ta Phoi area, Lao Cai Province, covering an area of approximately 4 km². The deposit occurs in the northeastern limb of the Hoang Lien Son anticlinorium, within the Phan Si Pan structural zone. It is primarily composed of metamorphosed sedimentary suites of the Sin Quyen Formation, along with small undated intrusive bodies situated adjacent to the large intrusive mass of the Po Sen Complex. The deposit is primarily hosted in metamorphic rocks of the second unit of the Sin Quyen Formation (PPsq₂), which is a key geological factor closely associated with copper ore formation in the study area [4, 14].

The second unit of the Sin Quyen Formation is widespread in the Ta Phoi area and consists of quartz-feldspar-biotite schist, metasomatic rocks, amphibolite lenses, and graphite-bearing quartz-mica schist. The feldspar-quartz-biotite schist contains small amount to no graphite, exhibits a brown color, schistose structure, and lepidoblastic texture. Muscovite-sericite minerals (1–8%) are commonly enriched along orebody margins and fault zones. Accessory minerals include sphene, apatite, epidote, zoisite, and ore minerals.

The metasomatic rocks occur as bands in the central part of the area, while amphibolite appears as lenticular bodies within the metasomatic rocks, characterized by an opaque white color, interbedded with greenish layers. Amphibolite is commonly found along the hanging walls of copper ore bodies. The graphite-bearing quartz-mica schist is gray and exhibits a schistose structure. Copper mineralization is primarily hosted in metasomatic rocks, with lesser occurrences in feldspar-quartz-biotite schist. The second unit has a thickness exceeding 800 m (Figs. 3, *a–d*).

2.2. Igneous rocks

Granitoid formations of the Po Sen complex and granodiorite, diorite intrusions are widespread in the Ta Phoi area, along with the presence of lamprophyre dikes. Rocks of the Po Sen complex are distributed along the western and southwestern margins of the area, mainly represented by phase 2 and phase 3. Phase 2 consists of biotite granite and biotite-hornblende granite, while Phase 3 is characterized by light-colored dike rocks, including aplite granite and pegmatitic granite.

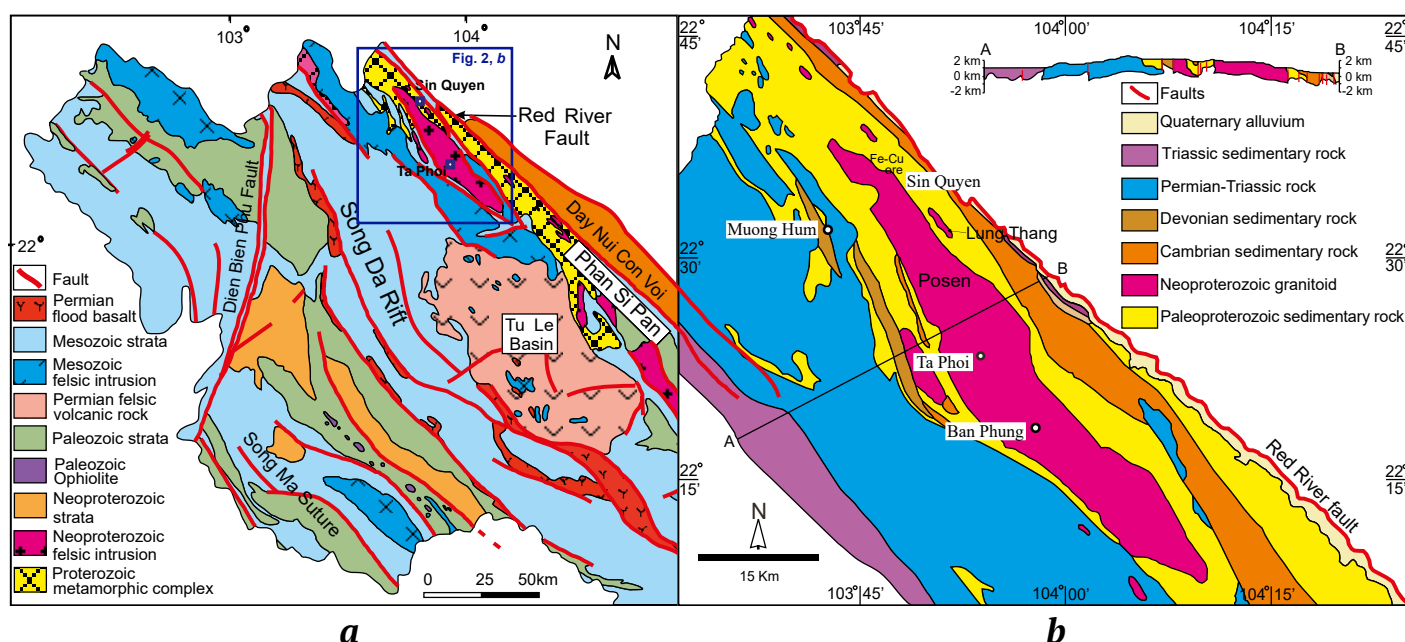


Fig. 2. Geological map of (*a*) northwestern Vietnam and (*b*) the Phan Si Pan zone and showing location of the Ta Phoi deposit (modified after [32])

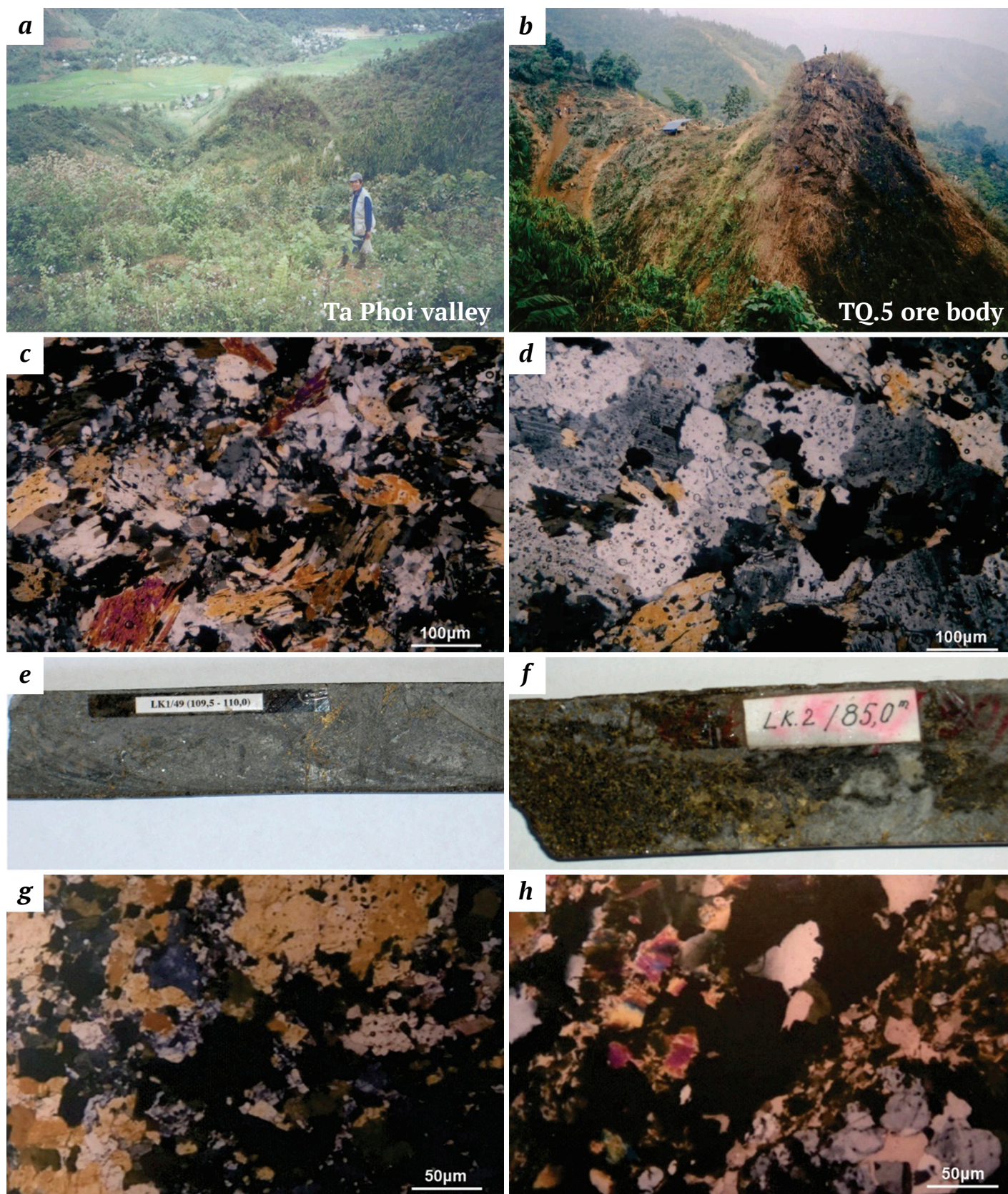


Fig. 3. Geological structure and material composition of the Ta Phoi deposit:

a, b – general view of the Ta Phoi valley and mining operations at the TQ.5 ore body (photo from [14]);

c, d – photomicrographs of rocks in transmitted light (magnification 35×, Nikon microscope): *c* – felsic schist (feldspar, quartz, biotite), drill core LK.2/28, depth 89–91 m; *d* – dark-colored metasomatic rock, drill core LK.1/13, depth 25–27 m (photo by Do Van Nhuan from [14]); *e–h* – manifestations of ore mineralization: *e, g* – disseminated ore in dark-colored metasomatic rock, drill core LK.1-T.1, depth 109.5–110 m; *f, h* – disseminated ore in felsic schist, drill core LK.2-T.1, depth 85 m (photo by Ly Quoc Su from [14])

U–Pb and $^{40}\text{Ar}/^{39}\text{Ar}$ dating methods have clarified the thermochronological history of the Po Sen complex. U–Pb analysis of composite samples of zircon grains by TIMS yielded an average age of 760 ± 25 Ma, clustering on the concordia line, while twelve SHRIMP U–Pb analyses provided a consistent age of 751 ± 7 Ma [38]. Combined with geochemical characteristics, these results indicate that the Po Sen complex is a Late Proterozoic magmatic complex.

Granodiorite and diorite rocks (namely Phin Ngan, Suoi Thau, Lung Thang massifs) are commonly found along the margins of ore bodies, with copper grades ranging from 0.01 to 0.4%. Copper mineralization within the diorite occurs as sparse dissemina-

tion and micro-veinlets along fractures. These rocks are gray to light gray, exhibit a massive structure, and have fine- to medium-grained textures, with localized weak deformation. Their crosscutting relationship with the surrounding rocks is unclear.

The absolute age dating results using the zircon U–Pb method for the granodiorite and diorite intrusions yielded ages of 776 ± 12 Ma for the Suoi Thau massif [48], 824 ± 4 Ma for the Phin Ngan massif [42], and 803 ± 3 Ma for the Lung Thang massif [47]. These results indicate that the formation of the granodiorite and diorite intrusions occurred during the Neoproterozoic. Moreover, most studies suggest that these intrusive bodies were generated in a subduction-related continental arc setting [42, 47, 48].

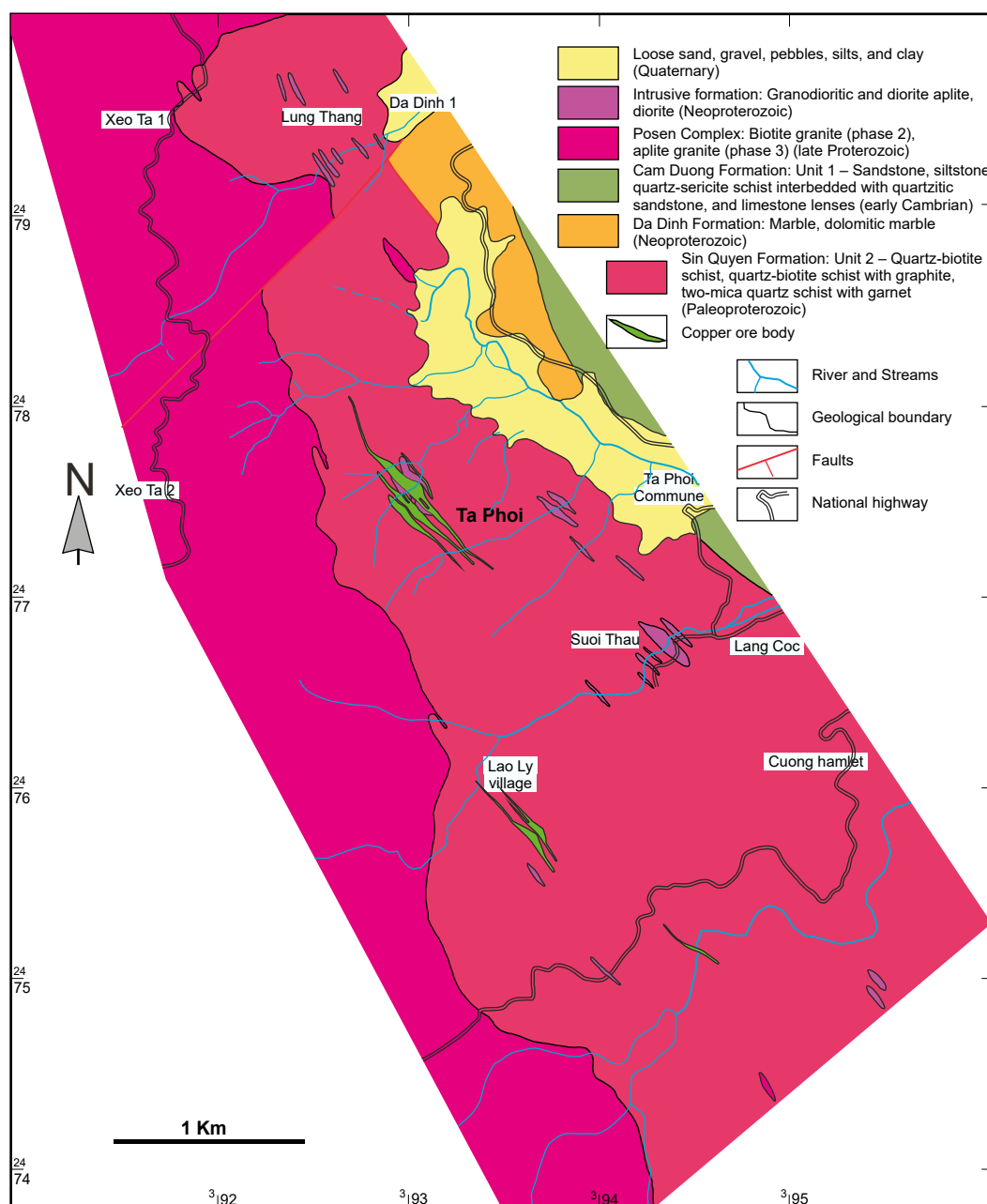


Fig. 4. Geological map of Ta Phoi area showing location of the Ta Phoi deposit (modified after [14])

Lamprophyre dikes intrude the surrounding rocks and are characterized by a grayish-green color, oriented structure, fine-grained texture and prismatic-granular texture. These dikes appear to have little to no association with copper mineralization.

2.3. Tectonics

The Ta Phoi ore deposit is located in the north-eastern limb of the Po Sen anticline, which exhibits a general monoclinic structure trending north-west-southeast and dipping to the northeast. Geological survey data indicate that surface rocks are strongly deformed, while drill core data reveal that at depth, both the host rocks and ore bodies maintain a consistent northeastward dip with dip angles ranging from 60 to 75° [4].

Along the Phoi 1 stream, a northwest-southeast trending fault, named Lang Phoi 1 Fault (F2), is observed. This fault is a subsidiary structure of the Ta Phoi Fault. The Lang Phoi 1 Fault cuts through and displaces rocks of the Sin Quyen Formation as well as biotite granite of the Po Sen Complex. Additionally, within the study area, the Ta Xeo 2 – Da Dinh Fault (F3) is identified. This fault extends along the Da Dinh

valley to Ta Xeo 2, with a total length of approximately 2.5 km. The Ta Xeo 2 – Da Dinh Fault displaces rock formations and intersects northwest-southeast trending faults [14] (Fig. 4).

2.4. Ore body distribution characteristics

The Ta Phoi copper deposit comprises 15 ore bodies, including lens-shaped and vein-type bodies. Among them, three large ore bodies (TQ.4, TQ.5, TQ.6) have been delineated, while the remaining 12 occur as smaller veins and lens-shaped clusters scattered throughout the area or along the margins of the larger ore bodies (TQ.1, TQ.2, TQ.3a, TQ.4a, TQ.7, TQ.8, TQ.9a, TQ.9b, TQ.10, TQ.10a, TQ.11, TQ.13) [14, 15]. These ore bodies dip northeastward at angle ranging from 60° to 85°, with strike length varying from 300 to 1200 m, thickness ranging from 1.5 to 94.8 m, and depths controlled up to 30–130 m. The primary ore minerals include chalcopyrite, cubanite, pyrite, and pyrrhotite, which exhibit irregular dissemination, occurring as isolated grains, clustered aggregates, or small ore pockets. These minerals also form veins filling microfractures and replacing pre-existing rock-forming minerals (Figs. 3, 5, Table 1).

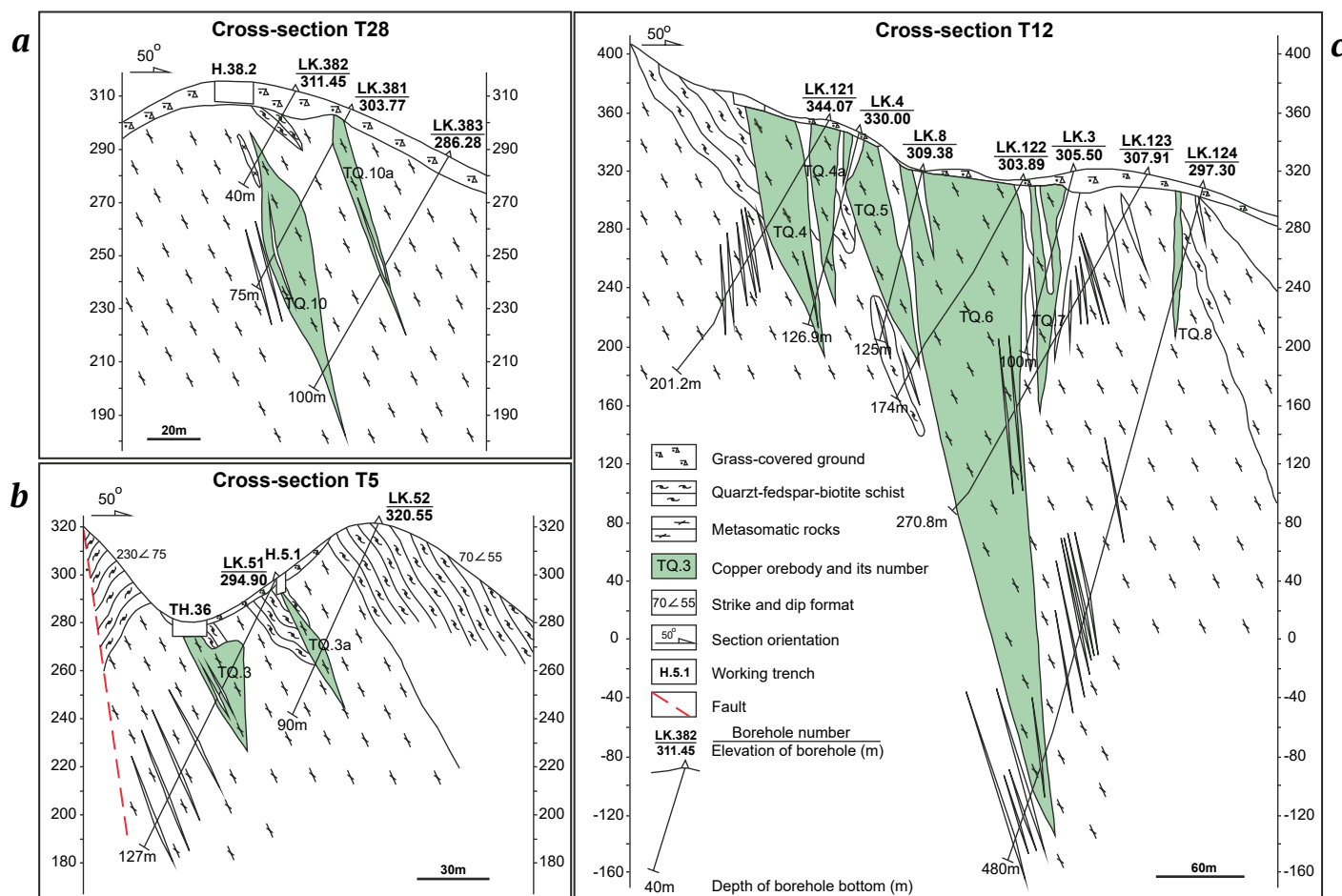


Fig. 5. Geological cross-sections along T5, T12, T28 lines showing TQ.3, TQ.3a, TQ.4, TQ.5, TQ.6, TQ.7, TQ.8 and TQ.10 orebodies [15]



2.5. Ore textures and structures

2.5.1. Types of ores and their properties

Petrographic and reflected light microscope analyses of copper ore samples from the study area reveal a complex assemblage of primary and secondary ore minerals. The primary sulfide minerals include chalcopryrite, bornite, pyrite, pyrrhotite, and cubanite,

while the secondary minerals such as covellite, chalcocite, malachite, and limonite occur as oxidation products in supergene alteration zones. Gangue minerals associated with the copper mineralization mainly comprise quartz and carbonate minerals.

Primary ore minerals include chalcopryrite, bornite, pyrite, pyrrhotite, cubanite, and magnetite.

Table 1

Morphological characteristics and composition of copper ore bodies in Ta Phoi deposit (after [14, 15])

Ore body number	Morphology of ore bodies	Length (m)	Dip direction	Dip angle	Average thickness (m)	Average copper grade (%)	Ore mineral composition
TQ.1	Vein	442	70°	65°	3.69	0.405	Pyrite 2%, chalcopryrite 1%, pyrrhotite 2%, marcasite in small amount, a arsenopyrite in small amount, rutin a few grains
TQ.2	Vein	300	65°	70°	2.00	0.447	Pyrite 3%, chalcopryrite in small amount, pyrrhotite 2%, graphite 1%, ilmenite in small amount
TQ.3a	Vein	210	60°	55°	12.05	0.455	Pyrite a few grains, chalcopryrite in small amount, covellite in small amount, graphite in small amount, ilmenite 1%
TQ.4	Large lense	580	50°	65°	21.04	0.698	Pyrite 1–2%, chalcopryrite 0.5–8%, pyrrhotite 10–55%, cubanite in small amount, graphite in small amount to 3%, covellite in small amount, molybdenite in small amount, gold 4–9 grains
TQ.4a	Vein	240	50°	65°	10.37	0.455	Pyrite 1%, chalcopryrite 8%, cubanite in small amount, covellite in small amount, molybdenite in small amount
TQ.5	Large lense	830	50°	70°	16.56	0.638	Pyrite in small amount to 5%, chalcopryrite in small amount to 8%, pyrrhotite 1–12%, cubanite in very small amount to 1%, graphite in small amount, covellite in small amount, hematite a few grains
TQ.6	Large lense	597	60°	75°	16.39	0.835	Pyrite in small amount to 5%, chalcopryrite 1–10%, pyrrhotite in small amount to 8%, cubanite 1–10%, covellite in small amount to 3%, rutin a few grains, limonite in small amount to 5%, gold 1–18 grains
TQ.7	Small lense	418	60°	75°	8.37	0.691	Pyrite in small amount to 5%, chalcopryrite 1–10%, pyrrhotite in small amount to 8%, cubanite 1–10%, covellite in small amount to 3%, rutile a few grains, limonite in small amount to 5%
TQ.8	Vein	270	60°	75°	5.53	0.587	Pyrite in small amount, chalcopryrite 15%, melnikovite in small amount, cubanite in very small amount to 1%, covellite 1%, limonite 1%
TQ.9a	Large lense	735	65°	65°	13.61	0.530	Pyrrhotite 10–18%, chalcopryrite in small amount to 2%, graphite in small amount to 3%, cubanite in very small amount, sphene a few grains
TQ.9b	Large lense	640	60°	60°	9.96	0.516	Pyrrhotite in very small amount to 10%, chalcopryrite 0.5–12%, pyrite 2%, arsenopyrite 1%, graphite in small amount, cubanite very scarce, sphene a few grains, covellite in small amount, and limonite 0.5%.
TQ.10	Small lense	340	50°	70°	11.69	0.568	Pyrrhotite in very small amount to 8%, chalcopryrite 1%, magnetite 3%, ilmenite 1–2%
TQ.10a	Small lense	190	50°	70°	13.79	0.763	Pyrrhotite 30%, chalcopryrite 4%, graphite 7%, pyrite 1%, sphalerite in very small amount
TQ.11	Vein	718	60°	65°	4.77	0.674	Pyrrhotite 2–6%, chalcopryrite 1%, graphite 2%, sphene a few grains, sphalerite in very small amount
TQ.13	Vein	400	65°	70°	3.09	0.481	Pyrite in very small amount to 2%, chalcopryrite 1–10%, graphite 1–2%, marcasite in very small amount to 3%, covellite in small amount, rutile in small amount

Chalcopyrite (CuFeS_2): The most abundant copper-bearing mineral, occurring as anhedral to subhedral grains with sizes ranging from 0.1 to 2 mm, typically between 0.1 and 1 mm. Chalcopyrite commonly exhibits disseminated, vein, and replacement textures, forming intergrowths with pyrite and pyrrhotite (Figs. 3, *a*, *b*). Under the microscope, chalcopyrite is characterized by its straw-yellow color with moderate reflectance.

Bornite (Cu_5FeS_4): Occurs as fine-grained disseminations or as replacement rims around chalcopyrite.

In some samples, bornite is partially replaced by covellite, indicating secondary enrichment (Figs. 3, *n*, *o*). It exhibits a distinct purplish-brown to reddish hue under the microscope.

Pyrite (FeS_2): Present as euhedral to subhedral grains, ranging in size from 0.1 to 2 mm, often forming intergrowths with chalcopyrite. Pyrite is commonly replaced by chalcopyrite and bornite along fractures and grain boundaries (Figs. 3, *e*, *f*). Under reflected light, pyrite appears bright yellow with high reflectance.

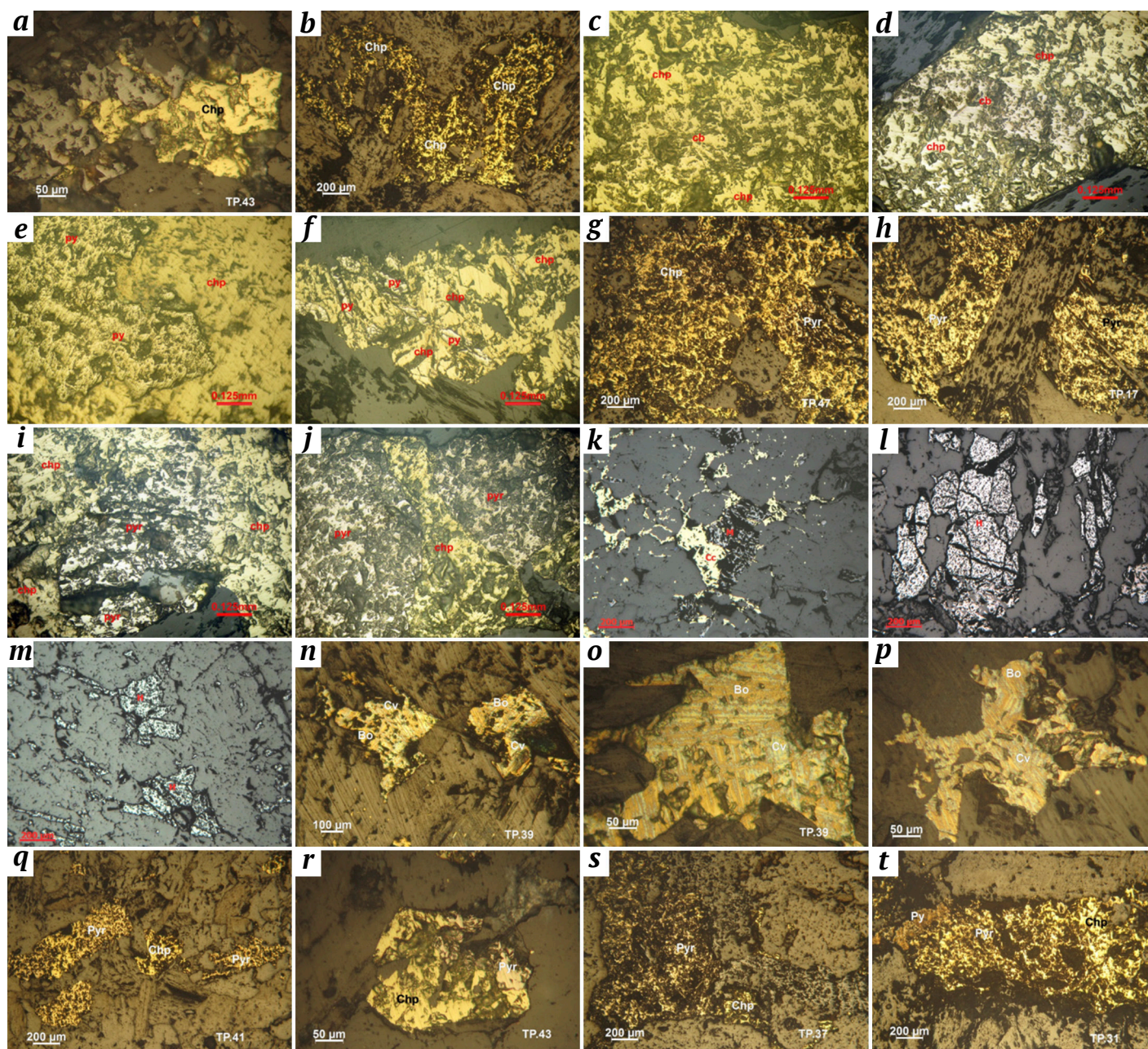


Fig. 6. Primary copper ore mineral assemblage in the Ta Phoi deposit:

a, *b* – disseminated chalcopyrite in a gangue matrix; *c*, *d* – syngenetic relationship between chalcopyrite and cubanite; *e* – chalcopyrite replacing pyrite; *f* – disseminated chalcopyrite and pyrite in an ore matrix; *g*, *h*, *i*, *j* – disseminated chalcopyrite and pyrrhotite in a gangue matrix; *k* – euhedral chalcopyrite grains replacing magnetite; *l*, *m* – subhedral hematite grains forming clusters within the rock matrix; *n*, *o*, *p* – bornite replaced by covellite through corrosive processes; *q*, *r*, *s*, *t* – euhedral chalcopyrite and pyrrhotite disseminated within the rock matrix



Pyrrhotite (Fe_{1-x}S): Found as anhedral grains up to 2 mm in size, often occurring in association with chalcopyrite and cubanite. Pyrrhotite grains exhibit weak anisotropy and are commonly replaced by later-stage sulfides (Figs. 3, *g, h, i, j*).

Cubanite (CuFe_2S_3): A minor phase in the ore, appearing as thin lamellar intergrowths within chalcopyrite. Cubanite has a darker yellow color with a faint pinkish tint under the microscope (Figs. 3, *c, d*).

Magnetite (Fe_3O_4): Occurs as fine, scattered grains within the ore, often showing replacement by chalcopyrite (Fig. 3, *k*).

Secondary ore minerals are covellite, chalcocite, limonite, and malachite.

Covellite (CuS): Originates as a supergene product replacing chalcopyrite and bornite, often appearing as deep blue rims around primary sulfides (Fig. 3, *p*).

Chalcocite (Cu_2S): Found in small amounts, typically replacing chalcopyrite in oxidation zones. It appears as a fine-grained, dark gray mineral with a metallic luster.

Limonite ($\text{FeO}(\text{OH}) \cdot n\text{H}_2\text{O}$): It is widespread in oxidation zones, pseudomorphically replacing pyrite and chalcopyrite. It is commonly associated with goethite and hematite.

Malachite [$\text{Cu}_2(\text{OH})_2\text{CO}_3$]: Occurs as green botryoidal crusts, often coating surfaces of fractures and voids within altered host rocks.

The results of mineralogical sample analysis indicate that the Ta Phoi deposit exhibits the following common ore textures and structures.

Disseminated and clustered structures: These are the most common structures observed in the ore bodies, where chalcopyrite, pyrite, pyrrhotite, and cubanite are dispersed as fine to medium-grained aggregates in the host rock matrix (Figs. 3, *q, r, s, t*). The distribution of ore minerals is irregular, with forming clusters of variable sizes within altered host rocks.

Massive structure: Pyrite, pyrrhotite, and chalcopyrite frequently occur as compact massive aggregates, forming sulfide-rich zones. These zones often appear as coarse-grained, tightly packed sulfides, replacing earlier mineral phases (Figs. 3, *c, e*).

Vein and stringer structures: Hydrothermal replacement and infill processes have resulted in the formation of sulfide-bearing veins and micro-veinlets, composed mainly of chalcopyrite, pyrrhotite, and minor chalcocite. These veinlets exhibit variable thicknesses and cut across the host rock, often filling fractures and microfractures (Fig. 3, *t*).

Replacement and corrosion structures: Secondary enrichment zones show formation of covellite, chalcocite, limonite, and goethite replacing and

corroding primary sulfides such as chalcopyrite and pyrrhotite. These minerals form rims around the primary sulfides, indicating manifestations of oxidation and supergene processes (Figs. 3, *i, l*).

Euhedral to subhedral grain texture: Chalcopyrite and pyrite frequently exhibit well-developed crystal faces, indicating crystallization under favorable conditions. This texture is more commonly observed in primary mineralization zones.

Anhedral grain texture: A prevalent texture in the sulfide ores, where chalcopyrite, pyrrhotite, and cubanite display irregular, intergrown morphologies due to replacement and overgrowth processes.

Colloform texture: Observed mainly in secondary minerals such as marcasite, melnikovite, and covellite, forming concentric layers around pre-existing sulfides. This texture suggests low-temperature hydrothermal precipitation.

Residual texture: Early-formed sulfides, such as pyrite and pyrrhotite, are partially replaced by younger sulfides like chalcopyrite and bornite, leaving behind embayed and corroded outlines.

Brecciated and fragmented texture: In faulted and sheared zones, sulfide minerals appear fragmented and cemented by later-stage hydrothermal minerals, forming breccia-like textures.

2.5.2. Paragenetic sequence

Based on the geological conditions of ore formation, the morphological relationships of minerals within the ore, and their genetic morphological characteristics, it is possible to identify characteristic mineral associations as well as the ore-forming periods and stages present in the study area. A summarized mineral associations are provided in Table 2.

The hydrothermal period consists of three ore-forming stages. Early stage is dominated by the formation of disseminated quartz and magnetite with minor pyrite. Main sulfide stage is characterized by origination of sulfide minerals, forming a mineral association of pyrite, pyrrhotite, chalcopyrite, and cubanite alongside quartz. The mineralization occurs predominantly as disseminated grains, with minor development in veinlets. Post ore stage represents the principal phase of copper ore formation. This stage produces a quartz–chalcopyrite–cubanite association, accompanied by extensive hydrothermal alteration of the host rocks, including epidotization, actinolitization, tremolization, and chloritization.

The supergene enrichment period consists of a single ore-forming stage, characterized by covellinization, chalcocitization, and limonitization of primary ore minerals (see Table 2).



Table 2

Mineral associations at the Ta Phoi deposit, northwestern Vietnam

Minerals	Hydrothermal mineralization			Epigenesis
	Quartz – mag-netite	Quartz – pyrite	Quartz – chalcopyrite – cubanite	Covellite – chalcocite – limonite
Quartz				
Magnetite	— — — — —	— — — — —		
Pyrite		— — — — —	— — — — —	
Molybdenite		— — — — —		
Chalcopyrite			— — — — —	
Cubanite			— — — — —	
Pyrrhotite			— — — — —	
Melnikovite			
Chalcocite				— — — — —
Covellite				— — — — —
Goethite				— — — — —
Hydrogoethite				— — — — —
Limonite				— — — — —

— — — — — Main (>5%)
 — — — — — Minor (1–5%)
 Locally occurring

3. Sampling and analytical methods

3.1. Study material and petrography observation

This study used sulfide copper ore samples and associated gangue minerals, including sphene and quartz, collected from both surface and subsurface exposures of the Ta Phoi deposit. Selected samples were prepared as polished sections and observed under optical microscopy and Scanning Electron Microscopy (SEM) for mineral identification, textural relationships, and alteration features of sphene and associated minerals.

3.2. Analytical methods

3.2.1. SEM analysis

SEM study was conducted using an FEI Quanta 200 microscope equipped with an EDS system at 20 kV and 20 nA. Back-scattered electron (BSE) imaging was applied to study zoning, morphology, and alteration features of sphene. Analyses were performed at the National Key Laboratory, China University of Geosciences (Wuhan).

3.2.2. Fluid inclusion microthermometry

Doubly polished quartz sections (~0.20 mm thick) were analyzed using a Linkam THMSG 600 heating-freezing stage mounted on an Olympus BX51 microscope. The fluid inclusion study was focused on primary, pseudosecondary, and secondary inclusions based on established classification criteria [49, 50]. Eutectic and melting temperatures were used to estimate salinity and fluid density, with calculations performed using the FLINCOR software. Temperature accuracy was $\pm 0.2^\circ\text{C}$ between -20°C and $+20^\circ\text{C}$.

3.2.3. Sulfur isotope analysis

Sulfur isotope measurements were conducted using a Delta V Plus mass spectrometer at the CNNC Beijing Research Institute of Uranium Geology. Results are reported in $\delta^{34}\text{S}$ values relative to the V-CDT standard, with analytical precision better than $\pm 0.2\text{‰}$ (2σ).

3.2.4. U-Pb isotope analysis of sphene

U-Pb dating of sphene was conducted at the State Key Laboratory of Geological Processes and Mineral Resources (GPMR), China University of Geosciences (Wuhan), using an Agilent 7700x ICP-MS system coupled with a GeoLas 2005 laser-ablation system equipped with a DUV 193 nm ArF-excimer laser. Analytical procedures and data reduction methods followed those described by Spandler et al. (2016) [51]. A laser spot size of 32 μm was used for all analyses, with ^{43}Ca serving as the internal standard isotope, previously measured by EPMA. NIST SRM610 was used as a bracketing external standard [51]. The laser fluence was set at 5 J/cm^2 , with a repetition rate of 10 Hz, the parameters optimized to enhance analytical sensitivity while minimizing elemental fractionation. Calibration of geochemical and isotopic data was achieved by performing one measurement of MKED1 and NIST SRM610 after every three ordinary sample analyses. The MKED1 reference material originates from the Elaine Dorothy Cu-Au-REE deposit in the Mount Isa Inlier, Queensland, Australia. Concordia diagrams and $^{206}\text{Pb}/^{238}\text{U}$ weighted mean age calculations were generated using Isoplot/Ex_ver3 [52].

4. Results and Discussions

4.1. Sulfur isotopic compositions of sulfide minerals

The analytical results of sulfide samples are summarized in Table 3. This study determined the $\delta^{34}\text{S}$ values for five chalcopyrite samples and one pyrite sample from the Ta Phoi deposit. The sulfur isotope compositions of these six samples range from +2.2‰ to +3.1‰, with an average of +2.85‰.

The sulfur isotope analyses of chalcopyrite and pyrite from the Ta Phoi deposit showed a narrow range close to 0‰, which is consistent with the mantle-derived sulfur signature (Fig. 7). This suggests that the source of ore-forming materials in the Ta Phoi copper deposit was relatively homogeneous magmatic reservoir.

4.2. Ore-forming fluids

Analyses of 8 quartz samples associated with copper ore identified 97 fluid inclusions with elliptical, triangular, or elongated elliptical morphologies. These inclusions are classified into two types: liquid-vapor (type I) and CO_2 - H_2O vapor inclusions (type II) (Table 4). Among them, type I inclusions (from 6 quartz samples) account for 77 inclusions, while type II inclusions (from 2 quartz samples) comprise 20 inclusions. Microthermometric measurements of the homogenization temperatures for type I (liquid-vapor) inclusions range from 163.1 to 375.6°C, with an average of 256.4°C. The dominant temperature range was 240–300°C. The freezing point temperatures vary between –10.5 and –1.0°C, predominantly between –5.0 and –3.0°C. For type II (CO_2 - H_2O) inclusions,

Table 3

Sulfur isotope compositions of chalcopyrite and pyrite crystals from ore samples of the Ta Phoi deposit

No.	Sample	Location	Mineral	$\delta^{34}\text{S}_{\text{V-CDT}}$	2 σ
1	TP-01	Surface, TQ.4	Chalcopyrite	2.6	0.2
2	TP-02	Surface, TQ.5	Chalcopyrite	2.4	0.2
3	TP-03	Surface, TQ.6	Chalcopyrite	2.2	0.2
4	TP-04	30m below surface, TQ.4	Chalcopyrite	2.9	0.2
5	TP-05	50m below surface, TQ.6	Chalcopyrite	3.1	0.2
6	TP-06	120m below surface, TQ.6	Pyrite	3.9	0.1
Average				2.85	

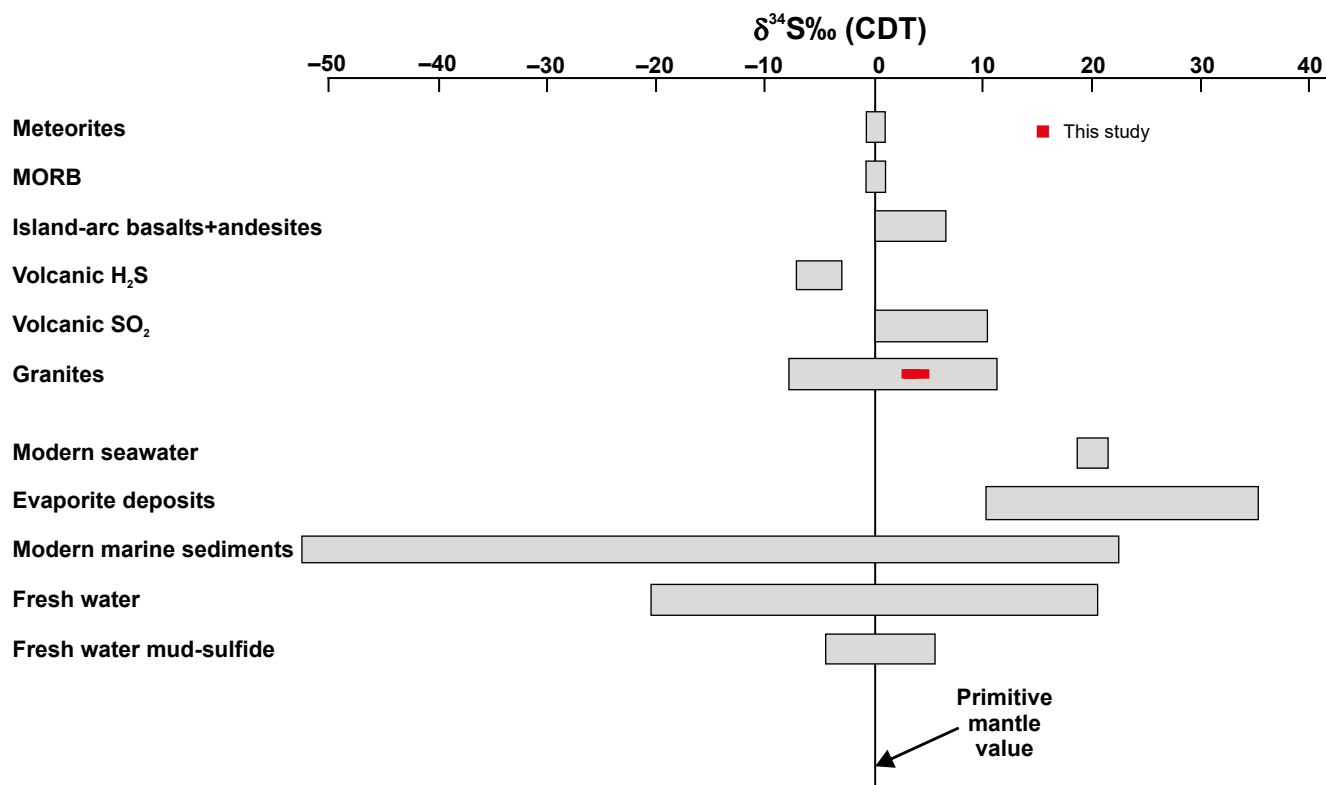


Fig. 7. Natural sulfur isotope reservoirs, showing copper forming material sources in the Ta Phoi deposit (data from [53–59])



homogenization temperatures range from 250 to 410°C, with an average of 350°C. The dominant temperature range was 330–360°C. The freezing point temperatures vary from –11.8 to –3.8°C, mostly between –6.2 and –4.8°C. The salinity of the fluid inclusions ranges from 2.1 to 16.25 wt %, with the majority falling between 4.0 and 6.6 wt %, and an average of 6.96 wt %. The fluid density ranges from 1.15 to 1.91 g/cm³, with an average of 1.35 g/cm³.

The fluid inclusion analyses indicated that the measured homogenization temperatures ranged from 163.1°C to 410°C, with a dominant range of 250°C to 350°C, classifying the ore-forming fluids as medium to relatively high temperature. The salinity values ranged from 2.1% to 16.25%, indicating a moderate salinity level. The ore-forming pressure varied between 43.98 and 99.85 MPa, while the formation depth ranged from 3.39 to 6.45 km, suggesting that the ore was formed at an intermediate depth.

4.3. Timing of copper mineralization

The U-Pb dating results for two samples of sphene are presented with the corresponding concordia diagrams shown in Fig. 8. In sample TP-12, 25 spot analyses performed on 10 sphene grains yielded concordant U-Pb ages, with a weighted average ²⁰⁶Pb/²³⁸U age of 810.7 ± 4.6 Ma (*n* = 25, MSWD = 0.82). Similarly, for sample TP-19, 25 spot analyses on 12 sphene grains produced concordant U-Pb ages, yielding a weighted average ²⁰⁶Pb/²³⁸U age of 819.5 ± 2.0 Ma (*n* = 25, MSWD = 5.2).

The U-Pb dating of sphene from the Ta Phoi copper deposit indicates that mineralization occurred between 810 and 820 Ma (Fig. 8). This age is comparable to the emplacement age of 860–740 Ma for granodiorite and diorite bodies such as the Phin Ngan, Suoi Thau, and Lung Thang massifs [11, 47, 65]. The spatial proximity of these intrusions to the Ta Phoi deposit suggests a genetic link between the copper mineralization and magmatic activity.

4.4. Origin and formation conditions

The Ta Phoi deposit is interpreted as a medium- to high-temperature hydrothermal-metasomatic deposit with a magmatic source of ore-forming materials. Copper ores are confined to the contact between the Sin Quyen Formation and hornblende diorite intrusions. They are mainly concentrated within altered rocks (with minor occurrences in quartz-feldspar-biotite schist) and are associated with a characteristic mineral association of tremolite-actinolite, albite, and epidote.

Moreover, the spatial proximity of the Neoproterozoic Phin Ngan, Suoi Thau, and Lung Thang granodiorite and diorite massifs to the Ta Phoi deposit suggests a potential genetic relationship between the two. This implies that the formation of the Ta Phoi deposit may have been influenced by tectonic processes associated with these magmatic intrusions. Specifically, the Phin Ngan, Suoi Thau, and Lung Thang massifs, which were formed in a subduction-related continental arc setting [11, 42, 47], may have played a crucial role in the mineralization process.

Table 4

Сводка данных по флюидным включениям на месторождении Та Фой

Sample	Type of inclusion	Quantity	$T_{m,ice}$, °C (mean)	T_h , °C (mean)	Salinity, wt % NaCl (mean)	Density, g/cm ³ (mean)	Pressure, MPa (mean)	Depth, km (mean)
TP-I.1	Type I	12	–2.9––2.1 (–2.53)	290–321 (304.5)	2.1–8.68 (5.19)	1.15–1.54 (1.29)	43.98–95.13 (66.56)	3.46–6.23 (4.76)
TP-I.2		14	–5.2––1.0 (–2.95)	163,1–372 (335.0)	3.06–14.25 (6.13)	1.16–1.68 (1.31)	44.53–99.85 (68.43)	3.50–6.45 (4.86)
TP-I.3		15	–10.5––2.3 (–3.94)	272–375,6 (314.24)	2.42–14.15 (7.42)	1.15–1.59 (1.32)	47.36–94.52 (69.70)	3.67–6.20 (4.93)
TP-I.4		12	–5.0––2.5 (–3.51)	240–350 (308.33)	4.63–11.55 (7.31)	1.13–1.51 (1.33)	46.06–93.44 (70.27)	3.39–6.15 (4.94)
TP-I.5		15	–5.1––2.5 (–4.21)	210–310 (266.67)	6.73–15.16 (9.99)	1.16–1.41 (1.29)	47.65–77.01 (64.18)	3.69–5.35 (4.65)
TP-I.6		9	–4.2––1.5 (–3.16)	170–285 (230.44)	7.02–16.05 (10.77)	1.18–1.47 (1.31)	49.19–87.55 (66.45)	3.79–5.87 (4.77)
TP-I.7	Type II	8	–11.8––3.8 (–5.81)	250–410 (333.5)	6.31–16.15 (11.62)	1.19–1.56 (1.35)	50.89–89.41 (69.94)	3.89–5.96 (4.96)
TP-I.8		12	–10.5––4.0 (–5.63)	280–405 (340.58)	7.73–16.25 (11.31)	1.20–1.91 (1.53)	48.34–91.69 (68.10)	3.73–6.07 (4.85)

Note: Salinities and density were calculated using the method proposed by [60, 61]; pressures were calculated using the method proposed by [62]; depths were estimated using the method proposed by [63,64]; $T_{m,ice}$ – final melting temperature of ice; T_h – homogenization temperature.

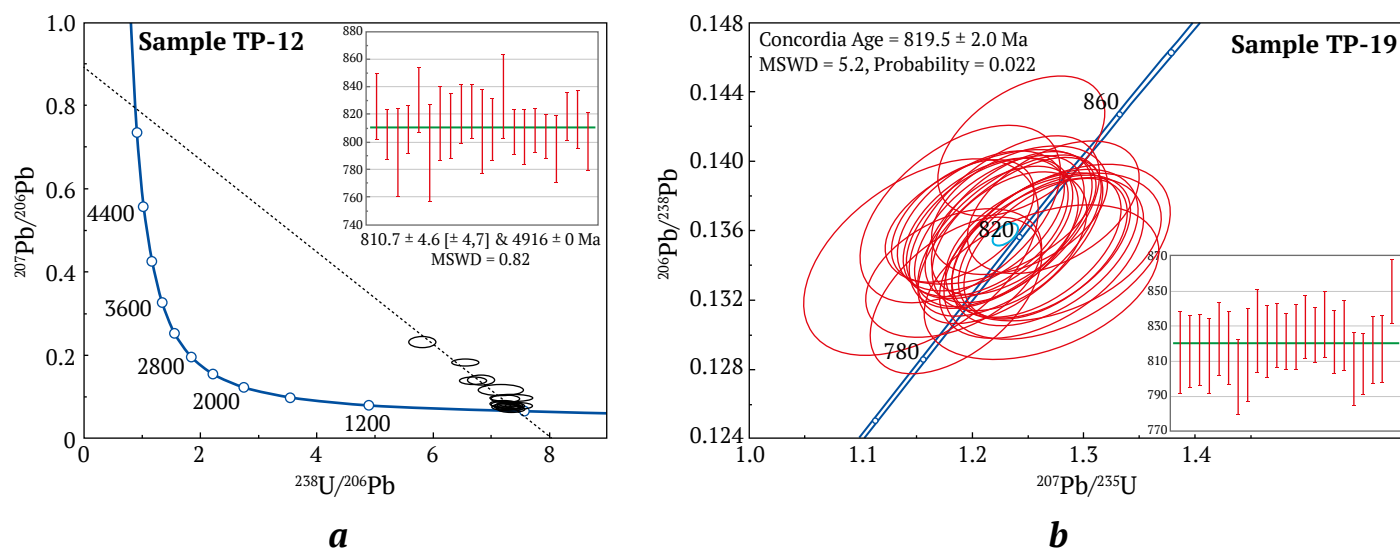


Fig. 8. Concordia diagrams for U-Pb isotopic dating of sphene from the Ta Phoi copper deposit:
a – Sample TP-12 (ore body TQ.4); b – Sample TP-19 (ore body TQ.6)

4.5. Comparison with well-studied porphyry copper deposits

The sulfur isotopic signatures (+2.2‰ to +3.1‰, average +2.85‰) observed in the Ta Phoi copper deposit fall within the typical range for mantle-derived sulfur, which is commonly reported in porphyry copper systems worldwide [66, 67]. For instance, sulfur isotopic values between 0‰ and +5‰ have been documented in sulfide minerals from porphyry Cu-Mo deposits in the Andes (e.g., Chuquicamata, El Teniente) [68], where magmatic sources dominate sulfur input. This consistency suggests that the Ta Phoi deposit, like classic porphyry systems, is also sourced from a relatively homogeneous magmatic reservoir.

In terms of fluid inclusion characteristics, the homogenization temperatures (163–410°C, dominant range 250–350°C) and salinities (2.1–16.25 wt % NaCl equivalent, averaging ~7 wt %) observed in the Ta Phoi deposit are comparable to those reported in porphyry copper systems globally [66–68]. For example, studies on the Batu Hijau (Indonesia) deposits have recorded similar fluid inclusion temperature ranges (250–400°C) and moderate to high salinities (3–16 wt % NaCl), indicative of magmatic-hydrothermal fluids undergoing phase separation and cooling during ore formation [69]. The depth estimates of 3.4–6.5 km at pressures of up to ~100 MPa in the Ta Phoi also align with typical porphyry copper deposit formation depths (2–6 km), further reinforcing this interpretation.

Additionally, the temporal constraint provided by U-Pb sphene ages (810–820 Ma) suggests that the Ta Phoi deposit formed synchronously with nearby Neoproterozoic magmatic intrusions (e.g., Phin Ngan,

Lung Thang, Suoi Thau). This timing of mineralization, spatial proximity, and geochemical affinity (e.g., sulfur isotope signatures, fluid composition) resemble the temporal and spatial relationships commonly observed between porphyry copper deposits and their causative intrusive bodies.

Taken together, the geological, geochemical, and fluid inclusion evidences from the Ta Phoi deposit collectively point to a magmatogene-hydrothermal origin, consistent with characteristics of porphyry copper systems. However, the dominant structural control and hydrothermal-metasomatic features observed in the deposit suggest that the deposit may represent a porphyry-related skarn or endoskarn system developed in response to magmatogene fluid migration along lithological and structural contacts.

4.6. Copper ore exploration potential and metallogenic implications

Data from the Phan Si Pan zone (including Sin Quyen, Ta Phoi, Phin Ngan, Lung Thang, and Suoi Thau deposits) suggest a major metallogenic event between 810 and 820 Ma.

U-Pb dating of granitoids across the zone and along the Ailao Shan–Red River belt confirms synchronous magmatism and mineralization [11, 65], pointing to a shared metallogenic system.

Given the wide distribution of granodiorite–diorite intrusions and their apparent link to the copper mineralization, the region holds high potential for additional undiscovered resources. In particular, areas such as Lung Thang and Suoi Thau remain underexplored and require further investigation.



Conclusions

This study enhances understanding of the Ta Phoi copper deposit through an integrated petrographic, geochemical, isotopic, and geochronological approach. The main findings are as follows:

Firstly, copper occurs in lensoid and vein-type bodies along NW-SE-trending structures. The ore association of chalcopyrite, bornite, pyrite, pyrrhotite, cubanite, and magnetite forms disseminated, anhedral- to subhedral-grained textures that record hydrothermal infilling and replacement.

Secondly, sulfur isotope compositions ($\delta^{34}\text{S}$) values for chalcopyrite and pyrite are magmatic in nature, pointing to nearby granodiorite-diorite intrusions (Phin Ngan, Suoi Thau, and Lung Thang massifs) as the primary metal and fluid reservoirs being sources of the deposit material.

Thirdly, U-Pb ages of hydrothermal sphene (819.5 ± 2.0 to 810.7 ± 4.6 Ma) fix the mineralizing

event in the Neoproterozoic and coincide with the age of intruding the regional intrusive suites, confirming a genetic link.

Furthermore, fluid inclusion microthermometry indicates moderate to high temperatures ($163\text{--}410\text{ }^{\circ}\text{C}$), moderate salinities (7–16 wt % NaCl eq.), trapping depths of $\sim 3.4\text{--}6.5$ km, and pressures of 44–100 Mpa, i.e. conditions typical of magmatogene hydrothermal systems.

Lastly, the magmatic sulfur signature, high-temperature saline fluids, and structural setting together suggest that Ta Phoi deposit represents a porphyry-related skarn (endoskarn) developed in a subduction-related convergent margin during the Neoproterozoic.

Collectively, these results refine the metallogenic framework of the Ta Phoi district and underscore its potential for further copper exploration in north-wester Vietnam.

References

1. Evans A.M. *Ore geology and industrial minerals: an introduction*. 3rd ed. Wiley-Blackwell; 1993. 403 p.
2. Misra K.C. *Understanding ore deposits*. Kluwer Academic Publishers; 2000. 845 p.
3. Robb L. *Introduction to Ore-Forming Processes*. Blackwell Publishing, Oxford; 2004. 373 p.
4. Tri T.V., Khuc V. (eds.) *Geology and earth resources of Vietnam*. General Department of Geology, and Minerals of Vietnam. Hanoi: Publishing House for Science and Technology; 2011. 645 p.
5. Fromaget J. *Études géologiques sur le Nord-Ouest du Tonkin et le Nord du Haut-Laos*. Hanoi; Service Géologique de l'Indochine; 1937. 153 p.
6. Thi P.T. Iron- and copper-bearing metasomatic rocks in the Lao Cai area. *Journal of Geology, Series A*. 1964;32(4):9–15. (In Vietnamese). URL: <http://idm.gov.vn/Data/TapChi/1964/A323.htm>
7. Hai T.Q. Further insights into ore-bearing metasomatic rocks in Sin Quyen. *Journal of Geology, Series A*. 1969;85–86(5–8):23–40. (In Vietnamese). URL: <http://idm.gov.vn/Data/TapChi/1969/a854.htm>
8. Cuong H.H., Han N.D. Ore-forming types in the Sin Quyen area. *Journal of Geology, Series A*. 1969;81–82(12):23–32. (In Vietnamese). URL: <http://idm.gov.vn/Data/TapChi/1969/a813.htm>
9. Mclean R.N. *The Sin Quyen iron oxide-copper-gold-rare earth oxide mineralization of North Vietnam*. In: Porter T.M. (Ed.) *Hydrothermal iron oxide copper-gold & related deposits: a global perspective. Volume 2*. Adelaide: PGC Publishing; 2001. Pp. 293–301.
10. Li X.C., Zhou M.F., Tran M.D. REE mineralization in the Sin Quyen Fe-Cu-LREE-(U-Au) deposit, Northwest Vietnam. In: *Abstracts of the Joint Assembly AGU-GAC-MAC-CGU*. Montreal, Canada; 2015.
11. Dung T.M., Luat N.Q., Hai T.T., et al. *Nature and formation age of copper mineralization in the northeastern Fan Si Pan belt and its metallogenic significance*. Fundamental research project in natural sciences, Code 105.01-2012.06, Ministry of Science and Technology; 2016. 50 p. (In Vietnamese).
12. Dac N.X., Zhao X.F., Hai T.T., et al. Two episodes of REEs mineralization at the sin quyen IOCG deposit, NW Vietnam. *Ore Geology Reviews*. 2020;125:103676. <https://doi.org/10.1016/j.oregeorev.2020.103676>
13. Anh T.T., Dung P.T., Hoa T.T., et al. 2010. *Enhancing mineral extraction efficiency and environmental protection: Investigating associated components in basic metal and rare earth mineral deposits in northern Vietnam*. State Science & Technology Programme, code KC.08.24/06-10. 459 p. (In Vietnamese).
14. Anh B.X. (Ed.) *Report on the assessment of copper ore potential and other mineral resources in the Ta Phoi area, Cam Duong Town, Lao Cai Province*. Hanoi: Intergeo Federation; 2007. (In Vietnamese).
15. San P.V. (Ed.). *Exploration report on copper ore in the Ta Phoi area, Lao Cai City, Lao Cai Province*. Hanoi: Geological Information and Archive Center; 2012. (In Vietnamese).
16. Metcalfe I. Permian tectonic framework and palaeogeography of SE Asia. *Journal of Asian Earth Sciences*. 2002;20(6):551–566. [https://doi.org/10.1016/S1367-9120\(02\)00022-6](https://doi.org/10.1016/S1367-9120(02)00022-6)



17. Metcalfe I. Palaeozoic and Mesozoic tectonic evolution and palaeogeography of East Asian crustal fragments: The Korean Peninsula in context. *Gondwana Research*. 2006. 9(1):24–46. <https://doi.org/10.1016/j.gr.2005.04.002>
18. Golonka J., Krobicki M., Paják J., et al. *Global plate tectonics and paleogeography of Southeast Asia*. Faculty of Geology, Geophysics and Environmental Protection. Arkadia, Kraków: AGH-University of Science and Technology; 2006. 128 p.
19. Hung K. T. Overview of magmatism in northwestern Vietnam. *Annales Societatis Geologorum Poloniae*. 2010;80(2):185–226. URL: http://www.asgp.pl/80_2_185_226
20. Pham T.H., Chen F., Wang W., et al. Zircon U-Pb ages and Hf isotopic composition of the Posen granite in northwest Vietnam. *Acta Petrologica Sinica*. 2009;25(12):3141–3152. (In Chinese with English abstract). URL: http://www.ysxb.ac.cn/en/article/id/aps_20091204
21. Wang W., Cawood P.A., Zhou M. F., Zhao J. H. Paleoproterozoic magmatic and metamorphic events link Yangtze to northwest Laurentia in the Nuna supercontinent. *Earth and Planetary Science Letters*. 2016;433:269–279. <https://doi.org/10.1016/j.epsl.2015.11.005>
22. Qi X., Santosh M., Zhao Y., et al. Mid-Neoproterozoic ridge subduction and magmatic evolution in the northeastern margin of the Indochina block: Evidence from geochronology and geochemistry of calc-alkaline plutons. *Lithos*. 2016;248–251:138–152. <https://doi.org/10.1016/j.lithos.2015.12.028>
23. Minh P., Hieu P.T., Thuy N.T.B., et al. Neoproterozoic granitoids from the Phan Si Pan Zone, NW Vietnam: Geochemistry and geochronology constraints on reconstructing South China–India Palaeogeography. *International Geology Review*. 2021;63(5):585–600. <https://doi.org/10.1080/00206814.2020.1728584>
24. Polyakov G., Balykin P., Hoa T.T., et al. Evolution of the Mesozoic-Cenozoic magmatism of the Song Da rift and its contouring structures. *Geologiya i Geofizika*. 1998;39(6):695–706. (In Russ.)
25. Anh T.V., Pang K.N., Chung S.L., et al. The Song Da magmatic suite revisited: A petrologic, geochemical and Sr–Nd isotopic study on picrites, flood basalts and silicic volcanic rocks. *Journal of Asian Earth Sciences*. 2011;42(6):1341–1355. <https://doi.org/10.1016/j.jseaes.2011.07.020>
26. Metcalfe I. Changhsingian (late Permian) conodonts from Son La, northwest Vietnam and their stratigraphic and tectonic implications. *Journal of Asian Earth Sciences*. 2012;50:141–149. <https://doi.org/10.1016/j.jseaes.2012.01.002>
27. Faure M., Lepvrier C., Van Nguyen V., et al. The South China block–Indochina collision: Where, when, and how? *Journal of Asian Earth Sciences*. 2014;79(Part A):260–274. <https://doi.org/10.1016/j.jseaes.2013.09.022>
28. Faure M., Lin W., Chu Y., Lepvrier C. Triassic tectonics of the southern margin of the South China block. *Comptes Rendus Geoscience*. 2016;348(1):5–14. <https://doi.org/10.1016/j.crte.2015.06.012>
29. Minh P., Hieu P.T., Hoang N.K. Geochemical and geochronological studies of the Muong Hum alkaline granitic pluton from the Phan Si Pan Zone, northwest Vietnam: Implications for petrogenesis and tectonic setting. *The Island Arc*. 2018;27(4):12250. <https://doi.org/10.1111/iar.12250>
30. Usuki T., Lan C.Y., Tran T.H., et al. Zircon U–Pb ages and Hf isotopic compositions of alkaline silicic magmatic rocks in the Phan Si Pan-Tu Le region, northern Vietnam: Identification of a displaced western extension of the emeishan large igneous province. *Journal of Asian Earth Sciences*. 2015;97(Part A):102–124. <https://doi.org/10.1016/j.jseaes.2014.10.016>
31. Tran T.H., Lan C.Y., Usuki T., et al. Petrogenesis of late permian silicic rocks of Tu Le basin and Phan Si Pan uplift (NW Vietnam) and their association with the Emeishan large igneous province. *Journal of Asian Earth Sciences*. 2015;109:1–19. <https://doi.org/10.1016/j.jseaes.2015.05.009>
32. *Geology of Vietnam: Stratigraphy*. DGMVN (Department of Geology and Minerals of Vietnam). Hanoi: Science Publisher; 1995. 359 p. (In Vietnamese).
33. Pham T.H., Lei W.X., Minh P., et al. Archean to Paleoproterozoic crustal evolution in the Phan Si Pan zone, Northwest Vietnam: Evidence from the U-Pb geochronology and Sr–Nd–Hf isotopic geochemistry. *International Geology Review*. 2022;64(1):96–118. <https://doi.org/10.1080/00206814.2020.1839976>
34. Lan C.Y., Chung S.L., Lo C.H., et al. First evidence for Archean continental crust in northern Vietnam and its implications for crustal and tectonic evolution in Southeast Asia. *Geology*. 2001;29(3):219–222. [https://doi.org/10.1130/0091-7613\(2001\)029<0219:FEFACC>2.0.CO;2](https://doi.org/10.1130/0091-7613(2001)029<0219:FEFACC>2.0.CO;2)
35. Nam T.N. 750 Ma U–Pb zircon age of the Po Sen Complex and tectonic implication. *Journal of Geology*. 2003;274:11–16. (In Vietnamese). URL: <http://idm.gov.vn/Data/TapChi/2003/274/t11.htm>
36. Zhao T., Cawood P.A., Wang K., et al. Neoproterozoic and Paleoproterozoic K-rich granites in the Phan Si Pan Complex, North Vietnam: Constraints on the early crustal evolution of the Yangtze Block. *Precambrian Research*. 2019;332:105395. <https://doi.org/10.1016/j.precamres.2019.105395>



37. Zhao T., Cawood P.A., Zi J. W., et al. Positioning the Yangtze Block within Nuna: Constraints from paleoproterozoic granitoids in North Vietnam. *Precambrian Research*. 2023;391:107059. <https://doi.org/10.1016/j.precamres.2023.107059>
38. Wang P.L., Lo C.H., Lan C.Y., et al. 2011. Thermochronology of the PoSen complex, northern Vietnam: Implications for tectonic evolution in SE Asia. *Journal of Asian Earth Sciences*. 2011;40(5):1044–1055. <https://doi.org/10.1016/j.jseaes.2010.11.006>
39. Pham T.H., Chen F.K., Thuy N.T.B., et al. Geochemistry and zircon U–pb ages and Hf isotopic composition of Permian alkali granitoids of the Phan Si Pan zone in northwestern Vietnam. *Journal of Geodynamics*. 2013;69:106–121. <https://doi.org/10.1016/j.jog.2012.03.002>
40. Pham T.T., Shellnutt J.G., Tran T.A., Lee H.Y. Petrogenesis of eocene to early Oligocene granitic rocks in Phan Si Pan uplift area, northwestern Vietnam: Geochemical implications for the Cenozoic crustal evolution of the South China block. *Lithos*. 2020;372:105640. <https://doi.org/10.1016/j.lithos.2020.105640>
41. Dung P.T., Usuki T., Tran H.T., et al. Emplacement ages, geochemical and Sr–Nd–Hf isotopic characteristics of Cenozoic granites in the phan si pan uplift, Northwestern Vietnam: Petrogenesis and tectonic implication for the adjacent structure of the red river shear zone. *International Journal of Earth Sciences*. 2023;112:1475–1497. <https://doi.org/10.1007/s00531-023-02307-4>
42. Li X.C., Zhao J.H., Zhou M.F., et al. Neoproterozoic granitoids from the Phan Si Pan belt, Northwest Vietnam: Implication for the tectonic linkage between Northwest Vietnam and the Yangtze Block. *Precambrian Research*. 2018;309:212–230. <https://doi.org/10.1016/j.precamres.2017.02.019>
43. Zhou M.F., Yan D.P., Kennedy A.K., et al. SHRIMP U–pb zircon geochronological and geochemical evidence for Neoproterozoic arc-magmatism along the western margin of the Yangtze Block, South China. *Earth and Planetary Science Letters*. 2002;196(1–2):51–67. [https://doi.org/10.1016/S0012-821X\(01\)00595-7](https://doi.org/10.1016/S0012-821X(01)00595-7)
44. Zhao J.H., Zhou M.F. Neoproterozoic adakitic plutons in the northern margin of the Yangtze Block, China: Partial melting of a thickened lower crust and implications for secular crustal evolution. *Lithos*. 2008;104(1):231–248. <https://doi.org/10.1016/j.lithos.2007.12.009>
45. Cai Y., Wang Y., Cawood P.A., et al. Neoproterozoic subduction along the Ailaoshan zone, South China: Geochronological and geochemical evidence from amphibolite. *Precambrian Research*. 2014;245:13–28. <https://doi.org/10.1016/j.precamres.2014.01.009>
46. Cai Y., Wang Y., Cawood P.A., et al. Neoproterozoic crustal growth of the Southern Yangtze Block: Geochemical and zircon U–Pb geochronological and Lu–hf isotopic evidence of neoproterozoic diorite from the Ailaoshan zone. *Precambrian Research*. 2015;266:137–149. <https://doi.org/10.1016/j.precamres.2015.05.008>
47. Dac N. X., Khan A., Ullah Z., et al. Neoproterozoic granitoids of northwest Vietnam and their tectonic implications. *International Geology Review*. 2024;66(16):2918–2939. <https://doi.org/10.1080/00206814.2024.2309470>
48. Dung T.M., Liu J.L., Li X.C., Cung D.M. Geology, fluid inclusion and isotopic study of the neoproterozoic Suoi Thau copper deposit, Northwest Vietnam. *Acta Geologica Sinica (English Edition)*. 2016;90(3):913–927. <https://doi.org/10.1111/1755-6724.12733>
49. Roedder E. *Fluid inclusions*. *Reviews in Mineralogy*. 1984;12:1–644.
50. Van den Kerkhof A.M., Hein U.F. Fluid inclusion petrography. *Lithos*. 2001;55(1–4):27–47. [https://doi.org/10.1016/S0024-4937\(00\)00037-2](https://doi.org/10.1016/S0024-4937(00)00037-2)
51. Spandler C., Hammerli J., Sha P., et al. MKED1: A new titanite standard for in situ analysis of SmNd isotopes and U–Pb geochronology. *Chemical Geology*, 2016;425:110–126. <https://doi.org/10.1016/j.chemgeo.2016.01.002>
52. Ludwig K. User's manual for Isoplot/Ex, version 3.00, a geochronological toolkit for Microsoft excel. *Berkeley: Berkeley Geochronology Center Special Publication*; 2003. 70 p.
53. Coleman M.L. Sulphur isotopes in petrology. *Journal of the Geological Society*. 1977;133:593–608. <https://doi.org/10.1144/gsjgs.133.6.0593>
54. Claypool G.E., Helser W.T., Kaplan I.R., et al. The age curves of sulfur and oxygen isotopes in marine sulfate and their mutual interpretation. *Chemical Geology*. 1980;28:199–260. [https://doi.org/10.1016/0009-2541\(80\)90047-9](https://doi.org/10.1016/0009-2541(80)90047-9)
55. Chambers L.A. Sulfur isotope study of a modern intertidal environment and the interpretation of ancient sulfides. *Geochimica et Cosmochimica Acta*. 1982;46(5):721–728. [https://doi.org/10.1016/0016-7037\(82\)90023-0](https://doi.org/10.1016/0016-7037(82)90023-0)



56. Sakai H., Casadevall T.J., Moore J.G. Chemistry and isotope ratios of sulfur in basalts and volcanic gases at Kilauea volcano, Hawaii. *Geochimica et Cosmochimica Acta*. 1982;46(5):729–738. [https://doi.org/10.1016/0016-7037\(82\)90024-2](https://doi.org/10.1016/0016-7037(82)90024-2)
57. Kerridge J.F., Haymon R.M., Kastner M. Sulfur isotope systematics at the 21oN site, East Pacific Rise. *Earth and Planetary Science Letters*. 1983;66:91–100. [https://doi.org/10.1016/0012-821X\(83\)90128-0](https://doi.org/10.1016/0012-821X(83)90128-0)
58. Ueda A., Sakai H. Sulfur isotope study of Quaternary volcanic rocks from the Japanese islands arc. *Geochimica et Cosmochimica Acta*. 1984;48(9):1837–1848. [https://doi.org/10.1016/0016-7037\(84\)90037-1](https://doi.org/10.1016/0016-7037(84)90037-1)
59. Chaussidon M., Albarede F., Sheppard S.M.F. Sulfur isotope variations in the mantle from ion microprobe analyses of micro-sulphide inclusions. *Earth and Planetary Science Letters*. 1989;92(2):144–156. [https://doi.org/10.1016/0012-821X\(89\)90042-3](https://doi.org/10.1016/0012-821X(89)90042-3)
60. Bakker R. *Optimal interpretation of microthermometrical data from fluid inclusions: thermodynamic modelling and computer programming*. Habilitation, Ruprecht-Karls-University; 1999.
61. Bakker R.J., AqSo_NaCl: Computer program to calculate P-T-V-X properties in the H₂O-NaCl fluid system applied to fluid inclusion research and pore fluid calculation. *Computers & Geosciences*. 2018;115:122–133. <https://doi.org/10.1016/j.cageo.2018.03.003>
62. Shao J.L., Mei J.M. On the study of typomorphic characteristics of mineral inclusion in the gold deposit from volcanic terrain in Zhejiang and its genetic and prospecting significance. *Minerals and Rocks*. 1986;3:103–111. (In Chinese with English Abstract).
63. Sibson R.H. Seismogenic Framework for Hydrothermal Transport and Ore Deposition. *Rev. Economic Geology*. 2001;14:25–50. <https://doi.org/10.5382/Rev.14.02>
64. Sibson R.H. Controls on Maximum Fluid Overpressure Defining Conditions for Mesozonal Mineralisation. *Journal of Structural Geology*. 2004;26(6–7):1127–1136. <https://doi.org/10.1016/j.jsg.2003.11.003>
65. Dac N.X., Son T.H., Tin Q.D., et al. In situ U-Pb isotopic dating method on titanite, and application to determine REE-Fe-Cu mineralization age of the Sin Quyen deposit, Lao Cai province. *Journal of Mining and Earth Sciences*. 2023;64(6):50–57. [https://doi.org/10.46326/JMES.2023.64\(6\).06](https://doi.org/10.46326/JMES.2023.64(6).06)
66. Seedorff E., Dilles J.H., Proffett J.M. Jr., et al. Porphyry deposits—characteristics and origin of hypogene features. society of economic geologists. *Economic Geology 100th Anniversary Volume, 1905–2005*. 2005:251–298. <https://doi.org/10.5382/AV100.10>
67. Sillitoe R.H. Porphyry Copper Systems. *Economic Geology*. 2010;105:3–41. <https://doi.org/10.2113/gsecongeo.105.1.3>
68. Berger B.R., Ayuso R.A., Wynn J.C., Seal R.R. *Preliminary model of porphyry copper deposits*. Open-File Report 2008–1321. Reston, VA: U.S. Geological Survey; 2008. 55 p. URL: <https://pubs.usgs.gov/of/2008/1321/>
69. Imai A., Ohno S., Primary ore mineral assemblage and fluid inclusion study of the Batu Hijau Porphyry Cu-Au deposit, Sumbawa, Indonesia. *Resource Geology*. 2008;55(3):239–248. <https://doi.org/10.1111/j.1751-3928.2005.tb00245.x>

Information about the authors

Khuong The Hung – Dr. Sci. (Earth Sci.), Lecturer, Department of Prospecting and Exploration Geology, Hanoi University of Mining and Geology, Hanoi, Vietnam; ORCID [0000-0003-1544-6470](https://orcid.org/0000-0003-1544-6470), Scopus ID [36716173500](https://orcid.org/36716173500); e-mail khuongthehung@humg.edu.vn

Ngo Xuan Dac – Dr. Sci. (Earth Sci.), Researcher, Vietnam Institute of Geosciences and Mineral Resources, Hanoi, Vietnam; e-mail dacbmks@gmail.com

Received 30.03.2025
Revised 14.06.2025
Accepted 16.06.2025



BENEFICIATION AND PROCESSING OF NATURAL AND TECHNOGENIC RAW MATERIALS

Research paper

<https://doi.org/10.17073/2500-0632-2025-06-419>

UDC 622.765:661.185.223.5



Application of polystyrene sulfonates for the depression of magnesium-containing silicates in copper-nickel ore flotation

A.A. Lavrinenko¹ , G. Yu. Golberg¹  , I.N. Kuznetsova¹  ,
O.G. Lusinyan¹  , V.A. Tverskoy²  

¹ Research Institute of Comprehensive Exploitation of Mineral Resources of the Russian Academy of Sciences,
Moscow, Russian Federation

² MIREA – Russian Technological University, Lomonosov Institute of Fine Chemical Technologies,
Moscow, Russian Federation

✉ lavrino_a@mail.ru

Abstract

It is very urgent to increase the efficiency of depressing magnesium-containing silicates (MS) in the course of the flotation of copper-nickel ores to reduce the content of magnesium in the concentrate, which causes a significant increase in energy consumption in pyrometallurgical processing of the concentrate. The use of polymer reagents containing sulfo groups seems to be a promising area of research. However, only lignosulfonates have been studied so far in this field. The question of the effectiveness of the depressing effect of other polymer sulfonates including polystyrene sulfonates (PSS), and their comparison with polysaccharides used in industrial conditions remains unclear. The purpose of this work is to study the depressing effect of PSS on the performance of bulk flotation of copper-nickel ores. Research objectives: to experimentally compare the effectiveness of the depressing effect of PSS and a reagent from the polysaccharide class on MS; to determine the modes of PSS use to reduce the magnesium content in the concentrate without significantly reducing the recovery of copper and nickel into the bulk concentrate; to establish the effect of molecular weight and the method of obtaining PSS samples on the effectiveness of their depressing effect. Laboratory experimental studies were carried out on the bulk flotation of copper-nickel ores from the Kola Peninsula, containing 15.7% of magnesium, 0.44% of nickel and 0.25% of copper. The effect of the following polymer anionic reagents on the flotation was studied: PSSs with molecular weight ranging from 89,000 to 208,000 g/mol; polyanionic cellulose (PAC-N) was used for comparison. To increase the effectiveness of these reagents, magnesium chloride was previously added. It was found that the lowest magnesium content in the concentrate of 14.7% was achieved using a composition of magnesium chloride and PSS against 16.7% without the depressants. It was shown that PSS provides a higher recovery of copper (by 7%) and nickel (by 8%) into the concentrate than when using PAC-N, since PSS, unlike polysaccharides, does not form chelate complexes with these metals. It was also shown that for PSS samples, the molecular weight within these limits has virtually no effect on the studied ore flotation performance. New scientific knowledge has been obtained about the effect of the consumption and properties of PSS on the flotation performance. It has been shown that the practical use of this class of reagents is advisable for the flotation of copper-nickel ores with a high magnesium content in cases where it is necessary to achieve the maximum possible decreasing the content of this element in the concentrate without significantly reducing the recovery of copper and nickel.

Keywords

flotation, copper-nickel ore, depression of magnesium-containing silicates, polystyrene sulfonates, magnesium cations, polyanionic cellulose


For citation

Lavrinenko A.A., Golberg G. Yu., Kuznetsova I.N., Lusinyan O.G., Tverskoy V.A. Application of Polystyrene sulfonates for the depression of magnesium-containing silicates in copper-nickel ore flotation. *Mining Science and Technology (Russia)*. 2025;10(3):280–288. <https://doi.org/10.17073/2500-0632-2025-06-419>



ОБОГАЩЕНИЕ, ПЕРЕРАБОТКА МИНЕРАЛЬНОГО И ТЕХНОГЕННОГО СЫРЬЯ

Научная статья

Применение полистиролсульфонатов для депрессии магнийсодержащих силикатов при флотации медно-никелевых руд**А.А. Лавриненко¹ , Г.Ю. Гольберг¹ , И.Н. Кузнецова¹ ,
О.Г. Лусинян¹ , В.А. Тверской² **¹ Институт проблем комплексного освоения недр им. академика Н.В. Мельникова РАН,
г. Москва, Российская Федерация² МИРЭА – Российский технологический университет, Институт тонких химических технологий
имени М.В. Ломоносова, г. Москва, Российская Федерация lavrin_a@mail.ru**Аннотация**

Весьма актуальной является задача повышения эффективности депрессии магнийсодержащих силикатов (МС) при флотации медно-никелевых руд для снижения содержания в концентрате магния, вызывающего существенное увеличение энергозатрат на пирометаллургическую переработку концентрата. Перспективным направлением представляется применение полимерных реагентов, содержащих сульфогруппы. Однако до настоящего времени изучено действие только лигносульфонатов. Остаётся неясным вопрос об эффективности депрессирующего действия других полимерных сульфонов, включая полистиролсульфонаты (ПСС), и их сравнении с полисахаридами, применяемыми в промышленных условиях. Цель настоящей работы: изучение депрессирующего действия ПСС на эффективность коллективной флотации медно-никелевой руды. Задачи исследований: экспериментальное сравнение эффективности депрессирующего действия ПСС и реагента из класса полисахаридов на МС; определение режимов применения ПСС, обеспечивающих снижение содержания магния в пенном продукте без существенного снижения извлечения меди и никеля в коллективный концентрат; установление влияния молекулярной массы и способа получения образцов ПСС на эффективность их депрессирующего действия. Выполнены лабораторные экспериментальные исследования по коллективной флотации медно-никелевой руды Кольского полуострова, содержащей 15,7 % магния, 0,44 % никеля и 0,25 % меди. Изучено влияние на флотацию полимерных анионоактивных реагентов: ПСС со значениями молекулярной массы от 89 000 до 208 000 г/моль; для сравнения применяли полианионную целлюлозу (ПАЦ-Н). Для повышения эффективности действия этих реагентов предварительно добавляли хлорид магния. Установлено, что наименьшее содержание магния в концентрате достигается применением композиции хлорида магния и ПСС и составляет 14,7 % против 16,7 % без депрессоров. Показано, что ПСС обеспечивает более высокое извлечение меди (на 7 %) и никеля (на 8 %) в концентрат, чем в случае применения ПАЦ-Н, так как ПСС, в отличие от полисахаридов, не образует хелатные комплексы с указанными металлами. Также показано, что для образцов ПСС значение молекулярной массы в указанных пределах практически не влияет на показатели флотации исследованной руды. Получены новые научные знания о влиянии расхода и свойств ПСС на показатели флотации и показано, что практическое применение этого класса реагентов целесообразно при флотации медно-никелевых руд с высоким содержанием магния в тех случаях, когда требуется достигнуть максимально возможного снижения содержания этого элемента в концентрате без существенного снижения извлечения меди и никеля.

Ключевые слова

флотация, медно-никелевая руда, депрессия магнийсодержащих силикатов, полистиролсульфонаты, катионы магния, полианионная целлюлоза

Для цитированияLavrinenko A.A., Golberg G.Yu., Kuznetsova I.N., Lusinyan O.G., Tverskoy V.A. Application of Polystyrene sulfonates for the depression of magnesium-containing silicates in copper-nickel ore flotation. *Mining Science and Technology (Russia)*. 2025;10(3):280–288. <https://doi.org/10.17073/2500-0632-2025-06-419>**Introduction**

The current stage of mining industry development is characterized by the involvement of relatively lean copper-nickel ores in processing [1–4]. A significant problem in the flotation of such ores is the presence of magnesium-containing silicate minerals (MS), including talc, serpentinite, and a number

of others [5, 6]. As a result of the extraction of these silicates into the concentrate, the content of harmful impurities, especially magnesium, increases. This, in turn, has an adverse effect on the subsequent processes of pyrometallurgical processing of the concentrate. For instance, according to [7], the effect of MS on the processing of nickel sulfide concentrate con-



sists in increasing energy consumption, increasing equipment wear, and growing the amount of sulfur dioxide atmospheric emission. This makes the problem of MS depression in copper–nickel ore flotation processes rather relevant.

Lowering MS recovery into flotation concentrate is achieved by using depressants that change the surface properties of these minerals by reducing the contact angle and/or increasing the negative surface charge. As a result, a potential barrier is created between a MS particle and an air bubble, which prevents the formation of a flotation complex and its extraction into the concentrate.

To date, various methods for depression of MS, mainly talc and serpentinite, have been developed. The first one is characterized by natural hydrophobicity due to the peculiarities of the crystal structure: weakly polar Si–O bonds predominate on the basal surface, which constitutes about 90% of the total surface of this mineral [8]. Therefore, the contact angle is relatively high, from 60 to 90° [9, 10]. Unlike talc, serpentinite is more hydrophilic, but its surface charge in acidic, neutral, and alkaline media (up to pH 11–12) is positive [11]. As a result of the mutual attraction of negatively charged sulfide particles and positively charged serpentinite particles, the latter are extracted into flotation concentrate. In this regard, various methods are used for talc and serpentinite depression.

Polysaccharides including carboxymethylated starches and celluloses (CMS and CMC, respectively), have become popular as talc depressants [12, 13]. They are characterized by a strong depressing effect not only on silicates, but also on sulfide minerals [14], i.e. low selectivity. Studies carried out at the IPKON RAS have shown that a domestically produced CMC sample manufactured under the PAC–N brand name (low molecular weight polyanionic cellulose) has a higher depressing capability against MS than foreign samples of reagents of the same class [15]. It is known that the effectiveness of CMC increases when combined with liquid glass, both in acidified [16] and in neutral form [17]. The papers [18, 19] have shown the possibility of effective depression of talc by lignosulfonates with the preliminary addition of calcium cations. The mechanism of depression in this case consists in reducing the hydrophobicity of talc under the influence of strong anionic sulfonate groups. At the same time, calcium cations contribute to an increase in the adsorption capacity of talc in relation to lignosulfonates. It is noted that the adsorption of lignosulfonate on chalcopyrite is lower than that on talc; this suggests that polymer reagents containing sulfo groups are selective in their depressing effect on

talc. The effect of other polymer sulfonates on the flotation of copper–nickel ores has not yet been studied both in Russia and abroad.

The results of monomineral talc flotation showed the depressing effect of sodium polystyrene sulfonates (PSS), which is slightly weaker than that of CMC and increases when magnesium or aluminum cations are pre-added [20].

For the depression of serpentinite during the flotation of copper–nickel ores, liquid glass in particular is used [21]. Its effect is mainly to neutralize the positive surface charge of this mineral by silicate anions. It is also known about the use of graphene oxide, which can selectively aggregate serpentinite [7, 22], organic phosphates, in particular sodium phytate [6], and acid treatment [23].

An analysis of the literature sources made it possible to establish the following:

- modern methods of MS depression using polysaccharides, liquid glass, and other reagents make it possible in some cases to effectively reduce the magnesium content in the concentrate, but at the same time reduces, and in some cases significantly, the recovery of copper and nickel into the bulk flotation concentrate due to the depression of the sulfides of these metals;
- to date, the effectiveness of the depressing effect of polymer sulfonates and polysaccharides has not been compared;
- the effect of PSS on monomineral talc flotation has been studied, but it is unclear what effect PSS has on the flotation performance of copper–nickel ore containing MS, including on the concentrate yield, its magnesium content, and the recovery of copper and nickel.

The purpose of this work is to study the depressing effect of polystyrene sulfonates on the performance of bulk flotation of copper–nickel ore.

Research objectives:

- experimental comparison of the effectiveness of the depressing effect of PSS and a reagent from the polysaccharide class on MS;
- determining the modes of PSS use that reduce the magnesium content in the concentrate without significantly reducing the recovery of copper and nickel into the bulk concentrate;
- establishing the effect of molecular weight and the method of producing PSS samples on the effectiveness of their depressing effect.

To achieve these goals, it was planned to conduct experimental studies on the flotation of copper–nickel ores with reagent compositions to achieve the lowest magnesium content in the concentrate without significantly reducing the recovery of copper and nickel.



Procedure of experiments

The studies were carried out with a sample of copper–nickel ore from the Kola Peninsula. The elemental composition of the ore according to X-ray fluorescence analysis was as follows: Si – 17.2, Mg – 15.8, Fe – 12.9, Al – 2.5, Ca – 2.0, S – 1.13, Ni – 0.44, Cu – 0.25, Cr – 0.20 %. X-ray phase analysis revealed the following minerals in the ore: antigorite, chlorite, amphibole, olivine, spinel minerals, pentlandite, violarite, pyrrhotite, chalcopyrite, chalcophyllite, etc.

The experiments were carried out on a laboratory flotation machine with a cell volume of 150 cm³ according to a scheme that involves sequential rougher and recleaner flotation of the initial ore sample with separate supply of reagents and appropriate stirring. A sample of an aqueous suspension of the initial ore (pulp) was prepared: the weight of the sample was 45 g, pH = 9. After mixing for 60 seconds, the reagents were sequentially fed in the following order: a depressant, collectors, and a frother. The contact time of each reagent with the pulp was 60 sec with permanent stirring. The froth product was sampled every 15 seconds. After 300 seconds of rougher flotation, a recleaner flotation of the cell product was carried out, with adding the above reagents sequentially in an amount equal to 40% of the consumption in the rougher flotation. The recleaner flotation lasted 180 sec. The combined concentrate and tailings were weighted. The grades of copper, nickel, magnesium, and silicon in them were determined by X-ray fluorescence analysis. The studies were carried out using parallel experiments. Statistical analysis showed that the discrepancy between the results in a pair of the parallel experiments was approximately ±0.8% (relative).

The effectiveness of the depressing effect of the studied reagents was determined based on the yield of concentrate γ , the recovery of copper ε_{Cu} and nickel ε_{Ni} into the concentrate; the grades of these metals (β_{Cu} and β_{Ni} , respectively) in the concentrate, as well as the content of magnesium β_{Mg} ; the Hancock–Luyken criterion (HL), which takes into account the values of ε , γ , as well as the grades of copper and nickel in the initial ore α :

$$HL = \frac{\varepsilon - \gamma}{100 - \alpha}. \quad (1)$$

Laboratory samples of linear sodium PSS, which were not previously used in ore flotation, were used as MS polymer depressants. The properties of the studied PSS samples are presented in Table 1. For comparison, carboxymethylated cellulose PAC–N manufactured by Policell CJSC with an average viscosity molecular weight of about 116,000 g/mol and a gamma number of 90% was also used as a polymer depressant.

Potassium butyl xanthate (PBX) and dibutyl dithiophosphate (DBTP) were used as collectors. To increase the effectiveness of the depressing effect of the polymer reagents, MgCl₂ was added, since the Mg²⁺ cation, according to [20], contributes to talc depression with the use of PSS.

Findings and Discussion

In the ore flotation without depressants but with the use of PBX and DBTP, the highest copper and nickel recoveries were achieved at PBX consumption of 112 g/t and that of DBTP of 84 g/t: 89.6% and 85.5%, respectively. This reagents composition was used in further experiments.

The depressing effect of polystyrene sulfonates on MS was studied using the example of the effect of L–50 in comparison with PAC–N (Fig. 1).

In Fig. 1, one can see that the optimal consumption of L–50 depressant is 700 g/t. At this consumption, the concentrate yield decreases from 49.8% to 44.6%. At the same time, copper recovery decreases from 89.7% to 88.5%, and nickel recovery, from 86.1% to 82.8%. A further increase in the depressant consumption leads to a significant decrease in the recovery of the metals into the concentrate. For instance, at L–50 consumption of 1,400 g/t, copper recovery into the concentrate was 79%, and that of nickel, 76.6%.

The data presented in Fig. 1, *b* show that effective results were obtained at a PAC–N consumption of 420 g/t. Under this flotation regime, copper recovery into the concentrate was 81.7%, and that of nickel, 76.6%, while the grades in the concentrate increased from 0.4 to 0.74% Cu and from 0.7 to 1.22% Ni.

An analysis of the beneficiation performance when using various depressants in accordance with the Hancock–Luyken (HL) criterion showed (Fig. 2) that the maximum HL criterion for both copper and nickel is achieved at L–50 and PAC–N consumption of 700 and 420 g/t, respectively.

Table 1

Properties of the studied polystyrene sulfonates

Reagent symbol	Medium viscosity molecular weight (MW), g/mol	Chain growth regulator; concentration, mol/l
L–50	97,000	Isopropanol; 0.3
L–51	89,000	Isopropanol; 0.9
L–54	89,000	Glycine, 0.9
L–55	96,000	Glycine, 0.9
L–5	93,000	Trimethylamine; 0.008
L–6	208,000	Trimethylamine; 0.041
L–7	176,000	Trimethylamine; 0.082

Thus, the optimal consumption of the depressants was 700 g/t for L-50 and 420 g/t for PAC-N, that corresponded to relatively low metal losses in the course of flotation. These values were adopted for further research to determine the most effective modes of the use of these reagents.

According to a number of studies, for example [20], the effectiveness of the depressing effect of polymer reagents on MS increases when multicharged cations, in particular Mg^{2+} , are pre-added. Therefore, in this study, the effect of the addition of this cation on the depressing action of PSS and PAC-N was investigated.

The results of experiments using L-50 and the preliminary addition of $MgCl_2$ at a consumption of 0 to 70 g/t showed that the lowest bulk concentrate yield was achieved at a consumption of $MgCl_2$ of 7 g/t through reducing the floatability of rock minerals due

to hydrophilization of their surfaces. This reduces the magnesium content in the concentrate by approximately 2.0% compared to the regime without the use of the depressants.

Figs. 3 and 4 show data characterizing the ore flotation with the following compositions of the studied depressants: 1 – without depressants; 2 – L-50, 700 g/t; 3 – PAC-N, 420 g/t; 4 – $MgCl_2$, 7 g/t + L-50, 700 g/t; 5 – $MgCl_2$, 7 g/t + PAC-N, 420 g/t.

The data in Fig. 3, *a* show that the lowest values of γ , approximately 27% and 25%, are achieved by using PAC-N and $MgCl_2$ in combination with PAC-N, respectively, that indicates the latter's high depressing capacity. At the same time, L-50, if used individually, even slightly increases the γ value that may be due to the manifestation of some flocculating ability of this reagent.

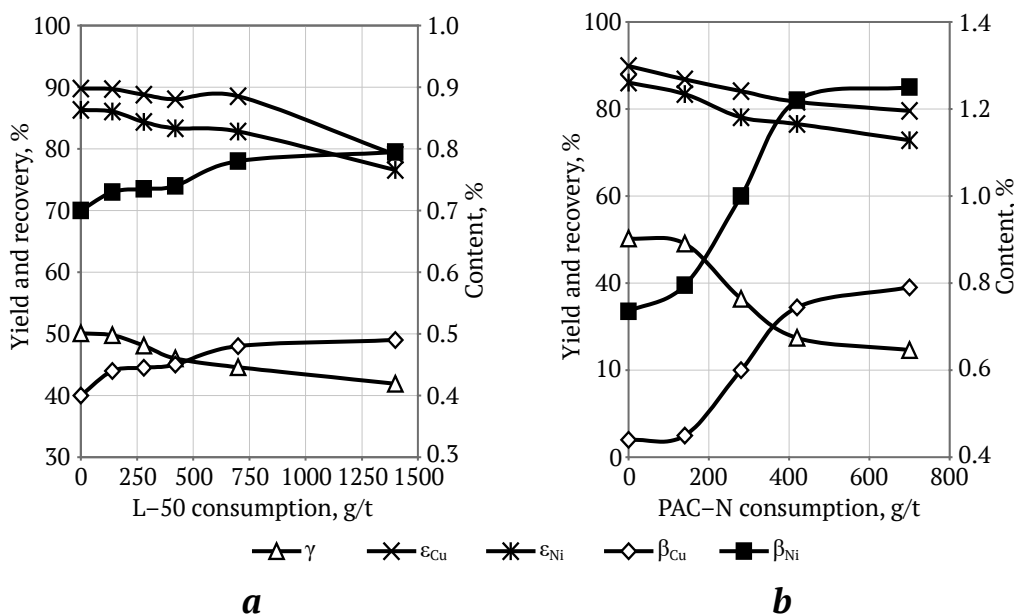


Fig. 1. The effect of depressant consumption on ore flotation: *a* – L-50; *b* – PAC-N

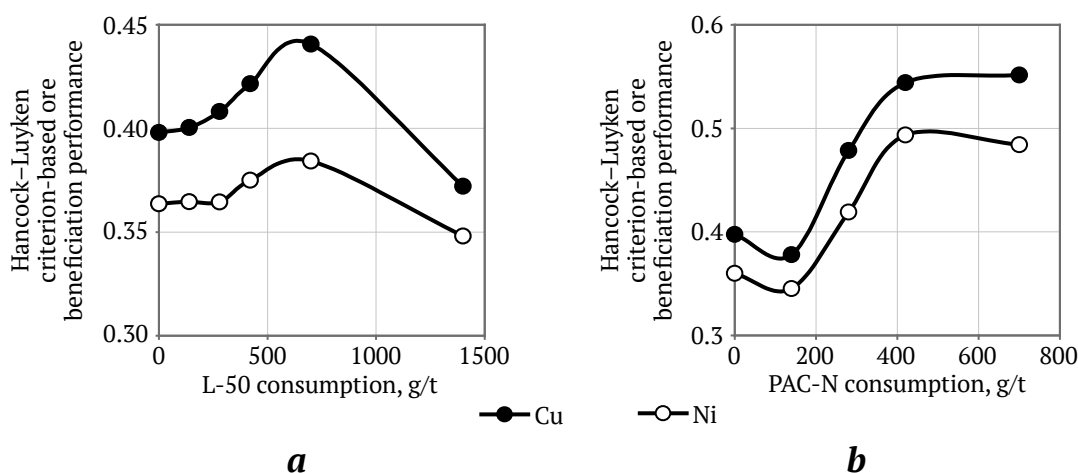


Fig. 2. The effect of depressant consumption on the ore beneficiation performance according to Hancock-Luyken criterion: *a* – L-50; *b* – PAC-N

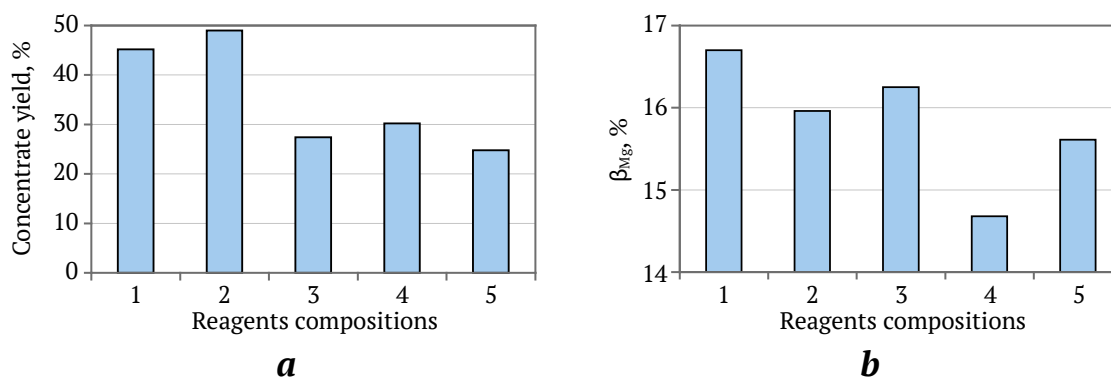


Fig. 3. The effect of depressant compositions:

a – on the concentrate yield; *b* – on the magnesium content in the concentrate

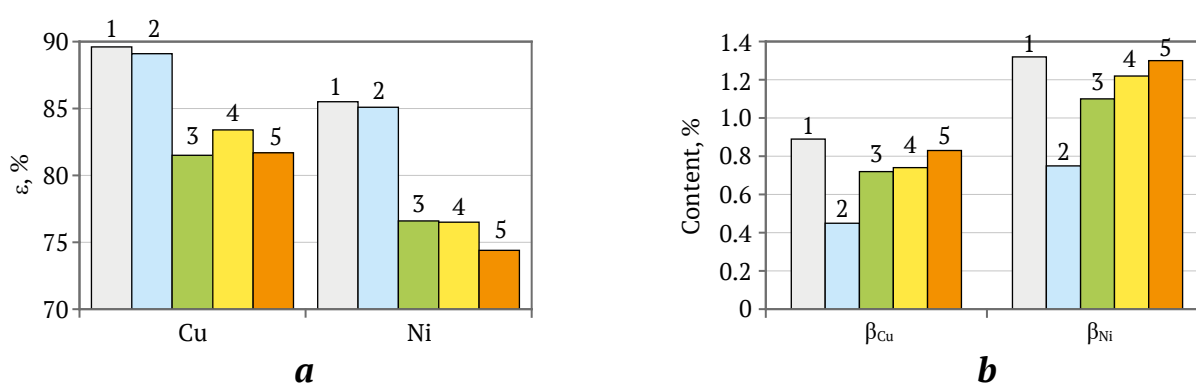


Fig. 4. The effect of depressant compositions: *a* – on the recovery of copper and nickel into the concentrate; *b* – on the content of copper and nickel in the concentrate

In the case of preliminary addition of $MgCl_2$, for L-50, the γ value decreases from 49 to 30%, and for PAC-N, from 27 to 25%. It is obvious that the difference in γ values with the use of $MgCl_2$ and a polymer reagent compared to the individual use of the latter for L-50 is 19% versus 2% for PAC-N. This is probably due to the fact that L-50 sulfo groups are more strongly attracted to the surface of minerals modified by Mg^{2+} ions than PAC-N carboxyl groups.

Fig. 3, *b* shows that composition No. 4 ($MgCl_2$ and L-50) provides the lowest magnesium content in the concentrate: 14.7% versus 16.7% for No. 1 (without depressants) and 15.6% for No. 5 ($MgCl_2$ and PAC-N). Overall, the magnesium content in the concentrate is reduced by about 2%.

Fig. 4, *a* shows downtrend of the recovery values ε with the use of the depressants. At the same time, L-50 reduces the recovery to a lesser extent than PAC-N, as can be seen from the comparison of compositions Nos. 2, 3 and Nos. 4, 5: in the case of individual use of the depressants, L-50 reduces the recovery of copper and nickel compared to the experiment without depressants by 0.5 and 0.4%, respectively, against 8.1 and 8.9% for PAC-N at its effective consumption. When $MgCl_2$ is first added to L-50, the recovery of cop-

per and nickel decreases by 6.2% and 9.0%, respectively, compared to the experiment without the depressants; for PAC-N, by 7.9 and 11.1%, respectively. The data in Fig. 4, *b* show that the least decrease in β is observed when $MgCl_2$ and PAC-N are used.

Thus, L-50 has an effect on MS in the presence of $MgCl_2$ only, and, at the same time, provides less effective depression as compared to PAC-N. A comparative analysis of the mechanisms of interaction between PSS and PAC-N with the MS surface, taking into account literature data, showed that for linear PSS macromolecules characterized by a smaller Kuhn segment length (4 nm versus about 20 nm), and, therefore, higher flexibility than PAC-N, some of the anionic groups are distant from the surface, or shielded, and therefore do not participate in the formation of surface charge. Unlike PSS, a PAC-N macromolecule has a wave-like, close to flat shape and is located along the mineral surface [24]. As a result, most of the anionic groups participate in the formation of surface charge. In contrast to PSS, a PAC-N macromolecule also contains hydrogen atoms capable of forming hydrogen bonds with electronegative atoms on the MS surface. This presumably determines the weaker effect of PSS on these minerals compared to CMC.

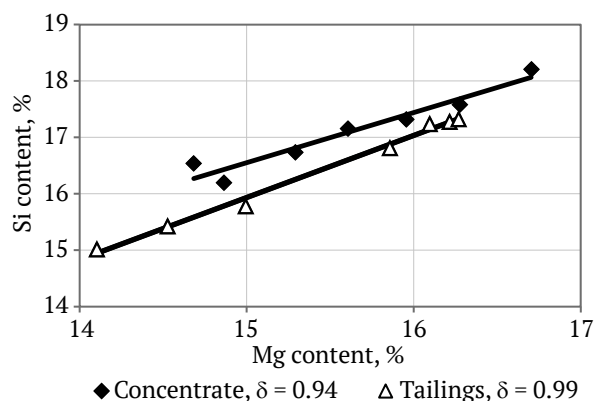


Fig. 5. Correlation between silicon and magnesium content in flotation products

At the same time, polysaccharides, in contrast to PSS, form chelated complexes with copper and nickel [25, 26], and this leads to a lower recovery of these metals into the concentrate when using PAC-N compared to L-50.

It was also found that the contents of silicon and magnesium in both concentrate and tailings are correlated with very high values of the determination coefficient δ , as can be seen in Fig. 5; this confirms that magnesium is mainly concentrated in silicate minerals.

The attempts to use other PSS samples for MS depression, which differ from L-50 in MM values, as well as by reagents for regulating chain growth, showed very similar recovery and content values in the bulk concentrate:

- for Cu – 85.7–87.0% and 0.48–0.59%, respectively;
- for Ni – 75.2–80.4% and 0.74–0.90%, respectively.

The analysis of the dependences of γ , as well as ε and β values for copper and nickel on the MM of these PSS samples showed that the determination coefficient δ does not exceed 0.21; this indicates that the MM value in the range from 89,000 to 208,000 g/mol has virtually no effect on the results of the ore flotation with the listed PSS samples. The reagents used to regulate chain growth during the polymerization of PSS (isopropanol, glycine, trimethylamine, see Table 1) also did not had an effect on the results.

Practical application

Based on the experimental data obtained, the use of PSS is recommended for the flotation of copper-nickel ores with a high magnesium content in cases where it is necessary to achieve the greatest possible restriction of the content of this element in the bulk concentrate without significantly reducing the recovery of copper and nickel, especially when the use of polysaccharide depressants does not significantly re-

duce the magnesium content in the concentrate and/or there is a significant decrease in the valuable metal recovery. PSS consumption is several hundred grams per ton; it is determined experimentally for a specific ore. Before applying PSS, it is advisable to add aqueous solutions of magnesium compounds so that the consumption of Mg^{2+} ions is about 5–10 g/t. At the same time, the expected magnitude of reducing the recovery of copper and nickel into the bulk concentrate will be lower compared to the use of CMC. This will make it possible to obtain an economic effect by reducing energy consumption for the subsequent pyrometallurgical processing of the concentrate.

It also seems appropriate to conduct separate studies with linear PSS samples with a MM of more than 1 million g/mol.

Conclusions

Based on experimental studies on bulk flotation of copper-nickel ore using sodium polystyrene sulfonate and PAC-N carboxymethyl cellulose, new scientific knowledge was obtained about the effect of the consumption and properties of polystyrene sulfonates on flotation performance.

1. It was found that in terms of reducing the concentrate yield, polystyrene sulfonate generally has a weaker depressing effect on magnesium-containing silicates than PAC-N. However, when using polystyrene sulfonate, the magnesium content in the concentrate is approximately 1% lower than when using PAC-N that allows reducing energy consumption in the course of the subsequent pyrometallurgical processing of the concentrate. Polystyrene sulfonate also provides a higher recovery of copper (up to by 7%) and nickel (up to by 8%) into the concentrate than when using PAC-N, since it does not form chelate complexes with these metals unlike polysaccharides.

2. It was found that the most effective MS depression is achieved by sequential applying magnesium chloride with a consumption of 7 g/t and polystyrene sulfonate with a consumption of 700 g/t. At the same time, the magnesium content in the concentrate is reduced by 2% compared to the flotation without depressants that justifies the use of this composition.

3. It was found that for the polystyrene sulfonate samples, the molecular weight ranging 89,000 to 208,000 g/mol, as well as the reagents used in the course of the synthesis process to regulate chain growth, have virtually no effect on the flotation results.

4. It has been shown that the practical use of PSS is advisable for the flotation of copper-nickel ores with a high magnesium content in cases where it is necessary to achieve the maximum possible decreasing the content of this element in the concentrate without significantly reducing the recovery of copper and nickel.



References

1. Boyarko G. Yu., Lapteva A. M., Bolsunovskaya L. M. Mineral resource base of Russia's copper: current state and development prospects. *Mining Science and Technology (Russia)*. 2024;9(4):352–386. <https://doi.org/10.17073/2500-0632-2024-05-248>
2. Svetlov A. V., Krasavtseva E. A., Goryachev A. A., Potorochin E. O. The challenge in mineral processing for low-grade ores and man-made waste: how to reduce the negative environmental impact from the mining industry? *Bulletin of the Kola Science Centre of the Russian Academy of Sciences*. 2020;12(3):21–33. <https://doi.org/10.37614/2307-5228.2020.12.3.003>
3. Gan F., Gao L., Dai H., et al. Study on beneficiation technology for rational utilization of low-grade copper nickel symbiotic ore. *Journal of Mining Science*. 2023;59(5):828–839. <https://doi.org/10.1134/S1062739123050150> (Orig. ver.: Gan F., Gao L., Dai H., et al. Study on beneficiation technology for rational utilization of low-grade copper nickel symbiotic ore. *Fiziko-Tekhnicheskiye Problemy Razrabotki Poleznykh Iskopaemykh*. 2023;(5):140–151. (In Russ.) <https://doi.org/10.15372/FTPRI20230515>)
4. Stepanova K. D., Kazantseva M. I. Impact of material composition of copper-nickel ores on their processing. *Mining Industry Journal*. 2021;(S5–2):17–23. (In Russ.)
5. Xie J., Sun W., Zhao K., et al. Upgrading of talc-bearing copper-nickel sulfide ore by froth flotation using sodium phytate as depressant. *Colloids and Surfaces A: Physicochemical and Engineering Aspects*. 2024;687:133561. <https://doi.org/10.1016/j.colsurfa.2024.133561>
6. Zhao K., Yan W., Wang X., et al. Effect of a novel phosphate on the flotation of serpentine-containing copper-nickel sulfide ore. *Minerals Engineering*. 2020;150:106276. <https://doi.org/10.1016/j.mineng.2020.106276>
7. Yin F., Zhang Ch., Yu Y., et al. Review on the challenges of magnesium removal in nickel sulfide ore flotation and advances in serpentine depressor. *Minerals*. 2024;14(10):965. <https://doi.org/10.3390/min14100965>
8. Dikmen S., Ersoy B., Dikmen Z. Adsorption behaviour of ionic and non-ionic surfactants onto talc a naturally hydrophobic mineral—a comparative study. *Eskişehir Technical University Journal of Science and Technology A – Applied Sciences and Engineering*. 2020;21:139–152. <https://doi.org/10.18038/estubtda.829712>
9. Douillard J. M., Zajac J., Malandrini H., Clauss F. Contact angle and film pressure: study of a talc surface. *Journal of Colloid and Interface Science*. 2002;255(2):341–351. <https://doi.org/10.1006/jcis.2002.8611>
10. Galet L., Goaldard C., Dodds J. A. The importance of surface energy in the dispersion behaviour of talc particles in aqueous media. *Powder Technology*. 2009;190(1-2):242–246. <https://doi.org/10.1016/j.powtec.2008.04.086>
11. Binbin Li, Guofan Zhang, Dezhi Liu, Jianhua Chen. Selective alteration mechanisms of sodium tripolyphosphate towards serpentine: Implications for flotation of pyrite from serpentine. *Journal of Molecular Liquids*. 2022;368(Part A):120687. <https://doi.org/10.1016/j.molliq.2022.120687>
12. Krasavtseva E. A., Goryachev A. A. Review of methods of talc depression at the flotation of copper-nickel ores. *Proceedings of the Kola Science Centre of the Russian Academy of Sciences*. 2019;10(6–1):149–154. (In Russ.) <https://doi.org/10.25702/KSC.2307-5252.2019.6.020>
13. Liao R., Deng J., Lai H., et al. An overview of technologies and selective depressing agents for separating chalcopyrite and talc. *International Journal of Metallurgical & Materials Engineering*. 2018;4:146. <https://doi.org/10.15344/2455-2372/2018/146>
14. Huang R., Liu J., Yang D., et al. Depression effect of CMC on sulfide ore flotation and its influencing factors. *Chinese Journal of Engineering*. 2024;46(4):627–636. (In Chinese) <https://doi.org/10.13374/j.issn2095-9389.2023.02.28.006>
15. Lavrinenko A. A., Kuznetsova I. N., Lusinyan O. G., Golberg G. Yu. Utilizing Russian polymer anion active depressants in the flotation of out-of-balance talcose copper nickel ore. *Izvestiya. Non-Ferrous Metallurgy*. 2023;29(5):5–14. <https://doi.org/10.17073/0021-3438-2023-5-5-14>
16. Xue J., Tu H., Shi J., et al. Enhanced inhibition of talc flotation using acidified sodium silicate and sodium carboxymethyl cellulose as the combined inhibitor. *International Journal of Minerals, Metallurgy and Materials*. 2023;30(7):1310–1319. <https://doi.org/10.1007/s12613-022-2582-5>
17. Lavrinenko A. A., Kuznetsova I. N., Golberg G. Yu., Lusinyan O. G. Joint use of sodium silicate and polysaccharides in the flotation of talcose copper-nickel ores. *Izvestiya. Non-Ferrous Metallurgy*. 2024;(2):5–15. <https://doi.org/10.17073/0021-3438-2024-2-5-15>



18. Fu Y., Zhu Zh., Yao J., et al. Improved depression of talc in chalcopyrite flotation using a novel depressant combination of calcium ions and sodium lignosulfonate. *Colloids and Surfaces A*. 2018;558:88–94. <https://doi.org/10.1016/j.colsurfa.2018.08.056>
19. Mai Q., Zhou H., Ou L. Flotation separation of chalcopyrite and talc using calcium ions and calcium lignosulfonate as a combined depressant. *Metals*. 2021;11(4):651. <https://doi.org/10.3390/met11040651>
20. Lavrinenko A.A., Kuznetsova I.N., Gol'berg G.Yu. Depression of flotation-sensitive silicates using polymeric anion active reagents. *Journal of Mining Science*. 2024;60(6):1022–1028. <https://doi.org/10.1134/S1062739124060176> (Orig. ver.: Lavrinenko A.A., Kuznetsova I.N., Gol'berg G.Yu. Depression of flotation-sensitive silicates using polymeric anion active reagents. *Fiziko-Tekhnicheskiye Problemy Razrabotki Poleznykh Iskopaemykh*. 2024;(6):160–167. (In Russ.) <https://doi.org/10.15372/FTPRPI20240617>)
21. Molifie A., Becker M., Geldenhuys S., McFadzean B. Investigating the reasons for the improvement in flotation grade and recovery of an altered PGE ore when using sodium silicate. *Minerals Engineering*. 2023;195:108024. <https://doi.org/10.1016/j.mineng.2023.108024>
22. Cao J., Tian X., Luo Y., Hu X. The effect of graphene oxide on the slime coatings of serpentine in the flotation of pentlandite. *Colloids and Surfaces A: Physicochemical and Engineering Aspects*. 2017;522:621–627. <https://doi.org/10.1016/j.colsurfa.2017.03.043>
23. Feng B., Lu Y., Feng Q., et al. Mechanisms of surface charge development of serpentine mineral. *Transactions of Nonferrous Metals Society of China*. 2013;23(4):1123–1128. [https://doi.org/10.1016/S1003-6326\(13\)62574-1](https://doi.org/10.1016/S1003-6326(13)62574-1)
24. Wang J., Somasundaran P. Adsorption and conformation of carboxymethyl cellulose at solid-liquid interfaces using spectroscopic, AFM and allied techniques. *Journal of Colloid and Interface Science*. 2005;291(1):75–83. <https://doi.org/10.1016/j.jcis.2005.04.095>
25. El-Saied H., Basta A.H., Hanna A.A., El-Sayed A.M. Semiconductor properties of carboxymethyl cellulose-copper complexes. *Polymer-Plastics Technology and Materials*. 1999;38(5):1095–1105. <https://doi.org/10.1080/03602559909351633>
26. Hosny W.M., Abdel Hadi A.K., El-Saied H., Basta A.H. Metal chelates with some cellulose derivatives. Part III. Synthesis and structural chemistry of nickel (II) and copper (II) complexes with carboxymethyl cellulose. *Polymer International*. 1995;37(2):93–96. <https://doi.org/10.1002/pi.1995.210370202>

Information about the authors

Anatoly A. Lavrinenko – Dr. Sci. (Eng.), Chief Researcher, Head of the Laboratory, Research Institute of Comprehensive Exploitation of Mineral Resources of the Russian Academy of Sciences, Moscow, Russian Federation; ORCID [0000-0002-7955-5273](https://orcid.org/0000-0002-7955-5273); e-mail lavrin_a@mail.ru

Grigory Yu. Golberg – Dr. Sci. (Eng.), Leading Researcher, Research Institute of Comprehensive Exploitation of Mineral Resources of the Russian Academy of Sciences, Moscow, Russian Federation; ORCID [0000-0002-7968-3144](https://orcid.org/0000-0002-7968-3144), Scopus ID [41761734500](https://scopus.org/authorid/41761734500); e-mail gr_yu_g@mail.ru

Irina N. Kuznetsova – Cand. Sci. (Eng.), Senior Researcher, Research Institute of Comprehensive Exploitation of Mineral Resources of the Russian Academy of Sciences, Moscow, Russian Federation; ORCID [0000-0002-5980-8472](https://orcid.org/0000-0002-5980-8472), Scopus ID [57201564209](https://scopus.org/authorid/57201564209); e-mail iren-kuznetsova@mail.ru

Oganes G. Lusinyan – Cand. Sci. (Eng.), Lead Engineer, Research Institute of Comprehensive Exploitation of Mineral Resources of the Russian Academy of Sciences, Moscow, Russian Federation; ORCID [0000-0002-5655-1747](https://orcid.org/0000-0002-5655-1747), Scopus ID [57201648662](https://scopus.org/authorid/57201648662); e-mail lusinyan.oganes@yandex.ru

Vladimir A. Tverskoy – Dr. Sci. (Chem.), Professor, MIREA – Russian Technological University, Lomonosov Institute of Fine Chemical Technologies, Moscow, Russian Federation; ORCID [0000-0003-4348-8854](https://orcid.org/0000-0003-4348-8854), Scopus ID [6604012434](https://scopus.org/authorid/6604012434), ResearcherID [H-8042-2017](https://orcid.org/H-8042-2017); e-mail tverskoj@mirea.ru

Received 11.06.2025

Revised 15.07.2025

Accepted 17.07.2025









MINING MACHINERY, TRANSPORT, AND MECHANICAL ENGINEERING

Research paper

<https://doi.org/10.17073/2500-0632-2025-03-401>

UDC 622.45

**Reliability analysis of mine ventilation fans
based on Markov process theory**P.V. Vyatkin¹ , N.G. Valiev²  , D.I. Simisinov²   , E.B. Volkov²  ¹ AMZ Ventprom JSC, Artyomovsky, Russian Federation² Ural State Mining University, Yekaterinburg, Russian Federation 7sinov@m.ursmu.ru**Abstract**

The reliability of mine ventilation fans plays a crucial role in aerological systems and is determined by a combination of various geological, mining-technological, and structural factors, most of which are stochastic in nature. The problem of quantifying the reliability indicators of mine fan installations is addressed using various mathematical methods for modeling random processes. This study considers the possibility of applying Markov process theory to develop a methodology for calculating the operational reliability of centrifugal main mine ventilation fans, using the VShTs-16 as an example. The limitations of applying Markov processes to reliability analysis are demonstrated, particularly due to the condition of stochastic independence of failures. The use of homogeneous Markov processes has its constraints, since the transition intensities between individual system states are not always constant. In such cases, it is impossible to construct a system of differential equations with time-dependent coefficients. When stochastic dependence is present in failure flows of mechanical systems, the application of Markov process theory remains possible, but the most effective tool for reliability analysis in such cases is the Monte Carlo numerical simulation method.

Keywords


Markov processes, technical system, stochastic processes, reliability, correlation analysis, failure, ventilation fans, main mine ventilation fan

For citation

Vyatkin P.V., Valiev N.G., Simisinov D.I., Volkov E.B. Reliability analysis of mine ventilation fans based on Markov process theory. *Mining Science and Technology (Russia)*. 2025;10(3):289–297. <https://doi.org/10.17073/2500-0632-2025-03-401>

ГОРНЫЕ МАШИНЫ, ТРАНСПОРТ И МАШИНОСТРОЕНИЕ

Научная статья

**Исследование надежности шахтных вентиляторов
на основе теории марковских процессов**П.В. Вяткин¹ , Н.Г. Валиев²  , Д.И. Симисинов²   , Е.Б. Волков²  ¹ АО «АМЗ «Вентпром», г. Артемовский, Российская Федерация² Уральский государственный горный университет, г. Екатеринбург, Российская Федерация 7sinov@m.ursmu.ru**Аннотация**

Важнейшую роль в аэрологических системах играет безотказность шахтных вентиляторных установок, надежность которых определяется комплексом различных геологических, горнотехнологических и конструктивных факторов, преимущественно стохастического характера. Задача определения количественных показателей надежности шахтных вентиляторных установок решается с применением различных математических методов моделирования случайных процессов. В работе рассматривается возможность использования теории марковских процессов для разработки методики расчета эксплуатационной надежности шахтных вентиляторных установок на примере вентилятора шахтного центробежного главного проветривания ВШЦ-16. Показана ограниченность применимости марковских процессов к анализу теории надежности по условию стохастической независимости отказов. Использование модели однородных марковских процессов имеет свои границы, т.к. интенсивности переходов между отдельными состояниями системы далеко не всегда являются постоянными величинами.



В этом случае невозможно составить систему дифференциальных уравнений с зависящими от времени коэффициентами. При наличии стохастической зависимости в потоках отказов механических систем применение теории марковских процессов возможно, но в этих случаях наилучшим инструментом для анализа надежности является численный метод статистических испытаний Монте-Карло.

Ключевые слова

марковские процессы, техническая система, стохастические процессы, надежность, корреляционный анализ, отказ, вентиляторная установка, вентилятор шахтный главного проветривания

Для цитирования

Vyatkin P.V., Valiev N.G., Simisinov D.I., Volkov E.B. Reliability analysis of mine ventilation fans based on Markov process theory. *Mining Science and Technology (Russia)*. 2025;10(3):289–297. <https://doi.org/10.17073/2500-0632-2025-03-401>

Introduction

According to Rostekhnadzor, aerological risk factors in underground mining remain at a high level. With enterprises transitioning to underground mining under complex geological and mining-technological conditions, and with increasing mining depths in operating mines, the efficiency requirements for ventilation and degassing systems are becoming more stringent [1–3]. The failure-free operation of mine ventilation fans plays a key role in aerological systems.

The reliability of mine ventilation fans is influenced by a range of geological, mining-technological, and structural factors, most of which are stochastic in nature [4, 5].

Quantitative indicators of reliability are determined using various mathematical methods for modeling random processes. The fundamental concepts and reliability measures of ventilation fans were first introduced through the state function method, the critical path method, the statistical method, and statistical simulation [6, 7], as well as fuzzy logic approaches [8].

The mathematical framework of reliability theory is broad, but mathematical statistics, probability theory, and the theory of random processes hold a central position. The concept of reliability in complex technical systems has led to the extensive use of Markov process theory as a mathematical tool. This approach has been successfully applied in analyzing the operability of complex electronic devices and systems [9, 10]. Reliability theory itself, as a general engineering discipline, was shaped largely by advances in radio electronics, computer technology, and rocket engineering, although reliability issues were first raised in the 1930s by specialists in structural mechanics and power systems. Consequently, the mathematical methods most widely adopted in reliability theory were those that met the requirements of computing technology.

The analysis of mechanical system operability emerged later as a second direction in the develop-

ment of general reliability theory. The mathematical toolkit of this field was significantly enriched by methods and theories that had been deeply developed and broadly applied in electronics. In some cases, however, such borrowing has been applied without sufficient consideration of the specifics of the systems under study and without adequate analysis of the physics of failures. This is particularly relevant to the use of Markov process theory in analyzing the reliability of mechanical systems. In studies [11–13], the authors employ Markov process theory to develop methodologies for engineering calculations of the reliability indicators of specific mechanical engineering products and their manufacturing processes.

Theory

According to the definition in [14], a Markov process is a random process $\xi(t)$, $t \geq t_0$, that satisfies the condition

$$p(s, x, t, B) = P\{f(s, x, t) \in B\}, B \subseteq R^1, t \geq s,$$

under

$$\xi(s_1) = x_1, \dots, \xi(s_m) = x_m, \xi(s) = x,$$

independently of x_1, x_2, \dots, x_m .

This property, known as the Markov property, expresses the independence of the future behavior of $\xi(t)$, $t \geq s$, from its past prior to s , given the current state $\xi(s) = x$. The conditional probabilities

$$p(s, x, t, B) = P\{\xi(t) \in B | \xi(s) = x\},$$

referred to as transition probabilities of a Markov process, describe the likelihood of the process moving from state $\xi(s) = x$ to a state $\xi(s) \in B$, where $B \subseteq R^1$. The corresponding function $p(s, x, t, y)$, $-\infty < y < +\infty$ is called the transition density. Accordingly, the states of failure-free operation and failure of mine ventilation fans can be described by these transition probabilities.

When assessing the reliability of complex technical systems, the methods of queuing theory are



commonly employed, which generally involve studying steady-state regimes of simple ergodic systems [15, 16]. All failure flows that transfer such a system from an operable to an inoperable state are simple and therefore imply statistical independence of the constituent random events.

Consequently, verifying the statistical independence of failure flows is a prerequisite for applying continuous-time discrete Markov processes to evaluate the reliability of mine ventilation fans as elements of complex technical systems.

From probability theory, by definition, random variables ξ_1, \dots, ξ_n are independent if the algebras $A_{\xi_1}, \dots, A_{\xi_n}$ generate by them are independent. Since each algebra A_{ξ_i} consists of events of the form $\{\xi_i = B\}$, $B \subseteq R^1$, this is equivalent to stating that random variables are independent if, for any sets B_i

$$P\{\xi_1 \in B_1, \dots, \xi_n \in B_n\} = \prod_{i=1}^n P\{\xi_i \in B_i\}.$$

According to a well-known theorem in probability theory, the independence of algebras $A_{\xi_1}, \dots, A_{\xi_n}$ is equivalent to the independence of the partitions $\alpha_{\xi_1}, \dots, \alpha_{\xi_n}$ generating them. This yields another equivalent definition: random variables ξ_1, \dots, ξ_n are independent if, for any sets $x_{1j_1}, \dots, x_{nj_n}$

$$P\{\xi_1 = x_{1j_1}, \dots, \xi_n = x_{nj_n}\} = \prod_{i=1}^n P\{\xi_i = x_{ij_i}\}.$$

The covariance (or correlation moment) of two random variables ξ and η is defined as

$$\text{cov}(\xi, \eta) = \mu_{\xi\eta} = M(\xi - M(\xi))(\eta - M(\eta)), \quad (1)$$

and it follows directly that $\text{cov}(\xi, \eta) = M(\xi\eta) - M(\xi)M(\eta)$. Equation (1) can also be expressed as

$$\text{cov}(\xi, \eta) = \int \int (x - M(\xi))(y - M(\eta))dF(x, y),$$

where $F(x, y)$ the joint cumulative distribution function of the two-dimensional random vector (ξ, η) . In particular, if (ξ, η) has density $p(x, y)$, then

$$\text{cov}(\xi, \eta) = \int_{-\infty}^{+\infty} \int_{-\infty}^{+\infty} (x - M(\xi))(y - M(\eta))p(x, y)dx dy.$$

Covariance is used as a measure of dependence between random variables. This is justified by the well-known equality in probability theory, $\text{cov}(\xi, \eta) = 0$, which holds for independent random variables ξ and η with finite variances. However, the value of the covariance of ξ and η depends on the choice of measurement units for these variables, and therefore this characteristic is not always convenient to use. Free from this drawback is the characteristic known as the correlation coefficient. By definition, the correlation

coefficient of random variables ξ and η is the ratio of their covariance to the product of their standard deviations:

$$\rho_{\xi\eta} = \frac{\text{cov}(\xi, \eta)}{\sigma_{\xi}\sigma_{\eta}}.$$

The operating conditions of mine ventilation fans give rise to both dependent and independent failures. For example, failures such as “impeller looseness on the shaft” and “bearing wear” are dependent. In contrast, “bearing wear” and “failure of the motor control system” are independent. Let ξ and η represent such failure events. Clearly, the correlation coefficient of independent random variables ξ and η equals zero, i.e., $\rho_{\xi\eta} = 0$ if ξ and η are independent. Random variables ξ and η are called uncorrelated if their correlation coefficient $\rho_{\xi\eta} = 0$. Thus, independence implies uncorrelatedness. The converse does not hold in general – specifically, when only second moments are known: $\text{cov}(\xi, \eta) = 0$ does not necessarily imply independence of ξ and η .

As an illustration, let ξ be a random variable with finite $M(\xi^3)$ and a density $\rho(x)$ symmetric about $x = 0$ i.e., $\rho(-x) = \rho(x)$. Define $\eta = \xi^2$. Then

$$M(\xi) = \int_{-\infty}^{+\infty} x\rho(x)dx = 0$$

due to the evenness $\rho(x)$. It follows, by the evenness of $\rho(x)$, that

$$\begin{aligned} \text{cov}(\xi, \eta) &= M(\xi)(\eta - M(\eta)) = M(\xi\eta) - M(\xi)M(\eta) = \\ &= M(\xi^3) - 0M(\eta) = M(\xi^3) = \int_{-\infty}^{+\infty} x^3\rho(x)dx = 0. \end{aligned}$$

Nevertheless, ξ and η are dependent: if x is any number such that $0 < \rho(|\xi| < x) < 1$, then for $y = x^2$

$$\begin{aligned} \rho(|\xi| < x, \eta < y) &= \rho(|\xi| < x, \xi^2 < x^2) = \\ &= \rho(|\xi| < x) > \rho^2(|\xi| < x) = \rho(|\xi| < x)\rho(\eta < y). \end{aligned}$$

Therefore, the uncorrelatedness of random events in a failure flow cannot serve as evidence of independence.

Moreover, even for correlated random variables with a bivariate normal distribution, the hypothesis of independence of random variables x and y in mathematical statistics [17] is tested using a sample $(x, y), \dots, (x_n, y_n)$ of size n , based on reliability statistics of mine ventilation fans

$$t = \frac{r_{xy}}{\sqrt{1 - r_{xy}^2}} \sqrt{n - 2},$$

where



$$r_{xy} = \frac{\sum_{i=1}^n (x_i - \bar{x})(y_i - \bar{y})}{\sqrt{\sum_{i=1}^n (x_i - \bar{x})^2 \sum_{i=1}^n (y_i - \bar{y})^2}}$$

is the sample correlation coefficient, and

$$\bar{x} = \frac{1}{n} \sum_{i=1}^n x_i, \quad \bar{y} = \frac{1}{n} \sum_{i=1}^n y_i$$

are sample means.

Using a two-tailed test at significance level α with $m = n - 2$ degrees of freedom, the null hypothesis H of independence of random failure probabilities is rejected if

$$|t| > t_{m; 1 - \frac{\alpha}{2}}.$$

For the same distribution parameters, the hypothesis may be tested against critical values of the correlation coefficient. In this case, under a two-tailed test for significance level α and $m = n - 2$ degrees of freedom, H is rejected if $|r_{xy}| > r_{m; q}$.

The critical values of the correlation coefficient are determined from statistical tables for $m = n - 2$ and $q = 1 - \alpha/2$.

Methods

In practical applications, verification of stochastic independence using the expressions described above is highly challenging. Consequently, an alternative explanation is often employed, although it is purely qualitative in nature: random variables ξ and η are defined as independent if the random mechanisms determining the distributions of ξ and η operate independently of one another [9].

Guided by this qualitative interpretation, in many cases the failures of individual components in mechanical systems cannot be regarded as independent events [18]. As an illustrative example, the operability of the assemblies of a main mine centrifugal ventilation fan VShTs-16 is considered.

The VShTs-16 fan is designed for mine ventilation in installations with bypass channels, operating in blowing or suction mode during shaft sinking, in heating and ventilation systems, for cooling electric machines, and for other industrial purposes. The fan is manufactured by AO AMZ Ventprom (Open Joint-Stock Company Artyomovsky Machine Engineering Plant VENTPROM).

The assemblies of the fan are subjected to disturbances in the air stream caused by unsteady aerodynamic forces arising from flow nonuniformity during interaction with the casing ribs and the blades of the guide and straightening devices [19].

Furthermore, variation in the mechanical loading on fan components is induced both by operational adjustment of the air supply into mine workings and by sudden pressure fluctuations resulting from abrupt changes in the characteristics of the external ventilation network, associated with the movement of equipment and personnel through airlock chambers and with the travel of conveyances in intake shafts [20]. Transient processes occurring in such complex mechanical systems exert a considerable influence both on the efficiency indicators of the units and on the reliability indicators of the system as a whole [21]. An analysis of the operational reliability of the fan under underground ore mining conditions, conducted by the authors, demonstrated that the unsteady nature of blade loading – caused by sudden gas outbursts or by pressure waves generated during blasting operations – results in a significant number of failures such as “impeller looseness on the shaft” and “bearing wear.”

Such failures lead to rotor imbalance, an increase in dynamic loads, and, consequently, accelerated bearing wear. Therefore, random events such as “impeller looseness on the shaft” and “bearing wear” cannot be considered stochastically independent. It is evident that reliance on such a qualitative criterion of statistical independence introduces significant uncertainty into the reliability analysis of mechanical systems. A definitive resolution of this issue can be achieved only through the application of rigorous quantitative criteria. In scientific and engineering practice, correlation analysis, as described in the theoretical section of this paper, is widely used to evaluate the dependence of random variables.

Accordingly, in the case of a normal distribution, even correlated random variables may, under the stated hypothesis, be regarded as independent.

It should be emphasized, however, that this approach is applicable only to a limited class of mechanical systems, since the normal distribution of failure flows is characteristic primarily of designs that are well optimized for reliability, i.e., exhibiting a high level of operational durability. For the components and mechanisms of such systems, gradual failures – wear, fatigue, corrosion, etc. – predominate over sudden failures. The majority of mining machines and stationary mine equipment cannot be attributed to this class due to the insufficiently high technical level of mining machine-building and, in particular, the severe conditions of their operation and maintenance.

For main mine ventilation fans, the failure-free operating time of mechanical components approximately follows the Gnedenko–Weibull distribu-



tion with parameters $a = 800$, $b = 1.31$, as well as its particular cases, the Rayleigh and exponential distributions with parameter $\omega = 0.264$. For centrifugal main mine ventilation fans, the logarithmic-normal distribution provides a more accurate description of the failure flow [12]. According to an analysis of the operational reliability of the VShTs-16 main mine centrifugal ventilation fan performed by the Artemovsk Machine-Building Plant, the probability of failure-free operation of these units at the Sibay and Uchaly mining and processing plants corresponds closely, under the Mises criterion ($\omega^2 = 2.38-3.64$), to the exponential distribution ($\omega^2 = 0.466-0.747 \cdot 10^{-4}$). Thus, statistical evaluation of stochastic independence in failure flows of mining machines and stationary mine equipment using sample correlation coefficients is, in most cases, infeasible. For such systems, nonparametric statistical methods, including Fisher's exact test and the χ^2 test, may be applied. In addition to their main advantage – the ability to be used under any distribution law – nonparametric methods, unlike correlation analysis, do not require large volumes of prior failure data and can be applied at the earliest (preliminary) stages of reliability analysis.

An analysis of the above example of testing the independence of the failures “impeller looseness on the shaft” and “bearing wear,” performed using the χ^2 independence test, confirmed the validity of the conclusion previously drawn from the qualitative evaluation of the physical mechanism. The hypothesis H of independence of these failures was tested using a contingency table of attributes (Table 1).

Table 1

Contingency of attributes
for the independence hypothesis

$j \rightarrow i$	$1 \rightarrow 2$	h_j
1	$16 \rightarrow 1$	17
2	$3 \rightarrow 8$	11
h_i	$19 \rightarrow 9$	28

The test statistic for the 2×2 contingency case is calculated using the following formula

$$t = \frac{h(h_{11}h_{22} - h_{12}h_{21})^2}{h_1h_2h_ih_j} = 13.68.$$

For a significance level of $\alpha = 0.05$ and degrees of freedom $m = (r - 1)(s - 1) - (2 - 1)(2 - 1) = 1$, the tabulated critical value of χ^2 is $\chi_{1;0.95}^2 = 3.84$. Since the calculated value $t = 13.68$ exceeds this threshold, hypothesis H must be rejected. This indicates that the failures of the VShTs-16 main mine centrifugal ventilation fan – specifically, “impeller looseness on

the shaft” and “bearing wear” – are stochastically dependent events.

Up to this point, the discussion has focused on the limitation of applying Markov processes to reliability analysis under the assumption of stochastic independence of failures. To address the possibility of stochastic dependence between failures of components in mechanical systems, Prof. A.S. Pronikov proposed a classification of complex technical systems from the perspective of reliability, distinguishing three categories: disjoint, dependent, and combined systems [18].

Disjoint systems are those in which the reliability of individual elements can be determined in advance, since the failure of an element can be regarded as an independent event. Such systems are more typical of radio electronics, where individual components – semiconductor devices, resistors, capacitors, etc. – perform independent functions and must ensure output parameters within specified limits regardless of the parameters of other components. Replacement of a failed element fully restores the operability of the entire system.

Dependent systems are those in which element failures are dependent events associated with changes in the output parameters of the system as a whole. For example, the reliability of a mechanical system designed for precise displacement of a driven link depends on the wear resistance of all components transmitting motion. However, the wear of each component cannot be limited independently of the others, since greater wear of one component may be compensated by the higher wear resistance of another.

Combined systems consist of subsystems with internally dependent structures but with independence between the subsystems themselves.

Although simplified, this classification of complex technical system structures makes it possible to select suitable methodological approaches for analyzing overall reliability and, in particular, for applying Markov process theory.

For systems with disjoint structures, the assumption of stochastic independence in failure flows of elements is valid, and the use of Markov methods is not constrained. By contrast, in mechanical systems with dependent structures, the applicability of Markov process theory is limited.

For complex technical systems with combined structures, the Markov approach is acceptable, with a certain approximation, only for analyzing reliability at the highest level, i.e., when the system is studied as an aggregate of subsystems.

It should be emphasized that these observations apply to the analysis of functional reliability, in which

element failure is understood as a breakdown or malfunction that results in system failure, i.e., cessation of operation.

In the case of parametric reliability, where element failure is defined as the deviation of its functional characteristic beyond permissible limits – leading to the system's main parameters falling outside the allowable range – the use of any assumptions based on stochastic independence of the studied failure flows is inadmissible. This is particularly important for mining machines and stationary mine equipment, which, as systems of high material intensity and large unit power, are highly sensitive to the stability of their basic parameters during operation.

Experimental studies

As an illustrative example, the operation of the VShTs-16 main mine centrifugal ventilation fan is considered under the assumption of no stochastic dependence in the failure flows. In this case, the probability of system failure does not depend on time or on previous states [22]. The system is assumed to exist within a single day in one of two states: operable, $P_1(t)$, or inoperable, $F_1(t)$. This two-state representation simplifies the analysis and enables estimation of transition probabilities between states.

Based on observed transitions over a time interval t , the probabilities can be expressed as a transition matrix

$$\|P_{ij}\| = \begin{pmatrix} P_{11} & P_{12} & \dots & P_{1n} \\ P_{21} & P_{22} & \dots & P_{2n} \\ \dots & \dots & \dots & \dots \\ P_{n1} & P_{n2} & \dots & P_{nn} \end{pmatrix}. \quad (2)$$

For the VShTs-16 fan, the probability of remaining operable during a given period (P_{11}) is 0.9, and the probability of transitioning to failure (P_{12}) is 0.1. The probability of recovery during the period (P_{21}) is taken as 0.99, while the probability of non-recovery (P_{22}) is 0.01. Taking these values into account, matrix (2) becomes

$$\|P_{ij}\| = \begin{pmatrix} 0.9 & 0.1 \\ 0.99 & 0.01 \end{pmatrix}.$$

The state diagram of the system, illustrating possible transitions between operable and inoperable states, is shown in Fig. 1.

Let the vector of initial state probabilities be defined as

$$P(0) = \begin{pmatrix} 0 \\ 1 \end{pmatrix},$$

then, for a homogeneous Markov chain, the probabilities of system states can be determined from the relation:

$$P_i(k) = \sum_{j=1}^n P_j(k-1) \cdot P_{ij}, \quad (3)$$

where k is the step number (months).

From expressions (1) and (2), the probability of failure-free operation in the first month is $P_1(1) = P_1(0) \cdot P_{11} + P_2(0) \cdot P_{21} = 0.99$, and the probability of failure is $P_1(1) = P_1(0) \cdot P_{12} + P_2(0) \cdot P_{22} = 0.01$. In the second month, the probability of failure-free operation is 0.9009, while the probability of failure is 0.0991. Subsequently, by applying computer modeling of the probabilistic process, the data obtained for several cycles (months) are presented in tabular form (Table 2).

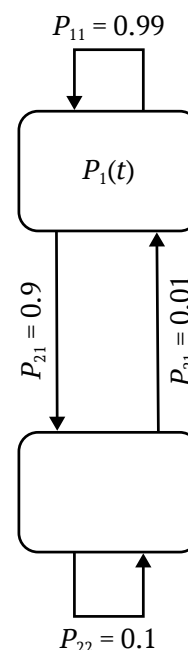


Fig. 1. State diagram of the system (VShTs-16)

Table 2

Simulation results

t , months	$P_1(t)$	$F_1(t)$	t , months	$P_1(t)$	$F_1(t)$
1	0.99	0.01	6	0.90826	0.09174
2	0.9009	0.099	7	0.90826	0.09174
3	0.9089	0.091	8	0.90826	0.09174
4	0.9081	0.0918	9	0.90826	0.09174
5	0.9082	0.09173	10	0.90826	0.09174

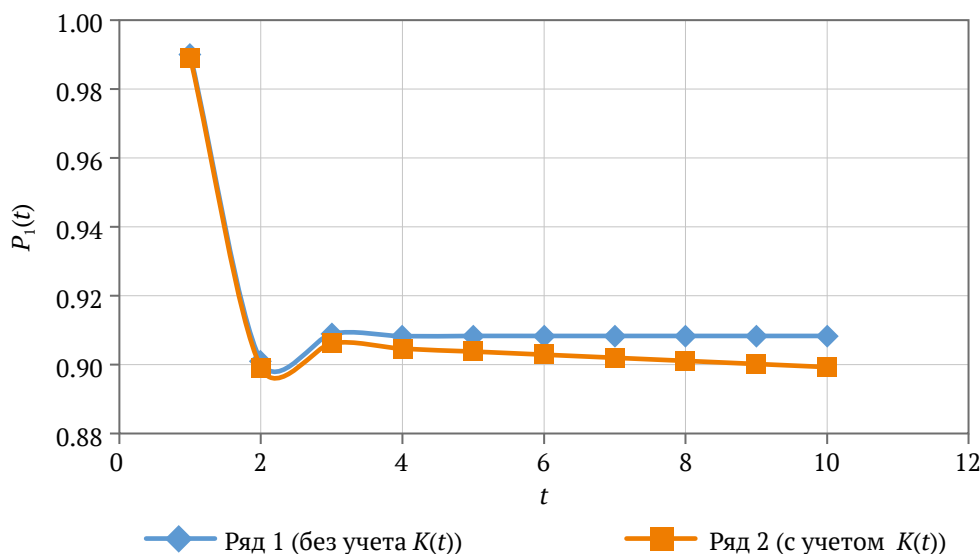


Fig. 2. Probability of the VShTs-16 remaining in an operable state over time

Discussion

Analysis of the obtained values indicates that this approach is generally straightforward to apply; however, it does not account for the cumulative effect of failures associated with system degradation [23]. Nevertheless, system reliability can be evaluated by applying formula (3), supplemented with stochastic coefficients $K(t)$ derived from the distribution laws of reliability indicators as functions of operating time t : $P = f\{P_i(k), K(t)\}$.

Table 3 shows the calculated probability of the VShTs-16 system remaining in an operable state, taking into account coefficients that reflect the degradation process of the technical system. It should be noted, however, that this calculation does not incorporate the frequency of random failures or the effect of individual component failures on overall system reliability.

The corresponding simulation results are illustrated graphically in Fig. 2.

Analysis of the dependence shown in Fig. 2 (series 2) indicates that the probability of the system remaining in an operable state decreases with increasing operating period and exhibits a nonlinear character. Thus, the qualitative determination of failure probability reduces to refining the stochastic coefficients.

Conclusions

The application of homogeneous Markov process models has inherent limitations, since the transition intensities between system states are not always constant. When transition intensities vary with time, calculations become significantly more complex, and in some cases certain intensities may not exist at all. In such situations, it is impossible to construct a system of differential equations with time-dependent coefficients. In mechanical systems, such dynamic transition intensities are typically associated with aging processes.

The analysis of the operational reliability of the VShTs-16 main mine centrifugal ventilation fan showed that the probability of failure-free operation of these units at the Sibay and Uchaly mining and processing plants corresponds closely, according to the Mises criterion ($\omega^2 = 2.38-3.64$), to the exponential distribution ($\omega^2 = 0.466-0.747 \cdot 10^{-4}$). Verification of the independence of the failures “impeller looseness on the shaft” and “bearing wear”, performed using the χ^2 independence test, did not confirm the independence hypothesis, since the calculated value $t = 13.68$ exceeded the tabulated critical value of 3.84. This finding demonstrates

Table 3

Simulation results with stochastic coefficients $K(t)$

t, months	$P_1(t)$	t, months	$P_1(t)$
1	0.98910	6	0.90286
2	0.89910	7	0.90196
3	0.90622	8	0.90106
4	0.90460	9	0.90016
5	0.90376	10	0.89926



that the failures of the VShTs-16 fan are stochastically dependent events.

To account for the influence of individual component failures on overall system failure, the determination of failure probability should incorporate refined stochastic coefficients. This approach may provide a foundation for developing methodological principles for monitoring and diagnosing the technical condition of ventilation systems, as well as for predicting

the residual service life of operating fans based on condition monitoring data.

In this context, the analysis of reliability may involve finite Markov chains and semi-Markov processes. When stochastic dependence is present in the failure flows of mechanical systems, the use of Markov process theory remains possible, but the most effective tool for reliability analysis under such conditions is the Monte Carlo numerical simulation method [24].

References

1. Ahaiev R., Prytula D., Kliuiev E., et al. The determination of the influence degree of mining-geological and mining-technical factors on the safety of the degassing system. In: *E3S Web of Conferences. II International Conference Essays of Mining Science and Practice*. 2020;168:00040. <https://doi.org/10.1051/e3sconf/202016800040>
2. Materova E.S., Aksenova Zh.A., Nikiforov A.A., et al. Development potential of the mining sector in the Russian Federation. *Ugol'*. 2024;(12):41–46. (In Russ.) <https://doi.org/10.18796/0041-5790-2024-12-41-46>
3. Balovtsev S.V. Assessment of ventilation circuits with regard to geological and geotechnical conditions of coal seam mining. *Mining Informational and Analytical Bulletin*. 2019;(6):173–183. <https://doi.org/10.25018/0236-1493-2019-06-0-173-183>
4. Chen Y., Liu R., Liu C., et al. Influence of blade installation angle spanwise distribution on the energy characteristics of mining contra-rotating axial flow fan. *Scientific Reports*. 2025;15(1):6444. <https://doi.org/10.1038/s41598-025-90797-4>
5. Kaledina N.O., Malashkina V.A. Indicator assessment of the reliability of mine ventilation and degassing systems functioning. *Journal of Mining Institute*. 2021;250:553–561. <https://doi.org/10.31897/PMI.2021.4.8>
6. Odeyar P., Apel D.B., Hall R., et al. A review of reliability and fault analysis methods for heavy equipment and their components used in mining. *Energies*. 2022;15(17):6263. <https://doi.org/10.3390/en15176263>
7. Ushakov V.K. Reliability and efficiency of mine ventilation. *Mining Informational and Analytical Bulletin*. 2015;(4):240–248. (In Russ.)
8. Kashnikov A.V., Kruglov Yu.V. Fuzzy logic-based determination of ventilation parameters in active mining areas. *Mining Informational and Analytical Bulletin*. 2023;(5):68–82. (In Russ.) https://doi.org/10.25018/0236_1493_2023_5_0_68
9. Reinschke K. *Zuverlässigkeit und Verfügbarkeit technischer systeme: theorie – praxis – berechnung*. Berlin: VEB Verlag Technik; 1973. 392 p. (In German) (Trans. ver.: Reinschke K. *Reliability and availability of technical systems: theory – practice – calculation*. Moscow: Mir Publ. House; 1979. 452 p. (In Russ.))
10. Petrochenkov A.B., Bochkarev S.V., Romodin A.V., Eltyshv D.K. Planning of electrical equipment operation process using Markov chain theory. *Elektrotehnika*. 2011;(11):20–24. (In Russ.)
11. Agbinya J.I. Markov Chain and its applications. In: *Applied Data Analytics – Principles and Applications*. 1st ed. New York: River Publishers eBooks; 2022. 15 p. <https://doi.org/10.1201/9781003337225-1>
12. Ssempijja M.N., Namango S., Ochola J., Mubiru P.K. Application of Markov Chains in manufacturing systems: a review. *International Journal of Industrial Engineering and Operational Research*. 2021;3(1):1–13. <https://doi.org/10.22034/ijieor.v3i1.26>
13. Wang Y., Xie B., E Sh. Adaptive relevance vector machine combined with Markov-chain-based importance sampling for reliability analysis. *Reliability Engineering & System Safety*. 2022;220:108287. <https://doi.org/10.1016/j.ress.2021.108287>
14. Rozanov Yu.A. *Introduction to the theory of random processes*. Moscow: Nauka; 1982. 128 p. (In Russ.)
15. Ignatov V.A., Manshin G.G., Kostanovsky V.V. *Elements of optimal maintenance theory for technical devices*. Minsk: Nauka i Tekhnika; 1974. 192 p. (In Russ.)
16. Ovcharov L. A. *Applied problems of queueing theory*. Moscow: Mashinostroenie; 1969. 324 p. (In Russ.)
17. Müller P., Neumann P., Storm R. *Tafeln der mathematischen statistik*. Berlin: VEB Deutscher Verlag der Wissenschaften; 1979. 272 s. (In German) (Trans. ver.: Müller P., Neumann P., Storm R. *Tables of mathematical statistics*. Moscow: Finansy i Statistika; 1982. 272 p. (In Russ.))



18. Pronikov A.S. *Reliability of machines*. Moscow: Mashinostroenie; 1978. 592 p. (In Russ.)
19. Russky E. Yu. Research of vibration reliability of axial fans rotors of the mine main airing. *Interexpo GEO-Siberia*. 2017;2(2):121–125. (In Russ.)
20. Kopachev V.F. Rationale for main fans service life in the conditions of changing load. *Izvestiya Vysshikh Uchebnykh Zavedenii. Gornyi Zhurnal*. 2020;(6):102–108. (In Russ.) <https://doi.org/10.21440/0536-1028-2020-6-102-108>
21. Kopachev V.F., Kopacheva E.A. Effect of transient processes on technical performance of compressed air production and handling systems in mines. *Mining Informational and Analytical Bulletin*. 2025;(1–1):106–119. https://doi.org/10.25018/0236_1493_2025_11_0_106
22. Ushakov V.K. *Mathematical modeling of reliability and efficiency of mine ventilation systems*. Moscow: Gornaya Kniga; 2003. 181 p. (In Russ.)
23. Potapov V.D., Prizyov A.D. *Simulation modeling of production processes in mining industry*. Moscow: Vysshaya Shkola; 1981. 191 p. (In Russ.)
24. Jones G.L., Qin Q. Markov chain Monte Carlo in practice. *Annual Review of Statistics and Its Application*. 2022;9(1):557–578. <https://doi.org/10.1146/annurev-statistics-040220-090158>

Information about the authors

Pavel V. Vyatkin – General Director, AMZ Ventprom JSC, Artemovskiy, Russian Federation; ORCID: [0009-0001-2477-4436](https://orcid.org/0009-0001-2477-4436), e-mail vyatkinpv@ventprom.com

Niyaz G. Valiev – Dr. Sci. (Eng.), Professor, Head of the Department of Mining Engineering, Ural State Mining University, Yekaterinburg, Russian Federation; ORCID [0000-0002-5556-2217](https://orcid.org/0000-0002-5556-2217), Scopus ID [55749527900](https://scopus.org/55749527900), AuthorID [284710](https://scopus.org/284710); e-mail Niyaz.Valiev@m.ursmu.ru

Denis I. Simisinov – Dr. Sci. (Eng.), Associate Professor, Head of the Department of Mining Equipment Operation, Ural State Mining University, Yekaterinburg, Russian Federation; ORCID [0000-0001-6095-0073](https://orcid.org/0000-0001-6095-0073), Scopus ID [6505975115](https://scopus.org/6505975115), AuthorID [435571](https://scopus.org/435571); e-mail 7sinov@m.ursmu.ru

Evgenii B. Volkov – Cand. Sci. (Eng.), Associate Professor, Head of the Department of Technical Mechanics, Ural State Mining University, Yekaterinburg, Russian Federation; ORCID [0000-0002-8313-3137](https://orcid.org/0000-0002-8313-3137), Scopus ID [57220450540](https://scopus.org/57220450540), AuthorID [795310](https://scopus.org/795310); e-mail gmf.tm@ursmu.ru

Received 22.03.2025

Revised 29.05.2025

Accepted 31.05.2025




DIGITAL TECHNOLOGIES AND ARTIFICIAL INTELLIGENCE

Research paper

<https://doi.org/10.17073/2500-0632-2025-04-402>

UDC 681.5:004.021

**Digital twins and digital technologies:
specific features and prospects in the coal industry****S.M. Nikitenko¹   , E.V. Goosen¹  , A.A. Rozhkov² , M.K. Korolev¹  **¹ Federal Research Center for Coal and Coal Chemistry, Siberian Branch of the Russian Academy of Sciences, Kemerovo, Russian Federation² Russian Energy Agency, Ministry of Energy of the Russian Federation, Moscow, Russian Federation nsm.nis@mail.ru**Abstract**

Across all sectors of the Russian economy, the adoption of digital technologies (DT) is accelerating, with high-tech industries leading the way. The coal industry, like other extractive sectors, has been slower to embrace these solutions, yet digitalization is advancing both at the industry level and within individual companies. One of the most dynamic areas of DT development is the adoption of digital twins (DTw), which form a core element of integrated digital management systems—acting as an integrator for cross-cutting technologies and sub-technologies. This article examines current approaches to studying and implementing digital twins in the coal sector. The objective is to highlight the specific features of digitalization processes, identify barriers, and outline promising directions for the adoption of DTw in the coal industry. To this end, the article systematizes conceptual and applied approaches to DTw, proposes an original framework for defining, structuring, and classifying digital twins based on maturity levels, and identifies both general and industry-specific trends in the development of DT and DTw. The analysis demonstrates that digital twins are a critical tool for managing value chains, and their effectiveness depends on the maturity of production and digital technologies and on the degree of their interoperability. The study compares and evaluates international and domestic experiences of DT and DTw adoption in mining and coal companies, as well as national-level models. It identifies barriers to adoption in the coal sector and offers recommendations for overcoming them. The research applies systems and comparative analysis, bibliographic review, generalization, and expert surveys. Data sources included media reports, websites of leading coal and mining companies, expert assessments, digital project case studies, consulting reports, and primary and secondary expert surveys. The findings show that digital transformation in the coal industry, including the adoption of DTw, lags behind other sectors. This gap is driven by both general and sector-specific factors: high costs and limited resources, scale effects, the absence of a clear development model and digitalization strategy, low levels of automation in production and management, insufficient digital infrastructure, and an acute shortage of personnel with digital competencies, particularly among executives.

Keywords

coal industry, digitalization, digital twins, typology of digital twins, analysis, experts, implementation, value chains, national models, infrastructure, management

Finding


This research was supported by the Russian Science Foundation (Grant Agreement No. 25-18-00647).

For citationNikitenko S.M., Goosen E.V., Rozhkov A.A., Korolev M.K. Digital twins and digital technologies: specific features and prospects in the coal industry. *Mining Science and Technology (Russia)*. 2025;10(4):298–305. <https://doi.org/10.17073/2500-0632-2025-04-402>



ЦИФРОВЫЕ ТЕХНОЛОГИИ И ИСКУССТВЕННЫЙ ИНТЕЛЛЕКТ

Научная статья

**Цифровые двойники и цифровые технологии:
особенности и перспективы в угольной отрасли**С.М. Никитенко¹  , Е.В. Гоосен¹  , А.А.Рожков² , М.К. Королев¹  ¹ Федеральный исследовательский центр угля и углехимии СО РАН, г. Кемерово, Российская Федерация² Российское энергетическое агентство, Минэнерго России, г. Москва, Российская Федерация nsm.nis@mail.ru**Аннотация**

В настоящее время широко развернулось внедрение цифровых технологий (ЦТ) во всех отраслях российской экономики. Наиболее активно в эти процессы вовлечены высокотехнологичные отрасли. Угольная отрасль, как и остальные добывающие отрасли, отстает во внедрении цифровых технологий. Тем не менее эти процессы идут как на уровне всей отрасли, так и на уровне отдельных компаний. Одним из наиболее популярных направлений развития ЦТ является внедрение цифровых двойников, которые являются частью единой цифровой системы управления компанией – технологией-интегратором всех сквозных ЦТ и субтехнологий. Статья посвящена анализу современных подходов к изучению и практике внедрения цифровых двойников в угольной отрасли. Цель статьи – показать особенности процессов цифровизации, выявить барьеры и перспективные направления внедрения цифровых двойников (ЦД) в угольной отрасли. Для реализации этой цели в статье систематизированы концептуальные и прикладные подходы к изучению ЦД, предложен авторский подход к определению, структуре и типологии ЦД на основе выделения этапов их зрелости. Выявлены общие и отраслевые закономерности развития ЦТ и ЦД. Доказано, что ЦД – это важнейший инструмент управления цепочками создания стоимости (ЦСС), который зависит от степени зрелости производственных и цифровых технологий, а также степени их интероперабельности. Проведены сравнение и оценка опыта внедрения ЦТ и ЦД в зарубежных и отечественных горнодобывающих и угольных компаниях и в страновые модели. Выявлены барьеры внедрения ЦТ и ЦД в угольной отрасли, предложены рекомендации по их устранению. При подготовке статьи использованы следующие научные методы: системный и сравнительный анализ, библиографическое исследование, обобщение, социологический опрос экспертов. Источниками данных послужили материалы СМИ и сайтов ведущих зарубежных и отечественных угольных и горнодобывающих компаний, экспертные оценки, кейс-стади цифровых проектов, аналитические отчеты консалтинговых компаний, материалы первичного и вторичного экспертных опросов. Проведенный анализ показал, что процессы цифровой трансформации и внедрения ЦД в угольной отрасли отстают от других отраслей. Причиной тому являются барьеры как общие для всех отраслей, так и специфичные для угольной отрасли: высокая цена цифровых технологий и нехватка ресурсов, значительный эффект масштаба; отсутствие четко выстроенной модели развития угольной отрасли и стратегии ее цифровизации; низкий уровень автоматизации производства и управления, недостаточность цифровой инфраструктуры; острая нехватка кадров и цифровых компетенций у руководителей компаний.

Ключевые слова

угольная отрасль, цифровизация, цифровые двойники, типология цифровых двойников, анализ, эксперты, внедрение, цепочки создания стоимости, страновые модели, инфраструктура, управление

Финансирование

Исследование выполнено при поддержке Российского научного фонда (соглашение № 25-18-00647).

Для цитирования

Nikitenko S.M., Goosen E.V., Rozhkov A.A., Korolev M.K. Digital twins and digital technologies: specific features and prospects in the coal industry. *Mining Science and Technology (Russia)*. 2025;10(4):298–305. <https://doi.org/10.17073/2500-0632-2025-04-402>

Introduction

The implementation of digital technologies (DT) is now rapidly expanding across all sectors of the Russian economy, with the most active engagement observed in high-tech industries. The coal industry, similar to other extractive sectors, lags behind in adopting digital solutions. Nevertheless, digitalization is progressing both at the industry-wide level and within individual companies.

One of the most prominent directions of DT development is the implementation of digital twins (DTw), which serve as an integral component of a unified digital enterprise management system – a technology that integrates all cross-cutting digital solutions and sub-technologies.

Recent advances in artificial intelligence (AI) have accelerated the adoption of digital twins (DTw) in extractive industries, including the coal sector.



DTw now make it possible to automate all key stages of value chains, support the integrated introduction of advanced technologies for deposit exploration, selective coal extraction, beneficiation, and the design of project coal blends, as well as optimize routes for coal transportation and processing.

The purpose of this article is to highlight the specific features of digitalization processes in the coal industry, identify barriers, and outline promising directions for DTw adoption. The objectives are as follows: 1 – To define digital twins and describe their distinctive features and current level of adoption in coal-producing countries; 2 – To identify and characterize the basic national models of coal industry digitalization management, and to determine the role of digital twins within these models; 3 – To identify barriers to the adoption of digital technologies and digital twins in the coal industry and to propose measures for overcoming them.

Data and methods

The study applied systems and comparative analysis, bibliographic review, generalization, and expert surveys.

Data were drawn from online and media sources, websites of leading international and domestic coal and mining companies, expert assessments, case studies of digital projects, consulting reports, and materials from primary and secondary expert surveys.

Research results

Since the early 2000s, the adoption of digital technologies (DT) and digital twins (DTw) has accelerated in the mining and coal industries. The initial introduction of enterprise resource planning (ERP) platforms made it possible to synchronize fragmented production operations, corporate processes, and reporting, significantly improving efficiency. This, in turn, drove major global investments in digital software and infrastructure aimed at developing local digital twins.

The term *digital twin* was first introduced into academic discourse in 2003, but its interpretation remains diverse [1]. Some authors define it narrowly as software that models objects and outcomes [2, 3], while others describe it as a key tool for monitoring and strategic management [4–6]. In international literature, the most widely cited definition presents a DTw as “...an integrated multiphysics, multiscale, probabilistic simulation of a complex product, enabled by a digital thread, that uses the best available physical models, sensor data, and input information to mirror and predict the behavior of its corresponding physical twin across its life cycle” [1]. More recent publications examine the role of DTw in managing companies, regions,

and value chains, accounting not only for technological but also for financial, organizational, and other aspects of complex system management [7, 8]. In Russia, research schools focusing on DT [9, 10] and DTw [11, 12] have emerged more recently, including studies on their application in the coal industry [15, 16].

In the authors’ view, a digital twin is a comprehensive management tool that creates a realistic virtual model of a physical object, continuously updated in real time.

Leading adopters of DT and DTw include major mining and coal companies in Australia, China, the United States, Canada, and Germany. These companies align DTw with priority digital technologies and apply them not only to individual units, technological stages, and mines, but also as tools for managing the entire value chain. In this article, the value chain refers to the full production sequence in the coal industry, from geological exploration to the sale of processed coal products [17–19]. The primary goals are to identify and maintain optimal operating modes in order to maximize productivity and reliability. This provides a basis for assessing the level of digital transformation and DTw adoption (Table 1).

Analysis of official reports and websites of mining and consulting companies allows for identification of levels of DT and DTw adoption. Level 0 is defined as the stage of standardization and automation of primary and auxiliary operations, marking the onset of basic digital technology adoption. At this level, production processes – including management – are extensively automated, and virtual models of individual products and operations, or quasi-digital twins, are introduced. Level 1 corresponds to the stage of business process optimization and reengineering in line with the requirements of digital technologies. It involves creating local digital twins (LDTw) for the most critical assets and processes, and synchronizing digital models with real business operations. Level 2 reflects the development of integrated digital twins (IDTw), achieved through the convergence of DTw with priority digital technologies. Level 3 represents the formation of a digital twin of the entire value chain (VC), capable of managing all its links and supporting both operational and strategic decision-making.

Alongside these adoption levels, two governance models of DT and DTw implementation in the coal industry have been identified: the corporate model, characteristic of developed economies (BHP, Anglo American, Glencore, and others), and the state-driven model, exemplified by China (China Shenhua Energy Company Limited, China Coal Energy Company Limited, etc.). These models differ in the structure of value chains and the maturity of DT and DTw (Table 2).



Table 1

Features of DT and DTw adoption in major mining and coal companies, 2024

Company	Country of registration / Coal asset location	Autonomous mining equipment and vehicles	Integrated Remote Operations Centers (IROC)	Digital twins at asset, process, and system levels	Artificial Intelligence and Generative AI	Level of digitalization
BHP	UK, Australia / Australia	+	+	+	+	3
China Shenhua Energy	China / China, Australia, Indonesia	+	+	+	+	2–3
China Coal Energy	China / China	+	+	+	+	2–3
Rio Tinto	Australia / no coal assets since 2018	+	+	+	+	2–3
Glencore	UK / Australia, Colombia	+	+	+	–	2–3
Anglo American	UK / Australia	+	–	+	–	2
PT Adaro Energy	Indonesia / Indonesia	+	–	+	–	2
Vale	Brazil / no current coal assets (formerly Mozambique, Australia)	+	–	+	–	2
Yankuang Energy Group	China / China, Australia	+	–	+	–	2
Tata Steel	India / India	–	–	+	–	1
ArcelorMittal	Switzerland / USA, Bosnia and Herzegovina, USA	–	–	+	–	1
Nippon Steel	Japan / indirect coal assets through joint ventures in Australia and the USA	–	–	+	–	1
Teck Resources	Canada / British Columbia	+	–	–	–	1
Peabody Energy	USA / USA, Australia, Venezuela	+	–	–	–	1
Coal India	India / India	–			–	0

Source: Compiled by the authors based on official company reports and websites, and data from McKinsey and GlobalData.

Table 2

Comparison of digitalization and DTw adoption in Australia, China, and Russia

Criterion	Australia	China	Russia
Governance model	Private–corporate	State-driven	None (pilot projects only)
Structure of value chains in the industry	Open, horizontally diversified, global	Closed, vertically integrated, domestic market-oriented	Closed, vertically integrated, export-oriented
Level of adoption	High	Medium	Initial
Core technologies	Autonomous equipment, blockchain	IoT, 5G, AI	Sensors, GIS, ERP systems
Safety	Predictive safety monitoring	Accident prediction models	Local solutions
Efficiency	+5–10%	+15–20%	+2–5%, often negative

Source: Compiled by the authors based on official company reports and websites, and data from McKinsey, Yakov & Partners, and GlobalData.



Another group of countries, including Indonesia, Mongolia, and Russia, is still in the process of shaping their digital transformation models.

In the corporate model, leading companies operate globally and benefit from geographic and functional diversification, which makes their value chains more flexible and resilient. Such groups include enterprises engaged in the mining, transportation, and processing of coal, ferrous and non-ferrous metals, and diamonds. They also encompass service, financial, and research organizations, as well as dedicated digitalization centers.

Case: BHP

BHP is the world's largest diversified mining and metallurgical company, with assets in more than 90 countries. Its sources of competitiveness include high-quality assets, proximity to consumers, transnational scale of operations, production and geographic diversification, and effective corporate governance across the entire value chain.

BHP is a global leader in the adoption of DT and DTw. The company has reached the third level of digitalization, completing the integration of IDTw, AI, and predictive analytics through a unified Integrated Remote Operations Center (IROC). This center functions as a local industrial hub of digital expertise: it monitors and analyzes trends in DT development, establishes standards for the use of DT and DTw, negotiates contracts with partners, and selects and supervises DT projects within both BHP and partner companies.

BHP collaborates with global leaders in DT and mining, including AWS (data analytics, IoT platforms), Siemens, and Schneider Electric (industrial automation). The company also engages in joint projects with Rio Tinto and Vale to standardize digital solutions, while investing in technology start-ups and the creation of innovation centers. In partnership with universities and the national research agency CSIRO, IROC contributes to the development of innovative digital and technological solutions.

Source: Official company website, consulting company data.

The BHP case represents one of the most successful examples of an open, predominantly corporate-driven model of coal industry digitalization. This model is based on close collaboration among leading global companies, supported by national governments, which provide the foundation for technological leadership.

In contrast, state-driven vertically integrated coal companies in China rely on government support and administrative resources to reduce operating costs and accelerate the adoption of DT and DTw, thereby nar-

rowing the gap with global leaders. The case of China Shenhua Energy exemplifies a closed, predominantly state-driven model of coal industry digitalization, aimed at strengthening technological sovereignty and economic security.

Case: China Shenhua Energy

China Shenhua Energy – is the largest coal company in the world. It is part of the state-owned energy holding China Energy Investment Corporation (CEIC). The company's key sources of competitiveness include its scale of operations, low production costs, strict vertical control of the entire value chain (VC) – from exploration to transportation, sales, and processing – state participation, and a focus on a protected domestic market.

A major factor is its status as a “national energy leader,” which allows the company to secure government subsidies, preferential loans, reduced tax rates, and guaranteed state contracts for coal and electricity. The government grants China Shenhua Energy priority access to the country's largest coal deposits and provides infrastructure preferences, such as the construction of railway lines and ports at public expense (e.g., Huanghua Port), while restricting foreign companies from entering the Chinese coal market. Through CEIC, China Shenhua Energy actively participates in drafting industry legislation and standards that reflect its interests. In implementing its projects, the company primarily cooperates with national technology firms: Huawei (5G technologies for “smart” mines), Alibaba (cloud-based AI solutions), and XCMG (autonomous mining equipment).

Source: Official company website, consulting company data.

The Russian coal industry and Russian companies lag far behind international leaders in terms of digitalization and DTw adoption¹. To clarify the situation, the authors conducted a survey in 2024 of ten experts representing the largest coal companies operating in the Kemerovo region. The results largely correspond to those reported by Bratarchuk et al., who carried out a similar survey in 2023 [15] (Table 3).

Experts agreed that Russian coal companies are not yet ready to adopt full-scale digital twins, while digital technologies are being introduced only in selected segments of coal value chains, primarily logistics and safety management (Table 4).

¹ Digitalization of the Russian Mining and Metallurgical Industry in 2024: Long-Term Optimism and Ambitious Goals. Moscow: Yakov & Partners, Tsifra Group; 2024. 20 p.



Table 3

Level of digitalization of Russian coal companies, 2023–2024

Technology	Data from Bratarchuk et al., 2023		Authors' survey data, 2024
	Share of investment in DT, % of total	Average age of deployed systems, years	Share of investment in DT, % of total
APCS	7.2	12.4	8.4
GIS	5.4	8.6	6.2
SCADA	4.0	10.2	5.0
MES	3.2	6.8	3.8
AI	1.2	1.8	1.0
DTw	1.6	2.4	1.2

Source: Compiled by the authors based on Bratarchuk et al. [15], official company reports and websites, and expert survey data.

Table 4

Priority areas of digitalization implemented in Russian coal companies

Company	Priority areas of DT adoption
Russian Coal JSC	Wireless data transmission systems Artificial intelligence technologies Logistics management
East Mining Company LLC	
CC KOLMAR LLC	
Kuzbassrazrezugol Coal Company JSC	
SUEK JSC	Integrated MES-based business process management systems Autonomous robotic technologies Local digital twins
Osinnikovskaya Mine (Raspadskaya Coal Company, EVRAZ coal assets)	
Barzasskoye Tovarishchestvo Open-Pit Mine (Stroyservice JSC)	

Source: Compiled by the authors based on official company reports and websites, and expert survey data.

The adoption of DT and DTw in Russia remains stuck between the first and second levels of digitalization. The DTw currently being introduced are local in scope and, even in large coal companies, fail to deliver the expected results.

Discussion and conclusions

The analysis showed that digital transformation and DTw adoption in the coal industry are lagging behind other sectors. This is due to both cross-industry barriers and challenges specific to coal mining, including:

- high costs of digital technologies and resource shortages, combined with significant scale effects;
- the absence of a coherent development model for the coal industry and a dedicated digitalization strategy;
- limited automation of production and management, combined with inadequate digital infrastructure;
- an acute shortage of personnel and a lack of digital competencies among company executives.

A further obstacle to DT and DTw adoption is the difficulty of assessing the real effects of digital transformation. At present, measurable indicators of objectives, as well as methodologies for evaluating the efficiency and effectiveness of DT implementation, are almost entirely absent. The indicators used for monitoring and ranking are largely oriented toward developed countries and remain unbalanced [20]. As a result, expert judgments and scoring-based evaluations are increasingly applied, but their main drawback is subjectivity. Without the development of national standards and assessment methodologies, these issues cannot be resolved.

In the authors' view, overcoming these barriers requires the development of a coal industry digitalization strategy, defining its key stakeholders, goals, and mechanisms. Under conditions of sanctions and heavy dependence on imported production and digital technologies, this is impossible without active state involvement. Since coal companies in Russia are privately owned, only a mixed model of DT and DTw adoption is feasible. A suitable instrument



for its implementation could be industrial competence centers (ICC) – a mechanism for collaboration between the state, industries, and IT companies launched in 2022. ICCs enable government, private companies, and research and educational organizations to establish standards and priorities for indus-

try digitalization, while co-financing and managing projects. To date, 36 ICCs have been created under the national project Effective and Competitive Economy in all key sectors of the economy on the principles of public–private partnership, but none yet in the coal industry.

References

1. Grieves M., Vickers. J. Digital twin: mitigating unpredictable, undesirable emergent behavior in complex systems. In: Kahlen F.-J., Flumerfelt Sh., Alves A. (eds.) *Transdisciplinary Perspectives on Complex Systems: New Findings and Approaches*. Springer, Cham; 2017. Pp. 85–113. https://doi.org/10.1007/978-3-319-38756-7_4
2. Schluse M., Rossmann J. From simulation to experimentable digital twins: simulation-based development and operation of complex technical systems. In: *IEEE International Symposium on Systems Engineering (ISSE)*. Edinburgh, UK; 2016. Pp. 1–6. <https://doi.org/10.1109/SysEng.2016.7753162>
3. Negri E., Fumagalli L., Macchi M. A review of the roles of digital twin in CPS-based production systems. *Procedia Manufacturing*. 2017;11:939–948. <https://doi.org/10.1016/j.promfg.2017.07.198>
4. El-Saddik A. Digital twins: the convergence of multimedia technologies. In: *IEEE MultiMedia*. 2018;25(2):87–92. <https://doi.org/10.1109/MMUL.2018.023121167>
5. Rasheed A., San O., Kvamsdal T. Digital twin: values, challenges and enablers from a modeling perspective. In: *IEEE Access*. 2020;8:21980–22012. <https://doi.org/10.1109/ACCESS.2020.2970143>
6. Ghahramanieisalou M., Sattarvand J. Digital twins and the mining industry. In: Soni A.K. (ed.) *Technology in Mining Industry*. IntechOpen; 2024. Pp. 1–30. <https://doi.org/10.5772/intechopen.1005162>
7. Zhang C., Xu W., Liu J., et al. A reconfigurable modeling approach for digital twin-based manufacturing system. *Procedia CIRP*. 2019;83:118–125. <https://doi.org/10.1016/j.procir.2019.03.141>
8. Ghahramanieisalou M., Sattarvand J. Applications of digital twin technology in productivity optimization of mining operations. In: *Applications for Computers and Operations Research in the Minerals Industries*. August 2023. Rapid City, USA: SME; 2023. Pp. 1–17.
9. Borovkov A.I., Ryabov Y.A., Shcherbina L.A., et al. *Digital twins in high-tech industries*. Saint Petersburg: Peter the Great St. Petersburg Polytechnic University Publishing House; 2022. 492 p. (In Russ.)
10. Prokhorov A., Lysachev M. *Digital twin: Analysis, trends, and global experience*. Moscow: Alliance Print; 2020. 401 p. (In Russ.)
11. Abramov V.I., Gordeev V.V., Stolyarov A.D. Digital twins: characteristics, typology and development practices. *Russian Journal of Innovation Economics*. 2024;14(3):691–716. (In Russ.) <https://doi.org/10.18334/vinec.14.3.121484>
12. Madatov D.A., Borisov V.V., Sivkov V.S. The future of digital twin technology. *Mezhdunarodnyy Zhurnal Informatsionnykh Tekhnologiy i Energoeffektivnosti*. 2025;10(1):10–15. (In Russ.)
13. Panov Yu.P., Grabsky A.A., Rozhkov A.A. Current state and prospects for digitalization of the Russian coal industry. *Proceedings of higher educational establishments. Geology and Exploration*. 2023;(5):8–21. (In Russ.) <https://doi.org/10.32454/0016-7762-2023-65-5-8-21>
14. Zhdanev O.V., Vlasova I.M. Digital transformation of the coal industry. *Ugol'*. 2023;(1):62–69. (In Russ.) <https://doi.org/10.18796/0041-5790-2023-1-62-69>
15. Bratarchuk T.V., Gladyshev A.G., Lukichev K.E. Development and implementation of digital twins for optimization and sustainable development of the coal industry in Russia. *Ugol'*. 2024;(11):108–116. (In Russ.) <https://doi.org/10.18796/0041-5790-2024-11-108-116>
16. Solovenko I.S., Rozhkov A.A. Digitalization of enterprises of the fuel and energy complex of Russia (the turn of the 21st century): The state of the art of the problem. *Tomsk State University Journal*. 2023;489:153–161. (In Russ.) <https://doi.org/10.17223/15617793/489/15>
17. Nikitenko S.M., Goosen E.V., Kavkaeva O. Modeling of flexible value chains based on clean coal processing technologies. *Russian Mining Industry*. 2023;(S2):126–134. (In Russ.) <https://doi.org/10.30686/1609-9192-2023-S1-126-134>
18. Nikitenko S.M., Pavlova L.D., Korneva A.V., et al. Formation and control of value chains in coal industry based on emerging technologies. *Mining Informational and Analytical Bulletin*. 2024;(8):163–179. (In Russ.) https://doi.org/10.25018/0236_1493_2024_8_0_163



19. Goosen E.V., Kagan E.S., Nikitenko S.M., Pakhomova E.O. Evolution of VAC in the context of coal industry advance in the conditions of digitization in Russia. *Eurasian Mining*. 2019;(2):36–40.
20. Kurlov V.V., Kosukhina M.A., Kurlov A.V. Model for assessing the digital maturity of an industrial enterprise. *Economics and Management*. 2022;28(5):439–451. (In Russ.) <https://doi.org/10.35854/1998-1627-2022-5-439-451>

Information about the authors

Sergey M. Nikitenko – Dr. Sci. (Econ.), Associate Professor, Head of the Laboratory of Value Chain Transformation in the Coal Industry, Federal Research Center of Coal and Coal Chemistry of the Siberian Branch of the Russian Academy of Sciences, Kemerovo, Russian Federation; ORCID [0000-0001-6684-4159](https://orcid.org/0000-0001-6684-4159), Scopus ID [56511552300](https://scopus.org/56511552300); e-mail nsm.nis@mail.ru

Elena V. Goosen – Cand. Sci. (Econ.), Associate Professor, Leading Researcher of the Laboratory of Value Chain Transformation in the Coal Industry, Federal Research Center of Coal and Coal Chemistry of the Siberian Branch of the Russian Academy of Sciences, Kemerovo, Russian Federation; ORCID [0000-0002-1387-4802](https://orcid.org/0000-0002-1387-4802), Scopus ID [57192160485](https://scopus.org/57192160485); e-mail egoosen@yandex.ru

Anatoly A. Rozhkov – Professor, Head of Analytical Research and Short-Term Forecasting Department for Coal Industry Development, Department of Analytics for Coal and Peat Industries, Russian Energy Agency, Ministry of Energy of the Russian Federation, Moscow, Russian Federation; ORCID [0000-0002-4541-0922](https://orcid.org/0000-0002-4541-0922); e-mail rozhkov@rosenergo.gov.ru

Mikhail K. Korolev – Researcher of the Laboratory of Value Chain Transformation in the Coal Industry, Federal Research Center of Coal and Coal Chemistry, Siberian Branch of the Russian Academy of Sciences, Kemerovo, Russian Federation; ORCID [0000-0001-8102-9830](https://orcid.org/0000-0001-8102-9830), Scopus ID [57246310900](https://scopus.org/57246310900); e-mail m.korolev.gm@gmail.com

Received 01.04.2025

Revised 21.06.2025

Accepted 27.06.2025



EXPERIENCE OF MINING PROJECT IMPLEMENTATION

Research paper

<https://doi.org/10.17073/2500-0632-2025-06-426>

UDC 330.1:622



Valuation of non-producing mining companies

A. N. Lopatnikov , A. Y. Rumyantsev

AAR LLC, Moscow, Russian Federation

alopatnikov@aarcapital.com

Abstract

It is not unusual for the valuations of mining companies and projects to be debated by mining investors, analysts and regulators. Difficulties understanding geological information, volatility of metals prices, high investment risks and poor historical returns on capital in the mining industry are among the reasons. An additional and important factor is the varying risk profile at different stages of a mining project. A non-zero probability of not advancing to production for a project with a positive feasibility study (FS) requires a careful analysis of its valuation methods and supportive data. Because each mining project is different, and public mining companies are a small part of the market, it's hard to compare them accurately. Once a company prepares a mineral resources report, the exploration costs cease to be a relevant value metric. We offer a practical valuation method for non-producing mining companies, accounting for development stage risks to determine market value. Recognizing the specific attributes of the mining industry, we show that the NPVs calculated using the expected cash flows and discount rates developed using the traditional CAPM framework provide realistic estimates of the project's value, that compare well to the market indications for the peer groups. We are also investigating the large gap between the NPV values in technical reports and the actual market values of mining companies.

Keywords

valuation of mining assets and companies, NPV, market value, feasibility study, risks of mining projects, discount rates

For citation

Lopatnikov A.N., Rumyantsev A.Y. Valuation of non-producing mining companies. *Mining Science and Technology (Russia)*. 2025;10(3):306–316. <https://doi.org/10.17073/2500-0632-2025-06-426>

ОПЫТ РЕАЛИЗАЦИИ ПРОЕКТОВ В ГОРНОПРОМЫШЛЕННОМ СЕКТОРЕ ЭКОНОМИКИ

Научная статья

Оценка горных компаний с проектами на стадии оцененных ресурсов и запасов до этапа строительства предприятия и добычи

А. Н. Лопатников , А. Ю. Румянцев

ООО «ААР», г. Москва, Российская Федерация

alopatnikov@aarcapital.com

Аннотация

Оценка горных компаний и проектов нередко становится темой дискуссий отраслевых инвесторов, аналитиков и регуляторов. Среди причин – сложности интерпретации геологической информации, высокая волатильность цен на металлы и минералы, повышенный риск при инвестировании и исторически невысокая доходность на капитал в отрасли. Дополнительный и существенный фактор – характерная для горных проектов стадийность, когда профиль риска проектов заметно меняется на разных этапах их развития. Ненулевая вероятность проекта – не перейти к стадии строительства горного предприятия и добычи даже при наличии исследования уровня Feasibility Study (FS) – требует особого внимания к выбору метода оценки и анализу исходных данных. Уникальность горных проектов и относительно небольшой размер рынка публичных компаний отрасли ограничивают надежность сравнительного анализа. После публикации отчета с оценкой ресурсов затраты перестают быть релевантной метрикой стоимости. Ниже мы описываем практический подход к анализу стоимости горной компании или проекта до этапа строительства, который позволяет учесть риски проекта на данной стадии, тем самым повысить надежность оценки его рыночной стоимости. Мы показываем, что несмотря на специфику отрасли использование в расчете NPV ожидаемых денежных потоков и традиционных методов расчета ставки дисконтирования (CAPM) позволяет получить адекватную оценку проекта, которая согласуется



с выводами сравнительного анализа. В работе приведен анализ причин нередко кажущегося парадоксальным значительного несоответствия между значением NPV в технических отчетах горных компаний и их рыночной капитализацией.

Ключевые слова

оценка стоимости горных активов и компаний, NPV, рыночная стоимость, Feasibility Study, риски горных проектов, ставка дисконтирования

Для цитирования

Lopatnikov A.N., Rumyantsev A.Y. Valuation of non-producing mining companies. *Mining Science and Technology (Russia)*. 2025;10(3):306–316. <https://doi.org/10.17073/2500-0632-2025-06-426>

Introduction

Valuing mining companies and projects in the early stages is considered more difficult than valuing an average company in most other industries, except for pharmaceutical companies, which have a similar risk profile. The reasons mining companies are difficult to value include challenges interpreting geological information, several distinct development stages of a project and the binary nature of risks at the exploration stage, the high volatility of metal prices, and the relatively small size of both the industry and most mining companies. This, combined with the fact that many companies in the industry are not publicly traded, makes some investors believe that valuation methods used in finance are not suitable for assets with this type of risk profile.

The purpose of this article is to explain the reason for the differences between NPV in technical reports and fair values, as well as to offer a way of assessing the market value of companies and projects with feasibility studies prepared, but before the start of mine construction and production. To achieve this purpose, the study addresses the following three issues. First, we identify and systematize the factors explaining the large differences between the NPV values provided in technical reports and the market values of mining projects. Second, we propose a practical approach to selecting a discount rate developed using the CAPM model that considers the changing risk profile of a mining project. Lastly, we compare the value estimated using the proposed approach with market multiples based on market capitalization.

NPV and public disclosure standards

Despite the unique characteristics of mining assets and the variety of methods available to investors for their valuation, they are all variations of one of three basic valuation methods or approaches: comparison with similar or comparable assets, justified equivalent costs, or the present value of the expected income.

NI 43–101 Standards of Disclosure for Mineral Projects, and a companion Form 43–101F1, require Technical Reports of the public companies (Preliminary

inary Economic Assessments (PEA), Pre-Feasibility Studies or Feasibility Studies) to include a section with economic analysis and its key assumptions. Specifically, Form 43–101F1 requires the report to include “a discussion of net present value (NPV), internal rate of return (IRR), and payback period of capital with imputed or actual interest”.

Neither the JORC Code 2012 nor the 2024 draft mentions NPV or requires its calculation disclosed in public reports [1]. However, the JORC Code requires disclosing all material information that impacts the economics of a particular mining project. This information includes economic assumptions considered in developing the modifying factors (i.e. mining method, processing, metallurgy, infrastructure, as well as economic, marketing, legal, social factors, including environmental and regulatory requirements) which must be included in technical reports with estimates of mineral resources and reserves.

In theory, NPV can be used to estimate the value of any asset; however, not every estimate of NPV results in the market value. The intended use of NPV defines how the key parameters are estimated, i.e. cash flows and discount rate. The main goal of estimating IRR and NPV in technical reports is to test if the project is economically feasible. Positive NPV means the project can be undertaken [2].

As a result, a useful practice of disclosing mining project NPV in public reports becomes a reason for confusion, since those NPVs have nothing to do with the market value of the project. Explaining the nature of value creation in mining and the confusion that arises from misinterpreting the intent of the technical reports vs market valuations, Michael Samis [3] noted that “*Industry professionals and observers are often confused by the large difference between an exploration company’s market cap and the NPV reported in its project NI43–101*”. NPVs provided in technical reports or announcements of public companies often tend to be significantly higher than market capitalization. An analysis of 100 mining projects in 2024 [4] showed that NPV reported in Feasibility Studies were on average 40–60% higher than their market values.



It is not unusual to see NPV of hundreds of millions of US dollars reported in a Pre-feasibility Study (PFS) or Feasibility Study (FS) by a company with a market capitalization of a few tens millions of dollars or less. A recent example is TriStar Gold's May 2025 announcement about the updated PFS that notes "There was no change to the mineral resources or reserves, the focus of the update study was the cost estimate since the release of the previous PFS, as well as to incorporate changes to the gold price and exchange rates" [5]. The markets positively reacted to the doubling of the project's NPV from 321 to 603 million US dollars in the updated PFS (calculated using USD2,200/oz and 5% discount rate)¹. At the same time the reaction to the increased NPV was rather subdued, the market capitalization of the company increased by 9.1% to reach USD36.5 million, which is roughly one-sixteenth of the NPV reported in the PFS.

Another example [6] is the updated Feasibility Study on a lithium project in Canada prepared by Frontier Lithium. The company with a market capitalization of USD90 million reported an NPV@8% of USD932 million.

The magnitude of the difference is way too high to assume a systematic mispricing of the mining projects by the markets. Neither can it be explained by the difference in the estimates made using different valuation approaches, e.g. comparative vs income based. In the following sections we explain that this value dichotomy is not a bug, but a feature of the mining companies at the exploration stage or Feasibility Study projects that did not reach mine construction and production phase.

NPV, Technical Value and Market Value

NPV logic is implicit in the definition of "Technical Value" in the VALMIN mineral assets and company valuation code, defined as follows "Technical Value is an assessment of a Mineral Asset's future net economic benefit at the Valuation Date under a set of assumptions deemed most appropriate by a Practitioner, excluding any premium or discount to account for market considerations".

The term "Technical Value" is not used or mentioned in the International Valuation Standards (IVS), International Financial Reporting Standards (IFRS) or economic literature. However, it is essentially an NPV developed using certain subjective inputs, raises questions and confuses. In the latest version, VALMIN attempted to harmonize its definitions with IVS. It was done in a clarifying statement that Technical Value

is equivalent to Investment Value in IVS. In our view it is not much of an improvement, since Investment Value under IVS is often nothing more than an NPV calculated using subjective user-specific assumptions. IVS2025 defines Investment Value as "the value of an asset to a particular owner or prospective owner for individual investment or operational objectives".

The assumptions used to calculate NPV in Technical Reports that make it significantly different from market value are as follows:

- use of a single set of cash flows instead of the expected cash flows. This approach implies that the project is guaranteed to reach production, and that its technical parameters, schedule and economic results will match the model;
- use of a "standardized" discount rate (normative), that does not reflect the risks and the cost of capital for the project during exploration and evaluation stages.

The first assumption could be appropriate for the valuation of an existing mine that reached the planned production level and sales volumes. However, even in this case, the use of a single discount rate for all projects is hard to justify for estimating the market value.

Based on empirical data, A. Dixit and R. Pindyck [7], noted that in financing new projects, investors tend to use not the opportunity cost or corporate WACC, developed using CAPM (Capital Asset Pricing Model), but a hurdle rate, which is much higher in real terms. The statistics of the mining industry show that the probability of a project reaching the stage of mine construction and production varies over life of the project. Even for bankable Feasibility Study projects this probability is markedly lower than 100%. The planned mining volumes cannot be achieved or be achievable for various reasons outside of the company's control. The research on the probability of mining companies failing to reach the stage of mine construction and production is limited. However, the available studies consistently report similar chances of moving between the stages for projects, that could be considered as a rough estimate of the risks at the respective stages.

It should be noted that the "stage" of a mining project is a broadly defined term subject to interpretation. The CIMVAL mineral valuation code mentions that "As applied to Mineral Properties, the Valuation approach depends on the stage of exploration or development of the Mineral Property. Mineral Properties can be categorized for convenience into four types; however, it should be noted that there are no clear-cut boundaries between these types, that the Mineral Property category may change over time, and that it may be difficult to

¹ At 10% discount rate NPV was calculated by the company to be equal USD393 million.



classify some Mineral Properties so they fit in only one specific category” [8]:

- prospecting and exploration projects without mineral resources;
- projects with mineral resources and reserves before final investment decision (FID) and mine construction;
- built and producing mines.

It is reasonable to expect that for the projects with resources and reserves, estimated according to one of the internationally accepted codes based on the CRIRSCO template, the stage of development will inversely correlate with their riskiness hence, positively correlate with their value, ceteris paribus. That said, no exploration or evaluation can ever remove all risks and uncertainties of a mining project. This explains why investors’ valuations of FS stage non-producing projects and producing mines differ.

Statistics that help better understand the risks of mining projects at different development stages were provided by J.P. Syles and A. Trench [9] in their study of global copper projects. The authors noted that a pyramid representation is the best illustration of “a flow of many projects to few through a hierarchical or linear stage-gating system”.

To illustrate the approximate probability of a mining project advancing to the next stage, in Table 1 we use the findings of the study to show the percentages at respective development stages.

According to J.P. Syles and A. Trench “As well as the expected large number of projects that do not make it from the raw prospect or early exploration stages into the advanced exploration stages, as would be expected,

a significant number do not also make it from advanced exploration to prefeasibility. The approximate percentage not converting from advanced exploration to prefeasibility is about 85 per cent in this sample, a greater percentage than the amount not making it from early exploration to advanced exploration (about 75 per cent). This suggests that a significant number of projects have an advanced level of exploration conducted on them, only to then subsequently prove uneconomic”.

Similar findings reported by others [10] are illustrated in Table 2.

AMC data [11] suggests that around 25% of FS projects fail. McKinsey (2017) [12] estimates that only 20% of FS stage mining projects were built as planned initially, many experienced multi-year delays and had lower parameters than planned. Other researchers found that 30% of mining projects do not advance beyond Feasibility Study because of problems obtaining regulatory approvals, technical issues, or failing to attract financing.

Table 3 illustrates the taxonomy of main development stages and appropriate valuation methods provided in VALMIN, CIMVAL, and SAMVAL mineral valuation codes.

Explaining the limitations of NPV for valuing mining projects P.F. Bruce [13] argued “The NPV-DCF method is invaluable for comparing the worth of various advanced exploration properties particularly those with similar technical and financial parameters. It is not appropriate to use the method rigorously on an Exploration Property which lacks the necessary technical and commercial parameters needed to properly apply the method.

Table 1

Global copper projects hierarchy

Project development stage	Construction and production	FS	PFS	Advanced Exploration	Early Exploration
Number of projects at this stage	66	75	92	664	2,870
Percentage of projects at this stage vs previous stage, %	88	82	14	23	N/A

Table 2

Probability of success at different phases of development

Year	Year 1	Year 2	Year 3	Year 4	Year 5	Probability of Success, %
Quarter (Q)	Q1-Q4	Q1-Q4	Q1-Q4	Q1-Q4	Q1	
Profile Engineering						50
Conceptual Engineering						70
Basic Engineering						90
Production						100



Any attempt to ‘invent’ parameters to engender the cash flow with some semblance of reality can be most misleading to the inexperienced or uninformed. Nevertheless, a crude conceptual cash flow model based on best judgement expectations of future mineral resource parameters is a useful in-house technique for putting an Exploration Property into perspective to support a ‘value’ or for justification of further exploration expenditure. The method applied to an Advanced Exploration Property will provide an indication of the value for ‘what can be seen’ on the property”.

It is fair to say that public companies’ disclosures note that NPV provided in the technical report does not reflect the project’s market value, which is often shown separately to illustrate the difference. As an example, presenting the results of a PFS prepared to restart its Madsen Mine, West Red Lake said the following “Madsen Mine NPV is CAD\$496 million using long-term gold price of USD2,640/oz. Developers often valued at ~0.4 times their asset value. Producers often valued between 0.7 and 1.0 times their asset value. WRLG’s market capitalization is ~CAD\$300M today”. Market capitalization did not change much after the mine restarted in May 2025 [14].

Why do the NPVs reported in PEA, PFS, or FS not represent market value?

Large differences between NPV reported in a PFS or FS and the market value of the mining project are explained by recognizing that a Feasibility Study is essentially a marketing product, supported by certain research and quantitative estimates. Its primary goal is “to sell” the project to investors. Investors usually consider not one project but select between several investment alternatives, making the use of a “single” discount rate appropriate. The task of the investor, therefore, is to make the right choice, not to estimate the market value of the specific investment.

For NPV to yield an estimate of the market value, the calculations should use the assumptions implicit in the market value definition and market inputs [15]. Mathematically, it means one should use the expected cash flows and the discount rate reflecting the risks of the projects. The main reason why NPV in a Feasibility Study differs from the market value is that the above conditions are not met.

The risks of a mining project can be accounted for in one of two key components of NPV, i.e. expected cash flows and/or the discount rate. Table 4 shows the examples.

Table 3

Comparative illustration of project stages and valuation methods

Valuation Approach			Applicability to Respective Project Stage		
Market Approach	Income Approach	Cost Approach	VALMIN	CIMVAL	SAMVAL
YES	NO	YES	Exploration projects	Exploration Projects	Early-stage exploration
YES	In some cases	In some cases	Pre-Development Projects	Mineral Resource Properties	Advanced stage exploration
YES	YES	NO	Development Projects	Development Projects	Development properties
YES	YES	NO	Production Projects	Production Projects	Production properties
NA	NA	NA	NA	NA	Dormant properties
NA	NA	NA	NA	NA	Defunct properties

Table 4

Accounting for risk when estimating the market value using NPV

Risk	Better modeled in	Comments
Systemic/Market risks	Discount rate	Expected return or return on an alternative investment
Time value of money and inflation	Discount rate	Present value
Financial risks	Discount rate	Uncertainty premium
Operating/project risks	Cash flows	Provisions for planned costs and contingencies
Technical and regulatory risks	Cash flows	Delays, likelihood of failure, cost overruns

Fig. 1 illustrates the risk structure of an exploration project. An estimate of value of a resource or reserves stage project can be made using a resource-based multiple or cash flows analysis, where exploration and evaluation data support it.

The fact that a company reported mineral reserves in a Pre-feasibility or Feasibility Study does not mean that all material risks of the project were removed; the remaining risks need to be reflected when estimating the market value of the project using NPV. Failing to do it is a major reason behind the differ-

ences between the valuations based on market multiples that use peer group market capitalization and NPVs in the technical reports.

To reflect the industry practice of using “standardized” discount rates in mining Feasibility studies for non-producing projects, mining analysts use an adjustment to NPV (or more precisely Net Asset value, of which NPV is the largest element). Fig. 2 provides an example of such conversion of NPV (or Technical Value) to the market value measured by market capitalization of a mining company, as presented by SRK [16].

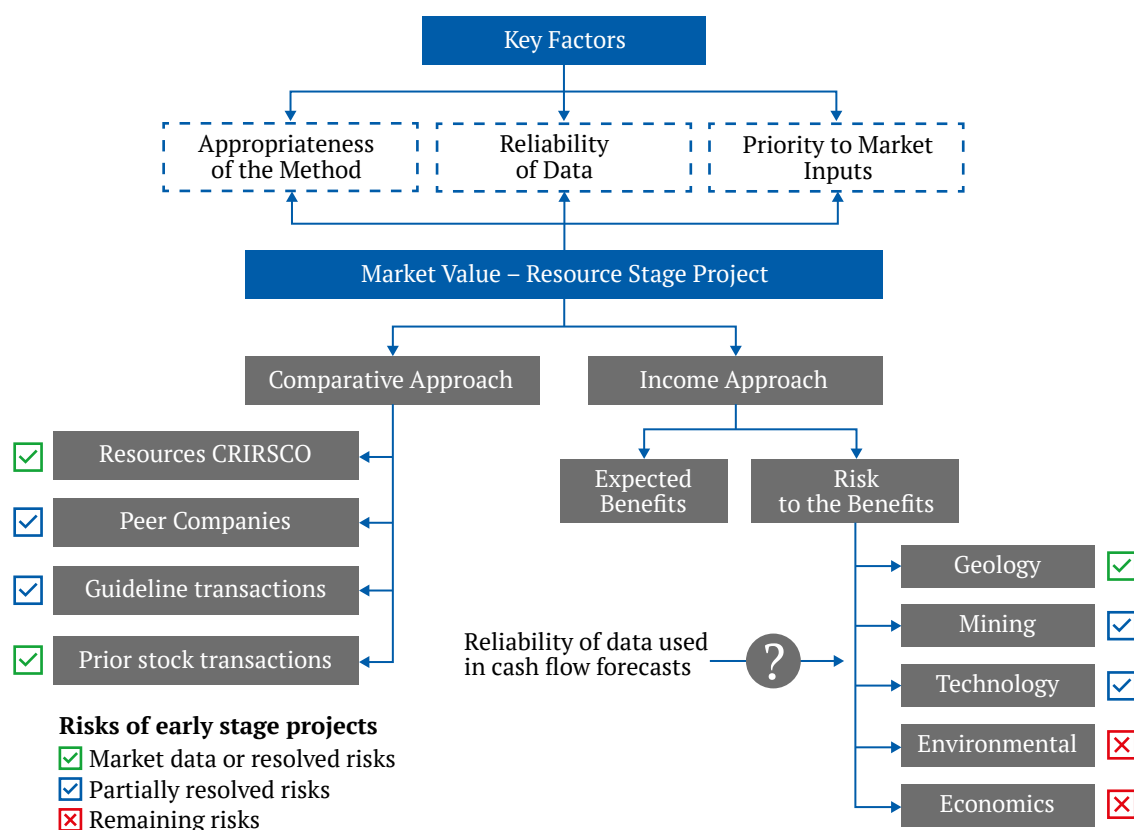


Fig. 1. Key factors and risks to be considered in valuations of exploration projects

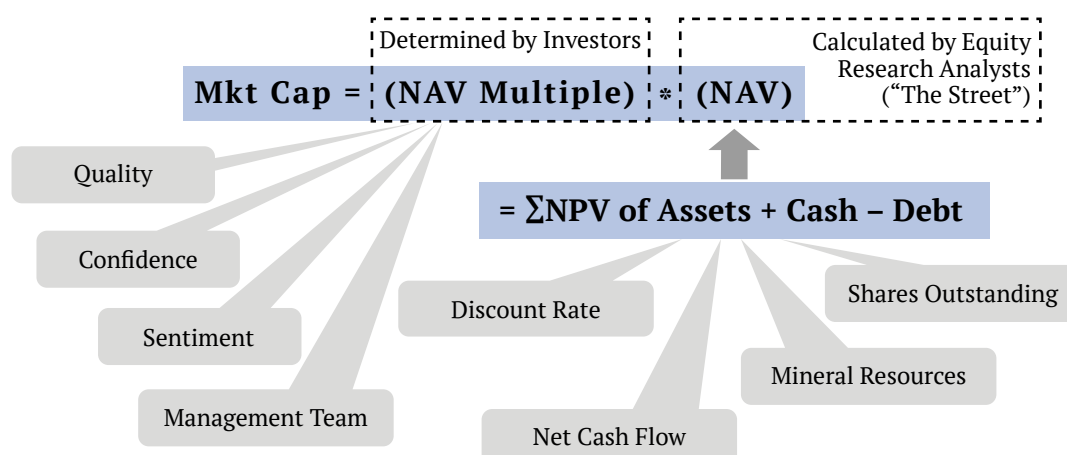


Fig. 2. Relationships between market value and NPV

BMO [17] describes the use of P/NAV multiple by analysis as follows “We apply NAV target multiples to each asset in our coverage universe based on our assessment of the asset’s risk, including construction/startup risk, production risk, geopolitical risk etc. We also consider opportunities, including potential for mine life extension. The multiples that we have applied range from 0.0 and 0.1x for early-stage, end-of-life, or otherwise higher-risk assets, and 1.0x for mature and stable operating mines as well as long-lived smelter assets”.

There is a practical problem with using P/NAV multiple to estimate the market value – its calculation is not transparent, and it is not obtained directly from the market. Furthermore, it is an ‘integral’ adjustment to NPV, not to its two key parameters, i.e. cash flows and discount rate.

Feasibility studies often report NPV for a base case scenario, which may not and often does not necessarily meet the definition of the expected cash flows for a project that has yet to be built and is not producing. This is evidenced by the absence of probabilistic adjustments in NPV developed for PEA, PFS and FS studies.

Some analysts compensate for the higher risks of the cash flows by using a higher discount rate, assuming that above-average risks require above-average discount rates, other things equal. While intuitively appealing, this adjustment is highly subjective and lacks academic support to sanity check the size of the adjustment.

The NPV presented in PEA, PFS, or FS is usually calculated using a “standard” normative discount rate that doesn’t reflect the condition and risks of the project. There may be some logic in using 5% real discount rate for producing gold mine, but it is hardly appropriate for a company that is yet to start building a mine.

Early-stage mining projects, prospecting and early exploration phases, are known to have the highest levels of uncertainty and the lowest amounts of information. Acknowledging there is no way of reliably estimating the value of such a project, investors choose to defer the valuation decision until additional data is obtained. A typical way of investing in early-stage projects is to share risks (costs) and secure the right to commence a more reliable valuation in the future by signing an option or a farm-in agreement. No mining valuation code recommends using NPV for projects at this stage of development.

Producing mines with stable mining and sales volumes or large multi-location companies are valued by market participants based on their projected cash flows or market multiples of publicly traded peers; however, the uniqueness of every mine and the re-

latively small size of the mining equity markets constrain the reliability of comparison. The most challenging task is usually the valuation of PFS or FS stage projects prior to mine construction and production.

Estimating the market value of projects and companies that did not start mine construction and production

The probability of entering production and reaching the expected mining volumes can be accounted for in the cash flows, the discount rate, or both. Alternatively, it can be addressed by using an integral adjustment, such as the previously mentioned P/NAV.

NPV of a gold mining project calculated in a Feasibility Study most often uses a ‘base’ real discount rate of 5% (equivalent to 7% in nominal terms, accounting for inflation). Lawrence Devon Smith [18] provided results of industry practitioners surveys undertaken over several years by CIM Mineral Economics Section to obtain an indication of common practice regarding discount rates for projects at different stages (Fig. 3). Respondents were asked to express the discount rates in real terms. Solid lines are mathematical averages of the responses; dashed lines indicate the ranges plus/minus one standard deviation. It is worth mentioning that the ranges are rather broad.

The publication also provided the average premiums over the ‘base’ discount rate, WACC for a producing mine, applicable for projects at different stages of development. We show them in Table 5.

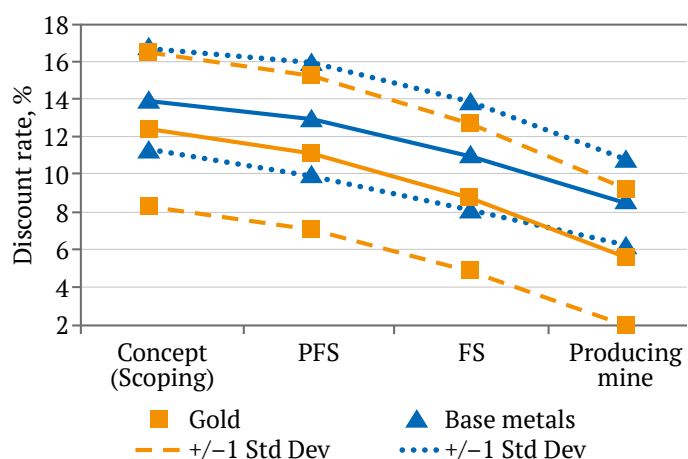


Fig. 3. Discount rates for cash flows in real terms for mining projects at different stages

Table 5

Premiums over the “base” discount rate for projects at different stages

Premium above WACC of a producing mine, %	FS	PFS	PEA/Scoping
Gold	3.3	5.7	6.9
Base metals	2.5	4.5	5.5

The survey results demonstrate the inverse relationship between project risk and discount rates used by market participants.

G. A. Davis [19] criticized the practice of using the discount rate as a receptacle of all and any risks. It is more appropriate to model the uncertainties of a specific project directly in the cash flows, not grossing up the discount rate with “specific” premiums lacking theoretical rigor and practical ways of calibrating them to risks.

The basic formula for the weighted average cost of capital or WACC is as follows:

$$WACC = R_e \cdot \frac{E}{E+D} + R_d \cdot (1-T) \cdot \frac{D}{E+D},$$

where R_e – cost of equity capital; $E/(E+D)$ – share of equity in capital; R_d – cost of debt; $D/(E+D)$ – share of debt in capital; T – corporate tax rate.

To estimate the cost of equity of smaller companies, the modified CAPM model is often used:

$$R_e = (R_f + CRP) + \beta \cdot ERP + SP,$$

where R_f – risk-free rate; CRP – country risk premium; β (Beta) – the coefficient that reflects the relationship between the asset risk and market risk; ERP – average equity risk premium over and above the risk-free rate; SP (size premium) – premium for smaller sized companies.

The following calculations illustrate how NPV would change for a Twin Hills project, developed by Osino Resources in Namibia, using the same cash flows assumptions, but selecting a different discount rate based on the modified CAPM.

The calculations are as of June 2023, the date of Osino Resources’ technical report, an FS prepared in accordance with NI43-101 (the company used the name DFS, Definitive Feasibility Study) [20]. DFS includes the details of the NPV calculations made in real terms assuming long-term gold price of USD1,750/oz and a discount rate of 5% resulting in NPV of USD 480 million. The company also illustrated the sensitivity of NPV to gold price, showing that at a gold price of USD1,950/oz, the project’s NPV would be USD656 million. In June 2023, spot gold prices ranged from USD1,910 to 1,970/oz. The consensus forecast predicted a gold price of USD1,500/oz in 5–7 years.

The assumptions we made in developing the discount rate were as follows:

R_f – considering the cash flow forecasts in the DFS were in USD, the risk-free rate was the yield of 10Y US treasury bonds of 3.7%.

CRP – country risk premium can be proxied by the spread between the US T-bonds and the project’s

country Eurobonds (if available) or a country with the same credit rating. According to Professor Damodaran, Namibia’s country premium was 5.5% in 2023.

ERP – equity risk premium, $R_m - R_f$, (Equity Risk Premium, «ERP») is the difference between the expected returns on a diversified portfolio of stocks and the risk-free rate. It can be interpreted as the average premium investors require for investing in stocks as an asset class. According to Kroll, mid-year 2023 ERP was 5.5%.

β – the coefficient showing the riskiness of the stock (or industry) relative to the market. To address the fact that companies’ Betas can be noisy, practitioners often use average betas for a representative peer group of companies from the same industry. The mining companies’ industry beta reported by Professor Damodaran was 1.17. It should be noted that this average beta was developed using the industrywide set of companies that include the large gold miners with betas well below one and junior gold mining companies with projects at the exploration stage that have significantly higher betas.

It is empirically established that betas tend to increase as company size goes down, the relationship holds for all industries. Our analysis of junior gold mining companies shows that their Betas start increasing significantly for companies in the 8–10th size deciles, those with market capitalization of below USD 1 billion. We show it in Fig. 4. The below trend betas for the companies from decile 9 are reflective of the composition of the decile that includes companies with operating mines, hence lower risks.

The average Beta for the set of junior gold mining companies from the 9th and 10th deciles was 1.5.

SP – size premium is the incremental return expected by investors in smaller-sized companies over and above the Beta of the stock.

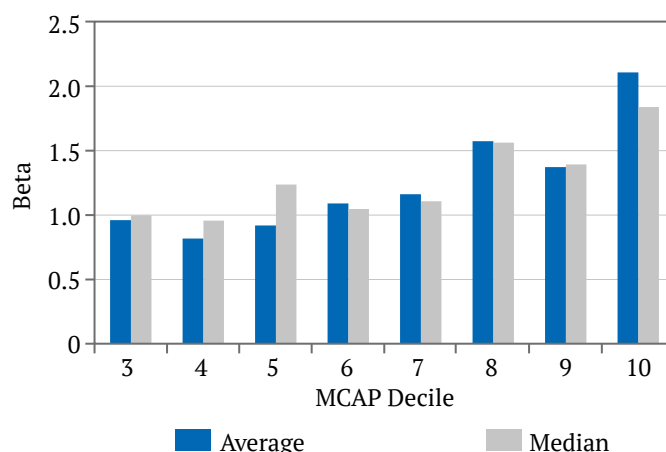


Fig. 4. Betas for different size deciles of junior gold mining companies

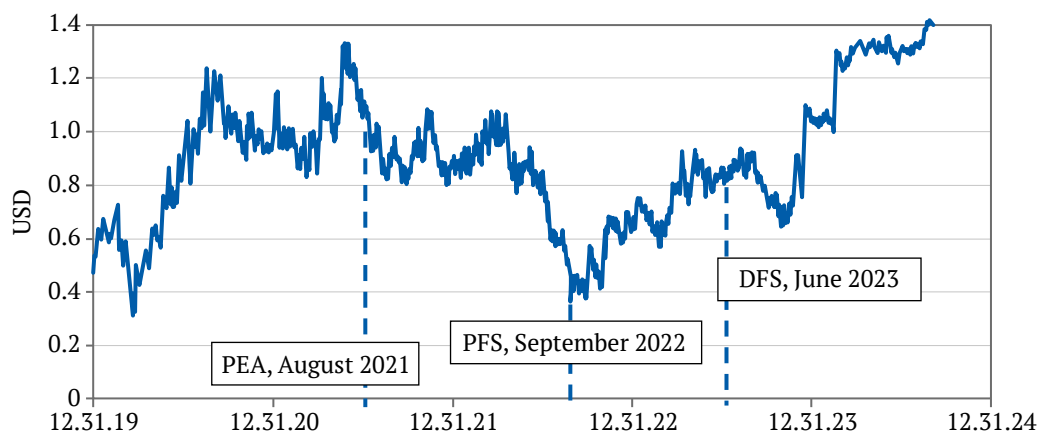


Fig. 5. Osino Resources share price, USD

Non-producing public junior gold mining companies have market capitalization below USD 500 million and are classified as microcapitalization stocks. Size premium for the companies of this size is estimated by Kroll as 2.9%. For smaller companies with a market capitalization below USD200 million, it is 4.7%.

Considering the above, the cost of equity for Osino Resources can be estimated as follows:

$$R_e = 3.7\% + 5.5\% + 1.5 \cdot 5.5\% + 2.9\% = 20.4\%.$$

Using industry average capital structure and Osino Resources' cost of debt, the company's WACC is estimated to be approximately 18% in nominal terms, or 16% in real terms. The calculated discount rate is significantly higher than real 5% rate selected in the DFS NPV calculations.

Using a 16% real rate developed using the modified CAPM with size premium adjustment and a cash flows probability adjustment of 88% for projects at FS stage, the resulting NPV would be USD150 million.

In June 2023, at the time when Twin Hill project DFS was published, base case NPV@5% in the technical report was USD464 million, whereas the market capitalization of the company was USD134 million, or about 30% of the reported NPV. Considering total resources of the project of 3.19 million oz of gold and the company's enterprise value (EV) of USD132 million, the market valued Osino Resources at USD42/oz.

The market valuation was also closer to the Rule of Thumb (or Yardstick Method) estimate of USD129–172 million. This empirical method uses market transactions data for gold companies and projects and usually works best for earlier stage resources projects but can also be used to test the reasonableness of NPV for non-producing mining projects that did not start mine construction [21, 22].

Fig. 5 shows the dynamics of the company's market capitalization. The dashed lines indicate the dates

Osino Resources published PEA (August 2021), PFS (September 2022), and DFS (June 2023).

The chart shows that the publication of the DFS did not materially change the market's opinion regarding the value of the Twin Hills project. This is not unusual assuming the typical value evolution profile for the mining companies known as the Lassonde Curve [23]. During the so-called 'orphan' period – when there is no investor committed to finance and develop the project, or until such a decision is made by the current owner – the value of a project often declines.

In December 2023, six months after the DFS was published, Dundee Precious Metals

offered USD214 million to buy Osino Resources, the owner of the Twin Hill project, at a premium

of 44.3% to Osino Resources' market capitalization. [24] In February 2024, Chinese Shanjin International Gold Co., Ltd. (previously Yintai Gold Co., Ltd.) made a better offer and acquired the project for USD272 million [25]. Following the acquisition, the buyer delisted Osino Resources from the TSX.

Despite a competitive bid and a high premium, the acquisition price was significantly lower than the DFS NPV, representing only about 60% of the reported value.

Discussion and Conclusions

The analysis of Feasibility Study level non-producing mining projects helps understand the reasons behind the systematic difference between NPV in technical reports and the market value of mining companies measured as their market capitalization.

Industry professionals and companies providing disclosure to investors have to better explain the differences in two value metrics, i.e. NPV and market value, since not all the users of such reports are equally experienced and knowledgeable about the pe-



cularities of the mining industry, and may therefore interpret them incorrectly. Market capitalization of a company and the volatility of its stock price provide important information about its market value and risks at different stages of project development.

The proposed method of estimating the market value of a non-producing company or project with completed PFS or FS but before the FID or construction of the mine considers the project's risks and improves the reliability of the estimate. We showed that despite mining industry specifics, the use of expected cash flows and traditional methods for selecting discount

rates (CAPM) when calculating NPV results in an adequate estimate of the project's value that reasonably compares with the market analysis using a peer group.

Important note: these discount rates should be used with the expected cash flows. Feasibility Study resource projects and earlier stage PEA and Pre-Feasibility Study projects require the application of risk-adjusted cash flows that account for the probability of achieving production.

The Rule of Thumb method can reasonably estimate market value and test NPV for early-stage projects.

References

1. JORC. JORC Code: Australasian Code for Reporting of Exploration Results, Mineral Resources and Ore Reserves (Draft for Public Comment, 1 August 2024). URL: https://www.jorc.org/docs/Draft_JORC_Code_01Aug2024_readonly.pdf
2. Samis M., Martinez L., Davis G.A., Whyte J.B. Using dynamic DCF and real option methods for economic analysis in NI43-101 technical reports. URL: <https://inside.mines.edu/~gdavis/Papers/ValMin.pdf>
3. Samis M. Exploration value differentials. Understanding the value differential attached to early-stage exploration projects. Presented at: IMVAL: Perspectives on Mineral Valuation; 2021 May 13. URL: https://imval.org/uploads/presentation/2021-05-13/Slides/IMVAL_May2021_Samis-Slides.pdf
4. Ovalle A. Analysis of the discount rate for mining projects. In: Castro R., Báez F., Suzuki K. (eds.) *MassMin 2020: Proceedings of the Eighth International Conference & Exhibition*. Mass Mining, University of Chile, Santiago, 2020. Pp. 1048–1064. https://doi.org/10.36487/ACG_repo/2063_76
5. TriStar Gold Updates Economics of PFS with After-Tax 40% IRR and US\$603 Million NPV5 and Provides Update on Permit. URL: <https://finance.yahoo.com/news/tristar-gold-updates-economics-pfs-110000667.html>
6. Frontier Lithium Inc. Corporate Presentation: Building North America's highest quality source of lithium. URL: https://www.frontierlithium.com/_files/ugd/dec7de_bb60250af14744c9b41b6b36c3890d26.pdf
7. Dixit A.K., Pindyck R.S. *Investment under uncertainty*. Princeton University Press; 1994.
8. Categories of Mineral Properties. In: *The CIMVAL Code for the Valuation of Mineral Properties*. Prepared by the Special Committee of the Canadian Institute of Mining, Metallurgy and Petroleum on the Valuation of Mineral Properties (CIMVAL).
9. Sykes J.P., Trench A. Resources versus reserves – towards a systems-based understanding of exploration and mine project development and the role of the mining geologist. In: *Ninth International Mining Geology Conference*. Adelaide, SA, 18–20 August 2014. <https://doi.org/10.13140/RG.2.1.5083.5600>
10. McCarthy P. Why feasibility studies fail. URL: <https://www.amcconsultants.com/experience/why-feasibility-studies-fail>
11. Dussud M., Kudar G., Lounsbury P., et al. *Optimizing mining feasibility studies: The \$100 billion opportunity*. URL: <https://www.mckinsey.com/industries/metals-and-mining/our-insights/optimizing-mining-feasibility-studies-the-100-billion-opportunity#/>
12. Méndez M. Real options valuations of the license of a copper mine. In: *FFM 2011*. (Revised September 2013). ESIC Business and Marketing School, Madrid, Spain. <https://doi.org/10.2139/ssrn.2708352>
13. Bruce P.F., Clarke D.E., Bucknell W.R. The company perspective on valuation methods for exploration properties. In: *Mineral Valuation Methodologies Conference*. Sydney. 27–28 October 1994
14. West Red Lake Gold shares jump on Madsen restart. URL: <https://www.mining.com/west-red-lake-gold-shares-jump-on-madsen-restart/>
15. *International Valuation Standards Council*. IVS 104: Bases of value. Para 30.5. In: *International Valuation Standards*. 2022.
16. Robson D.M. *What does it mean to create value in the mining industry?* CIM MES Discussion Group, Toronto. January 31, 2018.



17. *Initiating at outperform (speculative): where does the value go?* Turquoise Hill Resources, BMO Capital Markets. January 4, 2021. P. 35.
18. Smith L.D. *Mineral economics – risk adjusted cash flows: discount rates*. Risk & Long-Life Projects; 2013.
19. Davis G.A., (Mis)Use of Monte Carlo simulations in NPV analysis. *Mining Engineering*. 1995;47(2):75–79.
20. Armstrong R., Aucamp P.-J., Doundarov G., et al. *Definitive feasibility study of the Twin Hills Gold Project, Namibia*. National Instrument 43-101 Technical Report. URL: <https://osinoresources.com/wp-content/uploads/2023/07/Osino-DFS.pdf>
21. Roscoe W.E. Metal transaction ratio analysis – a market approach for valuation of non-producing properties with mineral resources. In: *VALMIN Seminar Series 2011–2012*. Perth, Western Australia, 18 October 2011. 17 April 2012, Brisbane, Queensland. The Australasian Institute of Mining and Metallurgy; 2012.
22. Araujo C.P. Valuation of mineral and coal assets. Presented at: *SMEDGE Conference*. 24 January, 2019.
23. *The Lassonde curve – understanding the mining life cycle*. SmallCapInvestor; 2023. URL: <https://smallcapinvestor.ca/the-lassonde-curve-understanding-the-mining-life-cycle/>
24. *Dundee to acquire Osino in \$214m deal*. Mining Technology; 2023. URL: <https://www.mining-technology.com/news/dundee-acquire-osino-214m-deal/>
25. *Yintai to acquire Osino Resources in \$272m deal*. Mining Technology; 2024 URL: <https://www.mining-technology.com/news/yintai-osino-resources/>

Information about the authors

Alexander N. Lopatnikov – Managing Partner, AAR LLC, Moscow, Russian Federation; ORCID [0000-0002-8267-4732](https://orcid.org/0000-0002-8267-4732); e-mail alopatnikov@aarcapital.com

Alexander Yu. Rumyantsev – CFA, Director of Financial Analysis and Valuation, AAR LLC, Moscow, Russian Federation; ORCID [0009-0007-4427-2269](https://orcid.org/0009-0007-4427-2269); e-mail arumyantsev@aarcapital.com

Received 26.06.2025
Revised 28.07.2025
Accepted 01.08.2025